National Library of Canada
Acquisitions and Bibliographic Services Branch
395 Wellington Street
Ottawa, Ontario
K1A 0N4

Bibliothèque nationale du Canada
Direction des acquisitions et des services bibliographiques
395, rue Wellington
Ottawa (Ontario)
K1A 0N4

Your file Votre référence

Our file Notre référence

NOTICE

The quality of this microform is heavily dependent upon the quality of the original thesis submitted for microfilming. Every effort has been made to ensure the highest quality of reproduction possible.

If pages are missing, contact the university which granted the degree.

Some pages may have indistinct print especially if the original pages were typed with a poor typewriter ribbon or if the university sent us an inferior photocopy.

AVIS

La qualité de cette microforme dépend grandement de la qualité de la thèse soumise au microfilmage. Nous avons tout fait pour assurer une qualité supérieure de reproduction.

S'il manque des pages, veuillez communiquer avec l'université qui a conféré le grade.

La qualité d'impression de certaines pages peut laisser à désirer, surtout si les pages originales ont été dactylographiées à l'aide d'un ruban usé ou si l'université nous a fait parvenir une photocopie de qualité inférieure.

Canada

Physical and Electrochemical Basis of Induction of Reversibility in MnO_2 Reduction and Reoxidation

Deyang Qu

ISBN 0-315-95970-3

UNIVERSITÉ D'OTTAWA
UNIVERSITY OF OTTAWA

Acknowledgments

Throughout the whole of life, there are only a few people who can dramatically influence one's life and future. Dr. B.E. Conway is one of those rare people in my life. From Dr.conway, I have learned not only the fundamental principles of electrochemistry, which can help me to bridge the discipline of fundamental electrochemistry to its practical applications, but also how to be a professional electrochemist. These experiences, however, will benefit my whole future career. Dr. Conway has been more than a good teacher to me; I sincerely appreciate his patience and encouragements, without which I cannot imagine how I could fulfil the requirements of presentation of a Ph.D thesis.

I wish also to thank Dr. W.A. Adams, director of ESTCO, for his kindly discussions; I have learned a lot from him, especially practical knowledge of batteries and electric vehicles.

I wish to thank Dr. James McBreen at Brookhaven National Laboratory, who introduced me to the new and powerful experimental method of X-ray absorption. I appreciate his kindness and patience in directing me in the running of the experiments on the Brookhaven National Synchrotron Light Source.

I also wish to thank Dr. L.J. Bai, who was Dr. Conway's senior research associate, for his selfless help and encouragement. I appreciate the long period friendship between his family and mine, and I believe it will last for ever.

I wish to thank, in addition, Prof. Y.H. Zhou for helpful cooperation and Dr. H.S. Wroblowa for fruitful discussions.

I also wish to thank all my colleagues , Qian, Rada, Sylvie, Mark, John, Gao..... I have always appreciated their help.

Special thanks are due to my parents, who not only introduced and encouraged me in the field of chemistry, but also sacrificed and struggled by every means to help me to fulfil my education.

I would like to thank my wife, Qiang Ren, for her constant sacrifice and encouragement throughout my studies, while she was working on her own Ph.D thesis during the same time. Without her company, I could not have a happy life in Ottawa.

Finally, I like to thank the Ontario Government for providing me, for one year, an Ontario Government Graduate Scholarship.

Special thanks are due to the Electrochemical Society for the award to me of the Battery Division's Student Award in 1993.

Abstract

"Chemically Modified" (CM) rechargeable MnO_2 cathode materials have been prepared, based on patents issued to Ford. The reaction mechanisms of the discharge and recharge of these materials have been extensively studied in the present work and compared with behaviour at Blank MnO_2 (without Bi) and regular γ-MnO_2, by various experimental techniques including classical electrochemical methods, as well as a newly developed *in-situ* uv-visible spectro-electrochemical method and a new *in-situ* X-ray absorption (XAS) electrochemical procedure. The roles of the soluble Mn(+III) species and Bi dopants in the discharge and recharge processes have been investigated in some detail.

Firstly, the presence of Bi(III) favours the formation of soluble $Mn(OH)_6^{3-}$ species in both the processes of discharge and recharge and, secondly, it appears to work as a "catalyst" for the steps involved in further reduction of $Mn(OH)_6^{3-}$ species to $Mn(OH)_2$ in discharge, and re-oxidation of $Mn(OH)_2$ to MnO_2 on recharge.

Based on the optical absorbance measurements, an heterogenous mechanism in which the soluble $Mn(OH)_6^{3-}$ intermediate is involved, is directly indicated as being the preferred pathway at CM MnO_2 and operates in parallel with the so-called homogenous mechanism in both the processes of reduction of MnO_2 and re-oxidation of reduced MnO_2 materials. Thus, from the soluble $Mn(OH)_6^{3-}$ species, either $Mn(OH)_2$ can be deposited, on

reduction, or MnO_2 re-formed on re-oxidation, on the porous electrode matrix at favourable and practically significant current-densities. The CM MnO_2 is then rechargeable over a practically useable voltage range and, importantly, over the 2-electron charge capacity. On account of the preferred heterogeneous pathway at CM MnO_2, high (up to 6C) discharge rates can be realized at a remarkablely constant plateau voltage, independent of discharge rate.

In the light of the mechanism studies, the electrochemical performance of the CM MnO_2 has been studied. The CM MnO_2 cathodes were characterized by (a) good multiple rechargeability, (b) high energy and power densities, (c) achievement of high charging/discharging rates at a surprisingly constant working voltage and (d) low cost.

Use of an ion-selective separator enables the CM MnO_2 to be used in a secondary alkaline MnO_2 battery system with a Zn anode, and an appreciable cycle-life to be realized which is not possible if ZnO_2^{2-} ions diffuse to the MnO_2 cathode.

These characteristics make the secondary CM MnO_2/Zn battery system a promising candidate for electric vehicle applications and also for many other market niches currently occupied by Ni-Cd secondary and MnO_2/Zn primary cells in the consumer market.

Contents

Chapter I

Introduction

1.1 Historical Background to Battery Science

As civilization has become more sophisticated and reliant on readily available sources of energy, so battery research and development has been stimulated. A battery is defined as a multi-cell, power-generating device which is able to convert stored chemical energy into work of an electrical nature. The stored energy is either potentially present in two or more chemical substances used that are reacted electrochemically together, as in the case of a non-rechargeable battery, or is induced in those substances by repeatable application of an external source of electrical work. In the latter case, a rechargeable battery is the result. During the last twenty-five years in particular, a number of new systems have become commercially available, but their full potential has not yet been realized.

Historically, it would appear from the archaeological work of Konig about 50 years ago [1] that, supposedly, some kind of galvanic cells were known to the Babylonians as early as 500 BC. During his excavations at a site near Baghsas, earthenware jars, approximately 15 cm high, were found, each containing copper

tubes having an inserted central iron rod cemented at the top with asphalt. This construction was seen to be strongly reminiscent of simple battery cells, and, on filling with naturally occurring acids, they would undoubtedly have produced reasonable currents when connected to an external circuit. Although their true purpose has been lost in antiquity, modern suggestions as to their use have included electroplating, medicinal therapy and use in religious rites.

However, in spite of this uncertain evidence that early electrochemical cells might have existed in the ancient world, it can be stated quite definitely that the development of modern battery systems and technology undoubtedly began with Volta's experiments about 200 years ago [2]. He combined metals such as copper, brass or silver (as positive electrodes) with tin or zinc as the opposite (negative) electrodes in simple salt electrolytes. Volta's discoveries were remarkable; he was able to obtain currents in the order of amperes, compared to the output of electrostatic generators in use at that time which could only deliver milliamperes, but at high voltages. Volta was also able to achieve high voltages but by combining a number of low voltage cells (1.0 ~ 1.2 V) into a series arrangement (pile).

The batteries at that time, however, were mainly used for laboratory work, initially for the preparation of the most electropositive or electronegative elements, and later for determination of thermodynamic and physico-chemical data. There

was little commercial interest initially in secondary batteries, since recharging had to be done from costly primary batteries which occupied much space. However, later with the invention and development of the d.c. dynamo, this problem was eliminated and rechargeable Pb-acid batteries were developed for electric vehicles before the end of the 19th century.

Modifications and improvements of Volta's cell were carried out by many innovators, especially Cruikshank [3], Daniell [4], Grove [5-6] and Bunsen [7]. All the cells were open and flooded with electrolyte, which made them dangerous or difficult to move. In 1860, Leclanché [8] constructed the first cell design having a restricted electrolyte, using manganese dioxide as the positive electrode material, in a mixture with carbon powder, and zinc as the negative electrode, which led to the present portable and sealed zinc-manganese dioxide battery systems.

1.2 The MnO_2 and Other Battery Systems

The search for clean and renewable power sources has been a major technological and environmental activity for some decades. Some "primary" and "secondary" battery systems have, however, been in the market and widely used for many years. Among them, the alkaline MnO_2 (primary) battery is the most widely used type in daily life except for the lead-acid battery employed in automotive applications and the Nickel-Cadmium battery for aircraft and military use, and for small

"rechargeable" electric appliances.

The unique performance and cost characteristics of the primary alkaline MnO_2 battery make it widely applicable so that an incentive for converting it into a rechargeable system is extremely appealing. Such an incentive is connected not only with energetics, material savings and environmental reasons but also with the possibility of entering the vast market (about $6 billion/year)[9] for rechargeable power sources for emergency power,portable telephones, remote communication systems, photographic equipment and other portable appliances. Such applications are currently dominated by the more expensive and toxic nickel/cadmium battery embodiment. Because of its toxicity and rather unfriendly influence on the environment, the Ni/Cd battery will soon be banned in North America[10], so clean, rechargeable and portable battery embodiments are at urgent stage of requirement. The rechargeable alkaline battery, however, is one of the replacement battery systems with the highest potential.

As solid-state cathode materials for aqueous battery systems, oxides of transition and other metals are preferred electrochemical reagents, e.g. PbO_2, Ni.O.OH, HgO, AgO, MnO_2, etc. Cathode materials that are rechargeable in a practically realizable way, with good cycle-life and attractive energy and

power densities[1], are however, relatively few, PbO_2 and Ni.O.OH being the predominant bases of practical acid or base electrolyte systems, respectively. MnO_2 has held a preeminent position as an excellent cathode material for primary batteries such as the Léclanché cell or the alkaline MnO_2/Zn cell for very many years.

Manganese dioxides are used extensively as active cathode materials in Léclanché or alkaline Zn/MnO_2 cells. Historically, manganese dioxide was known already in ancient Egypt and Greece, where it was used to modify the colour of glass. Pliny described a natural MnO_2 ore some two thousand years ago. It was first used in the positive electrode of a Volta-type pile by Ritter[11]. About 60 years later, Léclanché patented a wet primary MnO_2/Zn cell with ammonium chloride electrolyte and founded a battery factory in Brussels[12], later to operate at Yverdon, Switzland. In the 1880's, the French company Léclanché began to manufacture "dry" cells. The so-called alkaline cell, however, is a "late-comer". Although the first wet alkaline manganese dioxide/tin cell was patented in 1882 in Germany by Leuchs [13] and a wet MnO_2/Zn alkaline cell was patented in the U.S. by Yai in 1903 [14], the MnO_2/Zn alkaline battery was introduced industrially in the 1960's, which is close to the 100-year anniversary of the

---

* A number of special terms arise in the field of battery science and technology, such as the word "capacity" here. At the end of this chapter, an Appendix is given in which such terms are defined or explained. They also arise in later chapters of this thesis. They are not always well understood outside the field of battery research and development.

Léclanché cell (1966). Herbert's patented "crown" cell in the early 1950's [15] paved the way toward the commercialization of the alkaline MnO_2 battery.

The literature about manganese dioxide was already voluminous at that time, but the significance of the use of γ-MnO_2, especially the electrolytically produced form, was not clearly recognized until the studies performed by Brenet in the 1950's and 60's [16-19] brought it more attention.

1.3 Manganese Dioxide: its forms and its chemistry

Manganese dioxide has a number of allotropic forms and a wide variety of properties. Electrochemical activity of manganese dioxide depends on a number of factors, including but not limited to, its structure, surface area, pore volume and purity. It is generally difficult to predict the precise performance of a particular MnO_2 material in a given battery system at all completely by quantitative measurements. That is, MnO_2's with similar chemistry, molar volume and physical properties may perform in markedly different ways from each other in a given battery. The only decisive test for a manganese dioxide material is its performance in a given cell.

The name, manganese dioxide, is applied to a series of oxides of four-valent manganese. Materials used in the battery industry may be broadly categorized into three well recognized groups: natural manganese dioxide (NMD), chemically manufactured

manganese dioxide (CMD) and electrolytic manganese dioxide (EMD).

Natural manganese dioxide used to be the only available kind of battery-grade MnO_2 for Léclanché cells. This kind of MnO_2 was carefully chosen from manganese ores, which must have a high content of active MnO_2, favourable electrochemical properties and low content of deleterious impurities.

The so-called activity of a battery-grade CMD is the service it gives in terms of the specific discharge capacity of the batteries that are made from it. It is linked to the MnO_2 content of the CMD and the crystalline structure of the material. Manganese dioxide actually does not appear usually as stoichiometric "MnO_2" but rather as a mixture of various manganese oxides, because of the ability of Mn to present different oxidation state. The result is a series of oxides for which the chemical formulae could be expressed by MnO_x, with x around 1.92-1.96. Furthermore, H_2O combines intimately with manganese oxides so that it has been observed that the best NMD should have a content of combined water as high as 3 or 4%. Battery NMD contains a substantial amount of γ-MnO_2, although the quantity is difficult to assess since the γ-MnO_2 is intimately mixed with other crystallographic forms.

After World War II, synthetic manganese dioxide, either produced by chemical precipitation (CMD) and by electrolysis (EMD), has been developed and started to be used in growing quantities because of its better performance.

Much of the progress made in recent years in primary MnO_2/Zn cells is attributed to the production and improvement in electrolytic manganese dioxide. The latter is used almost exclusively in the fast growing alkaline manganese cell market. Manganese dioxide for batteries should be essentially free from impurities such as copper, nickel or cobalt, which would deposit on a zinc anode, facilitating corrosion of the latter, with H_2 evolution. These and other deleterious elements such as arsenic, vanadium, antimony and molybdenum must also be controlled, either in the headfeed or in the purification step, or both, in the production of high-purity, alkaline-grade, electrolytic manganese dioxide. Following strict purification procedures, EMD can meet these requirements. The electrodes, on which the manganese dioxide is deposited, are lead, carbon or titanium anodes. Today, most high-purity EMD is deposited on titanium anodes because of their inertness.

Chemical manganese dioxide (CMD), however, was developed in the mid-1950s by the Manganese Chemicals Corporation, providing, for the first time, production of battery-quality MnO_2 by a chemical process. The product was prepared to electrolytic manganese dioxide (EMD) specifications and was purchased in large quantities by the U.S. Government for government stockpiles. It later found wide acceptance in the mid-1950's in magnesium dry cells, where it is used almost exclusively today. In the mid-1960's the product was accepted in other battery systems with the advent of production in Europe, based on the

patented technology of the Manganese Chemical Corporation and the growth of the overall battery industry. Today the product competes with electrolytic manganese dioxide and maintains a significant market share of the synthetic manganese dioxide used in Léclanché cells. Special grades have been developed for the zinc chloride. alkaline and lithium battery industries.

The properties of chemical manganese dioxide differ from those of electrolytic manganese dioxide in four major ways: specific area, electrolyte absorption, density and morphology. The specific surface areas of most CMD products are higher than that of electrolytic manganese dioxide. Consequently, electrolyte absorption is considerably higher for CMD MnO_2 than for EMD. The higher porosity is also linked to a lower apparent density of CMD particles versus EMD. Further, Chemical Manganese Dioxide particles are typically more rounded in appearance than are EMD particles. These differences often require modification in formulation, moisture contents, carbon black contents and type of carbon blacks, for example, when either CMD or EMD is substituted for the other material in battery cathode preparation.

The production of Chemical Manganese Dioxide differs considerably from that of EMD. The patented process is based on the fact that certain types of manganese dioxide act catalytically to permit the efficient oxidation of manganese sulphate by sodium chlorate to produce manganese dioxide.

1.4 Factors Determining Rechargeability of Battery Materials

For a successful and practical rechargeable battery cell, its anodic and cathodic reactants must take part in reversible oxidation/reduction reactions that can be conducted repetitively. Also, the rechargeability of each of the electrodes must be approximately matched unless deliberate limitation ("anode limitation" or "cathode limitation") is desired in order to control the depth of discharge reached at one or the other electrode.

The anode material must normally be a reducing agent such as a metal (Zn, Cd, Pb, Fe, Al, Mg, etc.) or sometimes an oxidizable non-metallic substance, e.g. SO_2, $SOCl_2$, N_2H_4, NH_3 or H_2, as in fuel cells. Correspondingly,cathode materials must be oxidizing agents, usually oxides, sulphides, or SO_2, $SOCl_2$, or O_2 itself in fuel cells or Br_2 in the Zn/Br_2 battery and K_2CrO_4 in the old Grove cell.

There are two aspects of reversibility that are relevant to the operation of a battery system:

i) **"Materials reversibility"** - upon cycling, the original cathode or anode reactive materials must be regenerated, and must remain electrochemically accessible and conducting. Often, on cycling, some fraction of the active material can become isolated, so the capacity can become reduced on cycling. Also, some reduction of availability of material can arise after high rates of discharge. For some materials such as MnO_2, that are not

intrinsically good electronic conductors (contrast PbO_2), a conducting support matrix such as graphite must be provided in order to maintain electronic accessibility of the reactant.

An additional requirement, implicit in "materials reversibility", is reversibility of any *structural changes* that take place on discharge and subsequent recharge.

ii) Complementary to (i) is the question of **"kinetic reversibility"**, i.e. the extent to which polarization or overvoltage accompanies discharge or recharge at various rates. Such polarization is a fundamental aspect of kinetics of all electrode processes and is determined by the exchange current-density and the Tafel slope of the process concerned. The kinetic reversibility is important both in the anodic and cathodic processes and the overall (open-circuit) cell voltage (EMF) becomes reduced on discharge to an extent determined by the sum of the anode and cathode overvoltages, each dependent on the current-densities during current drain, at each of the respective electrodes.

iii) A third aspect, affecting practical rechargeability, is the Ohmic resistance of the electrode structures and the battery electrolyte and connectors. This resistance can change materially during discharge and recharge, depending on the types of materials involved and can also increase on cycling of a cell on account of "materials isolation" (see i above).

Simplistically, it might be thought that repetitive cycling of electrochemically oxidizable and reducible materials, subject

to Faraday's laws, should present no problem. However, solution of the problems identified in (i), (ii) and (iii) above forms much of the art and technology of battery science and development, and is usually by no means facile, as will be apparent in the description of the present work on rechargeability of MnO_2 and of the MnO_2/Zn cell combination.

Another aspect of rechargeability, related to "material isolation" on discharge, is its common dependence on "depth of discharge" (see Appendix). Rechargeability of some batteries, e.g. the regular lead-acid system, is often reduced if discharges are taken towards 90 ~ 100% of the theoretical capacity. Some of the active material then becomes irreversibly changed or isolated with respect to subsequent recharge for chemical or electrical reasons. On the other hand, the Zn/Br_2 cell can tolerate almost 100% depth of discharge over many cycles but it is less practical for day-to-day use.

1.5 Mechanism of MnO_2 Reduction and Re-formation

The cathodic and anodic mechanisms of rechargeability (reduction and reoxidation) of several kinds of MnO_2 have been widely studied by various methods and techniques since the 1960's, as well as the extents of rechargeability of manganese dioxide, especially in alkaline electrolyte.

Cahoon and Korner [20] postulated the following three steps for the reduction process in strongly alkaline electrolytes with

the help of both chemical and X-ray diffraction analyses. A mechanism was proposed which consists of the several steps listed below:

step 1: The manganese dioxide is electrochemically reduced according to the two following reactions which occur simultaneously:

$$4\ MnO_2 + 2\ K^+ + 2e + H_2O \rightarrow Mn_4O_7 + 2\ KOH$$

$$MnO_2 + 2\ K^+ + 2e + 2\ H_2O \rightarrow Mn(OH)_2 + 2\ KOH$$

step 2: The intermediate insoluble oxide product formed in step 1 then becomes the depolarizer which is electrochemically reduced in the following two reactions:

$$3\ Mn_4O_7 + 10\ K^+ + 10e + 5\ H_2O \rightarrow 4\ Mn_3O_4 + 10\ KOH$$

$$Mn_4O_7 + 6\ K^+ + 6e + 7\ H_2O \rightarrow 4\ Mn(OH)_2 + 6\ KOH$$

step 3: The insoluble product of the second step then becomes the "depolarizer" and is electrochemically reduced in the following manner:

$$Mn_3O_4 + 2\ K^+ + 2e + 4\ H_2O \rightarrow 3\ Mn(OH)_2 + 2\ KOH$$

Step 1 supposedly occurs during the first part of the discharge while the working voltage falls from the initial value of 1.46 to 1.20. Step 2 apparently operates in the working voltage range from 1.20 to 0.95. Step 3 occurs in the range below 0.95 V to the potential for complete reduction of the oxide to $Mn(OH)_2$. Much of this last part of the discharge usually occurs at a low working voltage of 0.4 to 0.5 V or less, vs the

Zn potential.

Bell and Huber [21], using X-ray diffraction analysis, found no evidence for $Mn(OH)_2$ being a reduction product at the beginning stage of discharge. Based on a theoretical treatment of the thermodynamics of oxide electrodes introduced by Vetter [22,23], a potential varying with composition indicates homogeneous phase reduction. When the potential remains constant over a given range of composition, a process involving an heterogeneous, two-phase system is indicated. These criteria are applicable only when the rate of solution of the oxide (hydroxide) is sufficiently low that the equilibrium between the oxide and/ or hydroxide ions in the solid phase and in the electrolyte is not appreciably disturbed and secondly when equilibrium between two heterogeneous solid phases can be established. In Bell and Huber's treatment, it was assumed that these restricting conditions were fulfilled. Three stages of the mechanism of reduction of γ-MnO_2 were postulated, as follows:

(i) MnO_2 - $MnO_{1.7}$ as a homogeneous, solid phase reduction;

(ii) $MnO_{1.7}$ - $MnO_{1.47}$ as an heterogeneous system;

(iii) Below $MnO_{1.47}$, an heterogeneous system.

In the first stage, the potential decreases continuously as the cathodic reduction process proceeds but in the second and third stages the potential remains practically at a characteristic, almost steady value. They also concluded that the process of reduction in the homogeneous (solid) phase

involves assimilation of protons into the crystal lattice by OH^- ion to O^{2-} proton transfer, coupled with electron injection from the external circuit, that leads to the dilation of the lattice of γ-MnO_2 upon discharge.

For the discharge of MnO_2 in alkaline electrolytes, the mechanism proposed by Kozawa, Yeager and Powers [24-30] is now widely adopted. They postulated a two-step mechanism for the reduction of γ-MnO_2 in alkaline solution. The first step is reduction from MnO_2 to $MnO_{1.5}$ (Mn.O.OH) and the second is from $MnO_{1.5}$ to $MnO_{1.0}$ [$Mn(OH)_2$]. In the first step, which was called the "electron-proton mechanism" (corresponding to the first stage of the mechanism mentioned above), the potential continuously decreases with extent of discharge, corresponding to the homogeneous mechanism (cf. ref. 22, 23) referred to on p.13, as also found for Li^+ ion intercalation, e.g. into TiS_2, while when the potential remains constant, or almost constant, over a given range of composition, an heterogeneous, two-phase system at equilibrium is indicated. Hence, the solid phase process must be homogeneous, with Mn(IV) and Mn(III) states being co-existent, as in an homogeneous redox reaction. The process can be formulated as

$$MnO_2 + H_2O + e \rightarrow \quad Mn.O.OH + OH^-$$

in which electrons and protons are transferred into the lattice of MnO_2 upon discharge.

It was assumed in the electron-proton mechanism that this

process can take place without changing much of the original structure. The electron and proton transfer processes can be conveniently illustrated as in Fig.1. As a result of electron exchange between Mn^{4+} and Mn^{3+} in the lattice, the position of Mn^{3+} (not the manganese ion itself) can move around in the entire lattice. At the same time, H_2O molecules (an abundant source of protons in aqueous KOH) may be decomposed at the solid-solution interface, with protons being introduced into the lattice, forming OH^- from O^{2-}. Since the OH^- in the lattice is rotating and vibrating, the O-H bond is broken, and H^+ is transferred to the adjacent O^{2-} to form OH^- again. Thus, OH^- also moves around in the entire lattice by means of the proton jumping from one O^{2-} site to another, like the mechanism of OH^- ion conduction in aqueous alkali solutions.

As the discharge proceeds, the concentrations of Mn^{3+} and OH^- in the lattice increase and, in an open-circuit condition, both of these species tend to become distributed homogeneously throughout the oxide lattice. At equilibrium, the electrode potential of the oxide in the homogeneous phase state, may be determined by the effective activity of the electron in the lattice, i.e. by the ratio of $[Mn^{3+}] / [Mn^{4+}]$ in the solid, because of the relatively free electron exchange between Mn^{3+} and Mn^{4+}. As long as the lattice parameters (distance between two adjacent O^{2-} ions and that between two adjacent Mn^{4+} cations) permit fairly free movement of protons (amongst O^{2-} sites) and electrons (through the Mn^{4+}/Mn^{4+} sites) in the manner described above, the

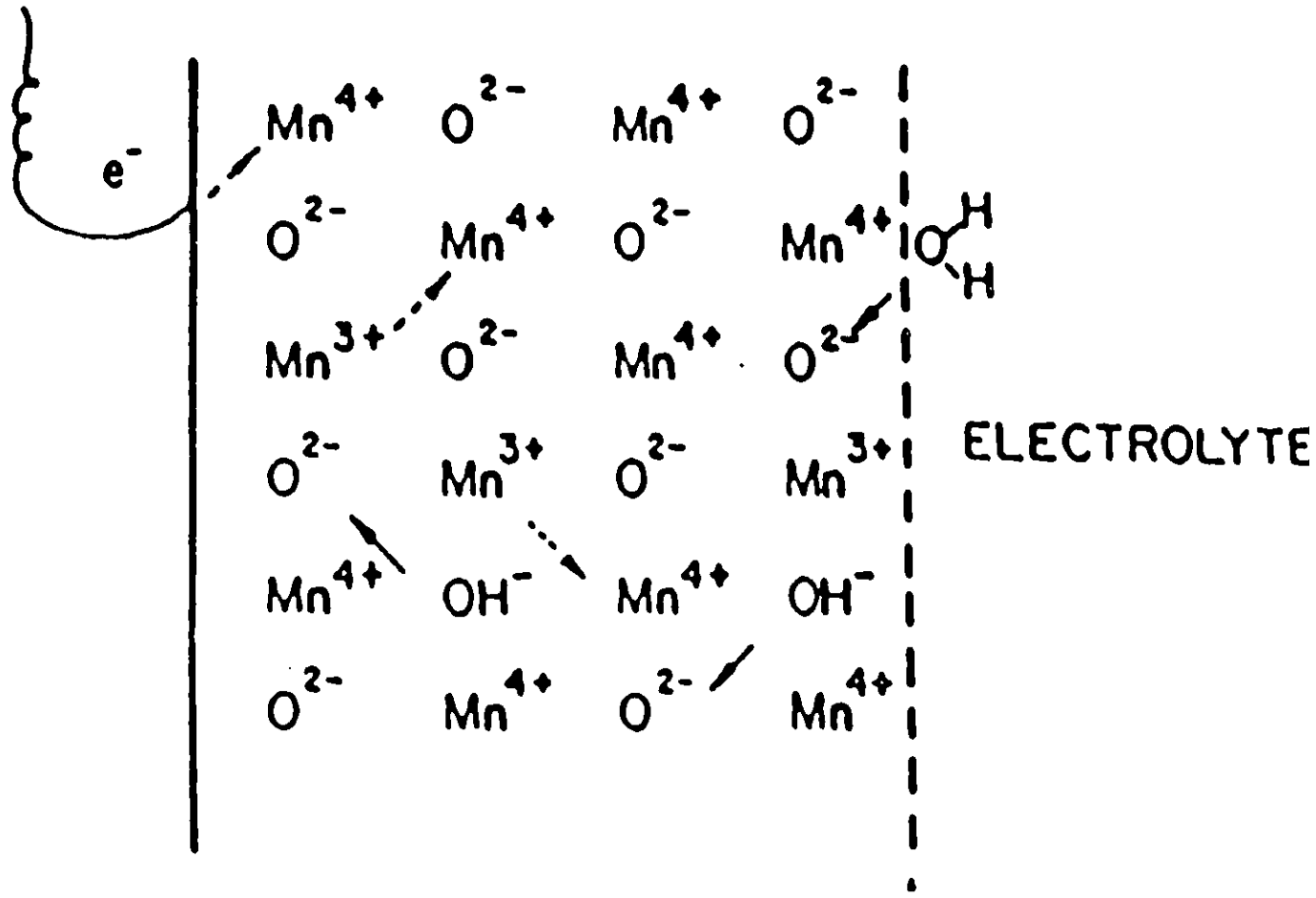

Fig. 1 Schematic representation of the initial discharge mechanism; movement of electrons (------→) and protons (——→) is indicated.

electrochemical reduction can take place through a homogeneous phase mechanism. However, as the discharge proceeds, the original MnO_2 lattice expands, because the ionic radius of OH^- (1.53 Å) is greater than that of O^{2-} (1.40 Å) and Mn^{3+} (0.62 Å) is greater than that of Mn^{4+} (0.52 Å). Therefore, at a certain stage, the crystal structure may be transformed to a new form in which such free movement of the electron and proton may not any longer be possible or is less facile.

The present and other work [31] reveals the involvement of Mn^{3+} ions or rather Mn(III) complexes as intermediates which are soluble and are introduced into the electrolyte solution phase upon discharge or recharge.

Because of the introduction of the proton and addition of the first electron, the original MnO_2 lattice expands, as mentioned above. At this stage, the product, α-Mn.O.OH (recently, δ-Mn.O.OH was suggested on the basis of results of an X-ray diffraction study [32]) can be recharged back to γ-MnO_2. The second step, which is to be regarded as a heterogeneous phase reduction, is believed to be a "dissolution-precipitation" type of mechanism involving an Mn(III) complex ion in solution, instead of a solid-solid phase change mechanism; the reaction mechanism of this second step involves the following stages [4]:

i) dissolution of a complex Mn(III) ion from Mn.O.OH, originating by reduction of the MnO_2;

ii) diffusion of Mn(III) ion species onto the graphite surface and to a significant extent into solution;

iii) charge transfer between the electrode and these Mn species, producing an Mn(II) species; then

iv) precipitation of $Mn(OH)_2$ on or in the porous graphite structure.

The solubility of Mn(II) and Mn(III) species was studied directly by Kozawa, Kalnoki-Kis and Yeager [31] by the polarographic method in various concentrations of KOH; in 9M KOH, the solubilities of these species are 4.4×10^{-3} M and 4.0×10^{-4} M, respectively, i.e. the solubility of Mn(III) is ten times higher than that of Mn(II). (In this strong KOH the Mn(III) is in the form of the complex anion $[Mn(OH)_6]^{3-}$ [33]).

Supporting Kozawa's mechanism, using an ultrathin electrolytic cell, a microscope for direct observation and an extraordinarily low-speed cyclic voltammetry (CV) (180 mV h^{-1}) technique, Ruetschi [34] directly observed morphological changes of γ-MnO_2 particles during discharge in various electrolytes, coupled with several reduction peaks in the CV. Associated with the first peak, a change in the shape of the original MnO_2 particles was observed. However, sudden dissolution of the grains started during the descending side of the peak; finally, only the bare substrate remained.

Associated with the second peak, small hexagonal platelets of $Mn(OH)_2$ crystallized out from solution onto the substrate. It is this kind of recrystallized $Mn(OH)_2$ that cannot be re-oxidised to the original form of γ-MnO_2. The dissolution-reprecipitation

processes can be illustrated as follows:

$$Mn.O.OH + H_2O + OH^- \rightarrow Mn(OH)_4^- \quad \text{(dissolution)}^2$$

$$Mn(OH)_4^- + e \rightarrow Mn(OH)_4^{2-} \quad \text{(reduction)}$$

$$Mn(OH)_4^{2-} \rightarrow Mn(OH)_2\downarrow + 2\ OH^- \quad \text{(crystallization)}$$

The anodic re-oxidation of manganese oxides in alkaline electrolyte was also studied by Liang and Kang [35] by means of a constant-current charging experiment and X-ray analysis. In agreement with Kozawa's two-step mechanism, two "states" of Mn(III) were proposed: so-called "active" and "inactive" forms. The former is produced from γ-MnO_2 through a homogeneous phase reduction, the product being α-Mn.O.OH. It could be expected that α-Mn.O.OH could be effectively re-oxidized to γ-MnO_2 since both γ-MnO_2 and α-Mn.O.OH have the same rhombic crystal structure, and since the mechanism of the cathodic reduction of γ-MnO_2 to α-Mn.O.OH is supposedly a homogeneous phase reaction. According to these authors, the anodic process may also be a homogeneous phase process.

The "inactive" form was produced from γ-MnO_2 after it had undergone such processes as:

a) a first-step reduction;

b) a second-step reduction which included:

(i) dissolution of Mn(III) oxide;

(ii) reduction of Mn(III) species in solution and

---

[2]In this work [34], the soluble complex-ion species was written as $Mn(OH)_4^-$; in ref.33, based on e.s.r measurements, the complex ion $Mn(OH)_6^{3-}$ was proposed.

(iii) re-precipitation of Mn(II) oxide which may include again a dissolution-and-precipitation process.

These conclusions were based on data obtained in their low sweep-rate linear voltammetry (25 $\mu V\ s^{-1}$) studies in conjunction with X-ray diffraction examination of the reaction products at various potentials.

McBreen [36] proposed a more detailed reaction pathway for the cathodic reduction of γ-MnO_2 and the anodic re-oxidation processes, based on data obtained in low sweep-rate cyclic voltammetry (25 $\mu V\ s^{-1}$) studied in conjunction with X-ray diffraction examination of the structures of the reaction products at various potentials. The X-ray analyses at -0.15 V and -0.33 V (vs Hg/HgO) confirmed the reported lattice dilation of γ-MnO_2 that occurs on discharge. At about -0.4 V, the distorted γ-MnO_2 diffraction pattern completely disappeared and spacings characteristic of $Mn(OH)_2$ appeared. In agreement with Kozawa and Powers' mechanism [24-30], the author proposed that after sufficient protons have been transferred into the γ-MnO_2 lattice, the latter collapses and forms an amorphous Mn(III) compound called α-Mn.O.OH. This α-Mn.O.OH can be reduced to $Mn(OH)_2$ and this reaction must involve a soluble intermediate. His results can be summarized in terms of the following steps in relation to the scheme in Fig.2:

(i) Protons are incorporated into the γ-MnO_2 lattice, causing lattice dilation and the

formation of an amorphous phase (α-Mn.O.OH);

(ii) Further reduction, resulting in conversion of the amorphous phase to $Mn(OH)_2$;

(iii) Oxidation of $Mn(OH)_2$, resulting in the formation of a mixture of γ-Mn_2O_3, γ-Mn.O.OH and β-Mn.O.OH, on recharge;

(iv) Further oxidation yielding δ-MnO_2 with reduction of δ-MnO_2 yielding Mn_3O_4; this Mn_3O_4 cannot be electrochemically oxidized but is reducible to $Mn(OH)_2$ which is then re-oxidizable to δ-MnO_2.

By means of the same techniques, β-MnO_2 was also studied by McBreen [37]. The open-circuit potential for β-MnO_2 is about 180 mV more negative than that for γ-MnO_2. The reduction current for β-MnO_2 does not exhibit two peaks; however, the general shape of the initial part of the reduction curve is similar to that found for γ-MnO_2. Apart from the first reduction, the linear sweep voltammetry (LSV) curves for both γ-MnO_2 and β-MnO_2 are very similar. The difference between β-MnO_2 and γ-MnO_2 was found [37] to be as follows: the reduction of β-MnO_2 in alkaline electrolyte differs from that of γ-MnO_2 in that, for β-MnO_2, there is no dilation of the crystal lattice in the initial stages of reduction, while later on in the reduction, Mn_3O_4 is formed. There are indications that the first reduction step of β-MnO_2 is an heterogeneous phase reaction, contrary to the case of γ-MnO_2.

Many other studies have also been reported on the

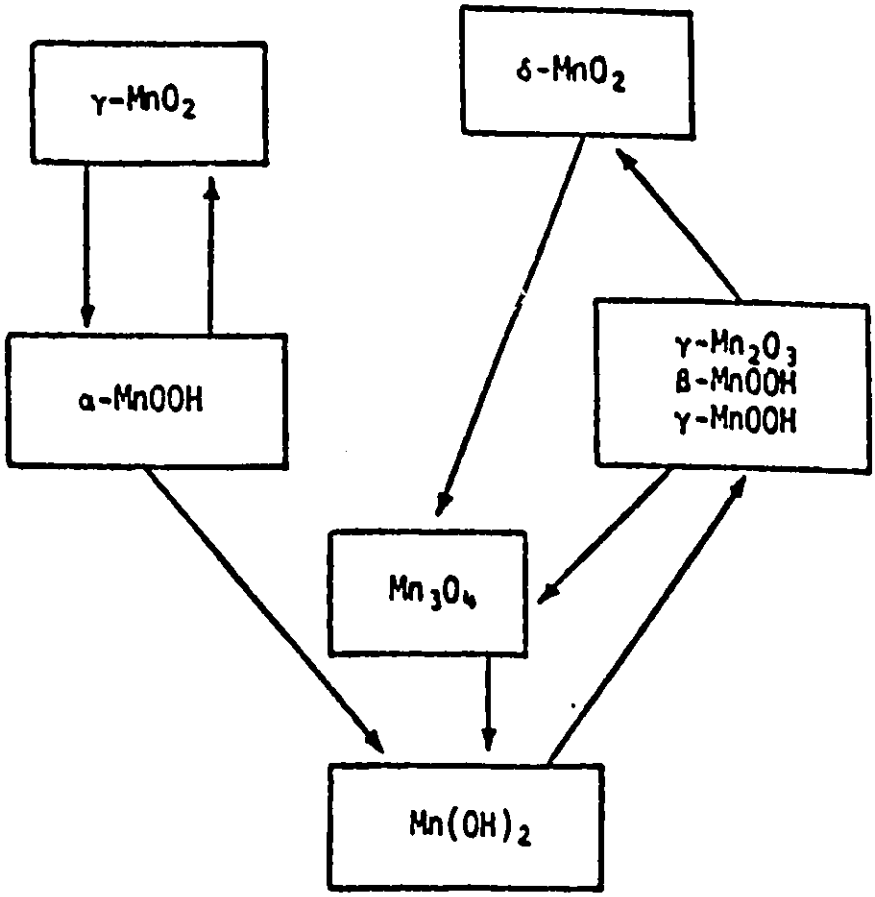

Fig. 2 Schematic representation of the reaction paths for the reduction and oxidation of manganese oxides in 7M KOH, according to McBreen {36]. First stage (γ-MnO_2/α-Mn.O.OH) allows partial rechargeability without chemical or physical modification.

mechanisms of MnO_2 reduction [38-44] and the re-oxidation processes [45] involving reduced MnO_2.

1.6 Rechargeability of MnO_2 Cathode Materials and MnO_2/Zn Cells

Although partially discharged dry Léclanché cells can be recharged , the success of such a process depends on a strictly defined set of conditions [12] the control of which, if not virtually impossible, is difficult in common practice, The rechargeability of presently existing alkaline cells is also limited to shallow discharge; however, their cycling regime is much less demanding than for Léclanché-type cells.

Various attempts have been made to make the alkaline manganese dioxide cell rechargeable. Rechargeable batteries are indispensable as subsidiary power sources or as auxiliaries in a large segment of industrial products. The necessity for their further development increases with the rapid expansion of industries using throw-away primary cells, and with the concern about energetic and environmental problems. Primary batteries contribute to a considerable energy waste (the energy expended in their manufacture may exceed by ten times the energy supplied by the battery itself during its lifetime), valuable material waste, and waste disposal problems.

Secondary batteries currently in use might have to be substituted by other types if the use of toxic lead and cadmium

were to be prohibited. The first relatively inexpensive, rechargeable MnO_2/Zn battery, designed for portable TV use, appeared for a short time on the market in the 1970's, The main reason for its lack of commercial success was its very short cycle-life (<30 cycles) coupled with inconvenience of its rechargeability requirements. Continued efforts have not brought much success, the primary reason being the inherently irreversible behavior of manganese dioxide electrodes with respect to discharge and recharge.

Although, fundamental studies of the structural, physicochemical and redox properties of MnO_2, which have continued since the 1960's, have provided a large amount of information concerning alkaline MnO_2 electrodes, as mentioned above, even now, neither the reaction mechanisms nor the factors affecting the rechargeable behavior are at all clearly understood. The uncertainties and contradictions that exist in the literature are largely due to the great variety and complexity of crystallographic forms (over 30 varieties of MnO_2 have been described) and poor, often overlapping X-ray diffraction (XRD) patterns that arise (the given species may need to be present in 50-99% concentration to be detected[46]).

The electrochemical behavior of manganese dioxide depends on its crystal structure and structural disorder, stoichiometry, presence of impurities, electrical conductivity and physical properties [47-50]. Standardization of MnO_2 in the form of International Common Samples (ICS) [5] introduced a valuable

reference for the study, evaluation and comparison of various results, thus diminishing the confusion arising from the use of different materials by different authors.

Significant progress has, however, been made by Kordech and co-workers [47,55,56] in developing a rechargeable MnO_2 cell of limited discharge capacity. There is much evidence for the two-step mechanism proposed by Kozawa, and only α-Mn.O.OH, which is the product of the first, homogeneous process of γ-MnO_2 reduction, can be re-oxidised back to its original form, γ-MnO_2; the second step, however, is irreversible. Hence, Kordesch's method of making the MnO_2 battery system "rechargeable" is to limit the depth of discharge to less than $MnO_{1.5}$ simply by means of restricting the anode capacity, i.e. the cell is "anode limited", based on the understandable fact that the proton migration is reversible as long as he original γ-structure is maintained.

In order to minimize dilation of the lattice in the process of introduction of the proton, pressure was used to restrict the expansion of the manganese dioxide electrode during discharge. The authors have shown that mechanically restrained MnO_2 electrodes indeed performed better than their free, unrestrained counterparts. Attempts to limit practical rechargeable cells to the required shallow depth of discharge have included voltage-controlled discharge cutoff, use of low electrolyte concentration (which forces zinc into early passivation) or limitation of the cell capacity by the zinc anode.

The first solution is inconvenient for the user, and the latter limits cell life on the negative side as well: the alkaline zinc electrode can survive prolonged cycling only in the presence of a two- to four-fold, excess of zinc (this delays the well known shape change on recharging and the loss of the active Zn surface). Further, in the Kordesch type of battery, only one third or less of "one electron" per Mn is practically available to be used, so that the energy-density is relatively low while limitation of the depth of discharge is inconvenient to users.

1.7 Doping Effects on Rechargeability of MnO_2

In order to develop a new type of rechargeable MnO_2 material, attempts have been made to introduce dopant ions into manganese oxide materials [57-64] using various methods. Various foreign ions were introduced, but the real breakthrough in the field occurred in the early 1980's by Wroblowa and co-workers [59-64], when the first truly rechargeable "Chemically Modified" (CM) MnO_2 materials, which had no constraints connected with the depth of discharge, were introduced by incorporation of Bi or Pb ions into manganese dioxide.

In recent years, various other researchers have also claimed modification methods to introduce Bi or Pb into the MnO_2 cathode material, which then can be recharged over the *two*-electron capacity [65].

Some researchers, however, have blamed the loss of rechargeability on the diffusion of zincate ions to the positive electrode and the formation there of nonreactive hydrohetaerolite [52-54] - a mixed Zn-compound containing trivalent manganese oxide. Although in the presence of zincate ions $Mn_2O_3 \cdot ZnO$ is indeed formed at a sufficient depth of discharge, MnO_2 electrodes were shown in the 1960's to be inherently nonrechargeable when reduced (in the absence of Zn or Zn ions) below the $MnO_{1.7}$ composition. Borden et al. [42] reported that alkaline zinc-manganese dioxide cells could be recharged over a considerable number of cycles if the discharge was limited to a relatively small fraction of the total manganese dioxide capacity. However, a few deep discharges severely reduced the rechargeability of the cells. The reasons for this electrode irreversibility have been variously attributed to γ-Mn_2O_3 [21], Mn_3O_4 and hydrohetaerolite [42] formation.

The effect of added Bi(III) was considered originally (60), however, in the light of the previously treated mechanisms of reduction and re-oxidation described earlier in this chapter. Since the reduction involves the insertion of protons and electrons, the cation radii consequently increase, resulting in substantial restructuring of the lattice. It was suggested that the effect of added Bi might be to stabilize the lattice towards such dimensional changes by modifying the "open structure" configuration.

On consideration of the redox mechanisms proposed in the

literature, these implied that rechargeability might be attained if the reactant had an open structure which could be maintained throughout the 2-electron redox cycle, thus improving the mobility of protons in the lattice, inhibiting pronounced volumetric changes, and preventing the collapse of the original structure to more stable, denser, and less electroactive and/or less conductive compounds. This premise led in turn to the synthesis of birnessites - complexes of tetravalent manganese, which belong to the group of phyllomanganates. Their structures have been described as infinite, two-dimensional sheets of edge-shared $[Mn^{IV}O_6]$ octahedra, separated by 7 or 10 Å, as shown in Fig.3. This structure may contain layers of water and hydroxyl ions bonded to the octahedral layers by foreign metal ions. The openness of the lattice and the possibility of stabilizing it by insertion of foreign cations seemed suitable for fulfilment of the demands of the working hypothesis.

Two kinds of methods were used (9,60,61) to introduce the dopants, Bi or Pb, into MnO_2; one was a co-precipitation method leading to a so-called "chemically modified" electrode; the other was a procedure of mechanically mixing Bi_2O_3 or PbO with γ-MnO_2, leading to a so-called "physically modified" electrode. Both the chemically modified MnO_2, referred to here as CM MnO_2, and the physically modified MnO_2, referred as PM MnO_2, have shown rechargeability at the two-electron level.

The modified MnO_2 electrodes not only are fully rechargeable (up to ca 90% material [2e] utilization) but also are

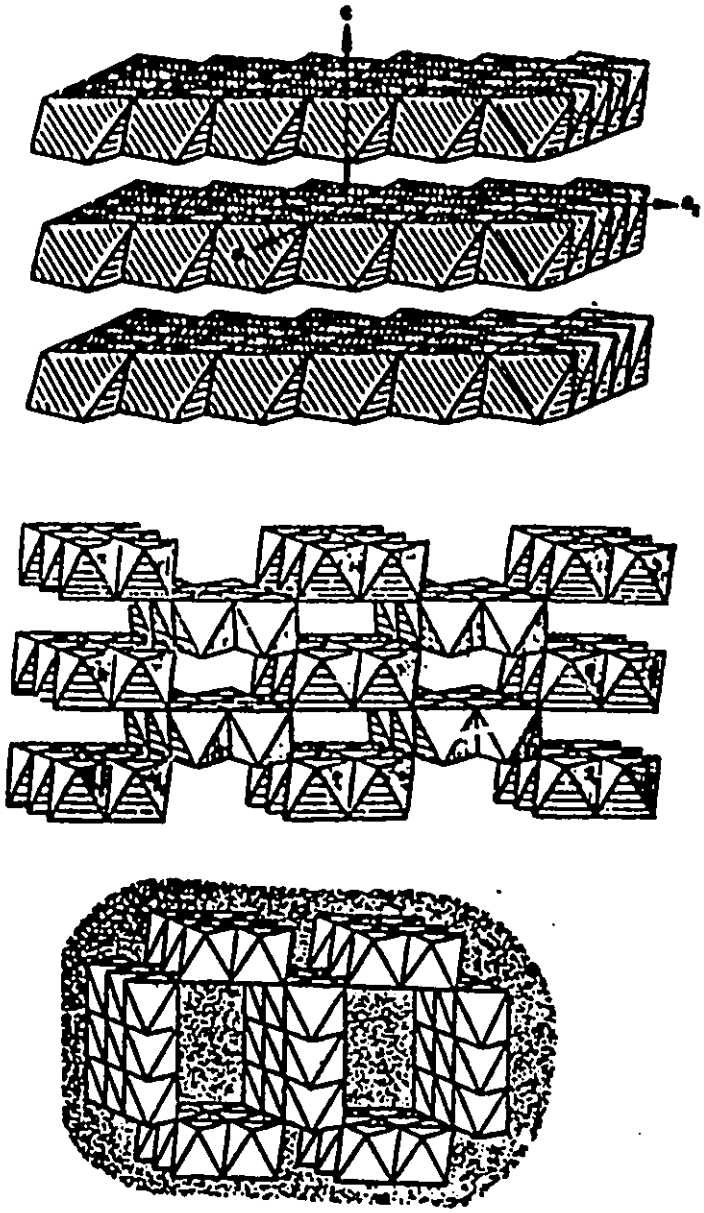

Fig. 3 Examples of MnO_2 structures: top, layers of edge-sharing octahedra of a phyllomanganate; middle, γ-MnO_2; bottom, romanechite.

insensitive - unlike the majority of battery electrodes- to overcharge and overdischarge, to changes of temperature and to dehydration. They are also capable of relatively high current drains, and have a lengthy shelf life.

The lattice-stabilizing effect of bismuth and lead cations lacks a direct confirmation owing to the low degrees of crystallinity of materials present at intermediate depths of discharge and charge. It is difficult, however, to account, on such a model of "open structure", for the fact that the influence of Bi(III) is already observable at low levels of 1-2 mol% in the MnO_2 material. Secondly, the CM MnO_2 becomes multiply rechargeable over the two-electron reaction. Considering that the Mn(III) intermediate is soluble, it is hard to understand the significance of the supposed "open structure" effect.

In alkaline aqueous electrolytes, the highest cell voltage can be achieved by coupling the manganese dioxide electrode with zinc. Unfortunately, zinc is highly soluble in alkali, as ZnO_2^{2-} ions, in which the concentration of zincate ions can reach over 2M (in 9M KOH) under electrochemical cycling conditions. The presence of zincate ions in the electrode shortens the cell cycle life, leading to the well-known phenomena of shape change, densification, and/or dendritic growth. The failure to produce a viable Ni/Zn electric vehicle battery has been due to these problems, which limit, at present, the cycle life of conventional Ni/Zn cells to 200-300 cycles.

However, apart from these inherent problems of the alkaline zinc electrode, the latter is also known to affect the performance of the conventional or CM manganese dioxide materials. Migration and diffusion of zincate ions to the positive electrode leads to the formation of electrochemically inactive hetaerolite. The same was observed (61) to occur in modified Mn-oxide/Zn cells.

Most of the results reported by Wroblowa (60,61) were obtained with electrodes having 1:10 MnO_2/graphite ratio; when the ratio was increased, however, the rechargeability of the CM MnO_2 electrodes was dramatically reduced. When Wroblowa and co-workers attempted to develop an actual MnO_2-Zn rechargeable battery, the rechargeability of the electrodes were also found to become dramatically reduced.

The loss of the rechargeability of the CM MnO_2, in the first case, was supposed by the author of this thesis, to be the result of both the mechanical loss of the soluble Mn(III) species (into solution) and the formation of a poorly conductive MnO_2 layer on the surface of the electrode during the deep discharge and recharge process. The loss of rechargeability of the CM MnO_2 electrode in the second case was found to arise on account of dissolution of Zn, leading to an high concentration of zincate ion which interferes with the rechargeability of $Mn(OH)_2$ due to irreversible formation of zinc birnessite.

Several attempts in the works of Wroblowa at Ford Motor Co., were made to overcome these difficulties, including

applying a number of organic materials to depress the solubility of zincate ions, and using an ion-selective membrane, e.g. Nafion, to block zincate-ion transfer to the cathode, but no appreciable improvements were reported.

Although the presence of zincate clearly affects the reactant utilization of the modified MnO_2 electrodes during cycling, the relative capacities (ratio of the actual discharge capacity to the theoretical value) of these unoptimized laboratory cells were better, even after 200 cycles, than the initial relative capacities of the best secondary (non-CM) MnO_2/Zn cells hitherto described in the literature. Various efforts have been made to solve the problem. The effects of using various separators have been studied including some work originating in the present research. It is clear that the use of membranes which would effectively impede the transport of zincate ions to the modified manganese oxide electrodes could further improve the capacity of MnO_2/Zn cells cycled for prolonged times but would tend to increase their internal Ohmic resistance.

The problem arising in the operation of the MnO_2/Zn system, caused by the dissolution of the Zn electrode, can be avoided by replacing the zinc anode by one of a different type. At the current stage of the present research, the author of this thesis proposed that a Metal-Hydride system could be a good replacement material in alkaline solution, although the open-circuit potential of the resulting CM MnO_2/Ni-hydride system

would seem to be too low (<1V) to lead to a practical system; in a non-aqueous solution, however, Li-CM MnO_2 and Li intercalated CM MnO_2 could be used. Alternatively, an Fe anode could be used but this is known to give rise to other problems, e.g. the gassing on recharge.

Since the mechanisms of reduction of CM MnO_2 and re-oxidation of it after discharge were not able to be completely characterized by Wroblowa and her co-authors, the problems could not be fully solved in their work at that time. The research described in this thesis in the following chapters extents substantially the understanding and phenomenology of the chemical and physical modification effects.

1.8 Appendix: special terms in the field of battery science and technology

a) Capacity or discharge capacity: the total withdrawable charge from a battery or from a given weight of active material or a given weight of the overall system. Capacity usually depends on discharge rate or previous recharge rate. Units are coulombs or ampere - hours. The "capacity" is not a capacitance (Farads) such as capacity of an electrode interface.

b) Energy-density: available electrical energy per unit weight (or volume) of the active material or overall battery weight. Usually expressed as Watt-hours per Kg

or per lb , and calculated as the integral of current (I) multiplied by time (t) of discharge and by the cell voltage, i.e. total charge x cell voltage. Energy-density usually depends on discharge rate.

c) Power or power-drain: the electrical current, I, times operating voltage (which may vary) that can be drawn from a battery. Units Watts (amps x volts). Achievable power depends on discharge rate. Also, achievable energy-density depends on power level of the operation of the battery, expressed by the "Ragone plot".

d) Power-density: as in (c), but calculated per kg or lb. Depends on discharge rate and achieved battery or cell voltage.

e) Discharge rate, "C-rate": "1C" is defined as the rate of discharge corresponding to discharge of the whole available capacity (see a) in 1 hour.

f) Depth-of-discharge: the % extent to which the practical or theoretical (based on the equivalent weight of active material and application of Faraday's laws) capacity of the battery is discharged in a given use or test regime. Usually determines effective practical capacity and rechargeability.

g) Cycle-life: the number of cycles of discharge and recharge (to a given depth of discharge) achievable with a given battery, cell or single electrode (in a test system). Usually depends on depth of discharge.

h) Watt-hours: measure of energy available in discharge of a battery, usually expressed per kg or lb (see b above), 1 Watt-hour ≡ 1 amp x 1 volt (watt) x 1 h of time, t, in seconds. Therefore 1 watt-hour = 1 x 3600 Joule.

i) "Cathode" and "anode" of a battery on discharge or recharge in relation to polarity of the electrodes: cathode is the electrode at which reduction processes occur but, in the spontaneous direction of discharge, the cathode is the electrode of positive polarity, e.g. MnO_2 (unlike the situation in electrolysis). Correspondingly, the negative plate is the electrode at which oxidation processes occur and is the anode of the battery, e.g. Zn. On recharge, the directions of the electrode reactions at the positive and negative plates are reversed.

j) Polarization: the deviation of the actual electrode potentials, or overall battery EMF, under current drain, from the thermodynamic reversible potentials or the thermodynamic, open-circuit EMF. In batteries and fuel cells, the polarization is usually mainly ohmic in origin due to resistance of the electrode and electrolyte materials, although kinetic (Tafel) polarization is always present, especially at low current-densities, relatively, since the latter polarization is log in I while the ohmic polarization

is linear in I.

k) Secondary Battery: a battery or cell having the capability of being multiply discharged and recharged, contrary to the situation with a "primary" battery. (These terms originated in the early literature of battery technology).

Chapter II

Aims of the research

Before commencing a detailed description of the experimentation conducted in the research, and its results, it will be useful first to give an introductory overview of the aims of the work.

1) First to reproduce the rechargeability behaviour of MnO_2 cathode material, modified chemically or mechanically by incorporation of Bi as Bi_2O_3 or Bi^{3+} ions in the MnO_2 lattice structure, as claimed in the patent of Wroblowa and described in related papers.

2) To investigate the physicochemical and electrochemical origins of the claimed induction of rechargeability of MnO_2 by Bi^{3+} or Pb^{2+} additions, from a fundamental point of view and also to try to provide a basis for understanding the mechanism of the Bi(III) doping effect, which leads not only to reversibility of the discharge/recharge cycle but also to 2-electron, rather than 1-electron, charge utilization. Understanding this effect requires more work on the mechanism of the discharge/recharge of the MnO_2 electrode ($Mn^{4+} \rightleftharpoons Mn^{2+}$) reaction itself and on the nature of the solid-state and interfacial processes

that are involved.

3) Having established (1) and made advances in (2), to set up MnO_2 electrodes first for "half-cell" rechargeability tests ("cycle-life" and "depth of discharge" testing) against a non-soluble anode. There were two purposes of experiments on the half-cell testing:

   i) to extend fundamental mechanism studies under conditions where the behaviour of the MnO_2 electrode is not influenced by the soluble Zn anode. Such testing can provide "first-hand" information on the MnO_2 cathode processes alone.

   ii) in the light of the mechanism studies, to try to solve the problem of the apparently required high carbon loading in the CM MnO_2 electrode (1:10 MnO_2:carbon ratio in Wroblowa's publication) by finding conditions under which good rechargeability could be maintained at higher MnO_2 : C ratios.

4) To investigate rechargeability of MnO_2 in single cells with zinc as the anode in KOH electrolyte and to evaluate the origin of the known deleterious effect of

dissolved ZnO_2^{2-} ion on the reversibility of reduction or reoxidation processes involving MnO_2. This aspect of the project involves investigations on separator membranes capable of selectively restricting transfer of zincate from the zinc anode side of a cell to the MnO_2 cathode side, with attempts to develop ion-selective separator materials to minimize the ZnO_2^{2-} interference and

5) In the light of work conducted in (1) to (4) above, to proceed to full cell cycle-life testing with the longer-term aim of commercial development and evaluation.

6) In the longer or extended term, to establish rechargeability behaviour over many cycles in battery-type modules with anode materials such as zinc, and also with Cd and metal-hydrides.

7) In a possible extension of the project, later to examine the reversibility of Li^+ ion intercalation into Bi-modified MnO_2 in comparison with untreated MnO_2 with regard to development of a rechargeable Li/modified MnO_2 battery system employing a non-aqueous electrolyte.

Chapter III

Experimental

3.1 Materials

Four kinds of MnO_2 cathode materials were used for investigation in the experiments; they are as follows:

3.1.1 Chemically Modified (CM) MnO_2

Chemically Modified MnO_2 material, a bismuth birnessite, was prepared according to Ford's patent [62] by co-precipitation from a mixture of $Mn(NO_3)_2$ and $Bi(NO_3)_3$ with various Bi/Mn mole ratios (in our experiments the range of the ratios was from 1/8.75 to 1/14).

A solution was made up by mixing $Mn(NO_3)_2$ with $Bi(NO_3)_3$ and maintained at a relatively constant temperature. NaOH was then added to the solution, causing $Mn(OH)_2$ and $Bi(OH)_3$ to be precipitated jointly as a suspension. While the suspension was being agitated, oxygen was passed through it, causing the $Mn(OH)_2$ to become oxidized and react to form a birnessite [Mn(IV)] compound which was filtered off for subsequent use. Thereafter, the compound was washed with water and dried.

3.1.2 "Blank MnO_2"

"Blank MnO_2" (no Bi being incorporated) was used as a comparative "reference" system; the preparation procedure was

the same as that for CM MnO_2 but without addition of the Bi component.

3.1.3 γ-MnO_2

γ-MnO_2 was the so-called International Common Sample, I.C. No.2, available for comparative measurements.

3.1.4 Physically Modified (PM) Electrode

A Physically Modified (PM) MnO_2 electrode material was made simply by milling together γ-MnO_2 with a proprietary Bi-treated carbon. The Bi/C composite is a commercially available material. The procedures to make the Physically Modified MnO_2 are described in a patent currently being applied for[75]. Appropriate amounts of γ-MnO_2 and Bi/C were weighed in the required ratio, then milled. The two materials were then mixed thoroughly. The product is the "physically modified" MnO_2 used in our experiments.

3.2 Construction of the MnO_2 working electrodes

MnO_2 samples of the above first three types (i.e. except PM MnO_2) were individually mixed thoroughly with lonza graphite KS44 (containing 5% Acetylene Blank) in an alumina mortar by extended milling for 15 minutes. Following this treatment, the mixture was subjected to high-speed milling in an electric coffee grinder for 20 minutes. The requirement of intimate mixing with graphite arises because MnO_2 itself is not a good electronic conductor so an inert, high dispersed conducting material must

be incorporated, as with the cathode mix used in the Léchanché primary cell. The successful incorporation of graphite plus acetylene black is an important and essential requirement for preparation of satisfactorily rechargeable MnO_2 cathodes having good rate capability.

Three kinds of MnO_2 powder electrode material were used in the experiments in order to examine the relation between electrode structure and loss or promotion of rechargeability:

(i) a non-pressed electrode, which was mounted as a hard paste in contact with and between two pieces of Pt mesh used as the current collector;

(ii) an electrode, which was compressed at a pressure of about 7.5 ton cm^{-2} into pellets, was mounted between two Pt-mesh sheets;

(iii) a specially rolled film: 5~10% wt (dry material) of Teflon suspension was used as a binder, then the active material (MnO_2/Teflon/graphite) was rolled to form a film which was then mounted between the Pt-mesh sheets or compressed on a Ni-mesh current-collector to form the positive electrode.

The ratio of MnO_2/graphite was, however, varied according to the requirements of various types of experiments. Unless

otherwise specified, the MnO_2/graphite ratio for electrodes used in the cyclic-voltammetry and constant-current discharge and recharge experiments was 1/10; for those electrodes used in the *in-situ* spectro-electrochemistry measurements, the ratio was 1/4; the MnO_2/graphite ratio in the electrodes used for the X-ray absorption measurements was 1/2. The MnO_2/graphite ratio is critical for optimum high-rate performance, a result connected with the internal resistance of the matrix since, unlike Ni.O.OH or PbO_2, MnO_2 or its reduction products are not good electronic conductors.

3.3 Electrolyte,reference and counter electrodes

9M aq. potassium hydroxide solutions were used as the electrolyte in all experiments at a temperature of 298K. Solutions were outgassed from O_2 by bubbling N_2 for 1 h before the experiments were begun. All potentials reported, unless otherwise specified, are referred to that of the Hg/HgO reference electrode made up with KOH of the same concentration as that of the experimental electrolyte. A Pt-mesh counter electrode was used.

3.4 Design of cells and electrode holders

3.4.1 The cells for the classical electrochemistry tests

As shown in Fig.4A, the cell was a 3-compartment, specially constructed, air-tight Teflon cell enabling strong KOH electrolyte to be used without the problems that would arise with a glass cell. A special Teflon electrode holder was used to accommodate and mount a compressed MnO_2+C electrode matrix by means of a screw-fitting plug. Another cell was of a flat-plate design, as shown in Fig.4B. It was made of Perspex, and could accommodate the special rolled MnO_2/graphite/Teflon-bonded electrode, referred to above; the cell was also designed to accommodate the special ion-selective separator membrane which was used to block zincate ion transfer by diffusion to the cathode compartment from the zinc anode in test-cell module experiments.

3.4.2 The cell used in the *in-situ* spectro-electrochemical measurements

A series of spectro-analytical experiments utilized a special small plate-geometry electrochemical cell (Fig.5) capable of accommodating a small MnO_2 electrode also having plate geometry, sealed to a 1 cm uv spectrometer cuvette. The spectro-electrochemical cell could be mounted directly in the cell chamber of a spectrophotometer. The *in-situ* uv-visible spectro-electrochemistry cell used in these experiments is shown in Fig. 5 and consisted of two parts: the upper was made of Pyrex and

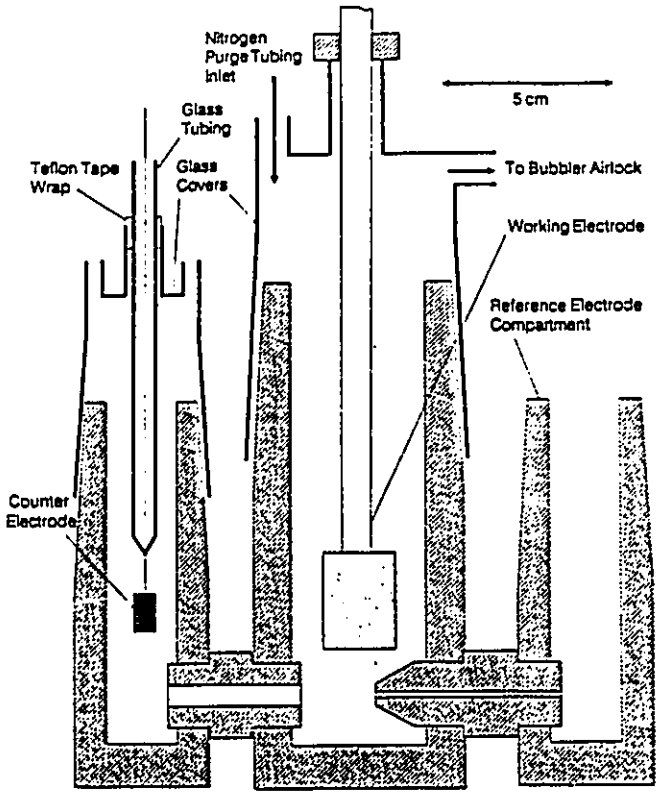

(a)

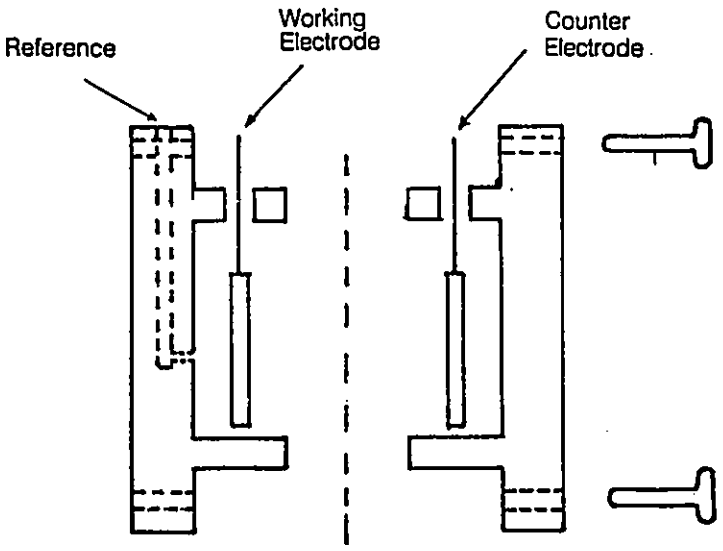

(b)

Fig.4 (a) Three-compartment air-tight Teflon cell
(b) Flat-plate electrochemical cell

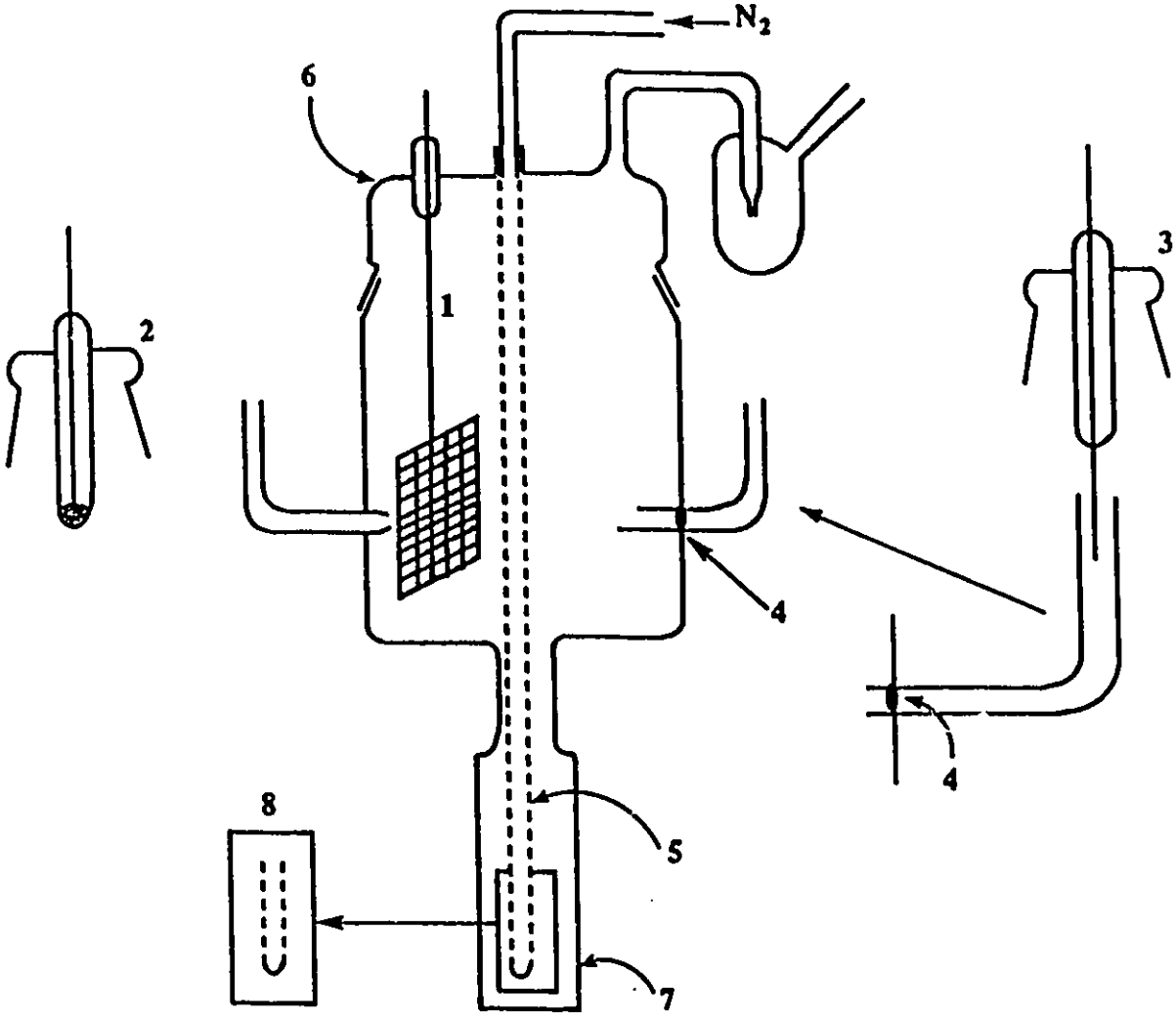

Fig. 5 Optical-electrochemistry cell. 1. MnO_2 working electrode; 2. Hg/HgO reference electrode; 3. Pt wire counter electrode; 4. membrane; 5. fine Teflon tube for bubbling of N_2; 6. Pyrex top; 7. quartz cuvette (1 cm); 8. perforated bottom of Teflon tube.

the lower, which was located in the optical pathway of the spectrophotometer, was made of quartz (a commercial 1 cm uv cuvette). The two parts were sealed together. Hg/HgO was used as the reference and Pt wire as the counter electrode.

The low-valent manganese species (Mn +III) of interest in the present work are formed during the reduction of MnO_2 or in reoxidation of reduced Mn species, but O_2 is unavoidably generated at the counter electrode. Since these Mn species are easily oxidized by O_2 in alkaline solution, an ionically conducting membrane was used to block the diffusion of this O_2 into the main compartment of the cell containing the MnO_2 cathode. During anodic recharge of the MnO_2 electrode, transfer of H_2 evolved at the Pt electrode was also blocked by the membrane.

A moveable fine Teflon tube, through which N_2 could be passed to the bottom of the quartz cell for bubbling, could be introduced through the top of the cell. There are two purposes of bubbling N_2 during the charge and discharge process: one is to initially expel any dissolved O_2 to avoid oxidation of the Mn(III) species; the other is to stir the solution to ensure that the soluble species formed from the MnO_2 electrode, located in the upper section of the cell, can be transported to the lower optical cuvette immediately. The Teflon tube was moved out of the light path when optical measurements were performed, with the cell remaining free of O_2.

It should be mentioned that employment of such a system

unavoidably and deliberately involves an electrode/electrolyte system with a significant volume of free electrolyte (ca. 9 ml) below the electrode in the cuvette and thus out of immediate contact with the working electrode material. For operation of this configuration, the solution in the cuvette in contact with the MnO_2 electrode was stirred with the N_2 admitted from the sliding capillary tube, prior to each of the optical absorption measurements.

In normal operation of an MnO_2/carbon cell, an "electrolyte starvation" situation is, of course, preferred, so that the amount of soluble Mn(III) species that becomes dissolved into the electrolyte is minimized, favouring charge recovery upon cycling.

3.4.3 The cell and electrode for Rotating Ring-Disk Electrode (RRDE) experiments

In one of the directions of the work, a rotating ring-disc electrode (RRDE) was used in order to characterize the formation of the soluble Mn(III) intermediate generated during discharge or recharge.

The cell used in the RRDE experiments was a specially designed three-compartment cell as shown in Fig.6. The main compartment, which was used to accommodate the rotating working electrode, was quite large and could contain about 600 ml KOH. The reason for using a large amount of electrolyte solution is to avoid turbulent flow which could result from the high-speed rotation of the working electrode. A fine Teflon tube with

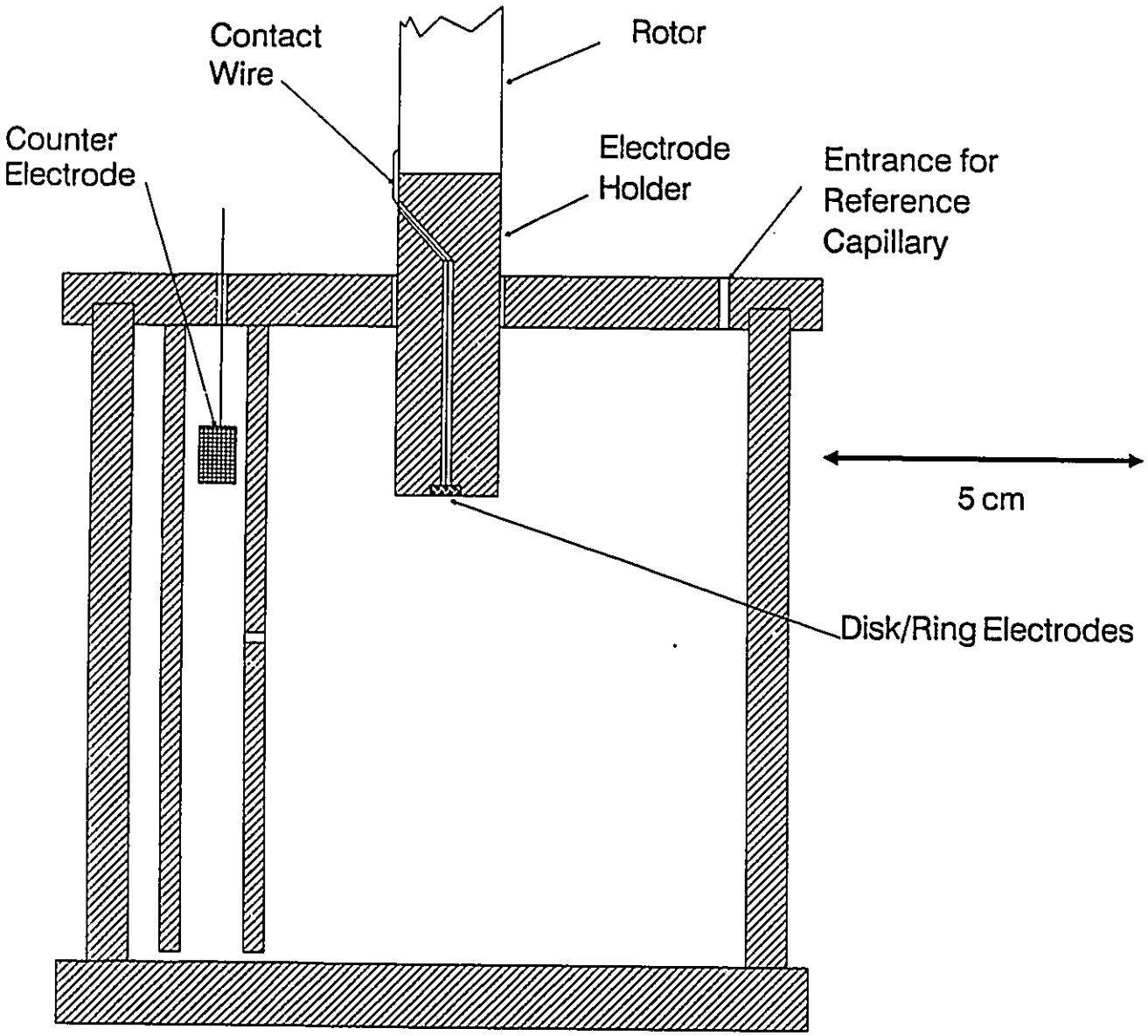

Fig.6 Electrochemical cell for RRDE experiments

perforated bottom, through which N_2 was passed to the bottom of the cell and dispersed throughout, was introduced through the top of cell.

3.4.4 The set-ups and cells used for *in-situ* X-ray absorption (XAS) experiments

There are two ways in which XAS data can be obtained: transmission and fluorescence experiments, so there are two types of *in-situ* spectro-electrochemical cells which can meet the requirements of each of these experimental methods, respectively.

The most common way to record XAS data is to do a simple transmission experiment, where the X-ray beam traverses the sample and the intensity is recorded before and after passing through the sample. When determination of edge-energy data is important, a reference sample with a third detector is used to accurately calibrate the energy scale. A typical transmission set-up is shown in Fig.7A.

Fig.8 shows an exploded view of the electrochemical cell for transmission measurements. The main body consisted of two machined acrylic plastic parts (7.6 x 7.6 x 1.9 cm). An acrylic window (0.75 mm thick) was glued on to each block. The cell consisted of a MnO_2 working electrode, one layer of filter paper (Whatman No.42) as an electrolyte absorbent separator, and a 0.125 mm Grafoil (Union Carbide Corp.) counter electrode. Electrical contact was achieved through a piece of Pt mesh which was pressed against the electrode. Hg/HgO was used as the

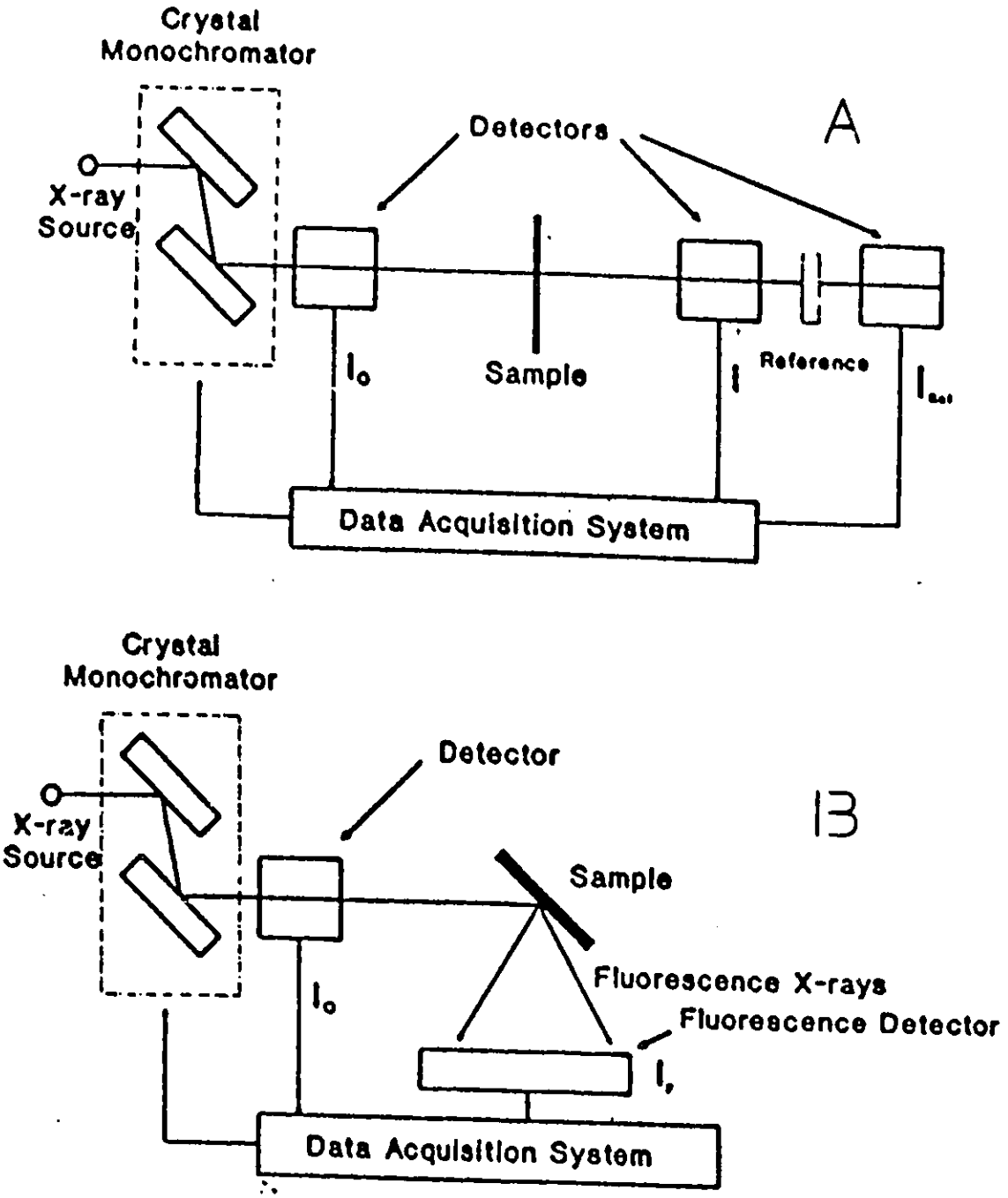

Fig. 7 (A) Experimental setup for transmission EXAFS.
(B) Experimental setup for fluorescence EXAFS measurements.

reference electrode. A reference electrode connection capillary was drilled in the plastic and was stuffed with filter paper to prevent dewetting. Contact to the main electrolyte was made via a piece of Nafion tubing which connected the reference electrode with the electrolyte inside.

In a dilute sample or a sample with low edge energy, where the absorption by the element of interest is less than 5% of the total absorption, the measured X-ray absorption will be dominated by absorption from the matrix and electrolyte. As a result, the signal-to-noise ratio will be low for transmission measurements. In this case, the alternative method of fluorescence detection can be used. Fluorescence is much more sensitive because the background absorption from the matrix will not contribute to the spectrum background. The greatest sensitivity is achieved through the use of energy discriminative detectors, particularly if the background is eliminated to prevent saturation of the detector. A typical fluorescence detection set-up is shown in Fig.7B.

Basically, the fluorescence cell is similar to the one used for the transmission mode experiments. Because the outlet fluorescence ray has a 45° angle with the inlet X-ray, an acrylic window was provided with a 45° angle against the pathway, instead being perpendicular to the pathway of the incoming X-rays as was the case for the transmission mode experiments.

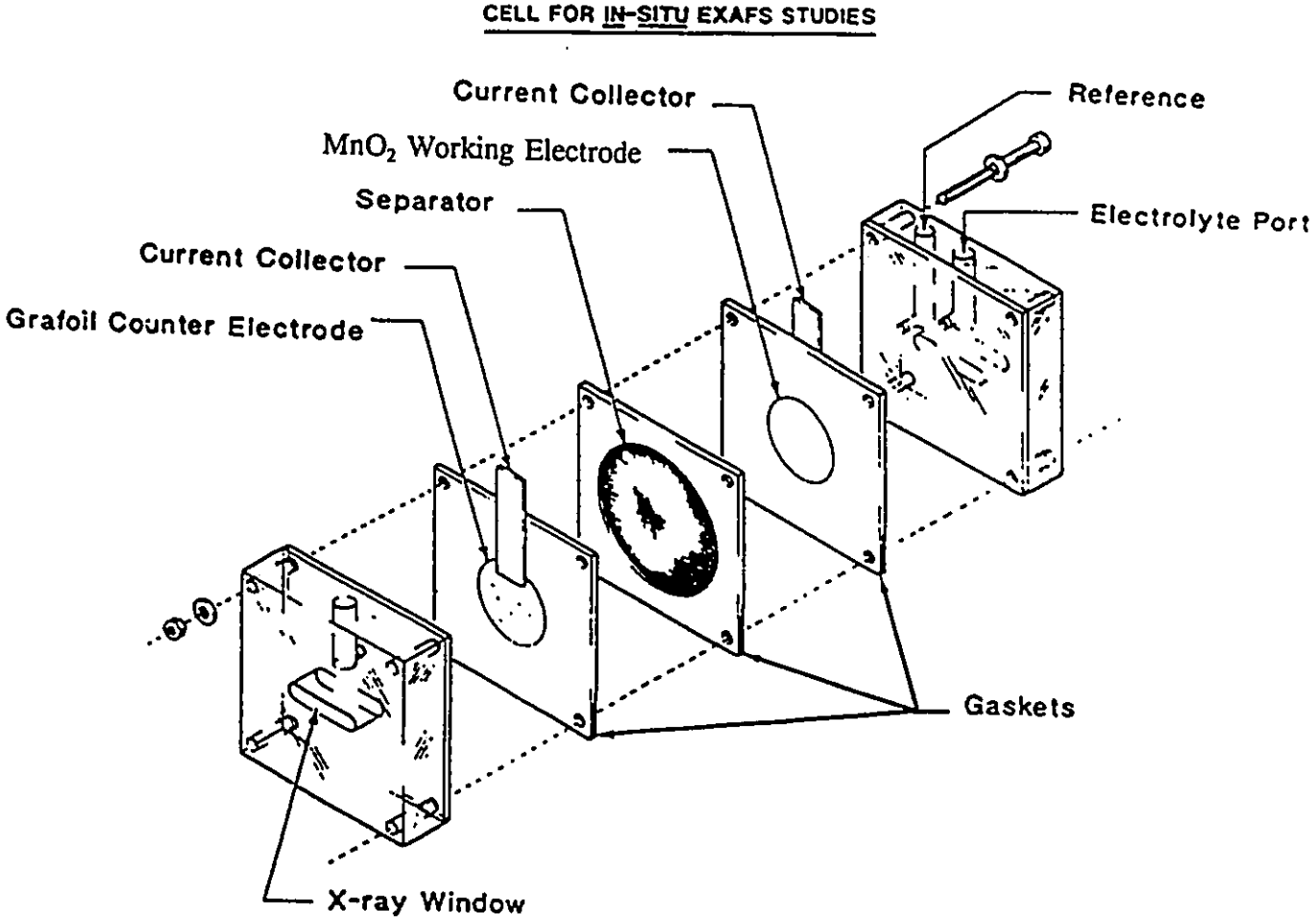

Fig. 8 Spectroelectrochemical cell for *in-situ* transmission EXAFS measurements.

3.5 Experimental Methods

3.5.1 Classical electrochemical methods

(i) *Cyclic-Voltammetry:* The electrodes used in the CV experiments were of the non-pressed type. After they were mounted into the holder, the electrodes were immersed in aq. 9M KOH solution for 1-2 hours to ensure that the whole electrode became wetted; it was then subjected to a linear potential sweep at various sweep-rates. Two procedures were used in these tests: one involved repetitive cycling, the other potential holding where the cathodic sweep was stopped at various potentials along the sweep range for a controlled period of time; then the direction of potential sweep was reversed to that for anodic polarization.

(ii) *Constant current discharge ("galvanostatic") experiments:* Here the MnO_2 electrodes were discharged and recharged in aq. 9M KOH solution at a certain constant current-density at 298K ±1 K.

(iii) *Constant-current discharge with the stationary detector electrode:* The electrodes used in these experiments were of the compressed type. The electrodes were mounted between two Pt-mesh supports which acted as current collectors. The MnO_2 working electrode and the Pt detecting electrode were separated by a thin perforated Teflon separator. Here, the soluble Mn species produced during discharge of the CM MnO_2 electrode was detected by its further reduction or its

reoxidation at the Pt detector electrode after it had diffused through the separator. Both the working and detector electrodes were encapsulated in a separator membrane and hand-pressed into the holder by screwing in a Teflon plug. If any soluble species were produced during discharge of the MnO_2 electrode, they could diffuse easily to the detector electrode close by where, at the potential of the latter, they would become reoxidized. Therefore any anodic current appearing at the detector electrode, additionally to the background current (due to reduction of any traces of oxygen), indicated the formation of the soluble Mn(III) species.

The potential of the detector electrode was held at -50 mV while the working electrode was being discharged. Potential control of both the generator electrode (the MnO_2 cathode) and the detector was achieved by means of a Pine Instrument Co. bi-potentiostat, as used with rotating ring-disc electrodes (see below). In order to get reproducible data, the Pt detecting electrode had to be thoroughly cleaned by HCl in order to make sure that there was no MnO_2 deposited on the surface of the electrode.

(iv) *Rotating Ring Disk Electrode (RRDE):* The MnO_2 electrodes used in the RRDE experiments had to be specially designed. A carbon/Teflon matrix, rolled as a film, was first fitted as a conducting disc into a circular depression (0.5 mm deep) of a rotating Au ring-disc system. The CM MnO_2 powder was then coated on to this matrix by pressure. The potential of the

Au-ring was controlled at -0.1 V.

3.5.2 *In-situ* spectro-electrochemical experiments

An important series of experiments was conducted spectro-electrochemically to detect, *in situ*, the formation of soluble Mn(III) species from CM or regular γ-MnO_2 under discharge or subsequent recharge. The special small plate-geometry cell, described in section 4.4.2, was constructed so that the formation of electrogenerated soluble species could be directly followed spectrophotometrically. Generation or removal of Mn(III) species on both discharge and recharge could be followed as a function of time and electrode potential as the soluble species diffused out from the MnO_2 electrode or was redeposited within it. The spectrophotometer also provided a wave-length scan read-out of the optical absorption which could be followed quite quickly at various times and after various periods of discharge or recharge. The kinetics of the processes involved in these experiments were determined by diffusion out of or back into the MnO_2/C cathode material matrix, aided by stirring of the solution with O_2-free N_2. Sufficient times were allowed for steady values of the Mn(III) concentrations to be attained.

There types of experiments were carried out by means of the *in-situ* uv-visible spectro-electrochemistry technique, as follows:

(i) *Constant current ("galvanostatic") discharge and recharge - optical experiments:* The MnO_2 electrodes

were discharged and recharged in aq. 9M KOH solution at a controlled constant current-density[3] [i=0.16 A (g MnO_2)$^{-1}$] at 298±1K and optical absorption measurements were taken in the solution below the electrode at various extents of percentage charge capacity along the discharge and recharge pathways.

(ii) *Constant potential discharge and recharge - optical experiments:* Here, the MnO_2 electrodes were potentiostatically held at various selected potentials along the discharge and recharge directions until the respective currents approached zero; then optical measurements were taken at those potentials. The current adjustment times varied from 0.5 to ca. 3h, depending on potential along the discharge or recharge curves.

(iii) *Multi-cycle, constant current discharge and recharge - optical experiments:* The PM MnO_2 electrode was used in these experiments. After having been immersed in the N_2-saturated 9M KOH solution for 24h, the electrode was discharged and recharged at a controlled constant current-density [again i=0.16 A (g MnO_2)$^{-1}$]. The discharge and recharge processes were interrupted at various stages, as percentages of the two-electron charge capacity, and optical absorption measurements were taken over a range of appropriate wavelengths. The

---

* Here and elsewhere in this work, current-densities are preferably expressed as A g^{-1} of active material. They could be converted to A cm^{-2} if a reliable *in-situ* estimate of the real accessible area of MnO_2 were available but this is difficult to determine satisfactorily.

electrode was discharged until its potential reached -0.6 V vs Hg/HgO (where Bi_2O_3 begins to be reduced to Bi metal, as indicated by cyclic voltammetry and in the very recent experiments, by means of XANES). Then it was recharged back to +0.2 V vs Hg/HgO at the same current-density as that for the process of discharge. After the electrode had become fully recharged, it was put on constant-current discharge again until the potential reached -0.6V.

The discharge and recharge processes were interrupted at various percentages of charge capacity in order to make the required optical measurements, which were conducted over the first to fifth discharge/recharge cycles. In those individual discharge/recharge cycles, charge recovery was e.g. ca. 100% in the fifth cycle. Ca. 10h were required to complete a single discharge and recharge optical experiment.

3.5.3 *In-situ* electrochemical X-ray absorption experiments

(i) *Brief introduction to the theory of X-ray absorption*[76-83]: In order to provide a background for presentation of the details of the experiments on X-ray absorption at the MnO_2 materials, it is first necessary briefly to describe the principles on which X-ray spectroscopy are based.

X-ray absorption spectroscopy (XAS) is simply the accurate determination of the X-ray absorption coefficient of a material as a function of photon energy, in an energy range that is both below and above the absorption edge of one of the elements in

the material. Absorption edges are abrupt changes in the absorption coefficient due to the X-ray beam having sufficient energy to photoionize core level electrons in the element. Each element has unique absorption edges that correspond to the binding energies of the inner shell electrons. Absorption measurements are usually done at the K or L edges. Each element has one K edge resulting from the photo-electric process in which the energy of the X-ray is absorbed by a 1s core state. All elements of atomic number above 9 have three L edges, which are the result of the corresponding processes for the 2s or 2p core states. The L_1 edge arises from the 2s, the L_2 edge from the $2p_{1/2}$ and the L_3 edge from the $2p_{3/2}$ core states. In practice, measurements are usually done at either the K edge or the L_3 edge. Absorption at the L_3 edge is much higher than at the other L edges. Measurements at the K edge are most suitable for elements of low atomic number (low Z) and for first row transition metal elements.

X-ray Absorption Near-Edge Structure (XANES): The fine structure in the XANES region can be explained in terms of (i) transition of the ejected photoelectron to unoccupied states in the vicinity of the Fermi level, and (ii) to the long mean-free-path of the low energy photoelectron which results in multiple scattering around the excited atom. The shape of the edge yields information on both the type and symmetry of the ligands around the excited atom. Edge shifts due to core-hole interactions are indicative of changes in oxidation state. Hence XANES yields

important chemical information about the absorbing atom.

Extended X-ray Absorption Fine Structure (EXAFS): In the XANES region, the low energy photoelectron has a long-mean-free path and can undergo multiple scattering. In the EXAFS region, the process can be explained by simple backscattering, and the theory has been worked out in detail. A small fraction of the outgoing photoelectron wave, associated with the excited electron, is backscattered by surrounding atoms. The EXAFS is a final state interference effect whereby, depending on energy (E), the backscattered wave interferes constructively or destructively with the outgoing wave. The EXAFS function, $\chi(\kappa)$, is,

$$\chi(\kappa) = \frac{\mu(E) - \mu_o(E)}{\mu_o(E)}$$

where μ and μ_o are the X-ray absorption coefficients of the absorbing atom in the material of interest and in the free state, respectively. The difference, $\mu - \mu_o$, depends on the local structure of the absorbing atom and represents the EXAFS. The division by μ_o normalizes the EXAFS to a per-atom basis.

Advantages and limitations of XAS in electrochemistry studies: The great advantage of XAS is that both the probe and signal are X-rays. This permits *in-situ* measurements in electrochemical cells since X-rays can penetrate the

electrolyte. EXAFS provides both structure and chemical information, which is important in studying the structure change of an electrode material during polarization. Since EXAFS only probes short-range order, it is very useful in the study of metal clusters and amorphous materials. The technique is element specific, so it can be used to probe the environment of the constituents of alloy catalysts, metal oxides and composite materials. The main limitation of XAS is that it is an averaging technique. If the element of interest is present in more than one or two chemical forms or phases, it is difficult to analyze the data.

(ii) *Experimental:* Both *in-situ* and *ex-situ* X-ray absorption (XAS) measurements were made at the Bi L_3 edge (13,419 eV) and at the Mn K-edge (6,539 eV). In the *ex-situ* experiments, washed and dried samples of the chemically modified MnO_2 from cycled cells were mixed with boron nitride powder and pressed into pellets that were then held in a sample holder between two layers of Kapton tape. In the case of the Bi L_3-edge, measurements were done at both 77K and 298K.

The *ex situ* measurements were done at both Beam line X11A and X23A2 at the NSLS (National Synchrotron Light Source, Brookhaven National Laboratory). The electron acceleration ring was operated at 2.58 GeV with a ring current of 110-240 mA. All the *ex situ* measurements were carried out in the transmission mode. Edge calibration was achieved through use of a Bi or Mn

foil, and a third reference detector.

The *in situ* X-ray absorption measurements were carried out on Beam Line X23A2. XAS spectra were obtained at the Bi L_3 edge, in the transmission mode, in a 3-electrode cell similar to that described previously by McBreen [76]. Attempts to perform corresponding *in situ* XAS experiments at the Mn K-edge in the transmission mode failed because of excessive absorption by the 9M KOH electrolyte and other components of the cell. However, experiments at the Mn edge were finally able to be carried out in a cell that permitted EXAFS measurements to be made in the *fluorescence* mode.

Fluorescence spectra were recorded using a Lytle detector. The quality of the data obtained in the fluorescence mode was excellent. The cell also permitted calibration of the edge through use of a reference Mn sample using signal detection in the transmission mode. All the *in situ* experiments were controlled electrochemically under potentiostatic conditions at selected potentials along the discharge/recharge curves. Spectra were usually recorded when the current, after a given adjustment of potential, had declined to a very small value. At some potentials (e.g. -0.4V on discharge and -0.15V on recharge), the current persisted for a long time (often for some hours). In these cases, several spectra were recorded and included several edge spectra which were taken within a small energy interval (-50 to 50 eV), together with complete EXAFS spectra.

The methods used for conducting the EXAFS data analysis have been described in several publications [74,78,85].

3.6 Instrumental

The principal instruments used in the work were a PARC 273 potentiostat controlled by means of M270 software, a PINE AFRDE4 bi-potentiostat and a PINE AFASR Rotator which were used in experiments conducted at a rotating ring-disc electrode. Constant-current discharge experiments were also carried out with a stationary detector electrode.

The uv-visible spectrophotometer used was a Perkin-Elmer Lambda 3B instrument.The output uv-visible data were recorded and accumulated by means of a Nicolet 310 Digital Oscilloscope. The atomic absorption spectrophotometer used was one of the Varian AA-1475 series. The digitized data were processed by a PC by means of appropriate software.

All the X-ray absorption experiments, both *in-situ* and *ex-situ*, were carried out on Beam Lines X23A2 and X11A at the National Synchrotron Light Source in Brookhaven National Laboratory, as mentioned earlier.

Chapter IV

Results and Discussion

Section I Classical Electrochemical Methods

4.1.1 Cyclic-Voltammetry

A general view of the stages of discharge and recharge of MnO_2 materials, and their reversibility, or otherwise, can be usefully gained by means of cyclic-voltammetry (CV).

Fig. 9 shows the 2nd cycle of cyclic-voltammetry applied to the CM MnO_2 electrode at a sweep-rate of 0.5 mV s^{-1} and Fig. 10 illustrates the cathodic capacity changes vs. the number of discharge/recharge cycles experienced by CM MnO_2, γ-MnO_2 and blank MnO_2. The significant rechargeability achieved with the CM material can be clearly observed, in agreement with the conclusions of Wroblowa's previous work. The difference of the first cycle response from those of subsequent ones originates partly from the unavoidable initial presence of adsorbed or absorbed oxygen in the porous, high-area electrode.

The observation that two cathodic peaks arise in the current-potential diagram (Fig. 9) suggests that they are respectively associated with the two stages of reduction of MnO_2 involving the first and the second electron, although the charges which are associated with each peak are not exactly

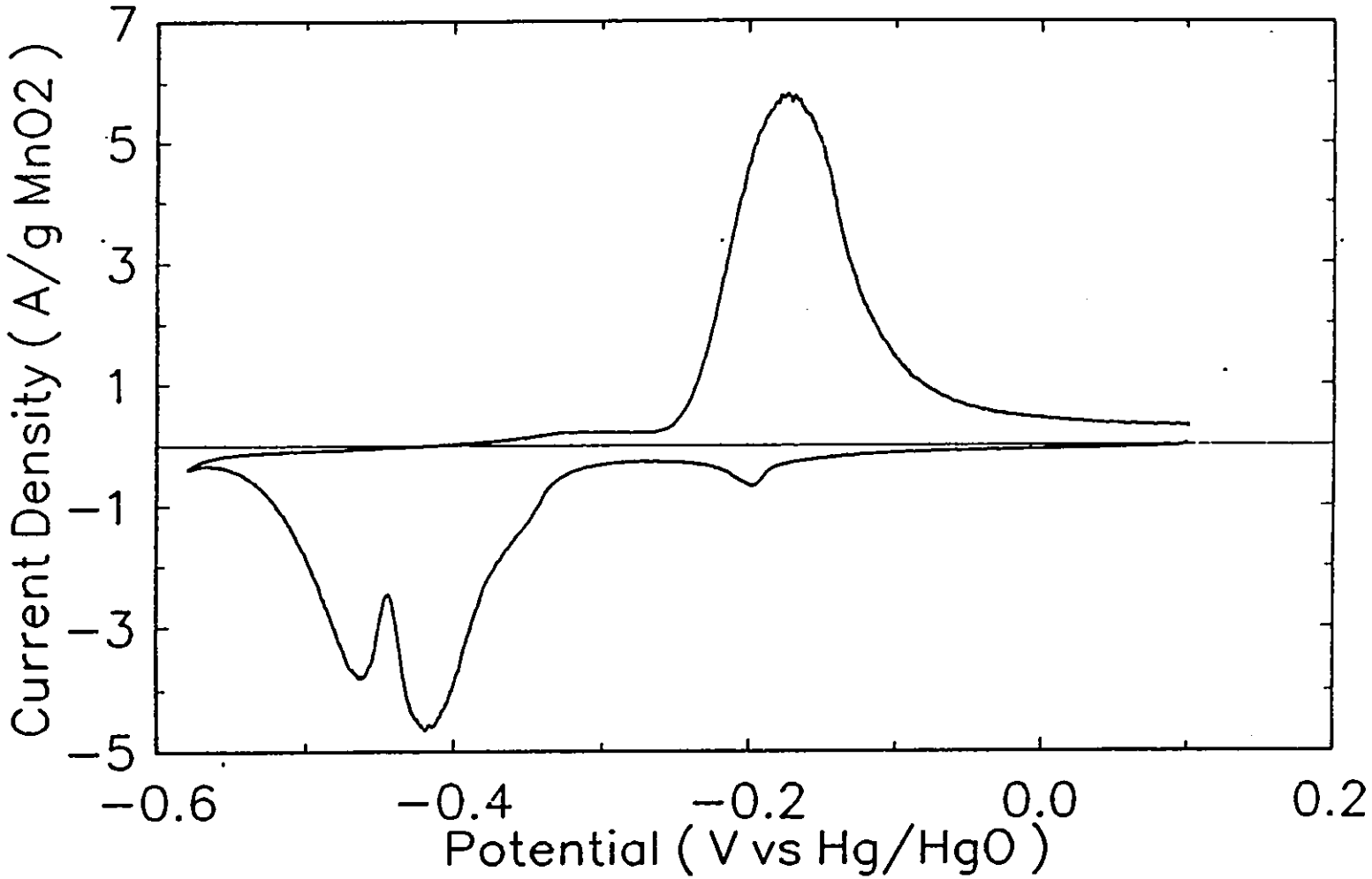

Fig. 9 Cyclic-voltammetry of CM MnO_2 in 9M aq. KOH solution at 298K. Sweep-rate 0.5 mV s^{-1}.

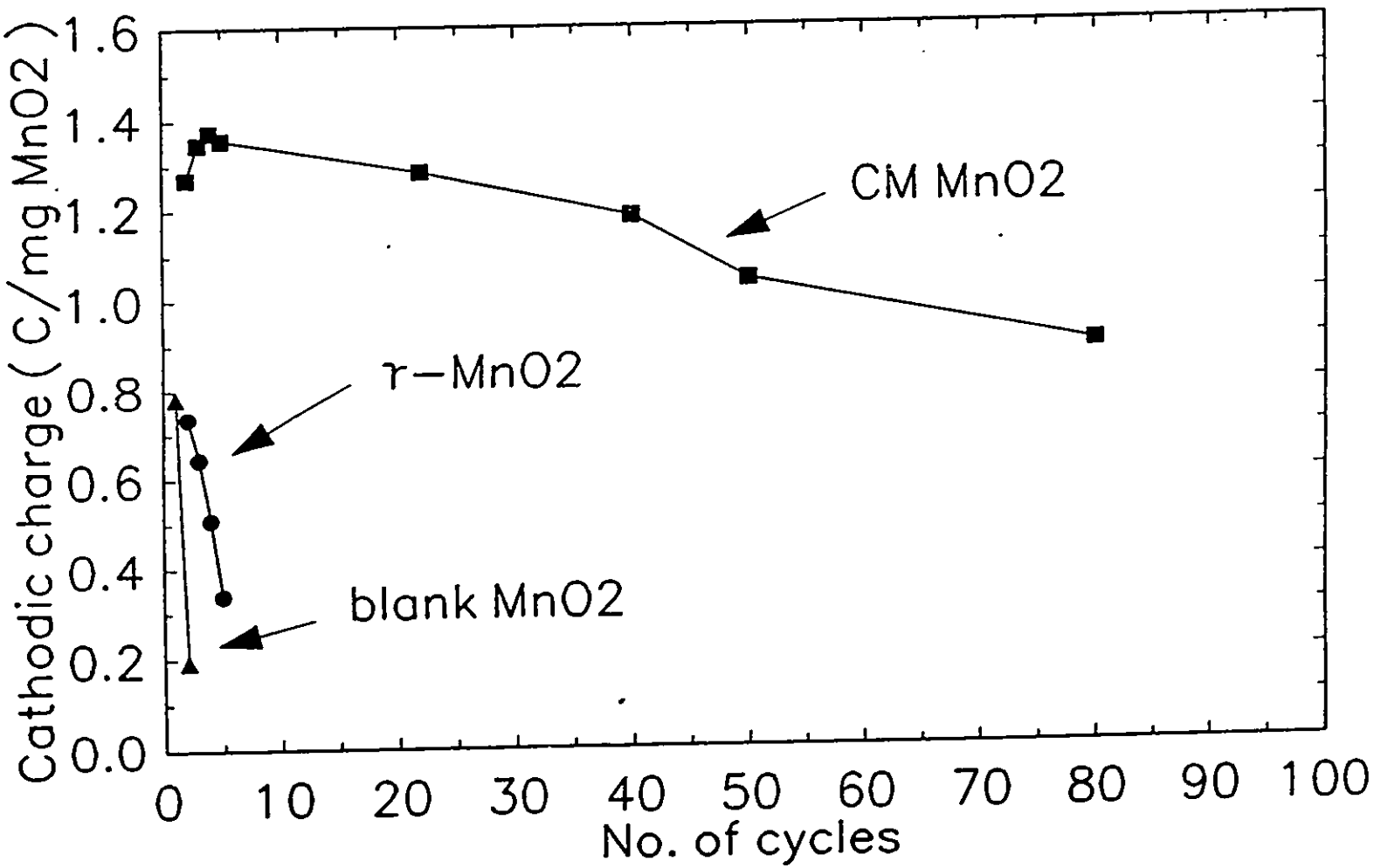

Fig. 10 Comparison between the cycle lives of CM MnO_2. γ-MnO_2 and blank MnO_2. The number of charge/recharge cycles represents the number of cycles covered in cyclic-voltammetry.(0.5 mV s^{-1})

same. (Other small peaks due to Bi reduction or reoxidation can also be observed, depending on the potential range covered in the CV). Sometimes, however, the two (Mn) peaks become combined into one, depending on the Bi/Mn ratio (high Bi/Mn material shows two peaks), the type of electrolyte (two peaks are better resolved in NaOH than in KOH [Fig.9] electrolyte), the surface area of carbon (two peaks are better resolved when the MnO_2 is mixed with high-area carbon) and the sweep-rate (at a sufficiently low sweep-rate, the two peaks merge into a single one, as in Fig. 11). These effects may arise because of the different conductivity of both electrolyte and electrode which can influence the further reduction of soluble Mn(III) in solution or that adsorbed on the porous electrode structure, as will be discussed later.

Figs. 11 shows the cyclic-voltammetry profiles for the CM MnO_2 at an extremely low sweep-rate of 4×10^{-5} V s^{-1}, while Fig. 12 shows, for comparison, cyclic-voltammograms for unmodified γ-MnO_2. The dotted lines in Figs. 11 and 12 represent the response behaviour on the 4th cycle, while the solid lines are those for the 5th cycle. The small cathodic peak C2 and the conjugate anodic peak A1 in Fig. 11 are associated with bismuth (III) reduction and Bi(0) reoxidation. The charge associated with the cathodic peak C1 and the anodic peaks A2 and A3 account for about 80% of two-electron capacity of the CM MnO_2 electrode material. In other words, the achievable energy density of the CM MnO_2 is almost twice that of γ- MnO_2 (see Fig. 12) which gives

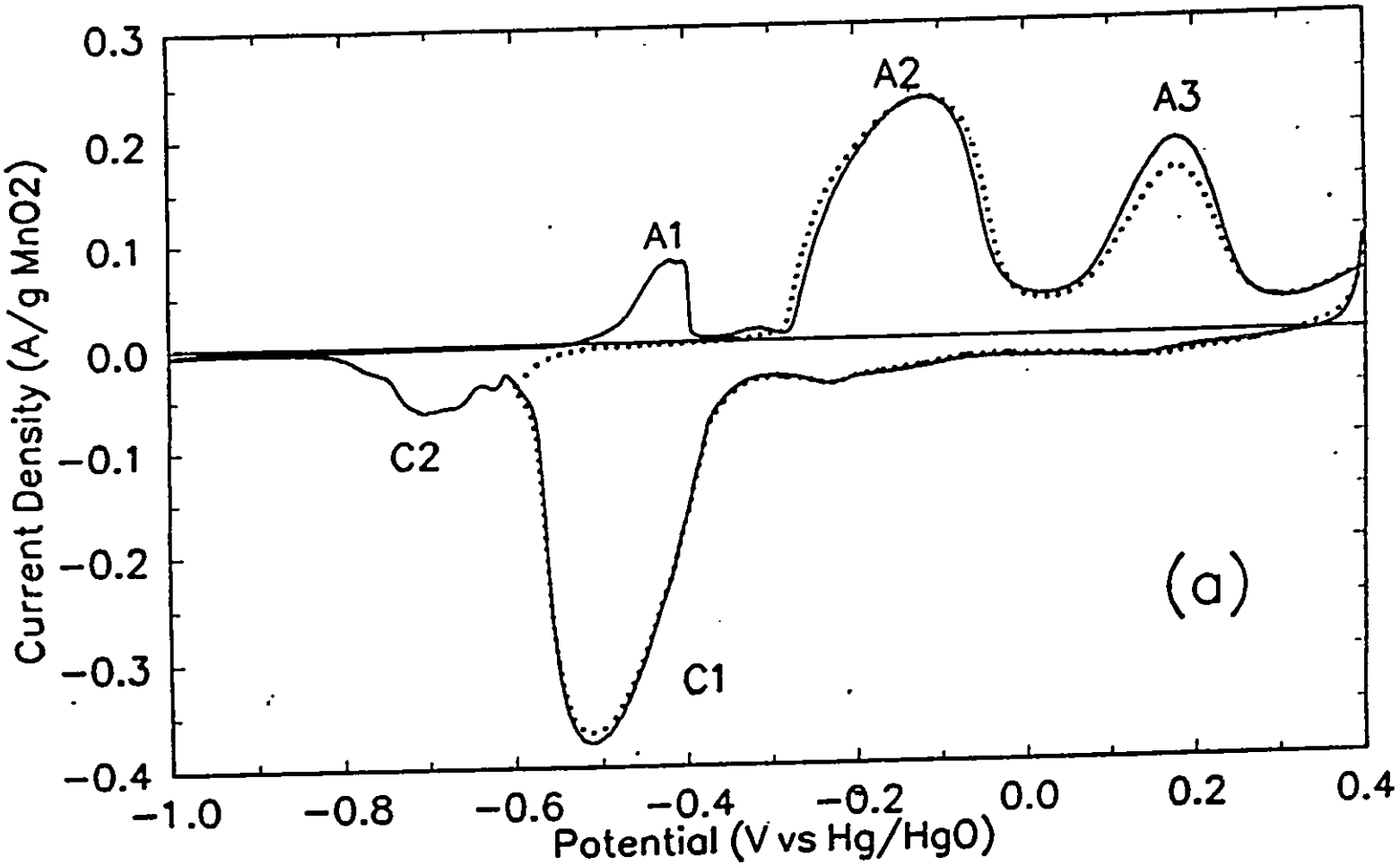

Fig. 11 Cyclic-voltammetry (CV) profiles for CM MnO_2 in 9M KOH at a sweep-rate of 4 x 10^{-5} V s^{-1}. The dotted line represents the 4th cycle, while the solid line is for the 5th cycle. Temperature: 298 K.

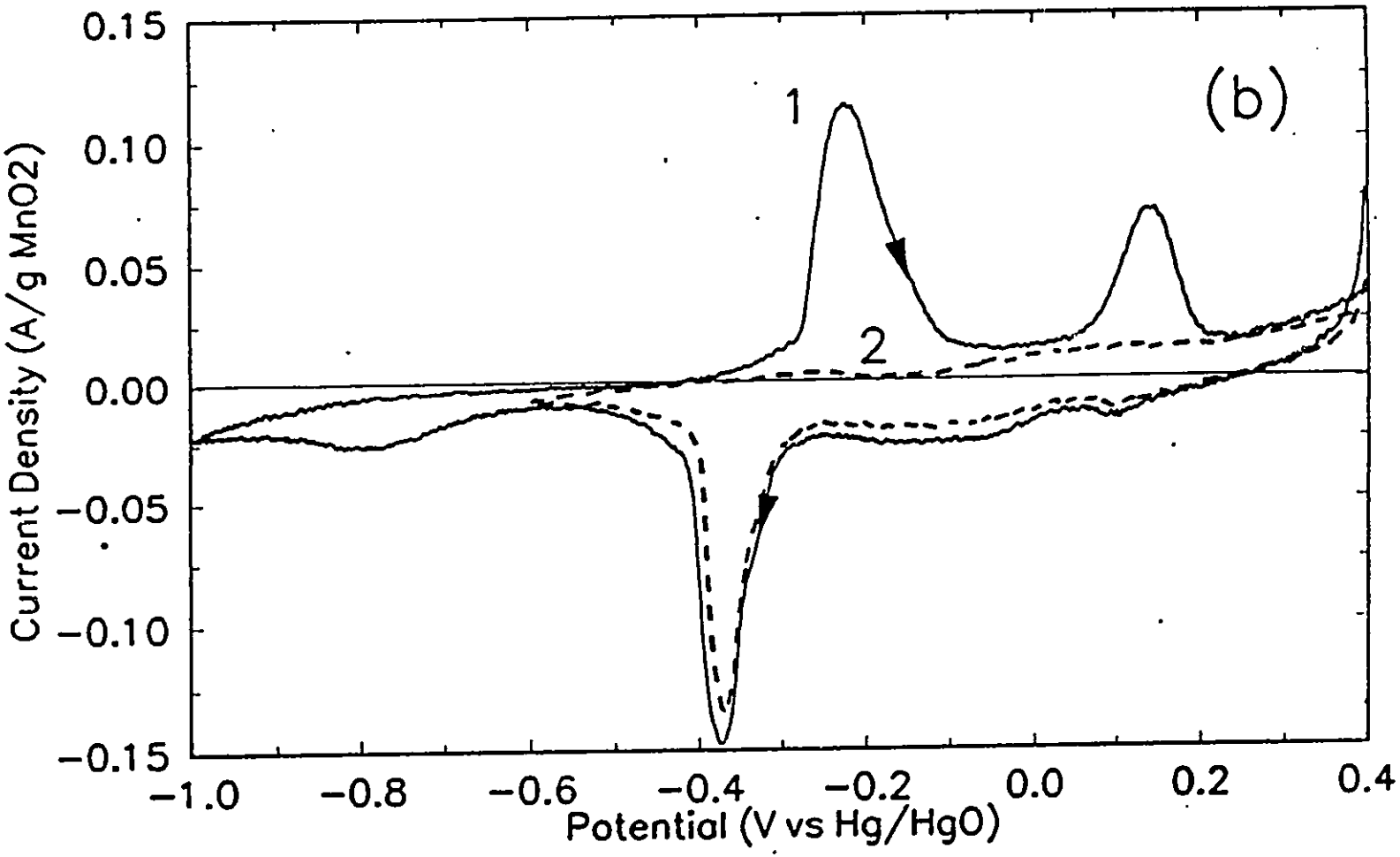

Fig. 12 Comparative cyclic voltammogram for γ-MnO_2 without Bi modification under the same conditions as in 11. The curve 1 (solid line) represents the 4th cycle, while the curve 2 (dashed line) is for the 5th cycle.

maximally only one-electron capacity with a cathodic cut-off potential at -0.6 V (36).

The most important feature of the behaviour of the CM MnO_2 electrode, as shown in Fig.11, is that 80% of the *two*-electron capacity can be discharged between 0.2 and -0.6 V and the same amount of charge can be delivered back on recharge, no matter if the electrode had been discharged previously to -0.6 (broken line) or to -1.0 V (dotted line).

Thus, the total two-electron capacity of CM MnO_2 can be discharged at an almost single-valued potential, viz. -0.4 V vs Hg/HgO [corresponding to a flat discharge profile (see below)]. This is again in contrast to the behaviours of "γ-MnO_2" (actually recharged γ-MnO_2 after deep discharge) and Blank MnO_2 for which the second electron can be utilized only if the discharge has been extended below -0.8 V vs Hg/HgO or 0.6 vs Zn (see Fig. 12). It is this characteristic which makes the second electron capacity unavailable for use in a practical γ-MnO_2 battery system.

It is interesting that the single cathodic peak, C1, in the CV shown in Fig.11, is associated with the two-electron reduction of CM MnO_2. This is contrary to the CV behaviours of "γ-MnO_2" and Blank MnO_2 which exhibit a second broad cathodic peak in the potential range -0.6 to -1.0 V (see Fig. 12), corresponding to distinguishable reduction of Mn(III) to Mn(II) after reduction of Mn(IV) to Mn(III). Usually, with higher sweep-rate and after extended recycling of the CM MnO_2 material,

two peaks in the cathodic current response become resolved at CM MnO_2 electrode (see Fig. 13 and cf. Fig 9).

It is important to note that γ-MnO_2 is only partly rechargeable after the previous reduction half-cycle has been taken to -1.00 V (Hg/HgO), as shown by curve 1 in Fig.12, while if the cycle is reversed at -0.6 V, the following anodic half-cycle (curve 2, Fig. 12) exhibits no recharging currents. Under the same conditions, CM MnO_2 will, repetitively, exhibit such recharging (Fig.11), even if the cathodic half-cycle has been extended only to -0.6 (Fig.11) rather than -1.0 V.

It should be emphasized, on the basis of the above results, that CM MnO_2 exhibits two unique characteristics:

(1) tolerance to deep discharge and

(2) capability of almost full discharge of the total two-electron capacity at an almost single valued potential, -0.4 V vs Hg/HgO (i.e., ca. 1.0 V Vs Zn) without deterioration in subsequent rechargeability.

This is in contrast to the behaviour of the γ-MnO_2 material which fails in this respect when more than the "one-electron" capacity is discharged, i.e., when the battery is discharged, (<0.6 V) to too low a voltage.

Fig.13 shows the CV profiles at a sweep-rate of 5×10^{-4} V s^{-1} for the CM MnO_2 cathode after 750 cycles. Two cathodic peaks in the range -0.4 to -0.6 V can now be observed. This result suggests that the C1 peak in Fig. 11 consists really of two peaks that overlap.

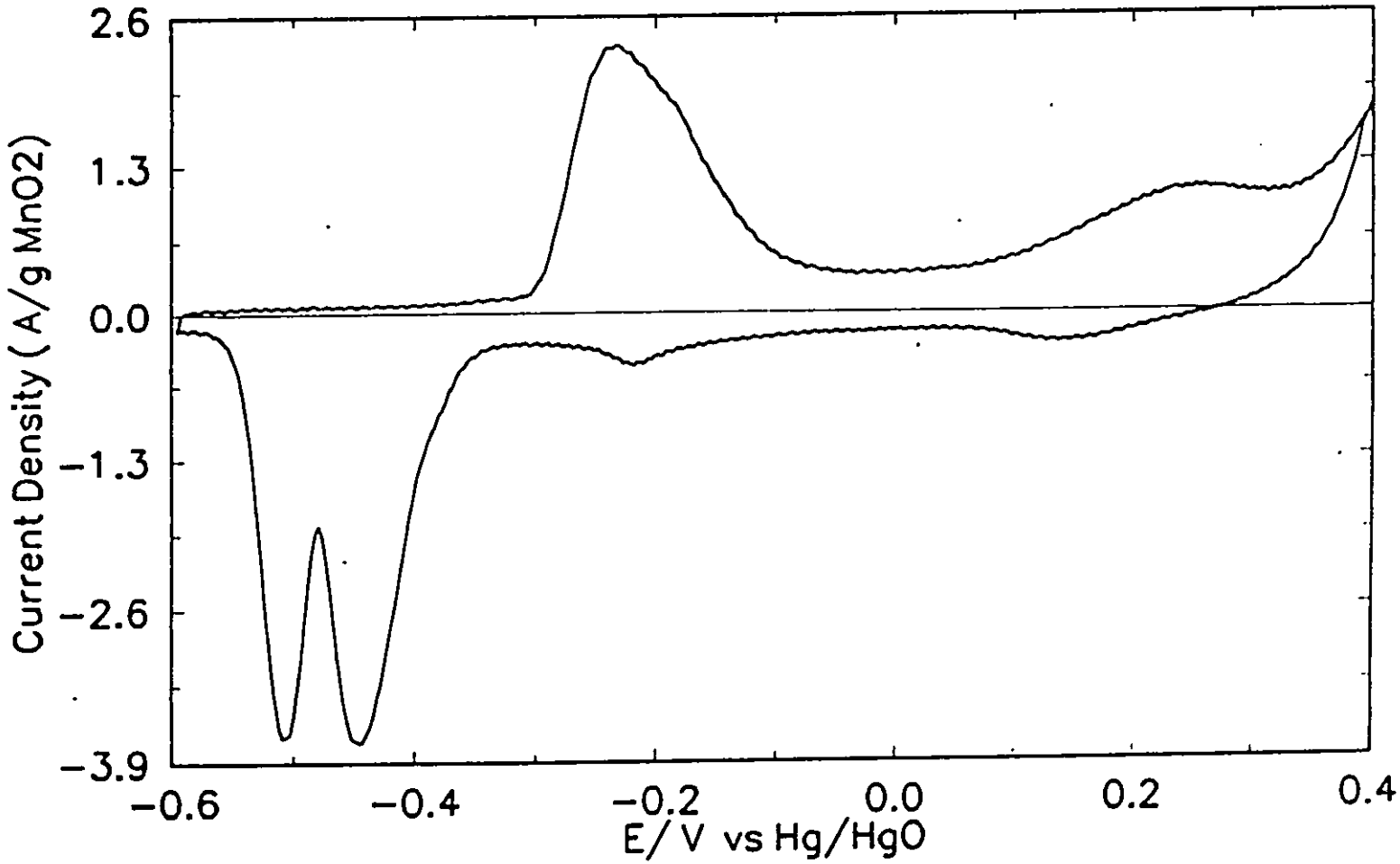

Fig. 13 CV profile at a sweep-rate of 5 x 10^{-4} V s^{-1} for the CM MnO_2 cathode (MnO_2 : graphite = 1 : 10) at the 751st cycle.

In irreversible processes studied by means of linear-sweep voltammetry, complementary kinetic information can be obtained by arresting the sweep at some defined potential in the swept range and then following the time dependence of the current.

Fig. 14 shows such behaviour in a potential-holding experiment: after a 1st cycle to reduce any adsorbed O_2, the potential sweep was stopped at various values along the swept potential range (Fig. 14A) and held until the cathodic current reached a stable value, eventually close to zero (except for curve 3); then the direction of potential sweep was reversed to that of anodic polarization. For curve 3, where the potential was held at -0.43 V (which is the potential corresponding to the flat region in the galvanostatic diagram, see Fig. 15 curve 2), the cathodic current kept decreasing until it reached point ☼ (where the current was not zero) whereupon it began to increase. Figs. 15C and D show the time dependence of the cathodic current during potential holding for curves 3 and 4, respectively.

It is necessary to point out again, from the results in Fig. 14, that the mechanisms of reduction of CM MnO_2 and γ-MnO_2 are dramatically different: the full 2e capacity of CM MnO_2 can be discharged at about -0.43 V and can then be re-charged, while γ-MnO_2 can only give 1e capacity if discharged in the range of -0.4 ~ -0.6 V, as mentioned previously, and cannot be re-charged unless it is further reduced to $Mn(OH)_2$ at about -1.0 V [36]. The above unique feature of CM MnO_2 gives electrodes of that material twice the usable energy density in comparison with regular γ-MnO_2

Fig. 14 Current variations in CV experiments (0.5 mV s^{-1}, started at 0.2 V and swept in the cathodic direction) on CM MnO_2 with potential holding :

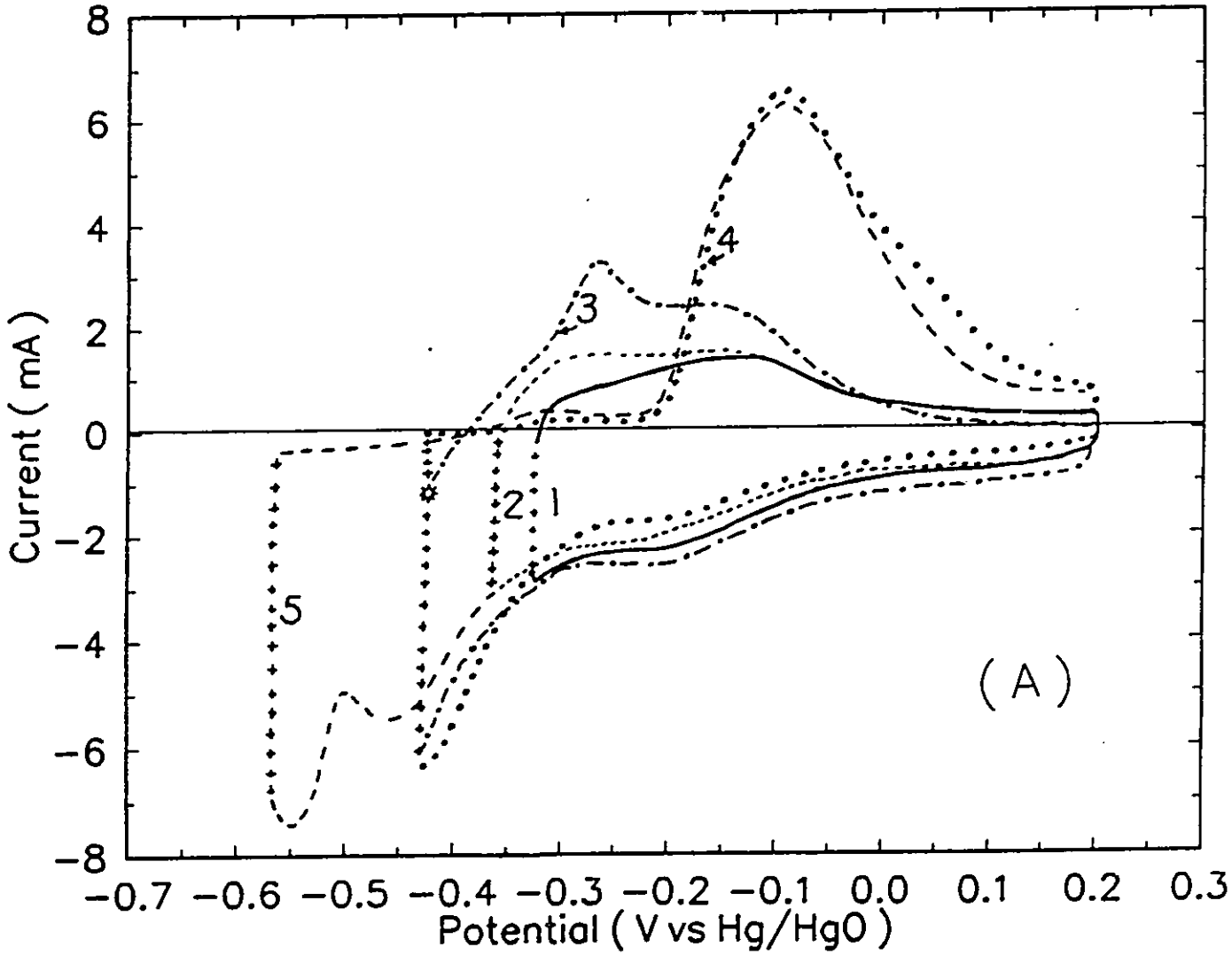

A) Potentials held at 1) -0.32; 2) -0.37; 3 and 4) -0.43 and 5) -0.57 V vs Hg/HgO until currents approached zero,(except curve 3,see following).

C) and D) Time dependence of the cathodic current during the potential holding experiments corresponding to curves 3 and 4, respectively.

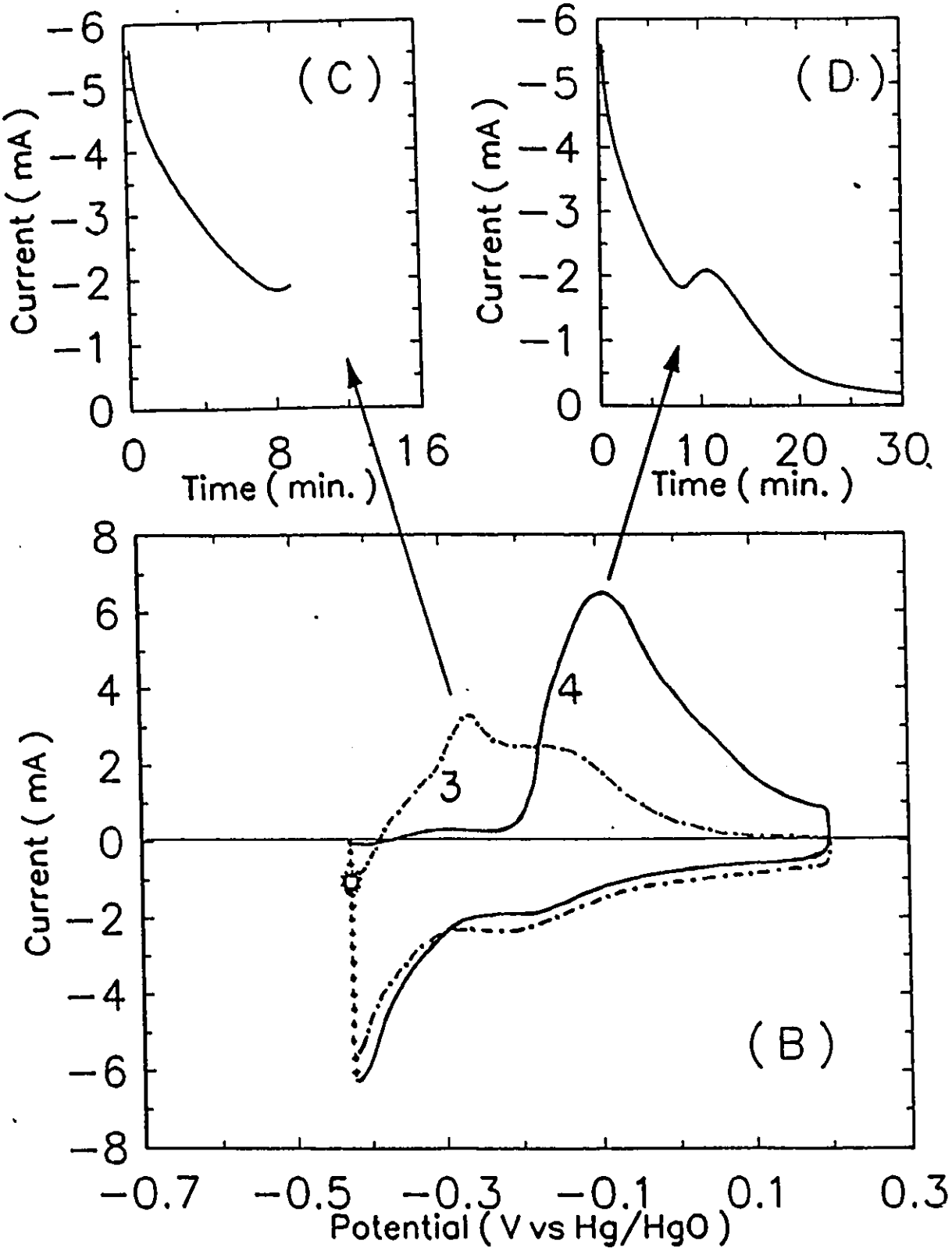

B) Potential held at -0.43 V vs Hg/HgO (curves 3 and 4).The time dependence of the current during holding is shown in Figs. 14C and 14D. Curves 3 and 4 are the same as those in A.

electrodes [88].

It can be observed from Fig. 14 that the highest anodic peak arises only in curves 4 and 5. In addition, there is a new peak in the potential range -0.3 ~ -0.25V, the current for which increases from curve 1 to 2 to 3. The anodic peak in curve 4 of Figs. 14A and B, which appears to be combined from two components, can be assumed to be associated with the two-stage process $Mn(OH)_2 \rightarrow [Mn(III)] \rightarrow MnO_2$. In curve 3, the anodic peak may be due to the re-oxidation of soluble Mn(III) species on the surface of the porous electrode. Since, in curve 3, the cathodic current had not reached zero when the current began to increase, the sudden increase of current in that curve suggests that the second electron reduction can take place, coupled with that involving the first electron, and at the *same* potential, when the first electron reduction has proceeded to a certain stage.

In Fig.14C, the current which decreases in the first 8 minutes results from the reaction of $MnO_2 \rightarrow Mn(III)$ and the sudden increase of the current results from another reaction which it would be reasonable to assume corresponds to $Mn(III) \rightarrow Mn(OH)_2$ (Fig. 14D).

Furthermore, the soluble Mn(III) species itself can be electrochemically re-oxidised to MnO_2 which can then be re-reduced and re-oxidised again and again, while the Mn(III) in the products of γ-MnO_2 reduction cannot be re-oxidised electrochemically [36,88].

4.1.2 Constant current ("galvanostatic") discharge/recharge

Fig. 15 shows a comparison of the constant-current discharge characteristic of CM MnO_2 (curve 2) with that of γ-MnO_2 (curve 1). Two regions can be distinguished in curve 1; in the first (from 0% to 35% of two-electron capacity), the potential keeps decreasing; a potential varying with composition indicates homogeneous phase reduction; in the second region (35% to 55% of two electron capacity), however, the potential remains constant over an appreciable range of compositions indicating co-existence of two phases at equilibrium. Thus the two regions in curve 1 correspond to the homogenous and heterogenous processes as proposed by Kozawa [25,26] but in curve 2 there is only one flat region and a small flat tail at its end, corresponding approximately to 10% of the flat region capacity, due in part to Bi_2O_3 reduction. Since almost no change of potential arises on discharge over about 80% of the total range of composition (Fig. 16), the first step of reduction of CM MnO_2 can be considered as an heterogenous process, based on Vetter's theory [22,23].

Theoretically, based on the Nernst equation, when one solid phase is electrochemically reduced to another solid phase at unit activity or to a saturated state of dissolved species (since the ratio of activities of higher to lower oxidation-state material remains constant during the discharge process), the OCP (Open Circuit Potential) of the system should remain constant as long as both phases co-exist. Although such

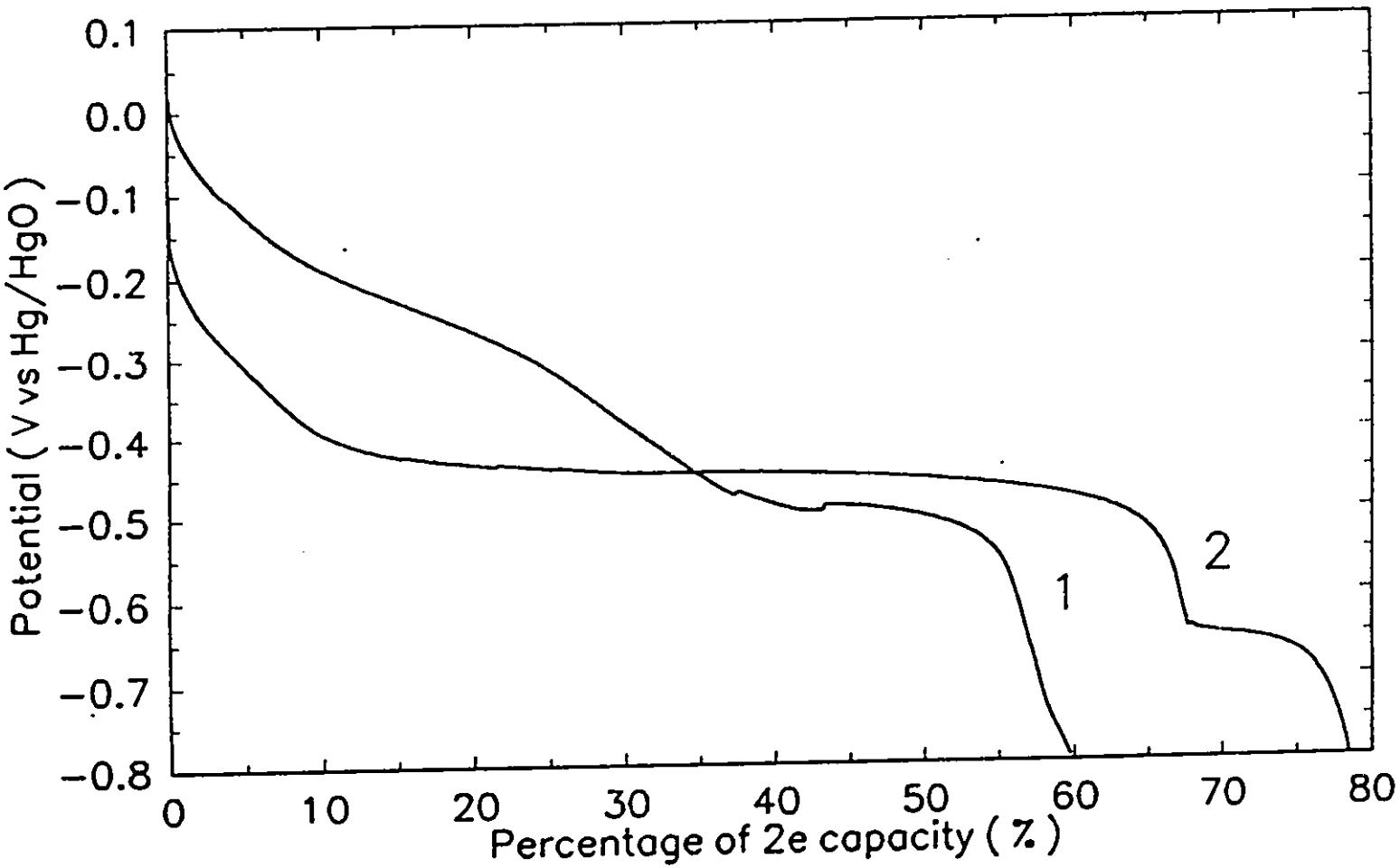

Fig. 15 Constant-current discharge of CM M.. (curve 2) and of γ-MnO_2 (curve 1). Current density 0.2 A g^{-1}.

criteria can only really be used for equilibrium conditions, in the present experiments, the discharge and recharge currents were relatively low, so the restricting conditions can be assumed to be almost fulfilled. Therefore the Mn(III) species, which is the first product of reduction of CM MnO_2, can be either in the solid state or dissolved in a saturated state (see below), or both.

In other experiments, it was shown that once the potential of the "flat region" of the discharge curve had been reached around 10% or less of discharge capacity, it remained almost *independent* of cathodic current-density from a C/10 rate up to the 6C rate, i.e. polarization effects in that state remain small in the continuing discharge of the CM material,even up to high rates.

Fig. 16 shows constant-current discharge curves for the CM MnO_2 cathode (MnO_2:graphite = 1:1, by weight) at C/10, and C/3 rates (see Appendix 1.8, e), respectively. The utilization of two-electron capacity of the CM MnO_2 is 70, 80, and 82% at C/3, C/5 and C/10 rates, respectively. (The theoretical two-electron capacity of MnO_2 is 0.617 Ah/g.) It seems that the discharge curves in Fig. 16 exhibit a remarkably flat voltage profile after an initial potential decline, covering most of the discharge time range, independent of the discharge rates. This characteristic will give a usefully constant or stable working potential (1 V vs Zn) and high specific power-density for the high discharge rates that the above results demonstrate are

attainable at the CM MnO_2 cathodes.

Figs. 17(a) and (b) show plots of E vs time and E vs capacity, respectively, for the same set of data under conditions of constant-current charging/discharging at substantially higher C rates as indicated in the above figure for the CM MnO_2 cathode. Here, an MnO_2 : graphite ratio of 1:10 is required in order to minimize internal ohmic polarization at these relatively high C rates. The utilization of two-electron capacity of the CM MnO_2 is 70, 70, 68, 67, 65, 59% at 2C, 3C, 4C, 5C, 6C, and 10C rates, respectively (using a cut-off cathodic potential of -0.6 V vs Hg/HgO).

Figs. 17A and 17B demonstrate that the CM MnO_2 cathodes with the higher graphite content not only can be discharged at up to a 6C rate, but also can be charged back at comparable rates. It is to be noticed that the experiments giving the results in Fig. 17 were all carried on the same CM MnO_2 electrode i.e., the electrode was first discharged and recharged at the 2C rate, then the 3C, up to the 10C rate, respectively. Therefore, the results in Fig. 17 also prove that the CM MnO_2 exhibits excellent rechargeability even at very high discharge/recharge rates.

Fig. 17 demonstrates that the constant-current charging/discharging profiles are almost independent of the charging/discharging rates up to 6C for the CM MnO_2 cathode having an high graphite content. This is an important characteristic of CM MnO_2 that makes it substantially different from γ-MnO_2 cathode material (85).

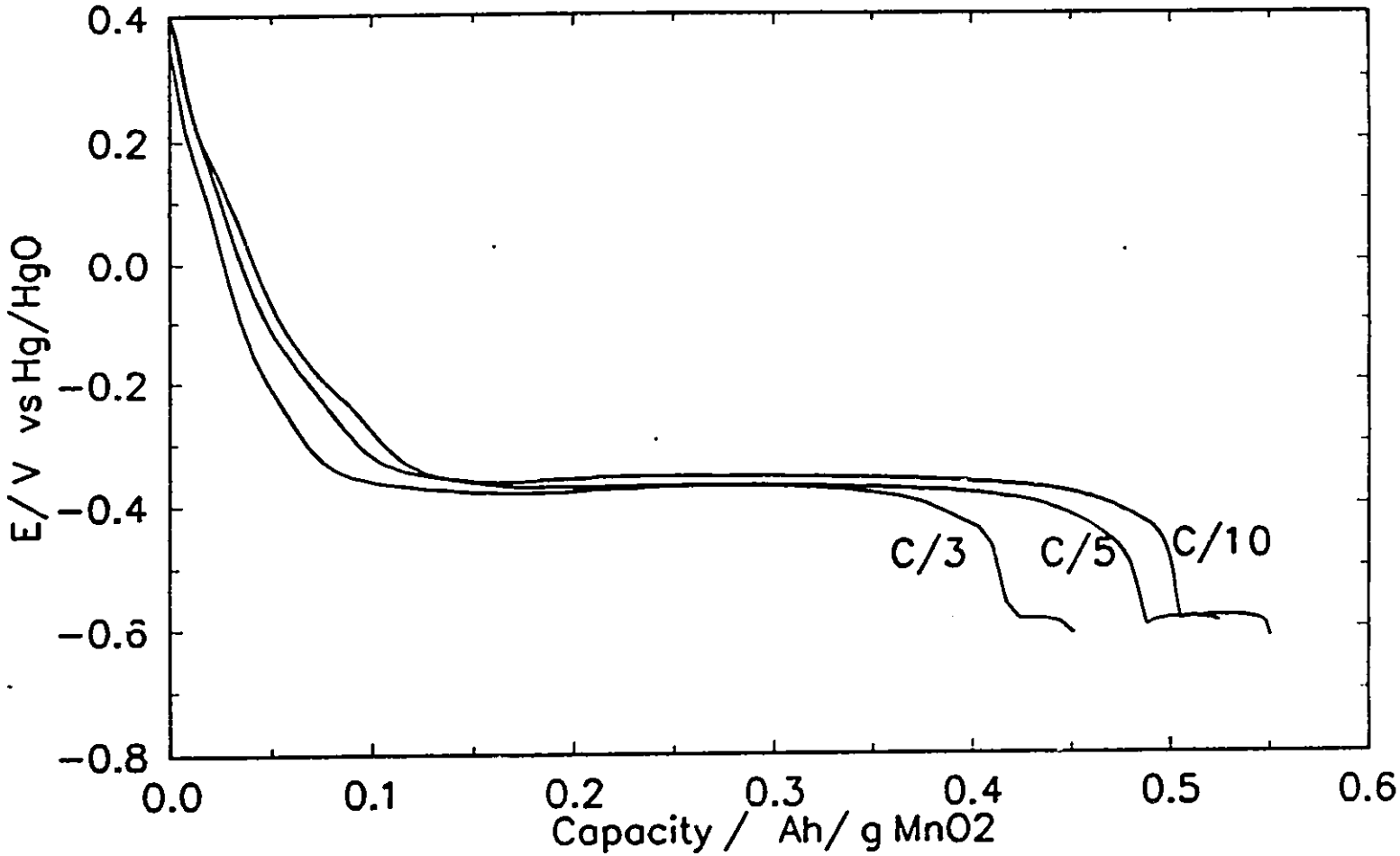

Fig. 16 Constant-current discharge curves for the CM MnO_2 cathode (MnO_2 : graphite = 1 : 1) at C/10, C/5 and C/3 rates, respectively. Temperature 298 K.

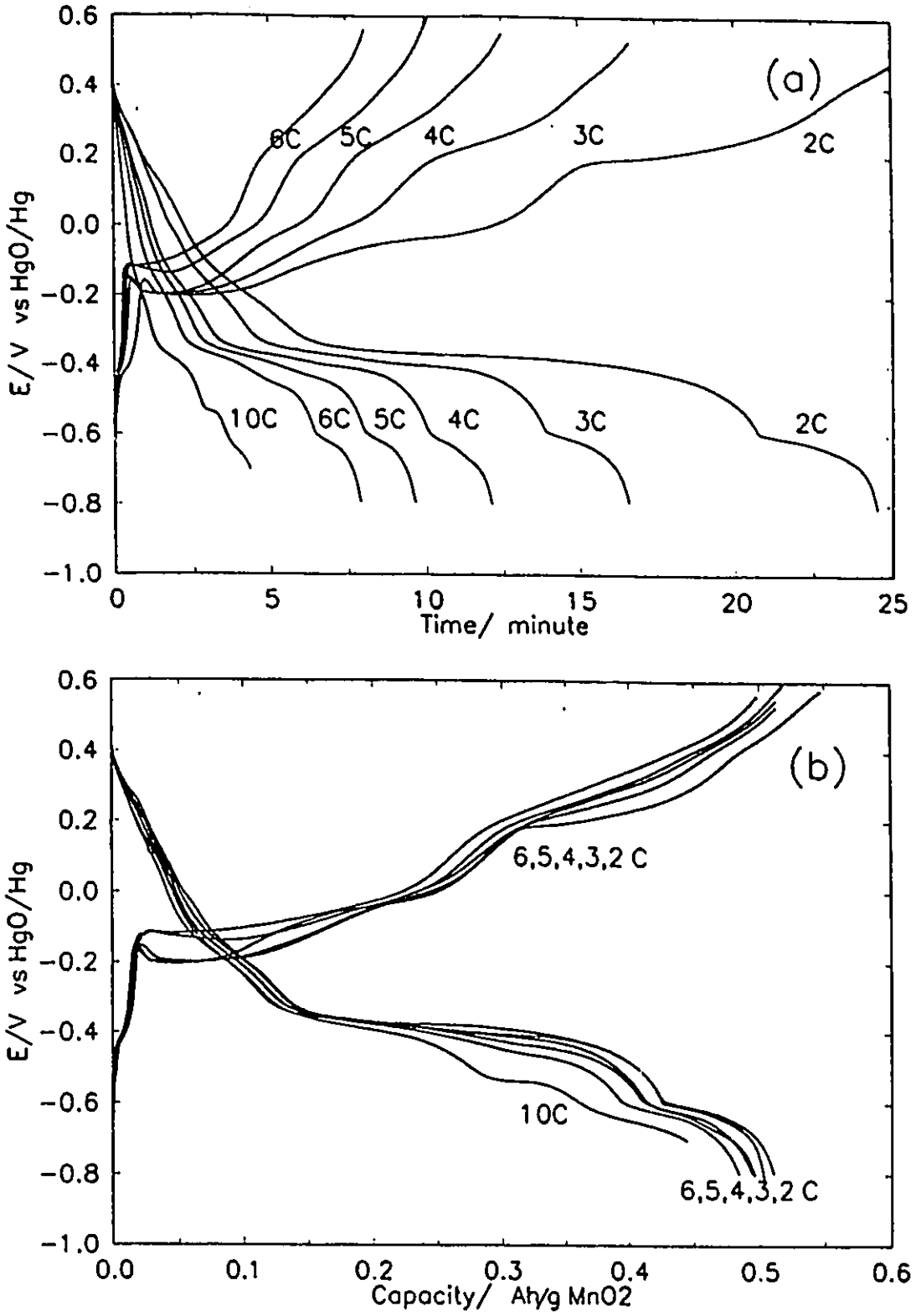

Fig. 17 Constant-current charging/discharging curves at the C rates indicated in the Figure for the CM MnO_2 cathode (MnO_2 : graphite = 1 : 10): (a) E vs time; (b) E vs capacity (Ah/g MnO_2).

Fig. 18 shows the plot of the plateau potentials corresponding to the flat voltage regions of the discharge curves, plotted vs discharge rate, for a CM MnO_2 cathode (MnO_2 : graphite = 1 : 10, as in Fig. 17). Corresponding round-number C rates are indicated. It is to be noticed that when the graphite content is higher, better charge/discharge current performance is realized for the CM MnO_2 cathodes, as those familiar with battery technology will understand. For high graphite content, as shown in the case of Fig. 17, the shapes of the discharge curves remained virtually unchanged up to a 6C rate. In other words, a stable working potential, about -0.4 V vs Hg/HgO, is still available up to such an high discharge rate, although this operating voltage plateau is significantly lower than the usual declining voltage range for discharge of regular γ-MnO_2 in the zero to one-electron charge capacity range.

Fig. 19 shows constant-current recharging curves, corresponding to the discharge curves in Fig. 16, for the CM MnO_2 cathode (MnO_2 : graphite = 1 : 1) again at C/10, C/5 and C/3 rates, respectively. Note that these results are achieved with a 1 : 1 MnO_2 to graphite ratio, thus giving good weight and volume energy density. The current efficiencies for the curves in Figs. 16 and 19 are close to 100%, the same as found in the CV experiments (see Figs. 11 and 13). The two distinguishable plateaux for each curve in Fig. 19 are associated with the two separate anodic peaks (A2 and A3) in Fig. 11. These results imply that the two-electron oxidation process, Mn(II) → Mn(IV),

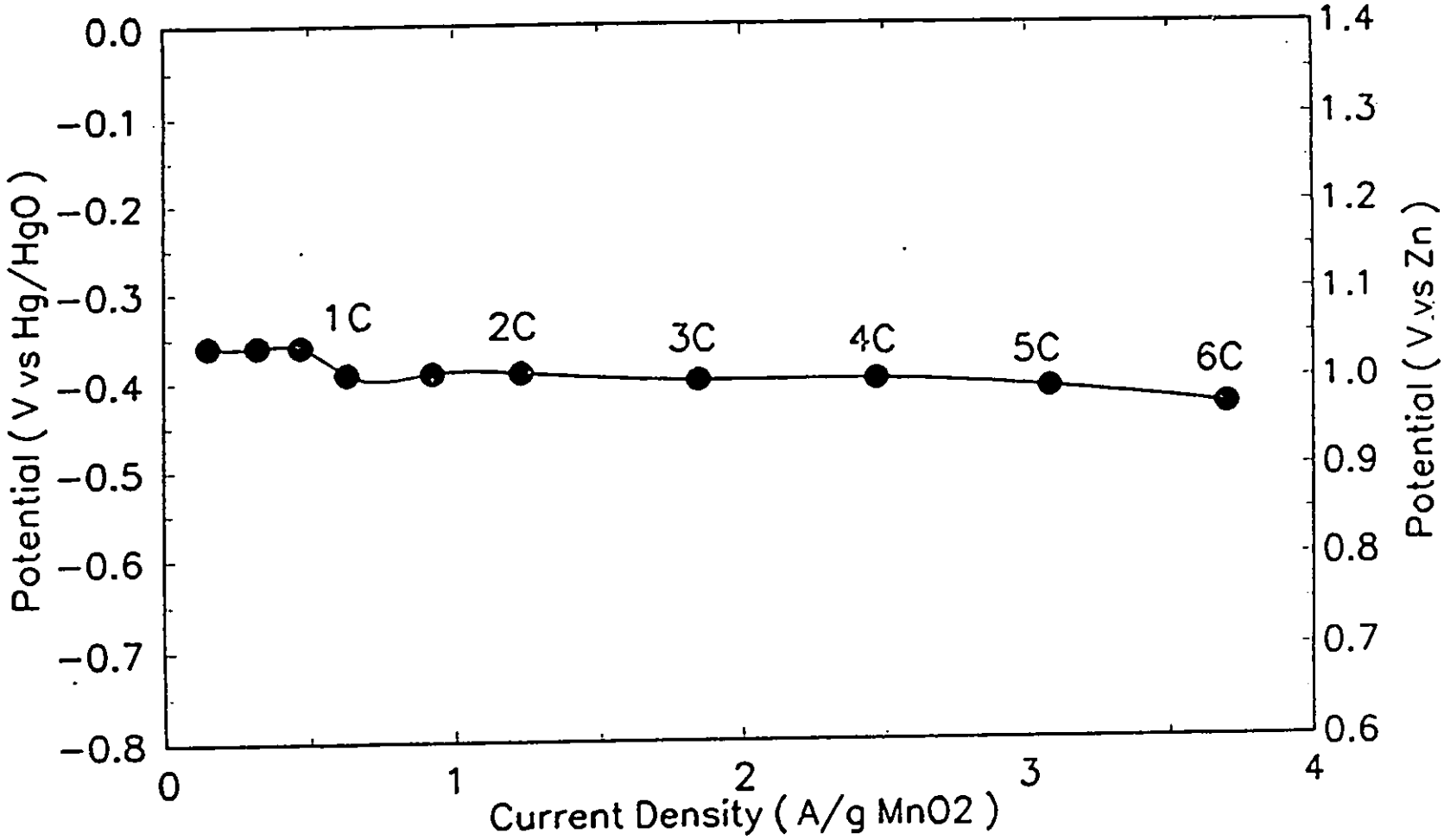

Fig. 18 Potential of the discharge plateaux for CM MnO_2 (MnO_2 : graphite = 1 : 10) as a function of current-density, corresponding to various discharge rates (in terms of C of multiples thereof).

is taking place in two stages: one at about -0.25 and the other at about -0.1 V vs Hg/HgO, respectively.

The capability for high-rate charging, as indicated in Figs. 17 and 19, is another remarkable and newly determined characteristic of the CM MnO_2 cathode. This feature is also very important for possible electric-vehicle power-train applications.

It is interesting to compare the discharge behaviour of CM MnO_2 and γ-MnO_2 (I.C. No.2). Fig. 20 shows discharge curves for both γ-MnO_2 and the CM MnO_2 at the same discharge rates, taken as C/10 and C/5 rates, respectively, the rates having been calculated on the basis of the theoretical two-electron capacity for each of the MnO_2 materials. Both electrodes were prepared in the same way (MnO_2 : graphite = 1 : 1 in this case) and charged to 0.4 V first, then subjected to discharge. It is clearly evident from Fig. 20 that at the C/5 and C/10 rate, γ-MnO_2 can only deliver 40% and 52%, respectively, of its theoretical full two-electron capacity, while the CM MnO_2 gives 80% and 83%, respectively, with a cut-off cathodic potential at -0.62 V vs Hg/HgO. The discharge curve for γ-MnO_2, shown in Fig. 20, has a small region at potentials higher than those of the curve for CM MnO_2, but the potential declines rapidly to -0.6 V. It is obvious from Fig. 20 that, as the discharge rate is increased from C/10 to C/5, the discharge profile for γ-MnO_2 declines significantly, while the change for the CM MnO_2 is small.

We have mentioned that the plateau voltages for discharge

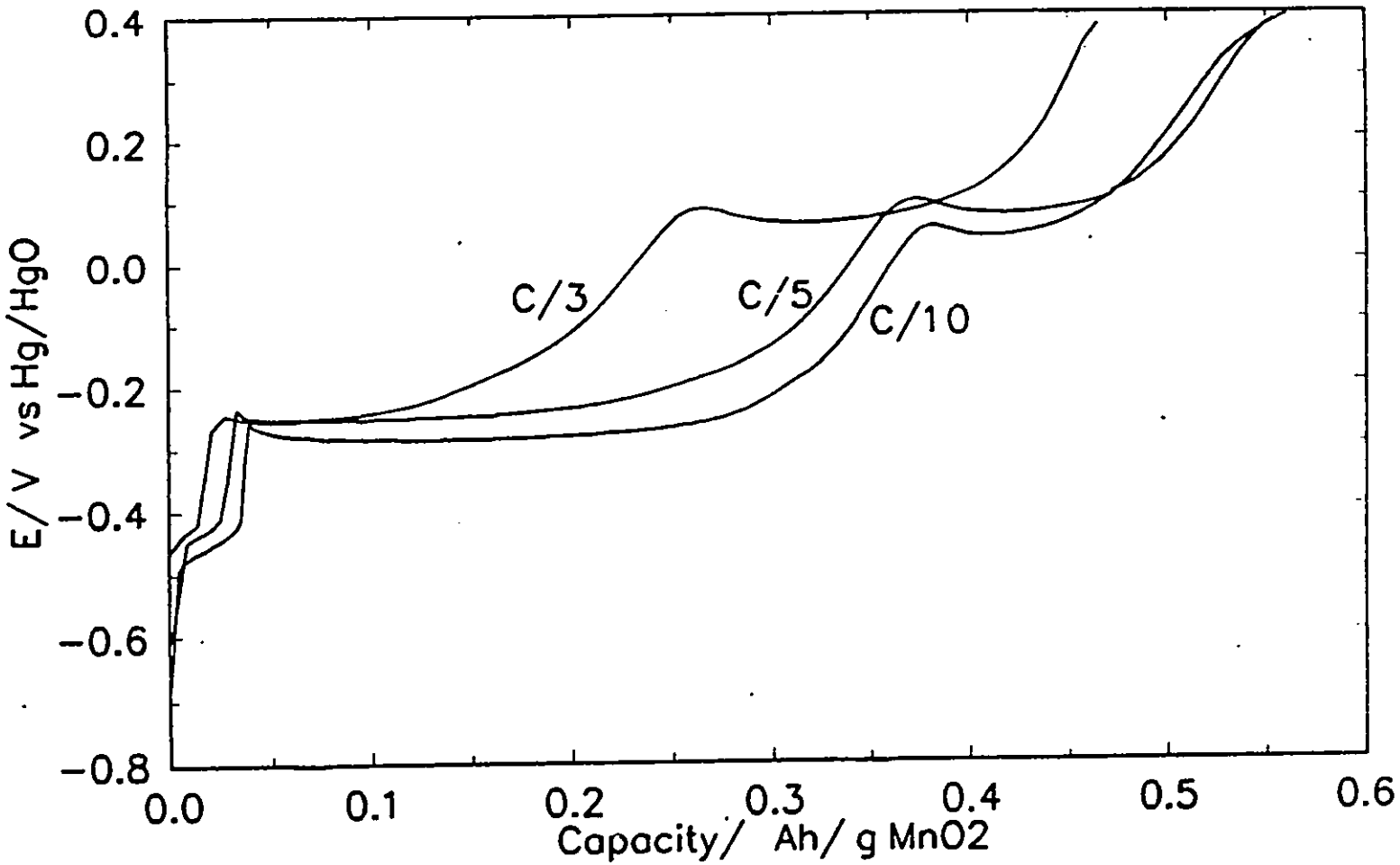

Fig. 19 Constant-current charging curves, corresponding to the discharging curve in Fig. 16, for the CM MnO_2 cathode (MnO_2 : graphite = 1 : 1) at C/10, C/5 and C/3 rates, respectively.

in Fig. 16 or Fig. 17 are about 1 V with respect to Zn/ZnO_2^{2-} in the same solution (ca. -0.4 ± 0.01V vs Hg/HgO). Such discharge voltages are, of course, about 0.2 to 0.3 V less than is achievable from a regular alkaline MnO_2 primary cell or initially with a partially rechargeable (30% of one-electron capacity) γ-MnO_2 at low discharge rates (see Fig. 20). Hence such a system with the CM MnO_2 would be unsuitable for many simple electronic or electrical devices, or appliances currently in the market place requiring a 1.5 V voltage source. However, this difficulty would not arise in electric vehicle applications where multiple series-stacking is involved in order to provide a required much greater operating voltage of 150 to 200 V per system. However, a proportionately large volume requirement would be unavoidable. However, such a CM MnO_2/Zn system, with the plateau working voltage indicated above, is comparable with the "Ni-Cd" battery.

From other related work (see section II of this chapter), in which comparative *in-situ* uv-visible spectroelectrochemical determinations of the extents to which the soluble Mn(III) intermediate arises, were made, it could be deduced that the mechanisms of the cathodic and anodic reactions of CM MnO_2 are different from those of γ-MnO_2 . The process of "proton/electron hopping" (25,27) in the lattice of MnO_2, which is believed to be the rate-determining step in the reduction of γ-MnO_2, may be bypassed by the so-called heterogeneous mechanism involving production of demonstrably soluble $Mn(OH)_6^{3-}$ ion. The proposed heterogeneous (two-phase) mechanism can provide a reasonable

heterogeneous (two-phase) mechanism can provide a reasonable interpretation of the observed phenomena, e.g., the relatively flat discharge and recharge profiles that are found (Figs. 16 and 17) and the much higher current-densities that can be realized experimentally in the present study for CM MnO_2 compared to those for γ-MnO_2 electrodes.

Based on two-electron capacity, the theoretical specific capacity and specific energy for the CM MnO_2/Zn system are 350 Ah/Kg, and 525 Wh/Kg, respectively (Table 2), which are very competitive performance figures vis a vis other secondary cell systems.

TABLE 1. Theoretical specific capacity and specific energy for the CM MnO_2/Zn system in comparison with those for several other common secondary battery systems(86)

Battery System	Cell voltage (V)	Specific capacity* (Ah/Kg)	Specific energy (Wh/Kg)
CM MnO_2/Zn	1.5	350	525
Ni oxide/H_2	1.5	289	433
Ni oxide/Cd	1.35	181	244
PbO_2/Pb	2.1	120	252

* Based on active anode and cathode materials only.

Table 1 lists comparatively the theoretical specific capacity and specific energy values for several commonly used secondary battery systems. It is clear that there is a great potential for building a practical high energy-density and high power-density CM MnO_2/Zn battery system, the theoretical specific capacity and energy of which are more than twice that of lead-acid and nickel-cadmium battery systems. This is a major attractive feature of the rechargeable MnO_2 material. Comparisons of the behaviour of non-CM MnO_2/Zn batteries with other battery systems, e.g., Pb/acid was made by Wruck et al., (85) with rather negative conclusions. However, as is shown here, quite competitive discharge and recharge rates are achievable if the MnO_2 is in the CM form.

Good cycle-life was achieved in our laboratory plate-geometry cells (see Fig. 4b) with about 40% of theoretical two-electron capacity of the CM MnO_2 still remaining active after one thousand discharge/recharge cycles or more. Fig. 21 shows a plot of the percentage of the theoretical two-electron capacity remaining after each cycle vs the cycle number for the CM MnO_2 cathode (MnO_2 : graphite = 1 : 10). The data shown in Fig. 21 were calculated from the results of CV experiments conducted at a sweep-rate of 0.5 mV s^{-1}. These results correspond to an effective average C rate of 12 over the current vs time profile of the CV.

It is to be noted that a "free electrolyte" cell, i.e., one with an excess of 9M KOH solution and a small amount of CM MnO_2

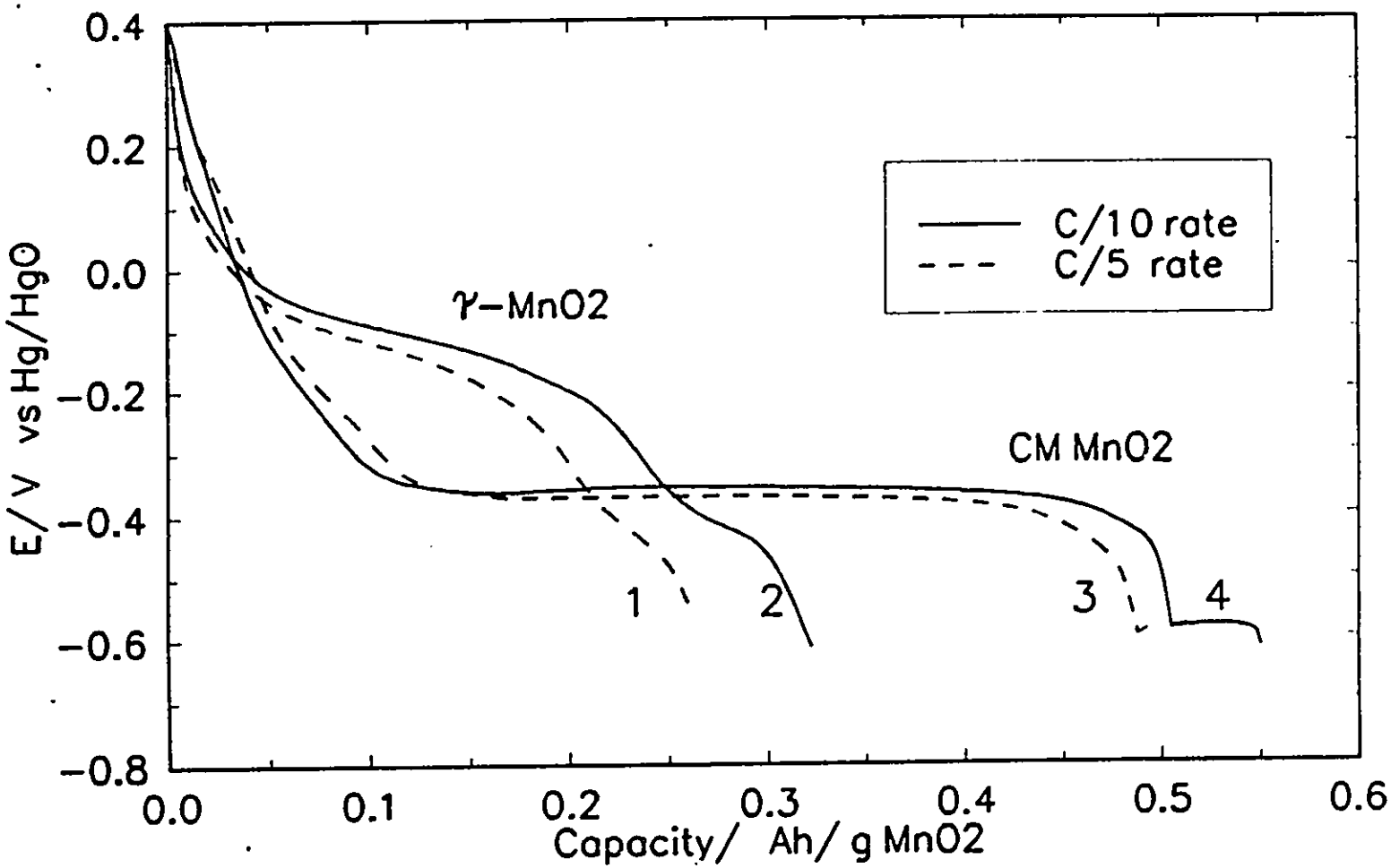

Fig. 20 Comparison of constant-current discharge curves for γ-MnO_2 (curves 1 and 2) (I.C. sample No. 2) and for CM MnO_2 (curves 3 and 4) at discharge rates C/5 (dashed lines) and C/10 (solid lines) respectively.

(ca. 20 mg per electrode) was used. Some appreciable part of the loss of the capacity shown in Fig. 21 is due to the formation and thence loss of soluble Mn(III) species into the solution during discharge and recharge of the CM MnO_2 electrodes. The role of dissolution of Mn(III) species in discharge of CM MnO_2 battery cathode material is very critical. In practical battery embodiments, there would be little difficulty arising from this situation, since a restricted electrolyte volume is normally used, i.e. virtually no free liquid electrolyte is present so that an "electrolyte starvation" situation obtains.

Fig. 22 shows discharge curves for a CM MnO_2 cathode (CM MnO_2 : graphite = 1 : 10) at the 1C discharge/recharge rate for the 3rd, 25, 41, 57, 63, 78 and 95th cycles. These results demonstrate that no significant decline arises in the discharge behaviour up to 95 cycles nor does it decline much in substantially extended further cycling. The charging rate was also 1C for the results shown in Fig. 22.

As described in 5.1.1, the two-electrons of CM MnO_2 can be utilized for reduction [Mn(IV) to Mn(III), Mn(III) to Mn(II)] almost at the same potential (about -0.4 V vs Hg/HgO). This aspect has been further proved by the *in-situ* spectro-electrochemical technique and *in-situ* XAS method, as will be described later in Sections 5.2 and 5.3. Hence, Mn(IV) and Mn(III) must be co-existent in two different phases in the early stages of discharge; Mn(III) and Mn(II) must also be co-existent in two different phases in the later stage of discharge, while

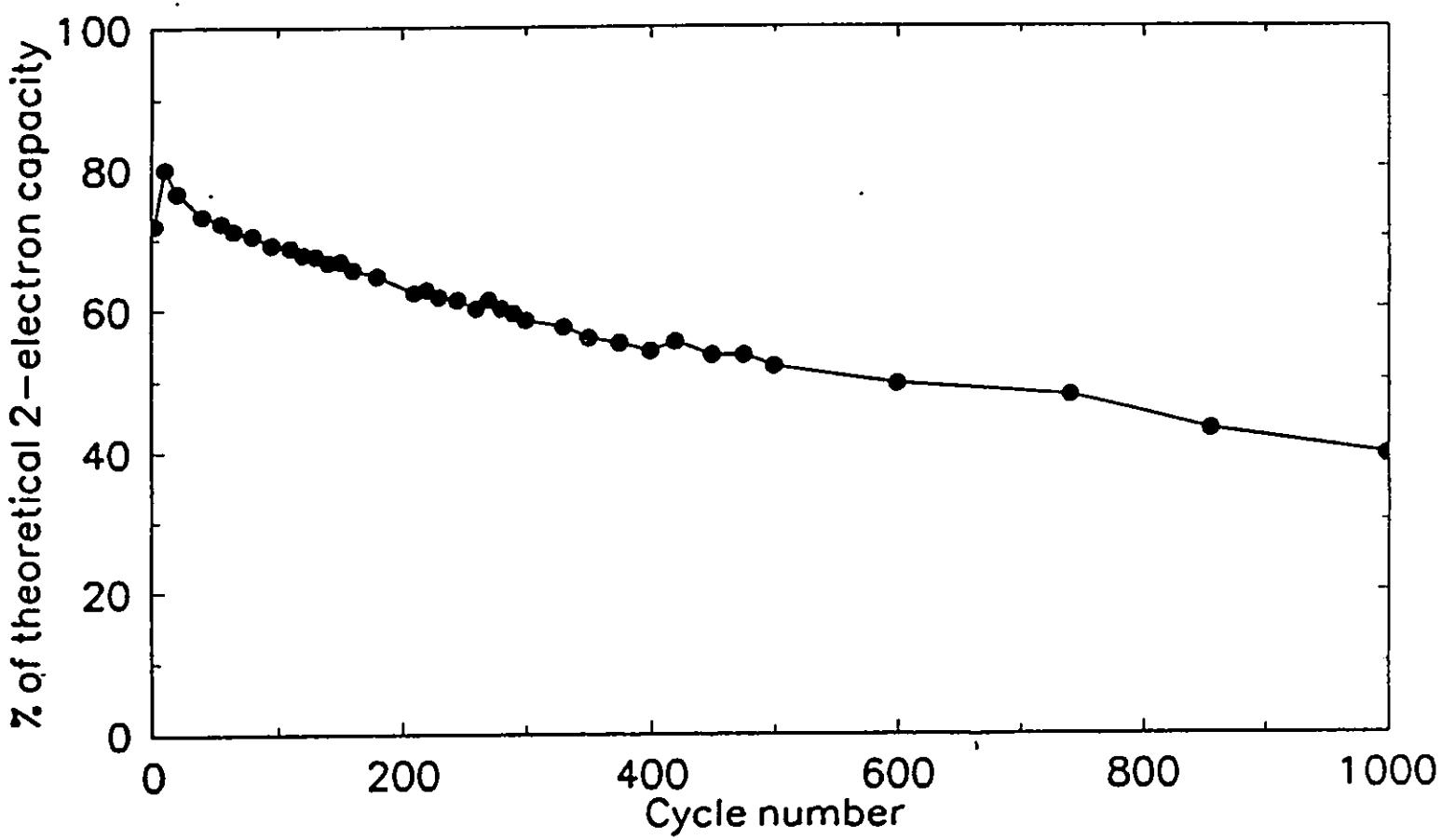

Fig. 21 Plot of the percentage of the theoretical two-electron capacity remaining after various cycles vs the cycle number, for the CM MnO_2 (based on cycle voltammetry experiments).

in the transitional region, which arises between the two extreme stages, the three phases, Mn(IV)/Mn(III)/Mn(II), must, presumably, be heterogeneously co-existent.

The soluble intermediate Mn(III) is the critical species in the process of discharge of the MnO_2 electrode. Studies on the behaviour and concentration of this species paves the way towards better understanding of the reaction mechanism.

4.1.3 Detection of Mn(III) Intermediate(s) in Solution with a Detector Electrode

The principle of this part of the work was the use of a Pt-mesh detector electrode (described in Chapter III) at which any diffusing, solution-soluble Mn(III) species could be detected by its re-oxidation current at the Pt electrode, set at an appropriate potential.

Figs. 23 and 24 show the results of constant-current discharge experiments using a stationary detector electrode, the potential of which was held at -50 mV vs. Hg/HgO. The electrodes were γ-MnO_2 (Fig. 23) and CM MnO_2 (Fig. 24), respectively. The upper curves in Figs. 23 and Fig. 24 show the results of constant current discharge and the lower ones the current response at the detector electrode. The dashed lines in Figs. 23(b) and 24(b) show the background reduction current of residual oxygen which was either in the solution or adsorbed in the porous MnO_2 electrode, and can also initially diffuse to the detector electrode. The positive oxidation current signal at the detector electrode would, of course, be added algebraically

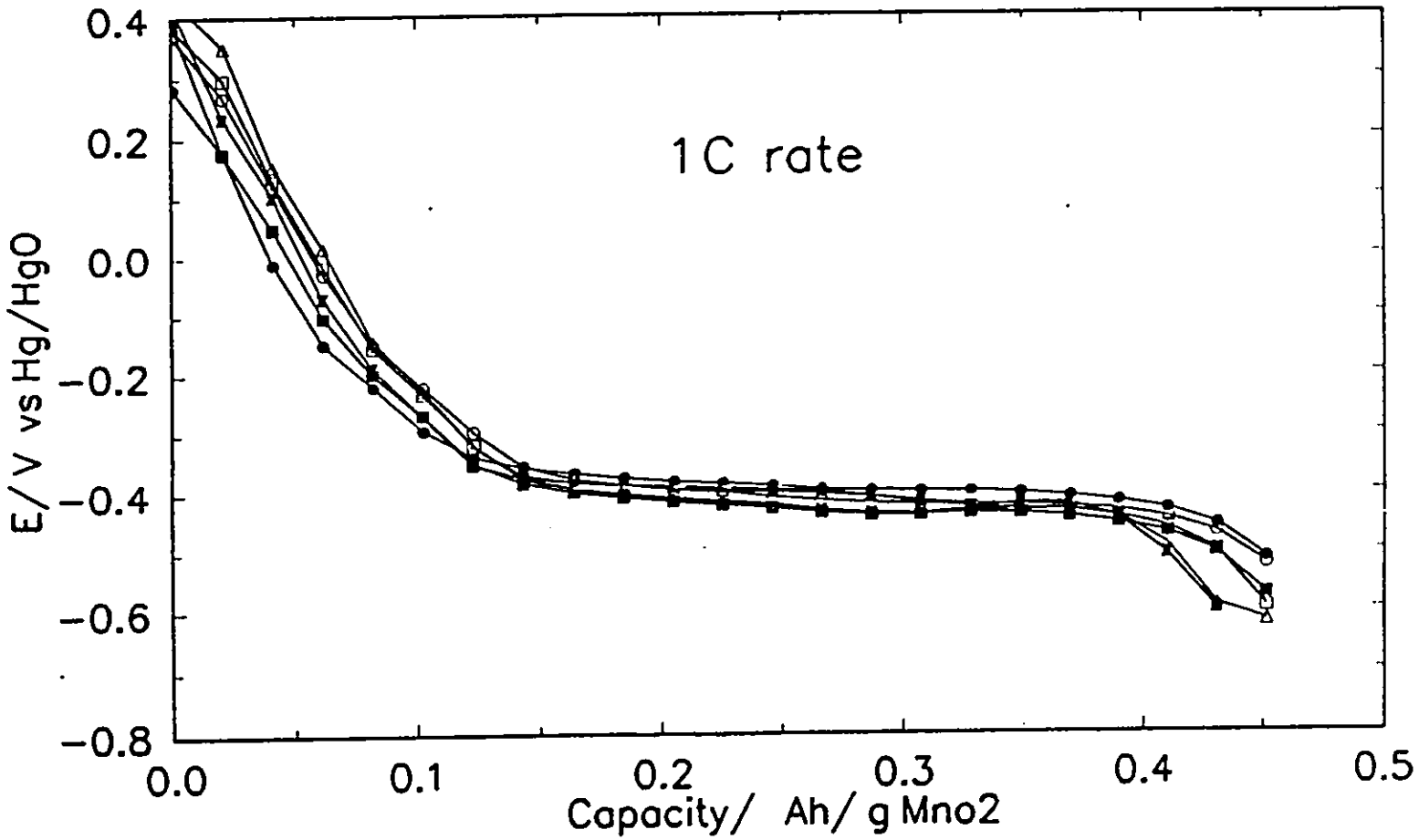

Fig. 22 Discharge curves for a CM MnO_2 cathode (MnO_2 : graphite = 1 : 10) at the 1 C discharge rate for the 3rd (•), 25 (○), 57 (□), 63 (△), 78 (▽) and 95th (△) cycles.

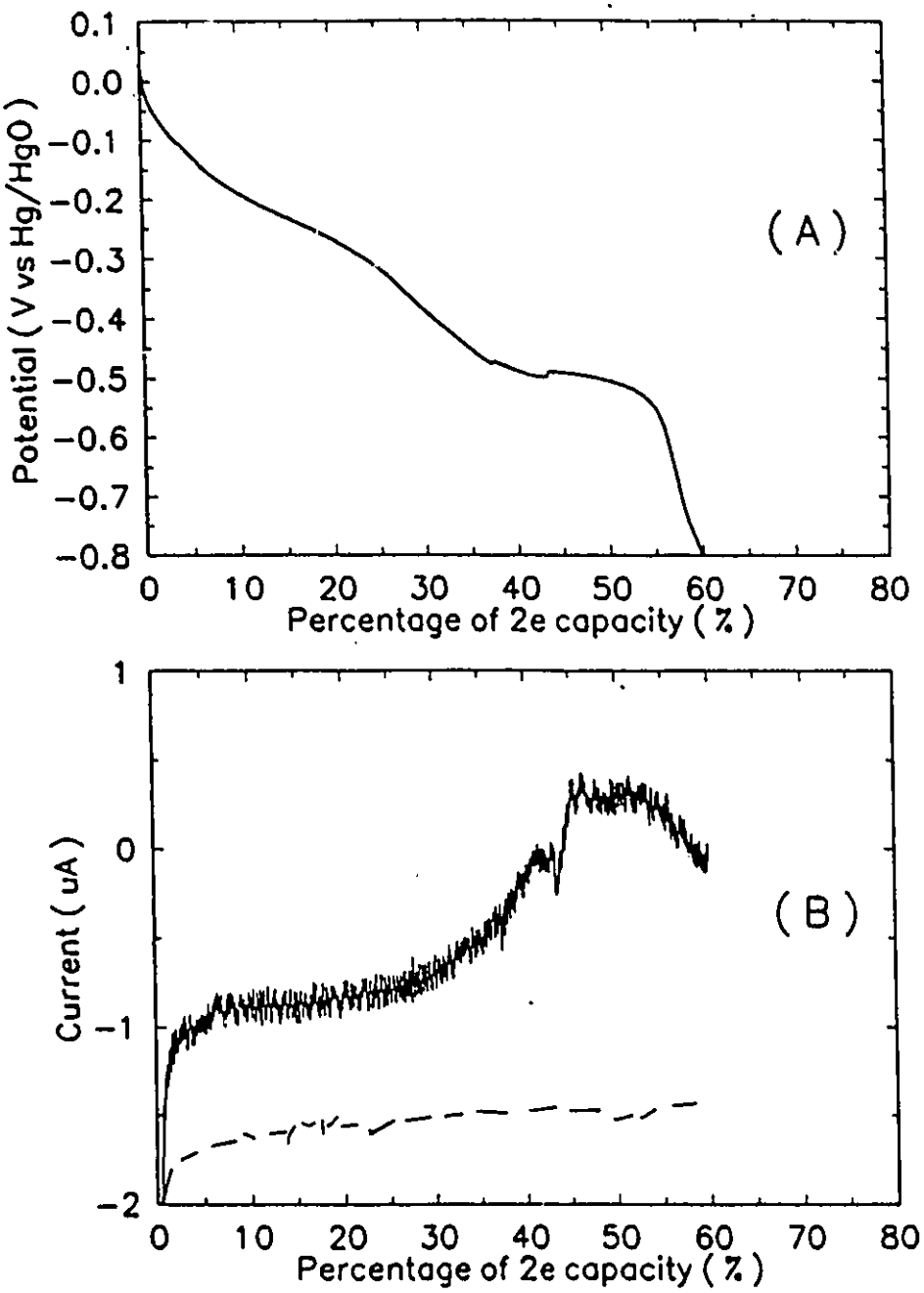

Fig. 23 Constant-current discharge of a γ-MnO_2 electrode showing the Pt detector electrode response. A. Constant-current discharge of γ-MnO_2; I density = 0.2 A g^{-1}. B. Response on the Pt detector electrode. Potential -50 mV vs Hg/HgO. Dashed line represents background current.

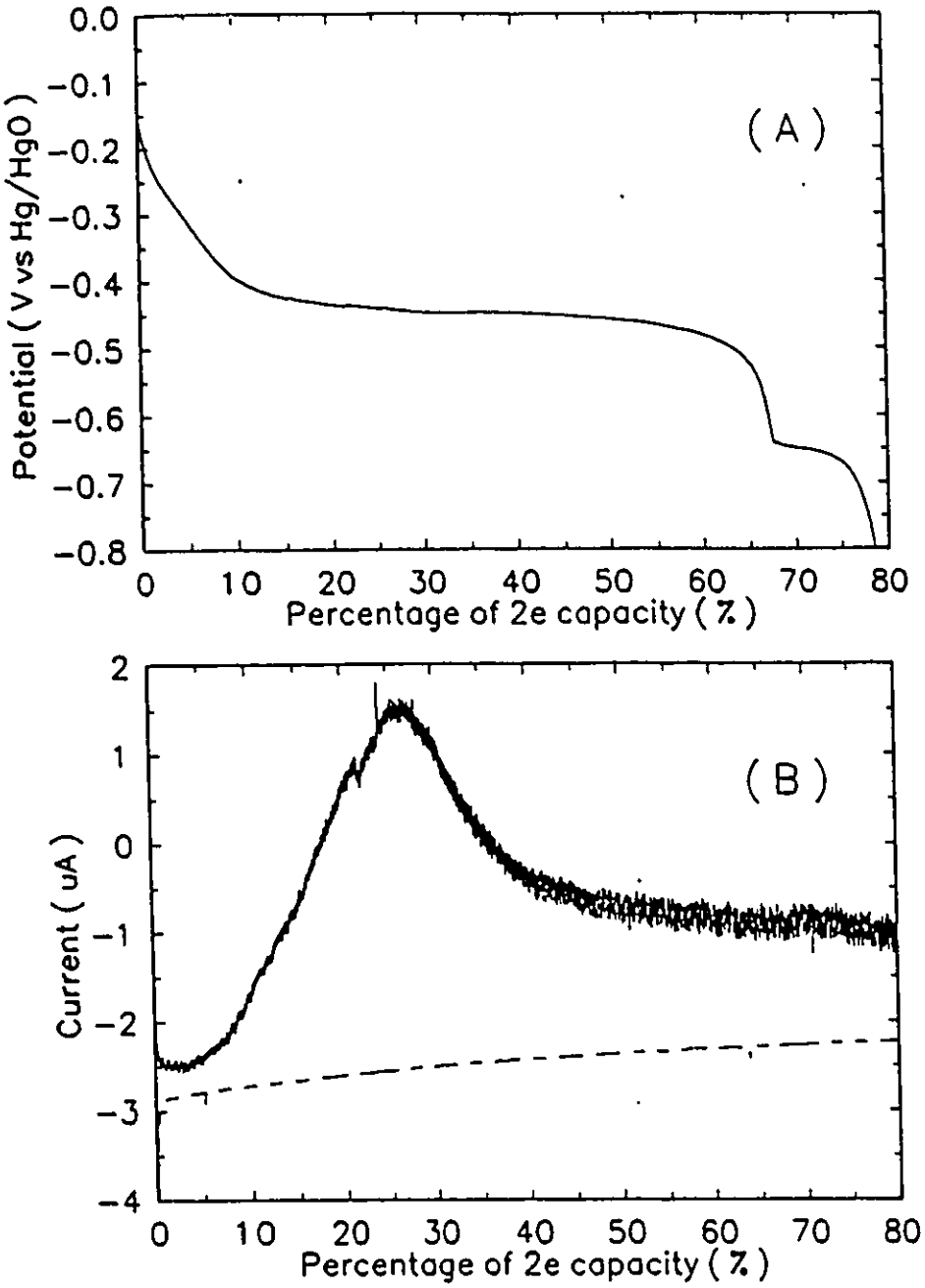

Fig. 24 Constant-current discharge of the CM MnO_2 electrode with the Pt detector/electrode. A. Constant current discharge of the CM MnO_2; current density = 0.2 A g^{-1}. B. Response on the Pt detector electrode. Potential = -50 mV vs Hg/HgO. Dashed line represents background current.

to the negative background reduction current for oxygen, referred to above.

In the first step of γ-MnO_2 discharge, which has been indicated as being largely to be homogeneous [24,25], there is already a small but significant detector response due to some dissolved species, indicating the beginning of participation of the heterogeneous mechanism; however, in the second step, which begins at approximately 30% of 2-e capacity, a significant increase of the signal arises which must result from generation of soluble species, as seen in Fig. 23(b). The soluble species may be $Mn(OH)_6^{3-}$ and it is evident that such species are generated from γ-MnO_2 but to a smaller extent than from CM MnO_2, referred to below.

These results are consistent with Kozawa's proposal [24] of a two-step reduction mechanism. In the case of CM MnO_2, Fig. 24 shows that soluble species are formed as soon as the discharge process begins. The discharge processes on the working and detector electrodes can be summarized as follows (see Fig. 24):

(i) In the range of 0%-5% of two-electron capacity, the "soluble" Mn(III) species, we suggest, remain adsorbed on the distributed surface of the porous electrode structure. Beyond ca. 5% of extent of discharge, adsorbed Mn(III) species will increase their occupancy of the C surface and the activity of soluble Mn(III) will tend to increase in the pores until the electrolyte there becomes saturated. So, during this step, the potential of the MnO_2 becomes reduced and no significant signal

yet arises at the detecting electrode. Thus, in the initial stage of discharge, a mixed heterogeneous and homogeneous mechanism would, in fact, apply.

(ii) The porous powder electrode becomes saturated by soluble Mn(III) species and the excess Mn(III) begins to diffuse out to the bulk solution, and can then provide a response signal at the Pt detector electrode. The potential of the MnO_2 electrode remains relatively stable (Fig. 24A) and the current at the detector electrode continues to increase (Fig. 24B).

(iii) The Mn(III) species then begins to be further reduced on the porous electrode, forming $Mn(OH)_2$ which begins to precipitate out of solution onto the substrate. In this step, the reductions of MnO_2 to Mn(III) and Mn(III) to $Mn(OH)_2$ are taking place simultaneously.

Another point must be mentioned about the above experiments: considering the time scale (3h) needed to discharge 100% of the theoretical two-electron capacity and the tightly constructed electrode, the experiments can be treated virtually as providing *in situ* detection of soluble Mn species, i.e. relatively no significant delay in the detector electrode response is seen. In other words, almost as soon as soluble low-valence Mn species are formed, a response is seen at the detector electrode. Similar results are found from the spectro-electrochemical measurements.

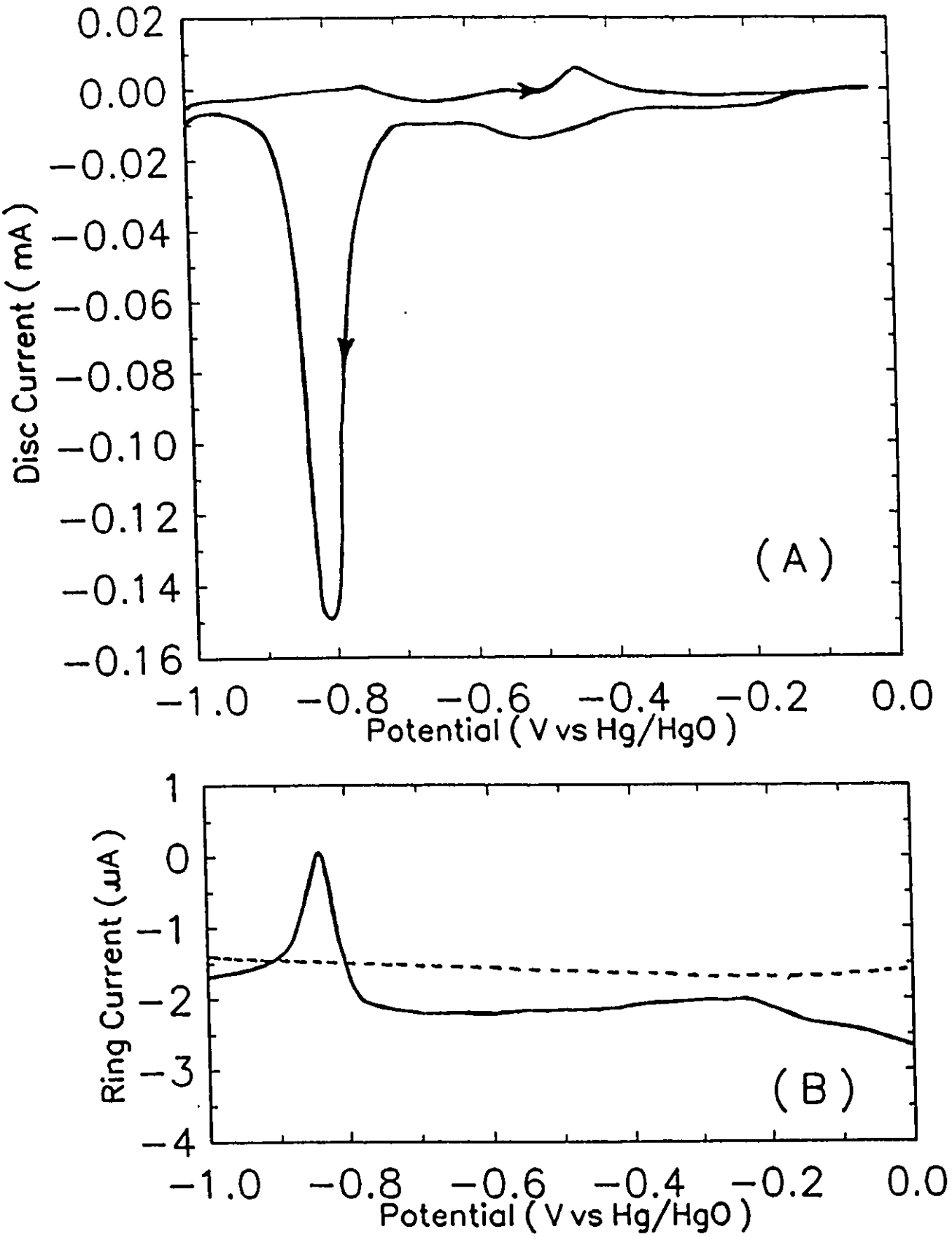

Fig. 25 A) CV profile of a CM MnO_2/acetylene black RRDE electrode, on the MnO_2 disc, at a sweep-rate of 0.5 mV s^{-1} and rotation rate of 2000 r.p.m.
B) Dependence of corresponding ring (Au) current on the electrode potential of the disc. The Au ring potential was held at -0.1 V vs Hg/HgO. Dashed line shows background current.

4.1.4 Detection of Mn(III) Intermediate(s) at the RRDE Electrode

Fig. 25 shows the results derived from experiments at a ring-disc electrode rotated at 2000 rpm with continuous bubbling of N_2. Fig. 25A shows the signal on the MnO_2 disc electrode while Fig. 25B that on the Au-ring held at -0.1 V. When the electrode is rotated, the soluble low-valence species formed at the disc are spun out to the ring and re-oxidised there.

Because the MnO_2 powder constituting the disc had to be hand-pressed onto the surface of the matrix, the contact between the MnO_2 particles and the carbon matrix could hardly be the same from one electrode to another, that is the contact resistance of the electrodes was unavoidably not uniform from one electrode to another; hence the cathodic polarization at each of the electrodes was not identical, so that some variation of polarization of the electrodes was unavoidable. However, considering the length of time (25 min.) which it took for the potential to change from the initial value (0.0 V) to the potential of appearance of the cathodic peak (about -0.75V), the MnO_2 particles can be treated as being firmly coated on the surface of the matrix otherwise they would have been thrown cut from the disc during the above period.

Fig. 26 shows the change of ratio of the anodic reoxidation charge to the cathodic reduction charge at the MnO_2 disc electrode, with electrode rotation rate.

Two aspects are to be noted here: firstly a significant

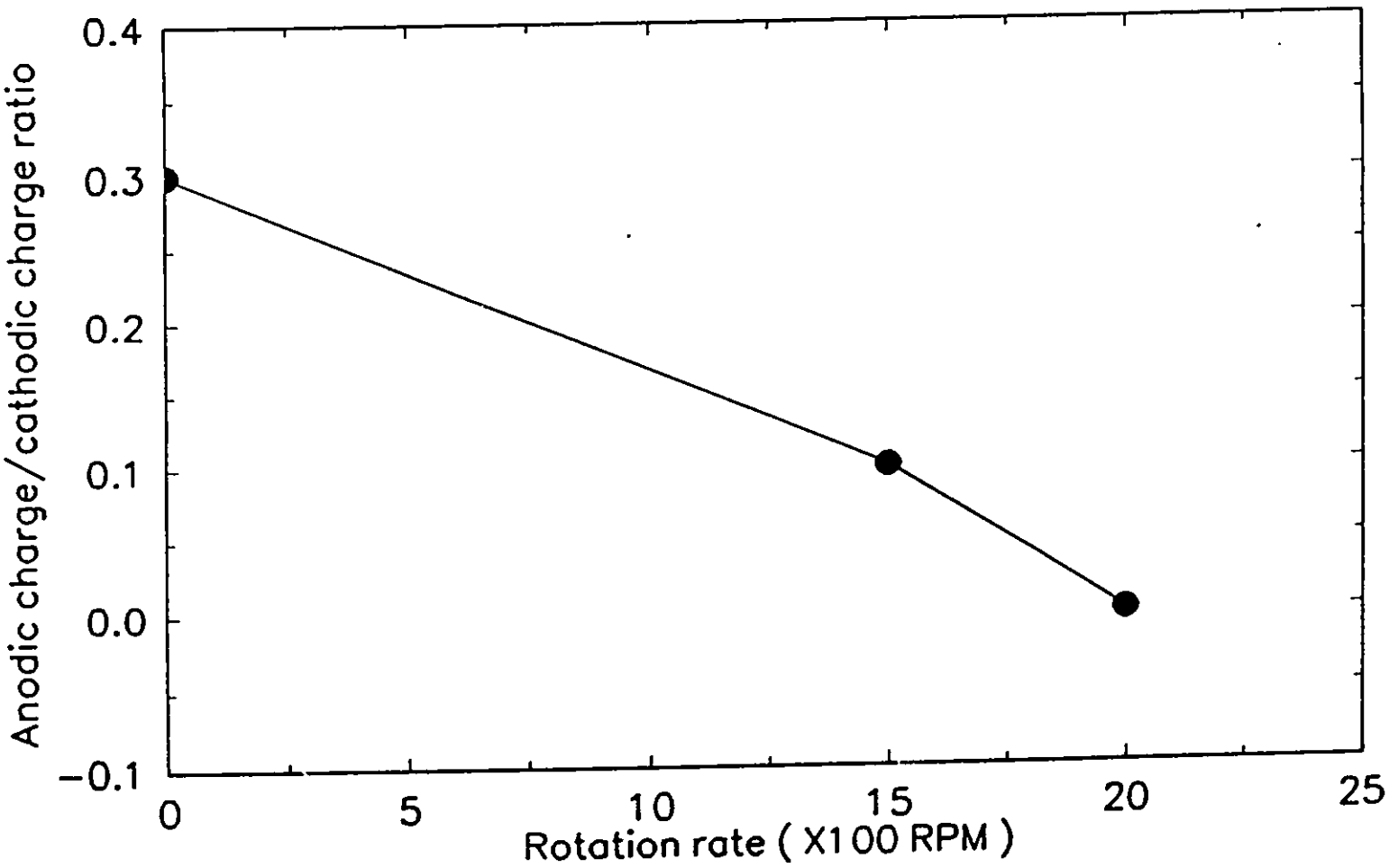

Fig. 26 The change of the ratio of anodic to cathodic charge at a CM MnO_2/acetylene black matrix electrode with rotation rate.

oxidation peak arises at the ring (Fig. 25B) corresponding to the peak for reduction of MnO_2 in the disc electrode (Fig. 25A) when the latter was rotated. This result supports the previous *in situ* observation of formation of soluble Mn species during discharge. Secondly, the ratio of the re-oxidation charge to the reduction charge at the MnO_2 disc electrode decreases with increase of rotation rate. When the rotation rate is high enough, *no* re-oxidation signal is detectable (Fig. 26); this shows that the CM MnO_2, like γ-MnO_2 [34], can be fully reduced to soluble species, assisted by rotation (mass-flow), given sufficient time.

Because the MnO_2 has to be accommodated in or at the porous carbon material, the soluble species tend to stay there, but if the rotation rate is high enough, the soluble species can be spun away to bulk solution soon after they are generated by reduction of MnO_2 and have diffused to the surface of the matrix. If the electrode is, however, kept stationary, most of soluble species can, of course, remain adsorbed or occluded in the vicinity of the electrode surface except for some small fraction that still diffuses into the bulk solution. These adsorbed and absorbed ions could be further reduced to $Mn(OH)_2$ precipitated onto the porous electrode and then re-oxidised to MnO_2 on recharge.

The electron-proton mechanism, proposed by Kozawa, probably best explains the first reduction step of γ-MnO_2. Because some Mn(IV) and Mn(III) should then be co-existent in the solid

phase, corresponding to the proposed homogeneous reduction mechanism, there should be no significant Mn(III) species dissolved into the electrolyte solution. Since only a very small amount of soluble Mn(III) species was detected in the first reduction step of γ-MnO_2 in our experiments, this theoretical assumption has now been supported experimentally. Of course, a relatively small fraction of Mn(III) could dissolve into the electrolyte solution, but the major fraction of the Mn(III) species evidently stays inside the solid phase, co-existing with Mn(IV). This co-existence of Mn(IV) and Mn(III) in one solid phase, obviously relies on the special structure of the γ-MnO_2. At that stage of discharge, the products can be delivered back as MnO_2 on recharge.

After sufficient protons have become transferred into the γ-MnO_2 lattice, upon reduction, the latter initially expands but then becomes degraded to an amorphous Mn(III) material which is non-rechargeable. Since the structure which allows the Mn species in different oxidation states to co-exist in a single phase, eventually disappears, so the Mn(III) species could dissolve into solution freely.

In the case of CM and Blank MnO_2, the situations are quite different from that of γ-MnO_2. Obviously, the structures of those two MnO_2 materials are different from that of γ-MnO_2. The electrochemical characteristics of the blank MnO_2 are only similar to those of the "γ-MnO_2" electrode in a state where the "lattice" has become collapsed (for example, the CV profile at

blank MnO_2 electrode on the first cycle is the same as that for the second and subsequent cycles of "γ-MnO_2" which has been deeply discharged to -1.0 V initially). In addition, relatively large amounts of soluble Mn(III) species are detected even in the early stage of discharge at CM MnO_2 and Blank MnO_2. These results suggest that the γ-MnO_2 type of lattice, which leads to the first electron reduction of γ-MnO_2 being by the homogeneous pathway, is not the same as that in both the Blank and CM MnO_2.

Section II. *In-situ* Spectro-Electrochemical Methods

4.2.1 Detection of Mn(III) Species by Spectroelectrochemistry

The aims of these experiments were

a) to establish if optically detectable, soluble Mn(III) intermediates were formed both on discharge and recharge of the three MnO_2 materials and

b) to relate their formation and consumption to the electrochemical discharging and recharging curves, i.e., to states of discharge and recharge of the active material.

The concentrations of the $Mn(OH)_6^{3-}$ species (as chemically identified in the work of ref. 89) involved were calculated on the basis of the Beer-Lambert law, $Ln[I_o/I] = \varepsilon LC$, where I_o is the intensity of incident light and I that after optical absorption in the cell. In this equation, the extinction

coefficient ε=385 [89] and the path-length L of the cell used was 1 cm. The concentrations of $Mn(OH)_6^{3-}$ species referred to elsewhere in this thesis were calculated as described above.

The cell and spectrophotometric procedure described earlier were employed in this part of the work in order to follow more quantitatively the production or consumption of Mn(III) species generated on discharge or recharge of the MnO_2 cathode preparations.

With excess electrolyte it is easy to observe a brown coloured soluble species being generated as a product of the cathodic process. The species and their dissolution into bulk solution are quite critical in the mechanism of discharge/ recharge of the MnO_2 material.

The solid line (Fig. 27) shows a typical optical absorption spectrum of soluble, low-valent Mn(III) species formed in the process of discharge of CM MnO_2. Hexacoordinated trivalent Mn complexes generally exhibit a single band in the 470 nm region [87,88]. Direct measurement of the spectrum of trivalent Mn in concentrated KOH solution confirmed this result in showing a single band in the visible region with a peak at 465 nm, which may therefore, with good reliability, be ascribed to the ion $[Mn(OH)_6]^{3-}$, based on ref. 89. Thus, quite positively, the low oxidation state Mn species could be identified as hydrous Mn(III) ion from the spectrum.

Such trivalent Mn species were found to be formed not only in the discharge process, but also in recharge. In Fig. 27 are

compared the absorption spectra of the species formed in discharge (solid line) with those in the recharge process (dashed line). It is seen that the shapes of the curves and the locations of maximum absorption (465 nm) are exactly the same. Hence the same Mn ion species are generated both in the cathodic and the anodic processes, i.e. the discharge/recharge processes are *chemically* reversible.

Considering the rechargeability of the material, it might be concluded, logically, that the mechanism of CM MnO_2 on discharge should be similar to that on recharge; at least both processes evidently involve the same intermediate(s). As was described earlier, Mn(III) species can also be detected at CM MnO_2 already at an early stage of discharge (unlike the behaviour of γ-MnO_2).

Fig. 28A shows typical optical absorption spectra of the soluble, low valent Mn(III) species formed in the process of discharge at CM MnO_2, Blank MnO_2 and γ-MnO_2 electrodes, while Fig. 28B shows the respective absorption spectra obtained in the process of recharge of the three types of MnO_2 electrodes. By comparing the spectra of the species formed in the discharge process (Fig. 34a) or the recharge process (Fig. 34b) at the three types of MnO_2 electrodes, it can be concluded that the shapes and the locations of the absorption maxima (465 nm) of all the curves in Fig. 34 are exactly the same. Hence, the same Mn ion species, which has been proven [89] to be $Mn(OH)_6^{3-}$, are formed not only in the cathodic and anodic processes of CM MnO_2

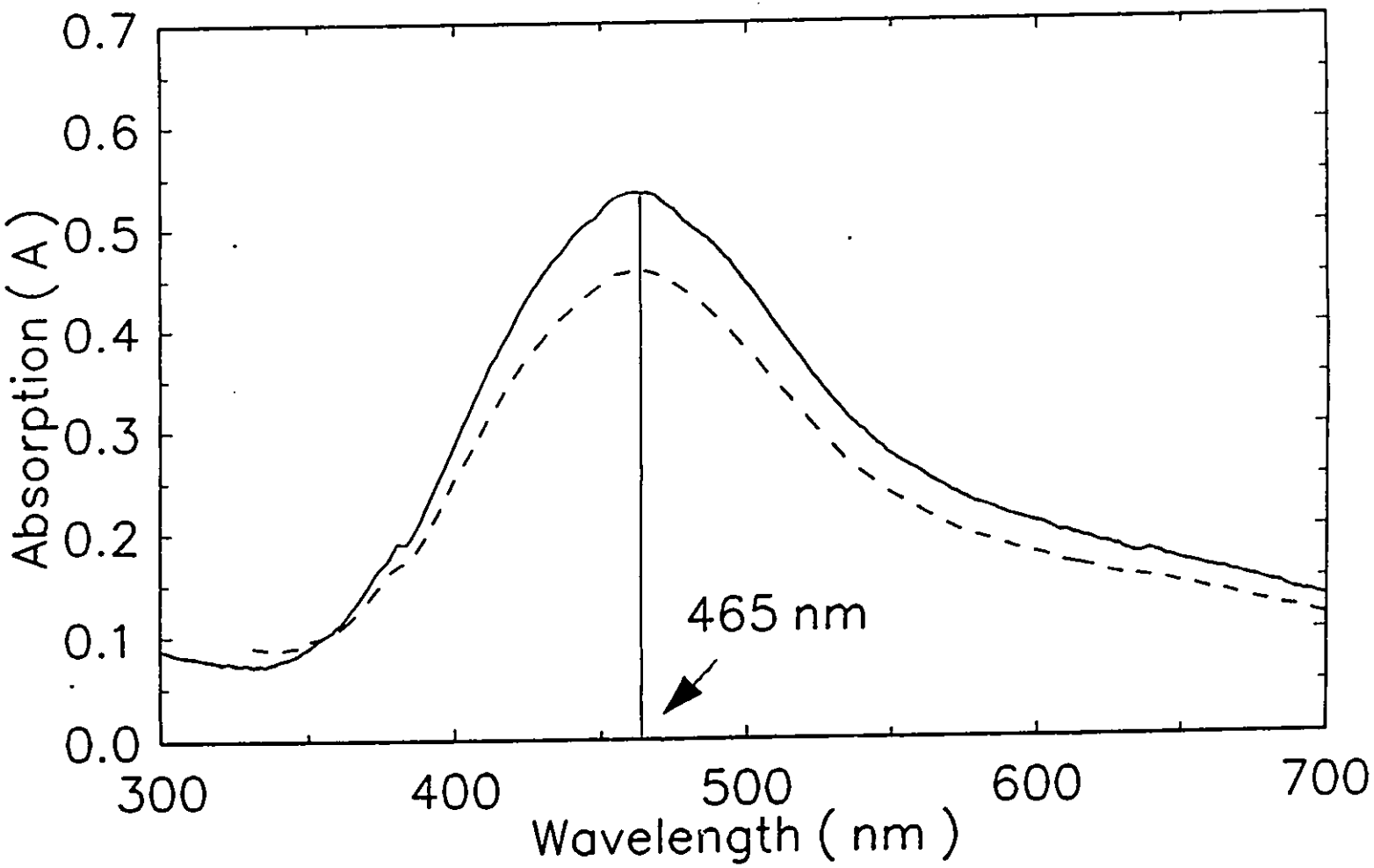

Fig. 27 UV-visible spectra of soluble Mn(III) species; solid line for 37% discharge; dashed line for 37% recharge of 2e capacity of a CM MnO_2 electrode.

electrode, but also in the cathodic and anodic processes of Blank MnO_2 and γ-MnO_2. In other words, the same Mn(III) intermediate species is generated in the polarization processes at all the three types of MnO_2, but to different extents.

4.2.2 Constant current discharge and recharge - optical experiments:

Figs. 29 and 30 show the solution-spectra observed at different states of charge established during constant current discharge or recharge. The states of charge are both expressed, for convenience of comparisons, as percentages of *discharge* capacity on both discharge (Figs. 29A and 30A) and recharge (29B and 30B) of CM MnO_2 and blank MnO_2 electrodes, respectively. Also, for other results presented in this thesis, the "percentage" also means the percentage of capacity referred to the discharge direction unless otherwise specified. This procedure facilitates plotting of discharge and recharge curves, e.g. as in Figs. 32, 33 and 34 on a common scale of "discharge" capacity. The first lines at 0% discharge or recharge capacity in both Figs. 29A and 30A are the background curves measured before polarization of the electrodes was commenced; no detectable absorption peaks are observed.

Separate experiments showed a) that double-layer charging of the carbon-support material contributed less than 3% to the discharge and recharge capacities referred to above and b) that reduction of Bi(III) to Bi(0) or reoxidation of Bi to Bi(III) (depending on potential ranges covered in cyclic voltammetry or

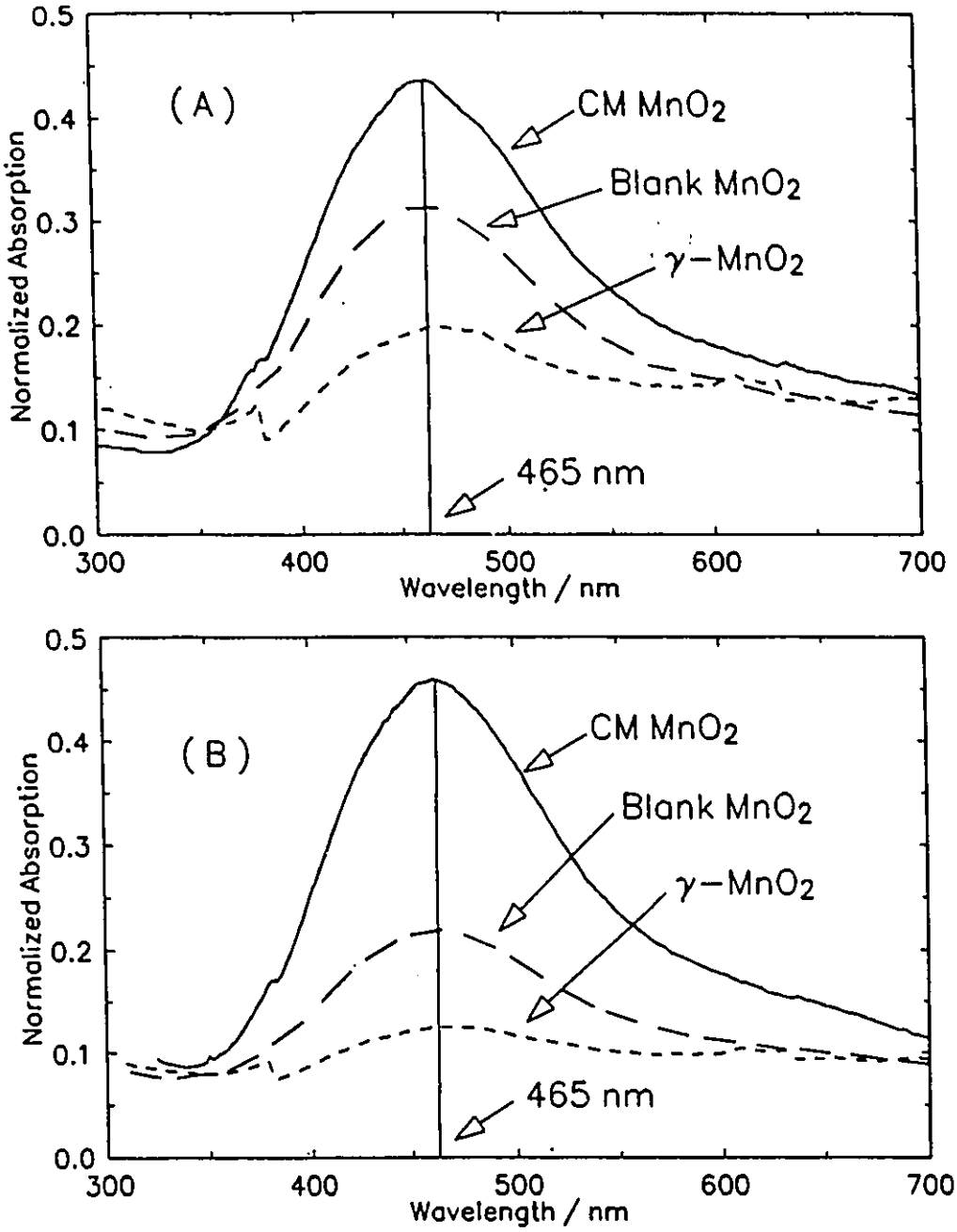

Fig. 28 (A) UV-visible spectra of soluble Mn(III) species formed in the processes of discharge at CM MnO_2 (solid line), Blank MnO_2 (long dashed line) and γ-MnO_2 (short dashed line).

(B) UV-visible spectra of soluble Mn(III) species formed in the processes of recharge at CM MnO_2 (solid line), Blank MnO_2 (long dashed line) and γ-MnO_2 (short dashed line).

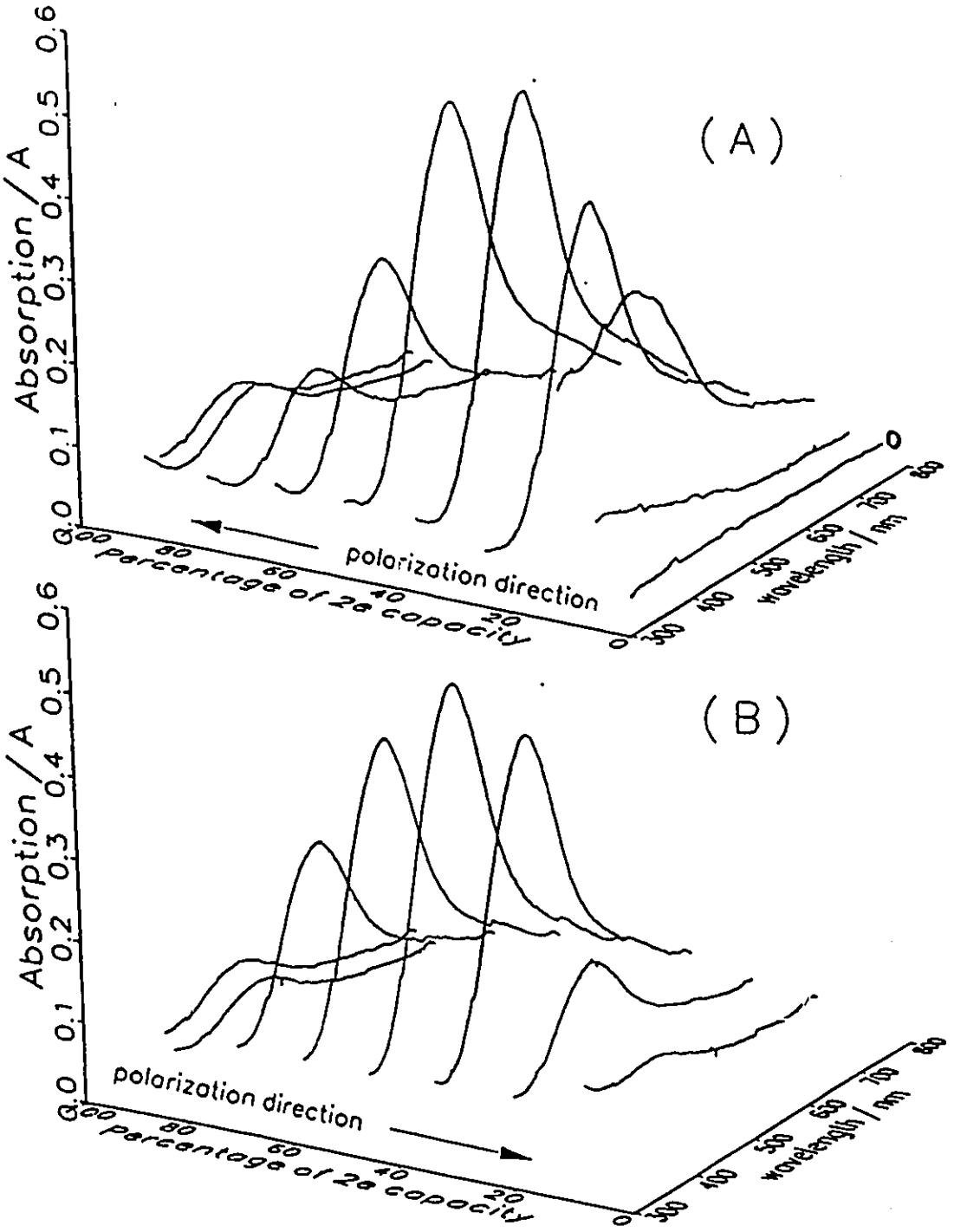

Fig. 29 The change of optical absorption spectrum of Mn(III) species with percentage utilization of discharge capacity (A) in the discharge process and (B) in the recharge process, at a CM MnO_2/Lonza graphite mixture (1:4).

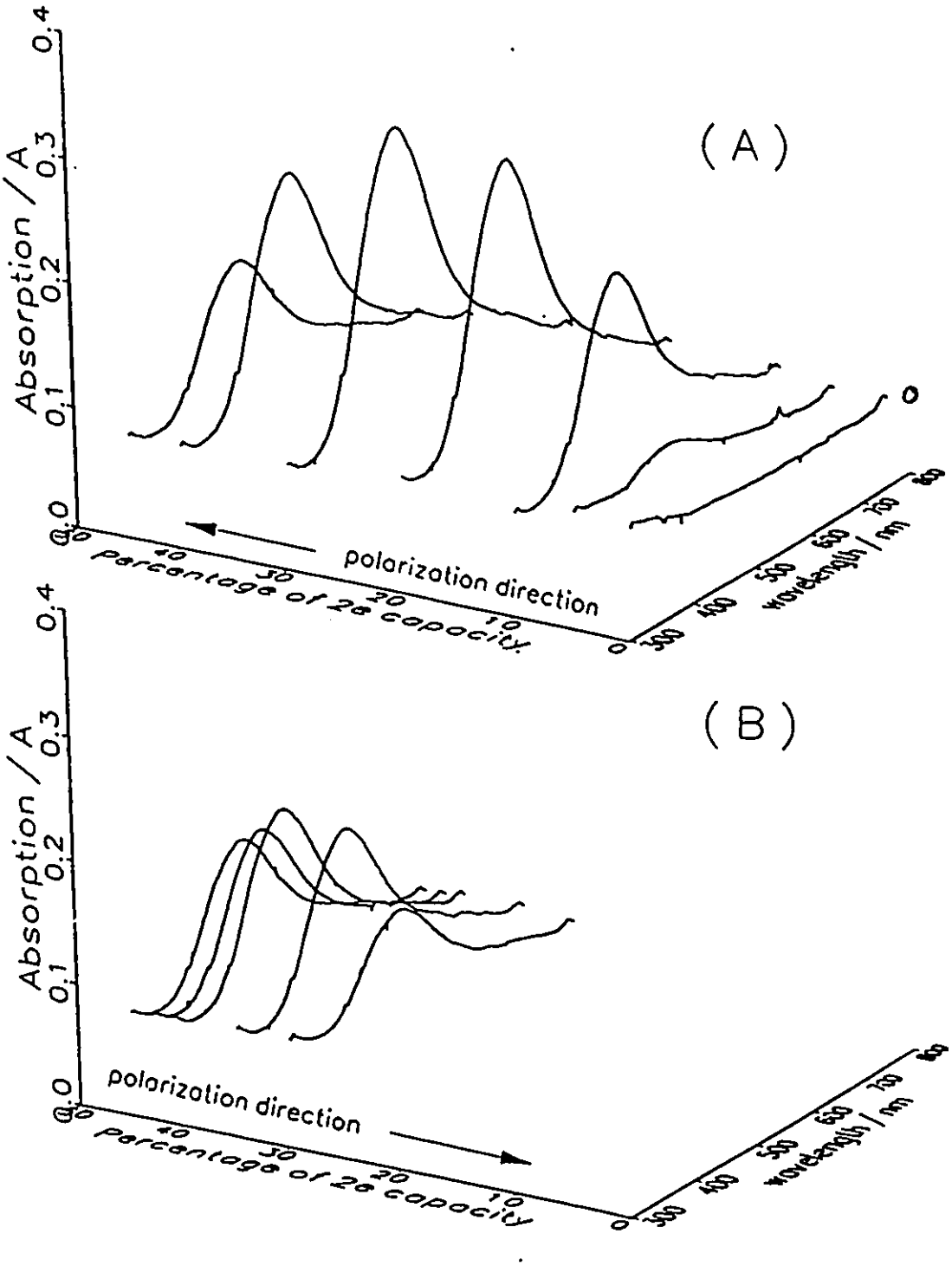

Fig. 30 The change of optical absorption spectrum of Mn(III) species under controlled constant-current conditions (0.16 A g^{-1}) with percentage utilization of capacity on discharge in the discharge process (A) and in the recharge process (B) at a "blank" MnO_2/lonza graphite mixture (1:4).

discharge/recharge galvanostatic experiments) gave rise to only a small fraction of the measured two-electron capacity of the CM MnO_2 and none at all if cycling was conducted above a potential of ca. -0.6 V vs Hg/HgO.

It is to be noted that due to the porous nature of the MnO_2 electrode and the consequent distributed resistance, mainly of the MnO_2 material (since strong aq. KOH is used as the electrolyte, cf. ref. 44), the active material utilization is not necessarily uniform during discharge, especially at high rates of discharge. However, close to 80% of 2e charge is realized at a 6C rate and this is little different from that at a relatively low C/10 rate. It is difficult to perform reproducible experiments much lower than the latter rate since discharge and recharge then require more than 20h.

From the practical point of view, one of the main and remarkable advantages of the CM material is that it can be discharged and recharged at *high* rates without either appreciable attenuation of capacity or lowering of the discharge plateau potential, as shown in Fig. 15 (Section 1 of this chapter).

The $[Mn(OH)_6]^{3-}$ is not a stable ion; it can be oxidized to MnO_2 by oxidizing agents such as O_2. It can also *disproportionate* in the following way, represented in terms of the simple cations:

$$2Mn^{3+} + 2H_2O = MnO_2 + Mn^{2+} + 4H^+$$

or to corresponding species in alkaline solution.

Considering the instability of the trivalent Mn state, there are two possibilities for interpretation of the decrease of $Mn(OH)_6^{3-}$ concentration in the discharge and recharge processes. One is the decomposition of $Mn(OH)_6^{3-}$, another is redeposition of Mn species back to the porous graphite electrode to form $Mn(OH)_2$ (further reduced) in the discharge process and MnO_2 (further reoxidised) in the recharge process.

In order to test the stability of dissolved low oxidation-state Mn species during periods of time involved experimentally interest, a time-dependence experiment was carried out under the same conditions as those in the electrochemical experiments, the results of which are shown in Fig. 31. The period of observation was up to 5 hours, which was the time needed for the single discharge or recharge half-cycles to be completed. The absorption was recorded at the maximum absorption wavelength (465 nm). The results show that the low-valent Mn species are, in fact, quite stable over the period of time involved in a single discharge/recharge cycle. Hence redeposition with reduction of Mn(III) in cathodic polarization is the main reason for the decrease of the $Mn(OH)_6^{3+}$ concentration and not auto-decomposition. In other words, during the discharge and recharge, the Mn(III) formed in the first electron transfer stage is soluble under both conditions and further discharge or recharge can drive the soluble species to solid state $Mn(OH)_2$ or to MnO_2 onto the porous graphite electrode.

Since the CM MnO_2 has been proved to be rechargeable, it is

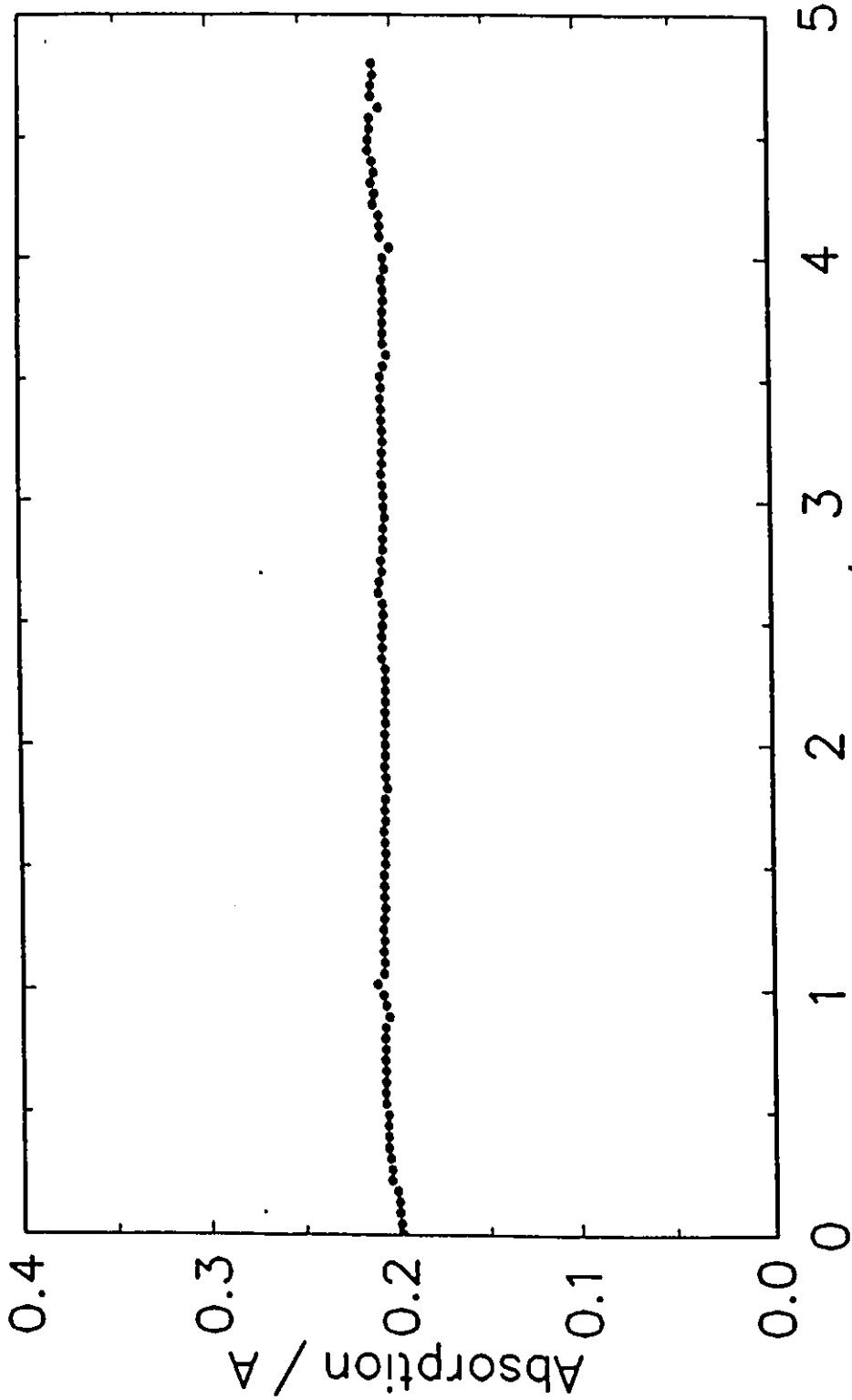

Fig. 31 Lack of change of the absorption of Mn(III) species with time.

logical to expect that the regenerated MnO_2 must be rechargeable, i.e. for CM MnO_2, the soluble Mn(III) species, both in solution or adsorbed on the porous electrode structure, can be reoxidized back to rechargeable MnO_2. The presence of Bi(III) is, however, essential for this behaviour to arise.

It should be emphasised that the $Mn(OH)_6^{3-}$ concentration was stable for 5 hours, but this does not necessarily mean that $Mn(OH)_6^{3-}$ is a stable ion over substantially longer periods of time. Actually, in our long-period cycling experiments, after two days or more, some solid MnO_2 was found to have become deposited on the walls of the cell compartment in which the MnO_2 electrode was accommodated, and on the separator. Of course, in a practical cell without "free electrolyte", such processes are minimized.

There remains another critical question about the soluble species before the discussion of the detailed reaction mechanism can be entered into, that is, how much Mn (absolutely) could diffuse into the solution. By means of Atomic Absorption Spectroscopy (AAS), the total amount of Mn species which diffused away from the electrode was therefore evaluated quantitatively. Two test experiments were carried out: in the first, all the Mn species including solid MnO_2 on the separator and on the walls of cell, and the $Mn(OH)_6^{3-}$ in the solution were collected. 5% of the total MnO_2 was found diffused into the solution. In the second test, just $Mn(OH)_6^{3-}$ in the solution was collected. The concentration of Mn(III) was found to be

$2.4x10^{-3}M$. The saturation concentration has been reported as $4.4x10^{-3}M$. The amount of the Mn(III) in the solution was equivalent to 2% of total MnO_2. The experiments took approximately 48 hours. In the uv-visible spectroelectrochemical measurements, the concentration was also found to approach the saturation value. The data are summarized in Table II.

TABLE II: Summary of Data on Formation of Soluble Mn(III) Species

Experiment	concentration of $Mn(OH)_6^{3-}$	percentage of total MnO_2	saturation concentration
1	6.1×10^{-3}	5 %	4.4×10^{-3}
2	2.4×10^{-3}	2 %	4.4×10^{-3}

Figs. 32A and B show comparisons of constant-current discharge and recharge curves with the maximum optical absorption of $Mn(OH)_6^{3-}$ species derived from Figs. 29A and B at 465 nm as observed simultaneously with the electrochemical response at various stages of discharge and recharge at a CM MnO_2/graphite mixture. The arrows on the curves indicate the directions of change of polarization; broad small background absorption values have been subtracted.

Figs. 33A and B show corresponding comparisons of the

discharge and recharge curves at the Blank MnO_2 (without Bi) electrode (compare Figs. 32A and B for CM MnO_2) with the 465 nm absorption of $Mn(OH)_6^{3-}$ species at various stages (expressed as % discharge capacity) of discharge and recharge. Again, allowances for the background absorption were made.

Figs. 34A and B show comparisons similar to those in Figs. 33A and B but for the I.C.γ-MnO_2 electrode, again with background subtraction. Finally, in Fig. 35 are compared the maximum absorption values for $Mn(OH)_6^{3-}$ species observed at (a) the CM MnO_2 (b) the Blank MnO_2 and (c) the γ-MnO_2 electrodes at various percentage extents of discharge.

From Figs. 29 and 30, it is seen that, before discharge there is no significant absorption over the whole wavelength range. Almost as soon as discharge begins, significant amounts of soluble $Mn(OH)_6^{3-}$ species are detectable at CM and Blank MnO_2 (solid lines in Figs. 32B and 33B) but appreciably less (Fig. 34B) at the γ-MnO_2 electrode. It is obvious and significant that small amounts of $Mn(OH)_6^{3-}$ are formed already at the *beginning* of discharge at each of the three types of MnO_2, but much *less* at the γ-MnO_2 than at the other two materials.

In the case of CM MnO_2, however, when discharge is started, absorption in the visible can be observed and continues to increase. At the stage of 25% of the two-electron capacity being discharged, the absorption density (Fig. 32B) is almost 80% of its highest value but 25% consumption of capacity is still an early stage in the overall discharge process (see Fig.

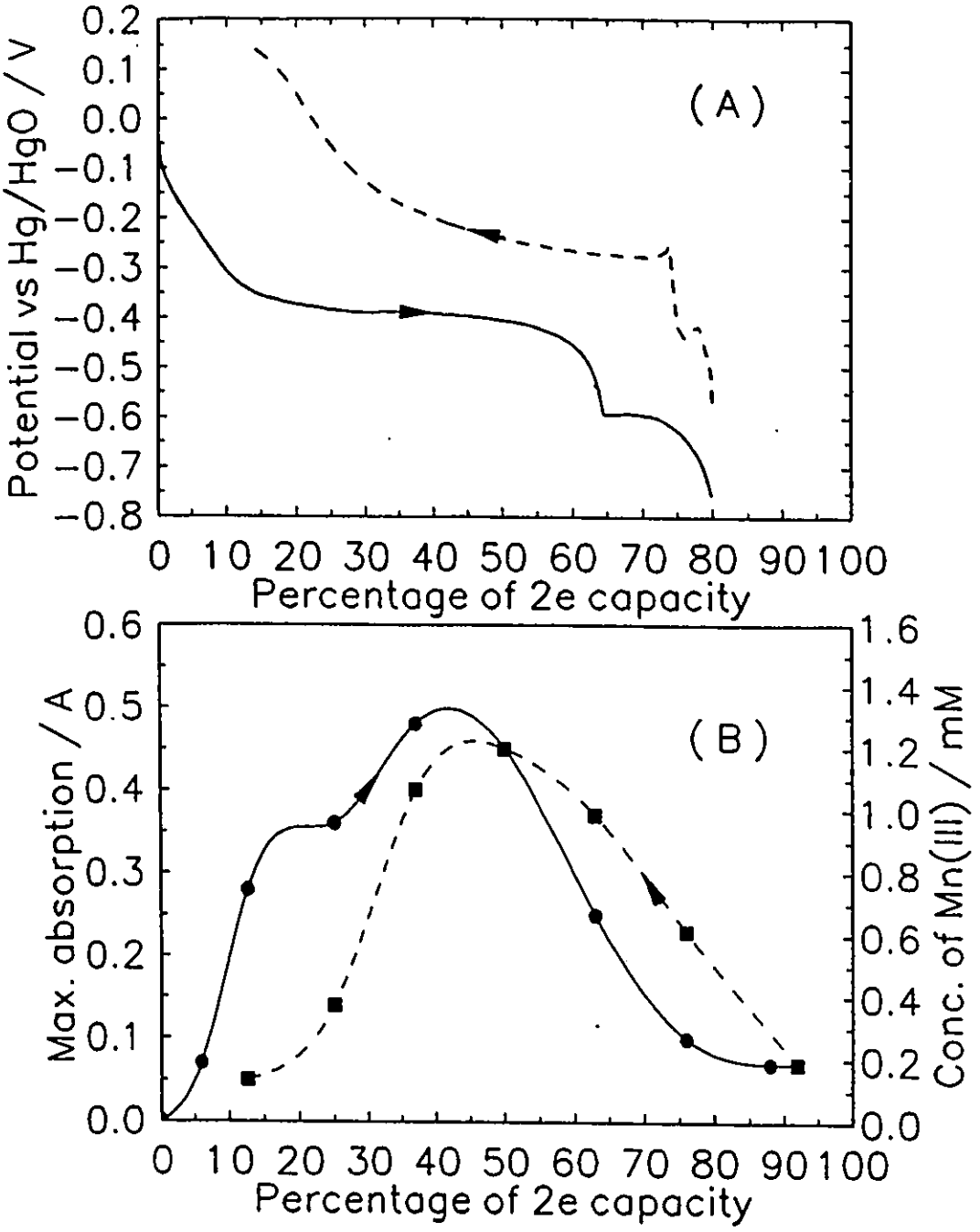

Fig. 32 Comparison of constant-current discharge and recharge curves (A) with maximum optical absorption at 465 nm at various stages of discharge and recharge (B). CM MnO_2/Lonza graphite=1:4; current-density=0.16 A g^{-1}; solid line: discharge; dashed line: recharge.

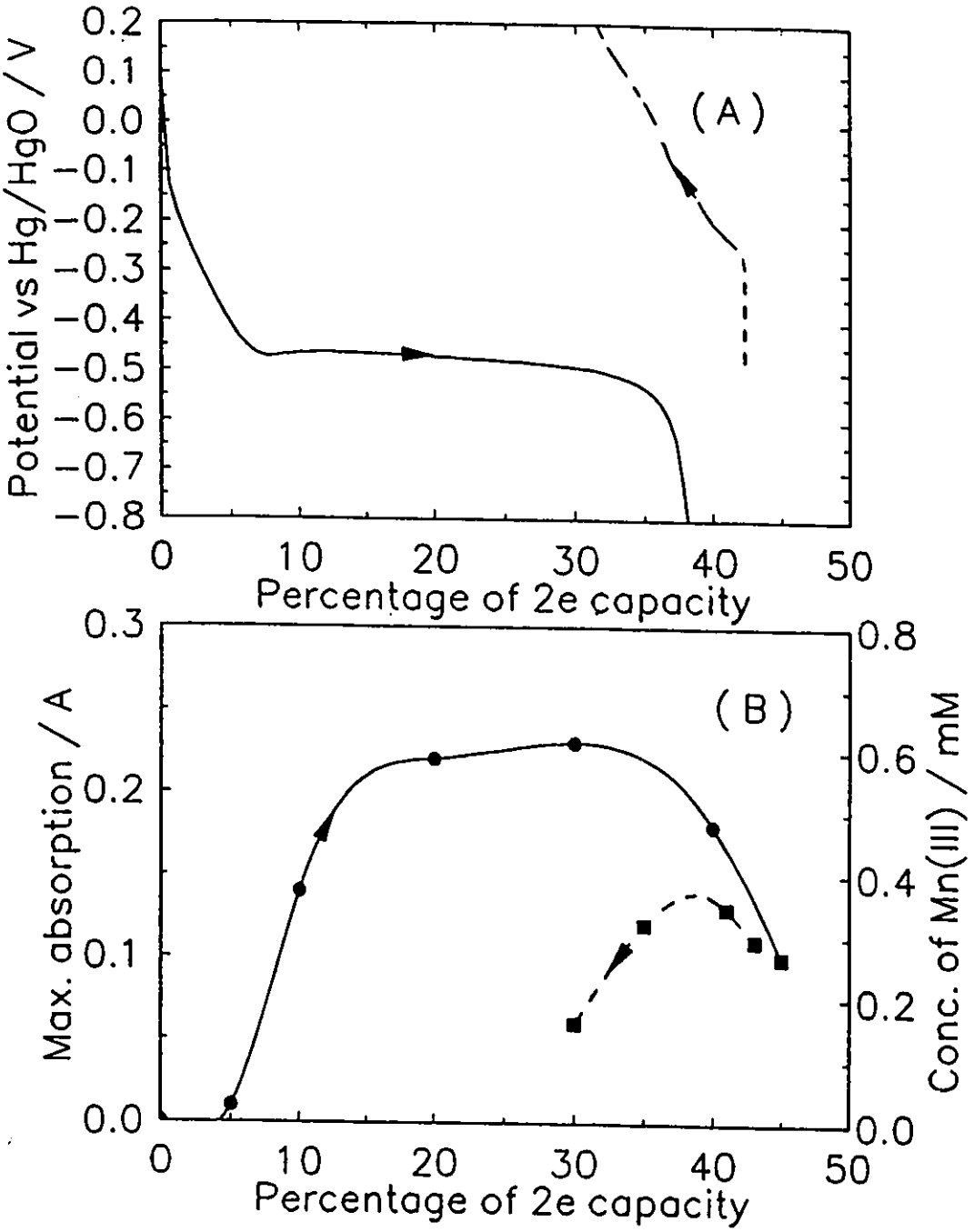

Fig. 33 Comparison of constant-current discharge and recharge curves (A) for "blank" MnO_2 with (B) maximum optical absorption at 465 nm at various stages of discharge and recharge. Blank MnO_2/Lonza graphite = 1:4; current-density=0.16A g^{-1}; solid line: discharge; dashed line: recharge.

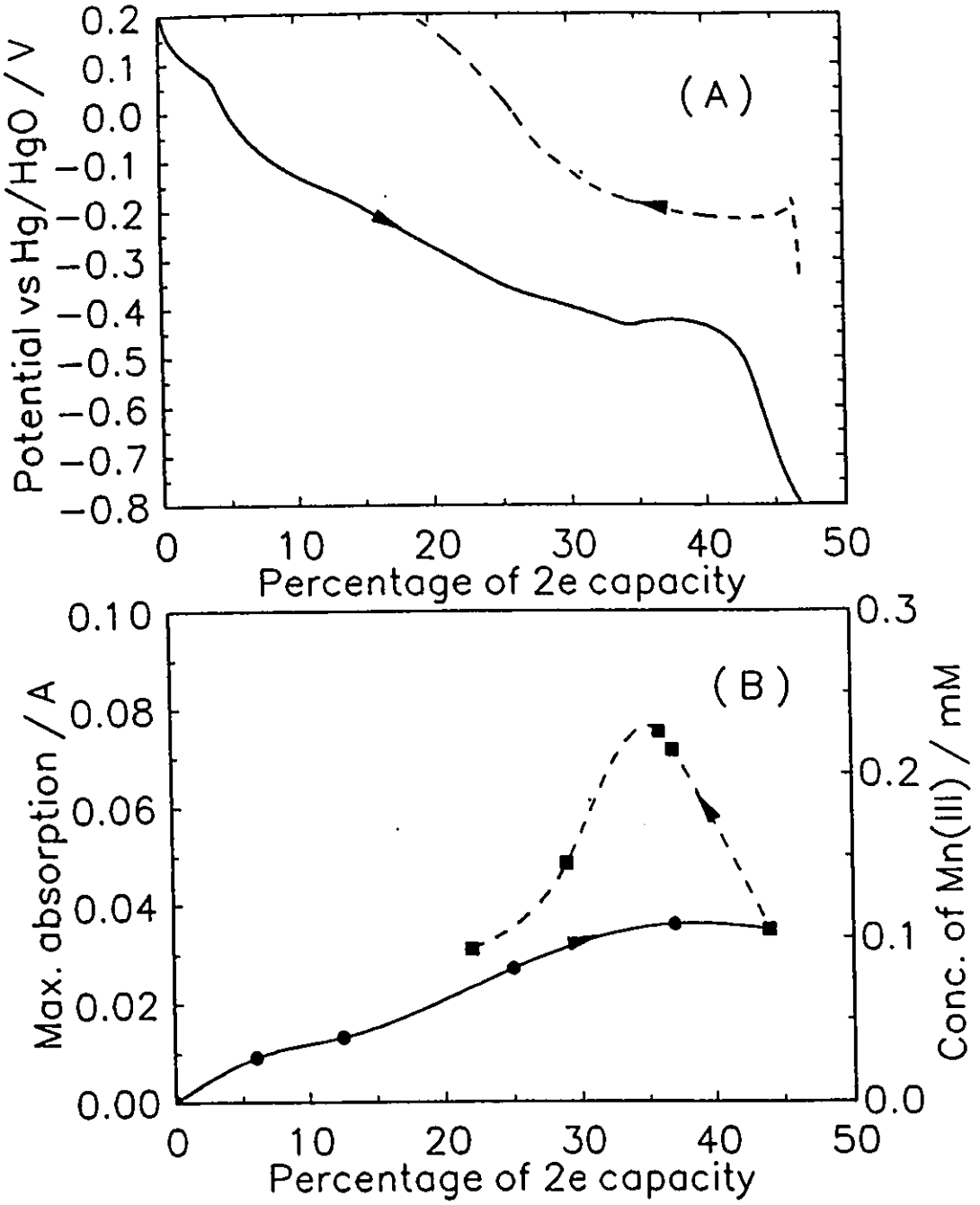

Fig. 34 Comparison of constant-current discharge and recharge curves (A) for γ-MnO_2 with (B) maximum optical absorption at 465 nm at various stages of discharge and recharge. γ-MnO_2/Lonza graphite=1:4; current-density=0.16 A g^{-1}; solid line: discharge; dashed line: recharge.

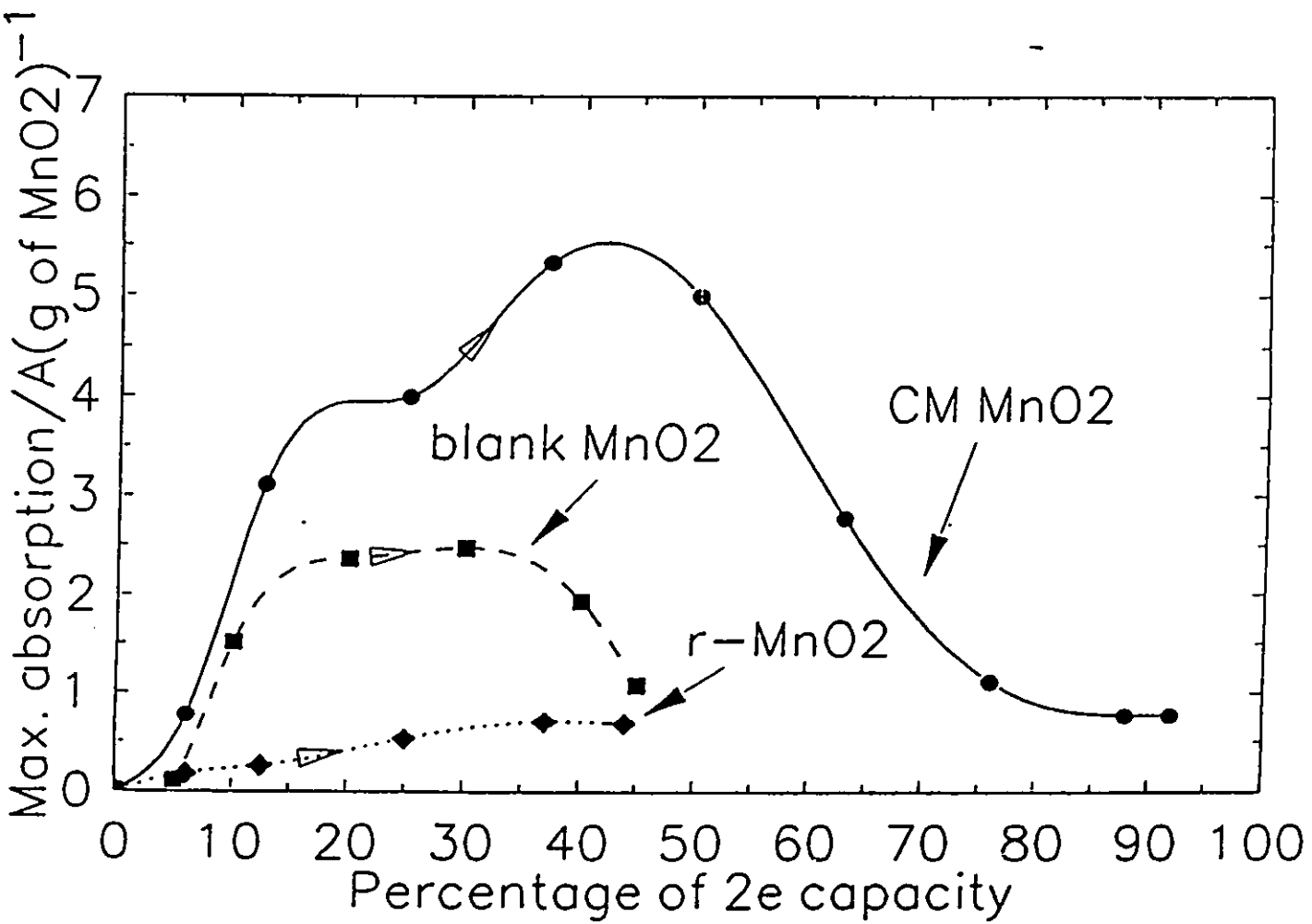

Fig. 35 Comparison of maximum optical absorption at 465 nm at various extents of discharge (%) in the process of discharge at CM MnO_2 (solid line), "blank" MnO_2 (dashed line) and γ-MnO_2 (dotted line). The concentrations of soluble Mn(III) were calculated based on the maximum absorption and the extinction coefficient (see text). MnO_2/Lonza graphite=1:4; current density=0.16 A g^{-1}.

32A). The concentration of $[Mn(OH)_6]^{3-}$ [corresponding to the optical absorption density, (see definition later) of Fig. 32B] increases in the early stage of discharge but the concentration begins to decrease in the range of 40% to 50% of two-electron capacity, with no significant decrease of the discharge potential (Fig. 32A). From Fig. 29b it is seen that similar to the cathodic process, in the early stage of recharge, the concentration of $[Mn(OH)_6]^{3-}$ increased with the polarization time (80% → 76% → 50%), and then the concentration begin to decrease in the range of 50% to 40%.

As in the case of discharge, the recharge potential (Fig. 32A) of the MnO_2 electrode did not change appreciably when the concentration of $[Mn(OH)_6]^{3-}$ began to decrease (see Fig. 32B). Comparing the density of the maximum absorption in both the discharge and recharge process (Fig. 32B), it can be seen that the densities of the maximum absorption in both cases are almost the same, i.e. the highest concentrations of soluble $[Mn(OH)_6]^{3-}$ ions in solution, formed in both the cathodic and anodic processes, are almost the same. It must be emphasised that there was a relatively large volume of free electrolyte (ca. 9 cm^3) in the optical cell.

It is seen e.g. from Fig. 32B that although a significant concentration of detectable soluble Mn(III) species arises both in discharge and recharge, in fact up to the solubility limit of ca. 4.4×10^{-3} M, it must be only a small amount of the total Mn in the given electrode, ca. 5%-10% or significantly less for

Blank or γ-MnO_2 . However, if excess free electrolyte is provided, as in the experiment of Ruetschi [34], all of the initial Mn (as MnO_2) can evidently pass into solution, given enough time. Therefore, in the present spectro-electrochemistry experiments, it appears that much of the Mn(III) species must remain absorbed in/on the graphite matrix but the amounts detectable in solution, which are different for given percentages of discharge capacity, still reflect different extents of participation of the homogeneous relative to the heterogeneous mechanism. Complementarily, the more extensive participation of the heterogeneous mechanism at CM MnO_2 is indicated thermodynamically by the extended flat (potential-independent) regions of the discharge curves (solid line in Fig. 32A).

In order to quantify the comparison between the behaviours of the three types of electrodes, "absorption density" was normalized as "A", *per gram* of MnO_2, with all three electrodes being made by using the *same* support materials and the *same* ratio of MnO_2 to C, and employing the *same preparation* procedure, so the apparent surface areas of the three types of electrodes should be the same. The N_2-desorption B.E.T method was employed to measure the actual "gas-accessible" surface areas. Three types of electrodes; γ-MnO_2, CM MnO_2 and the blank MnO_2, gave real specific surface areas of 15 m^2/g, 20 m^2/g and 19 m^2/g, respectively, i.e. each more or less of the same magnitude, a conclusion important for the comparative evaluation of the

behaviours of the three oxide materials. It can be reasonably presumed that, comparatively, the *in-situ* real areas g^{-1} of those three cathodic-material preparations, accessible to liquid aq. KOH electrolyte, will also be almost identical and certainly in order of magnitude.

Fig. 36 shows the maximum absorption densities, thus defined, recorded at the three types of MnO_2 electrodes at various percentages of capacity in the recharge process, following the discharge that gave the results in Fig. 35. In three experiments, each of the three kinds of MnO_2 electrodes was recharged up to +0.4 V vs Hg/HgO under constant current.

The present results serve to confirm and extend the preliminary results of the electrochemical detection experiments described earlier (section 4.1.3), and also the conclusion of earlier work of Kozawa et al. [26] and Ruetschi [34] which indicated the formation of soluble intermediates in γ-MnO_2 reduction. However, as shown above, *relative extents* of formation of the soluble Mn(III) species during discharge or recharge at electrodes having the same MnO_2 loading, are found to be quite different at the three materials.

These differences seem to reflect the particular characteristics of the mechanisms of reduction of each of the three types of MnO_2 materials investigated, as will be discussed later. Thus, it is seen from Figs. 35 and 36 that the *A* values for the CM MnO_2 are consistently well above those for γ-MnO_2 and blank MnO_2 throughout the course of the %-capacity curve,

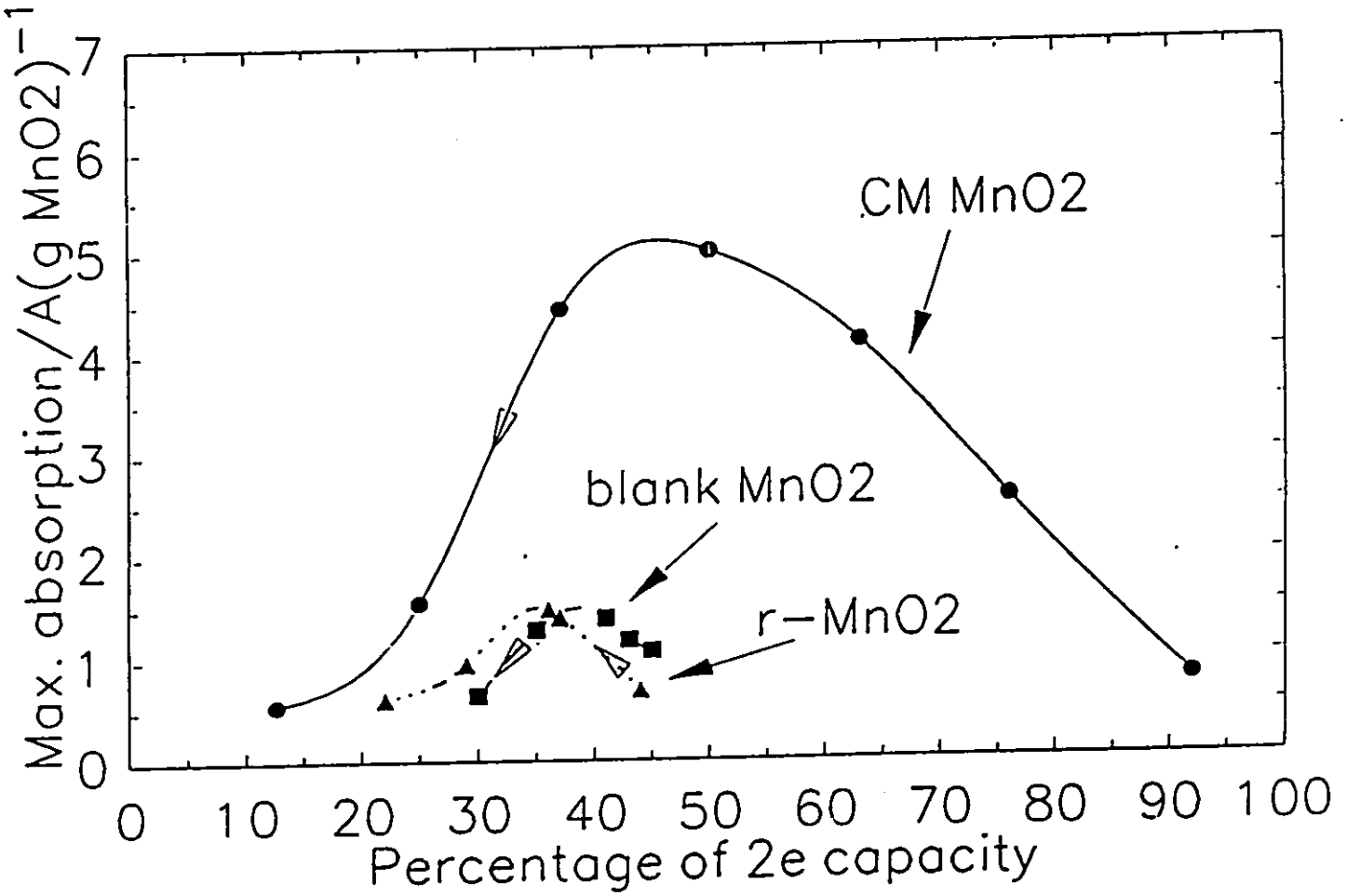

Fig. 36 Comparison of maximum optical absorption at 465 nm under constant current discharge 0.16 A g^{-1}, for various extents (%) of discharge in the processes of recharge of CM MnO_2 (solid line), "blank" MnO_2 (dashed line) and γ-MnO_2 (dotted line). The concentrations were calculated based on the maximum absorption and extinction coefficient. (MnO_2/Lonza graphite=1:4).

especially in the range 30-60%. Because both γ-MnO_2 and the Blank MnO_2 are non-rechargeable, at a given current-density the potentials of both γ-MnO_2 and blank MnO_2 electrodes reach +0.4 V vs Hg/HgO much faster than does the CM MnO_2; this is why the absorption curves for both the γ-MnO_2 and blank MnO_2 (Figs. 35 and 36) cover a much smaller range of charge capacity than that for the CM MnO_2.

4.2.3 Concentration of the Mn(III) intermediate in relation to the course of charging and discharging curves

In constant-current reduction of CM MnO_2 (solid line in Fig. 32B), the concentration of $Mn(OH)_6^{3-}$ increases continuously up to 1.3×10^{-3}M, which is near the saturation concentration (4.4×10^{-3}) of $Mn(OH)_6^{3-}$ in 9M KOH solution, then it decreases to 2.0×10^{-4}M. The curve thus exhibits a maximum which arises at around 40 percent of two-electron capacity. Logically, the peak point should correspond to the condition where the soluble Mn(III) species begins to re-precipitate, on discharge [as $Mn(OH)_2$] , out of the solution to form a solid phase on the matrix, i.e., on the surface of the porous graphite support material.

The maximum concentration of soluble Mn(III) species on *recharge* of CM MnO_2 appears at around 45% (dashed line in Fig. 32B) of the discharge percentage of two-electron capacity, where the potential on recharge is still relatively low and thus has not significantly increased (see dashed line in Fig. 32A). For

the Blank MnO_2, however, the situation is quite different from that at CM MnO_2.

Figs. 33A and B show constant-current discharge (solid line) and recharge (dashed line) curves for the Blank MnO_2, and the related curve for $Mn(OH)_6^{3-}$ concentration change, respectively. The redeposition (of Mn species as $Mn(OH)_2$) evidently does not begin until the discharge potential (Fig. 33A) significantly declines to below the "plateau" value (Figs. 33A and 33B) over which the first electron reduction is supposedly occurring. Also, compared with CM MnO_2, the rate of re-deposition (reduction) of soluble $Mn(OH)_6^{3-}$ species back to the electrode as $Mn(OH)_2$, as indicated by the slope of the curve of Mn(III) concentration vs charge capacity in Fig. 33B and Fig. 32B, is less at the Blank MnO_2 electrode. Thus, relatively to CM MnO_2, only small amounts of Mn(III) (both in the solution as $Mn(OH)_6^{3-}$ and in the solid phase as Mn_3O_4) are further reduced to $Mn(OH)_2$, so the discharged product is almost non-rechargeable in a practical potential range. For recharge of previously discharged Blank MnO_2 (see dashed lines in Fig. 33), the recharge potential increases rapidly because of the non-rechargeability of this MnO_2 material.

Based on the *in situ* optical electrochemistry experiments, conclusions can be summarized as follows:

(a) the soluble species are $Mn(OH)_6^{3-}$;

(b) they are formed both in the *cathodic* discharge and in the *anodic* recharge process;

(c) the same species are also generated, but in different amounts at Blank MnO_2 and γ-MnO_2, where a single absorption band of 465 nm is also exhibited; and

(d) the amount of $Mn(OH)_6^{3-}$ in solution increases already quite early in discharge (or recharge) and decreases in further stages of discharge (or recharge). Finally

(e) the quantities of Mn species which diffuse into the solution are determinable quantitatively, giving results which show that the solution becomes almost saturated with $Mn(OH)_6^{3-}$ around -0.3 V against HgO/Hg.

Considering that the maximum absorption values for both cathodic discharge and anodic recharge processes were almost the same, it can also be concluded that in both processes the concentration of $Mn(OH)_6^{3-}$ approaches saturation; this is virtually in agreement with what may be calculated from the extinction coefficient and the known solubility. In long-time cycling experiments, however, the $Mn(OH)_6^{3-}$ can disproportionate, giving rise to deposits of MnO_2 and $Mn(OH)_2$ on the walls of the cell and separator, or even be suspended in the electrolyte.

It appears that most of the "soluble" species remain adsorbed or absorbed in the porous electrode; the concentration of free $Mn(OH)_6^{3-}$ in the electrolyte can reach the saturation value but, in both the cathodic discharge and the anodic recharge, the soluble $Mn(OH)_6^{3-}$, both in solution and adsorbed on the porous electrode, can become redeposited respectively as

$Mn(OH)_2$ or MnO_2. Obviously, the latter materials can be recharged or re-discharged in the CM electrode, so the steps of redeposition could be one of the key processes in the rechargeability. It may be suggested that one of the roles of Bi is related to the redeposition from the soluble $Mn(OH)_6^{3-}$ (both in solution or adsorbed in the porous electrode), e.g. acting as a nucleation catalyst.

4.2.3 Multi-cycle, constant-current discharge and recharge of PM MnO_2

A number of experiments were carried out on multiple cycling of the ("Physically Modified") PM MnO_2 electrodes under galvanostatic conditions. Figs. 37A and B show, respectively, the electrochemical and optical results of such multi-cycle galvanostatic discharge (and recharge) experiments at a PM MnO_2 electrode during the first to the fifth discharges, annotated according to the cycle numbers. The maximum absorption values for $Mn(OH)_6^{3-}$ species arising at the CM MnO_2 are shown for comparison in Fig. 37B. In the first half-cycle of discharge, both the electrochemical and optical behaviours of the electrode were almost the same as those of γ-MnO_2 (see solid lines in Figs. 34A and B), i.e., only small amounts of soluble Mn(III) species arise. However, after subsequent discharge cycles, the "rechargeability" of the electrode (in terms of realizable capacity) progressively increases from the first to the fifth

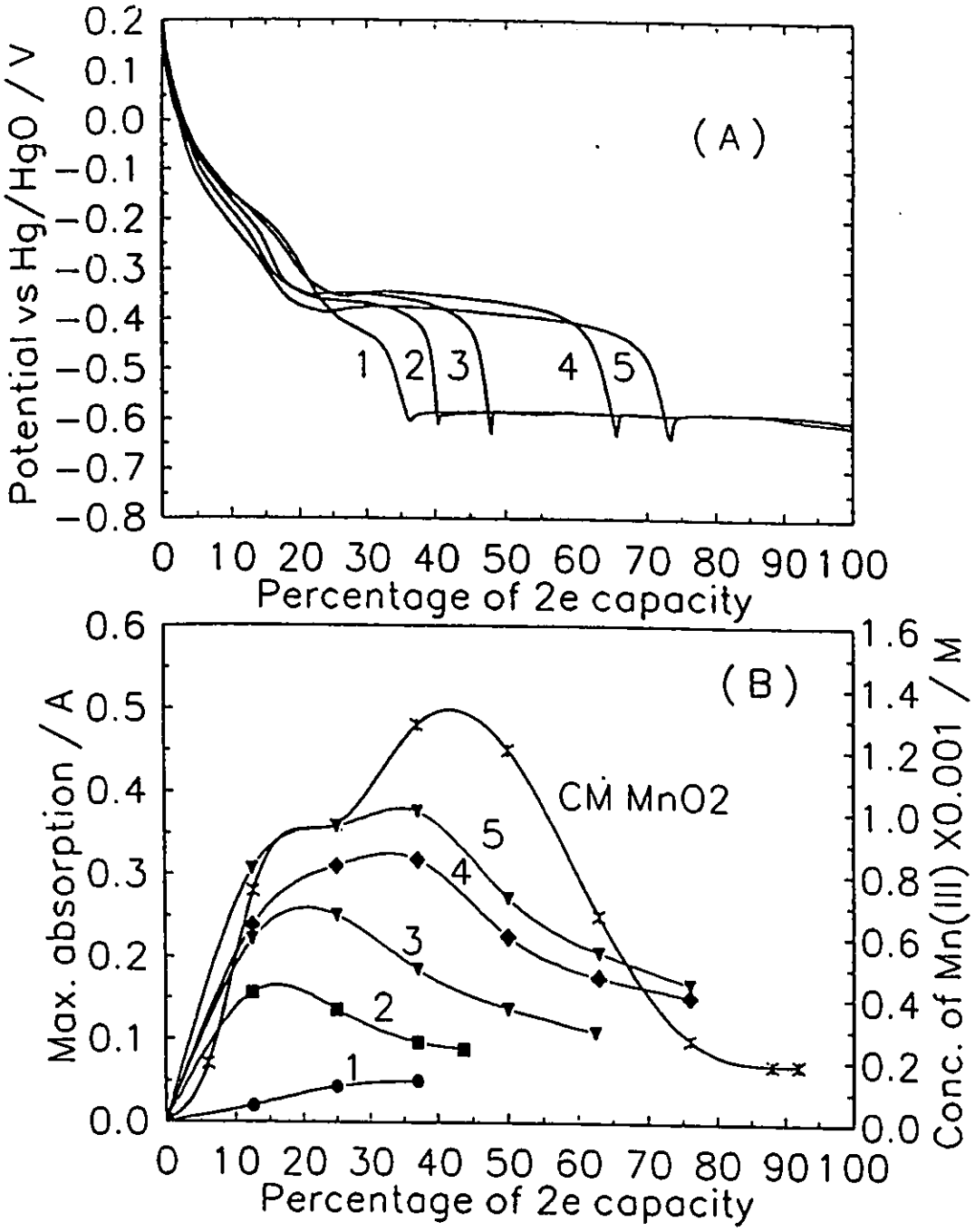

Fig. 37 Comparison of successive first to fifth constant-current (0.16 A g^{-1}) discharge curves (A) with the relative maximum absorption values at 465nm for various extents of discharge as percentage (B) at a PM MnO_2 electrode. PM MnO_2/Lonza graphite=1:4; the concentration of Mn(III) was calculated based on the maximum absorption and the extinction coefficient.

cycle (see Fig. 37A), while the amount of soluble Mn(III) species found on discharge increases correspondingly with the extent of the rechargeability, finally approaching the situation found with CM MnO_2 (Fig. 37B).

The behaviour on recharge is quite similar to that on discharge. Thus, it is evident that upon cycling, the behaviour of the PM material (curves 1 to 5) approaches that of the CM MnO_2 material (annotated as "CM MnO_2" in Fig. 37B) presumably because of a progressively improving micro-redistribution of Bi species homogeneously in the MnO_2.

From Fig. 37B in relation to 37A it can be seen that the extent of formation of soluble Mn(III) species is directly related to the realizable charge capacity (Fig. 37A) which increases over the first to fifth cycles of the PM MnO_2. The behaviour of γ-MnO_2 was shown in Fig. 34.

4.2.4 Optical and electrochemical experiments under controlled-potential discharge and recharge conditions

In previous sections, we have shown how the production or consumption of the soluble Mn(III) species is related to the extent of discharge or recharge of the MnO_2 materials. In relation to the cyclic-voltammetry curves for reduction of, and reoxidation to, MnO_2, as described previously, it was of interest to connect the changes of optical absorption to *potential* over the cycled ranges of potential required for discharge and/or recharge.

Figs. 38A and B show the spectra observed at various

potentials in the discharge and recharge processes, respectively, at a CM MnO_2 electrode. Figs. 39A and B show, respectively, the cyclic-voltammogram for a CM MnO_2 electrode in relation to the maximum absorption values for $Mn(OH)_6^{3-}$ recorded separately at various potentiostatically-controlled potentials in both discharge and recharge directions. The hysteresis between the concentration profiles as a function of potential on discharge and recharge closely follows the irreversibility in the current vs potential relations of the cyclic-voltammogram, as in Figs. 39A,B.

It should be emphasised that each of the measurements of optical absorption (Fig. 39B) was not recorded until each respective current at the electrode had relaxed for 0.5 to 3h, following each change of potential, and approached "zero" (e.g. 95% down from its original transient value) while the electrode was held at each of the selected 10 to 12 potential values in Fig. 39B.

Fig. 40 shows the spectra of $Mn(OH)_6^{3-}$ species observed at different potentials during discharge at the Blank MnO_2 electrode. Figs. 41A and B provide a comparison of the cyclic-voltammogram for the Blank MnO_2 electrode (Fig. 41A) with the profile of *A* values for $Mn(OH)_6^{3-}$ at 465 nm in the discharge process over the same range of potentiostatically-controlled potentials (Fig. 41B). Conditions were as for the results in Fig. 39B.

Further comparisons were made between the maximum

"absorption densities", A, recorded at different potentials in the discharge process for a CM MnO_2 electrode and a corresponding Blank MnO_2 electrode (Fig. 42) made by the same procedure and with the same MnO_2 loading. A substantial effect of the Bi(III) in the CM MnO_2 is readily seen from these plots as was also noted in reference to Fig. 35. The potential at which $Mn(OH)_2$ begins to be redeposited from the soluble $Mn(OH)_6^{3-}$ back on the porous electrode matrix is almost 200 mV more positive at the CM MnO_2 electrode (-0.35 V vs Hg/HgO) than at the "blank" MnO_2 (-0.55 V vs Hg/HgO). Furthermore, the rate of the redeposition at CM MnO_2 is higher than that at the "blank" MnO_2.

4.2.5 Comparative behaviours of CM, PM and γ-MnO_2 materials

Based on the results and discussion recorded above, it is clear that the electrochemical behaviours of γ-MnO_2, CM MnO_2 and Blank MnO_2 are by no means the same although they are related. When the γ-MnO_2 is fully discharged, the product is expected to be the same as that formed from the Blank MnO_2; with Bi(III) physically included in the electrode materials, the behaviour of the resulting PM γ-MnO_2, which prior to modification is intrinsically non-rechargeable over the potential range of +0.1 to -0.6 V vs Hg/HgO, becomes like that of "CM MnO_2" after a couple of discharge and recharge cycles (Fig.37). In fact, the initial discharge and recharge processes at a PM MnO_2 electrode evidently have the same function as that of the "Chemical Modification" process, i.e. providing an intimate distribution

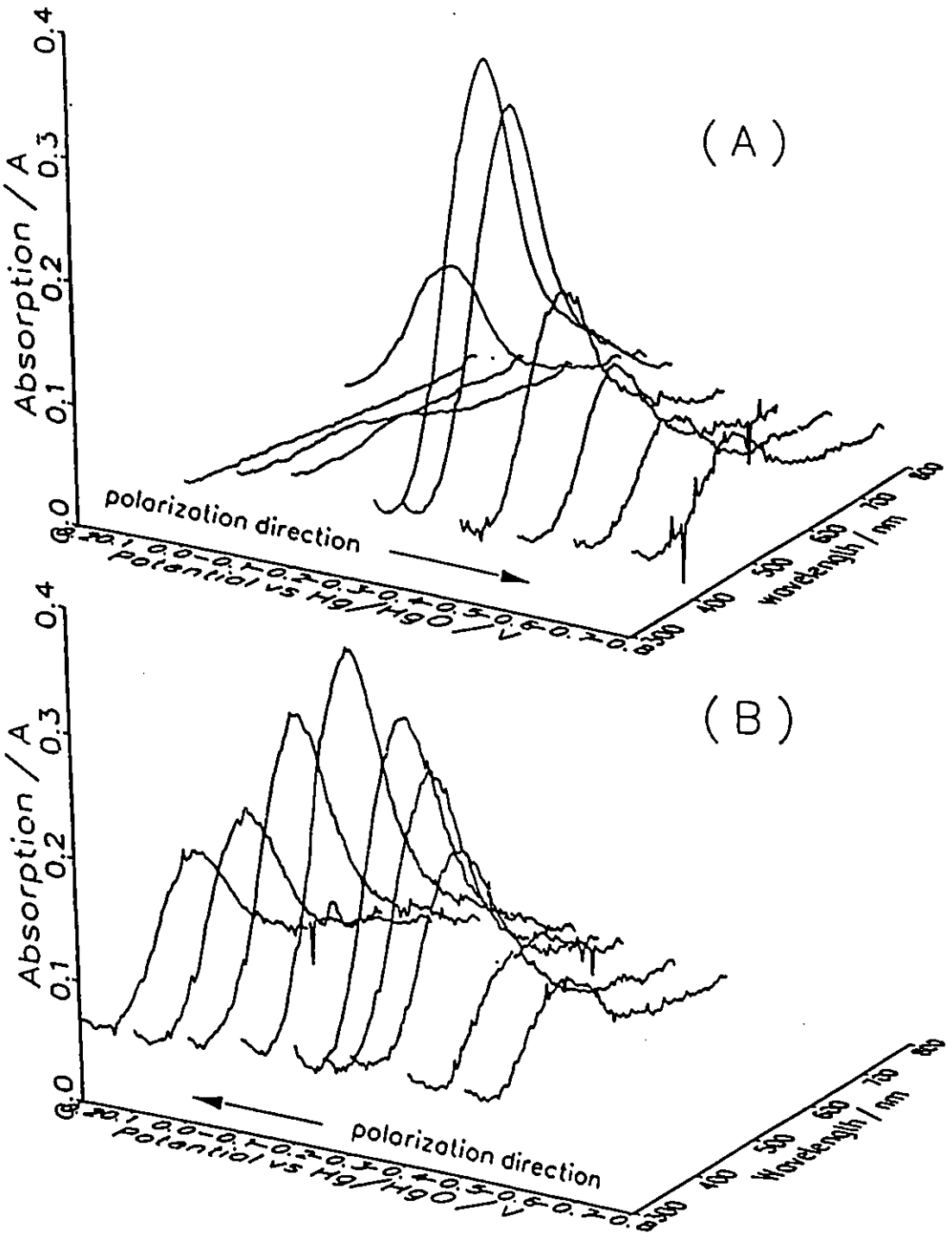

Fig. 38 The change of optical absorbance of Mn(III) species with potential under conditions of potentiostatic discharge at various controlled potentials (A), in the recharge process at a CM MnO_2/Lonza graphite=1:4 (B).

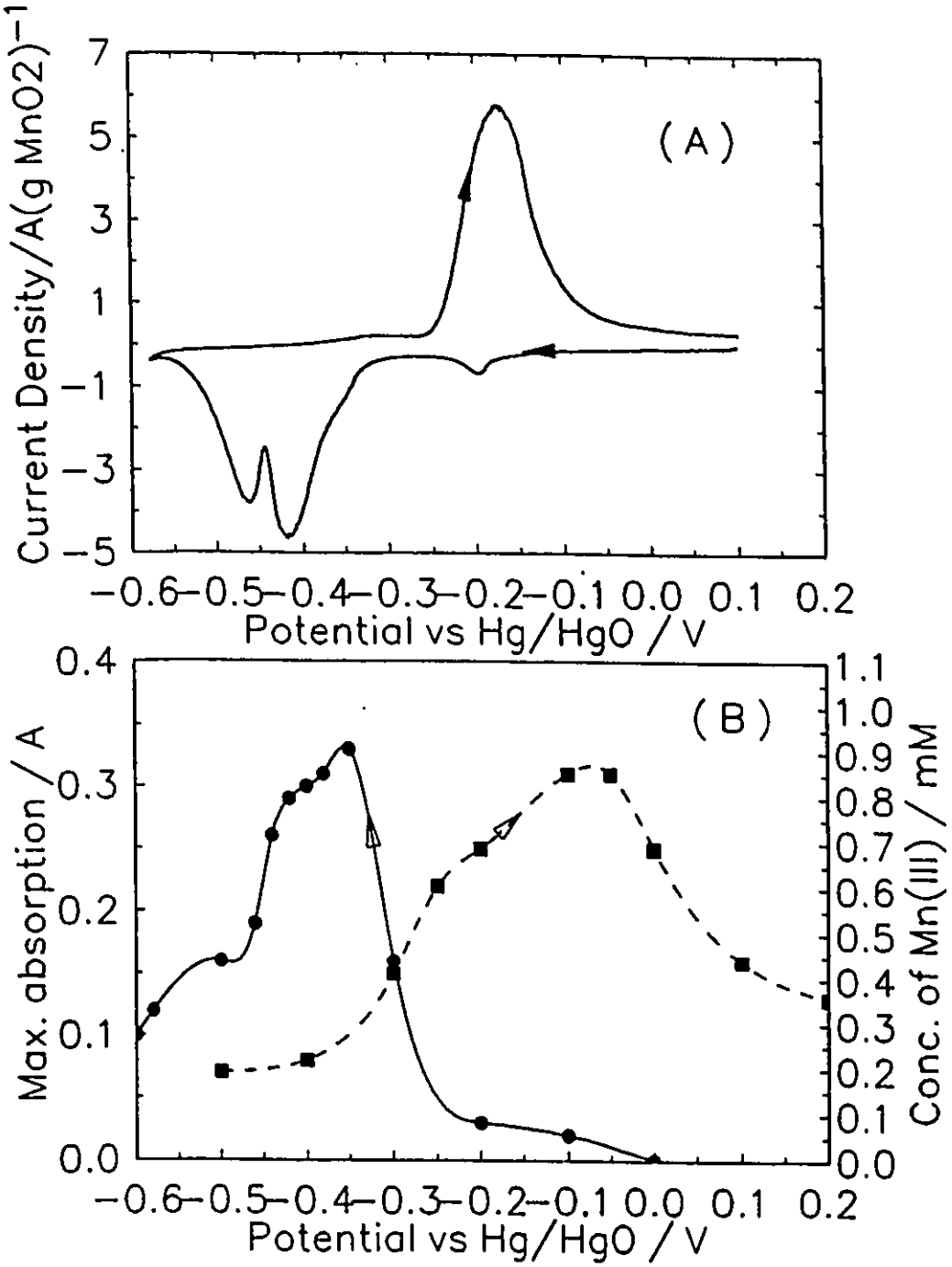

Fig. 39 (A) Correlation of anodic and cathodic half-voltammograms at 0.5 mV s^{-1} with (B) changes of maximum optical absorption at 465 nm at various discharge and recharge potentials. CM MnO_2/Lonza graphite = 1:4; solid line: discharge; dashed line: recharge.

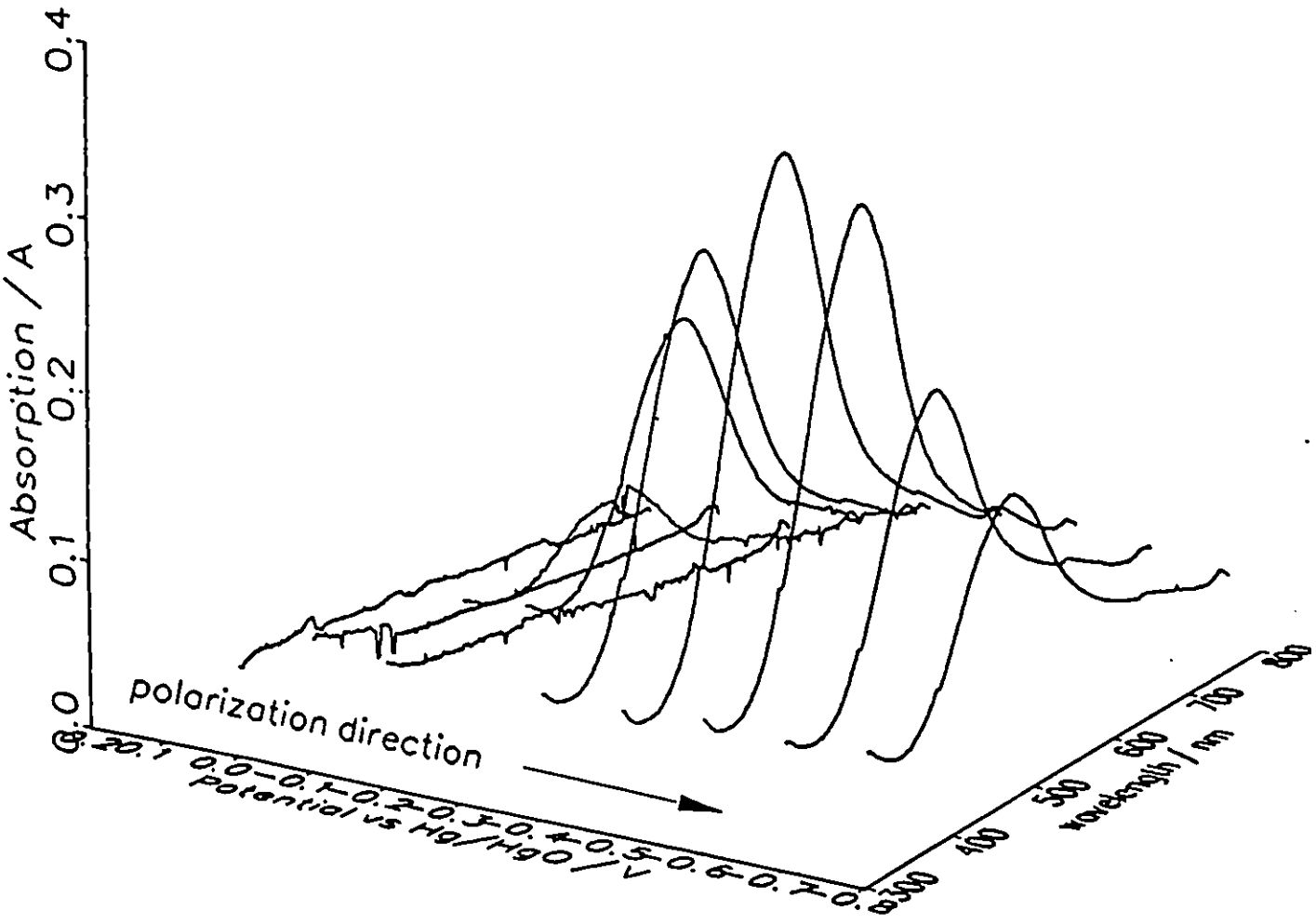

Fig. 40 The change of optical absorbance of Mn(III) species at a series of potentiostatically controlled potentials in the discharge process at a "blank" MnO_2 electrode. MnO_2/Lonza graphite = 1:4.

of Bi(III) species in the MnO_2 reactant. More directly, in the PM material with the help of the Bi(III) dopant, the dissolution and re-precipitation of $Mn(OH)_2$ from the soluble Mn(III) species in the processes of discharge and recharge seem to have the same functions as those of "co-precipitation" of Bi_2O_3 and MnO_2 with O_2 bubbling during the chemical modification process.

As was stated earlier, soluble $Mn(OH)_6^{3-}$ species are found in the discharge and recharge processes at all three types of MnO_2 (γ-MnO_2, Blank MnO_2 and the CM MnO_2) but the *amounts* of the species formed at various stages of discharge or recharge are quite different for a *given mass* of MnO_2. Considering the homogeneous "electron-proton hopping" mechanism for the first electron reduction of γ-MnO_2 proposed by Kozawa and co-workers, and the evidence for formation of soluble species in the discharge and recharge processes at all the three types of MnO_2, the present results suggest that an alternative and parallel heterogenous pathway, in which the soluble $Mn(OH)_6^{3-}$ intermediate is involved, is always coupled with the homogeneous pathway, rather than being distinct after the first electron stage of discharge. Thus, at the different types of MnO_2, especially CM MnO_2 *vis a vis* γ-MnO_2, *different extents* of parallel participation of these pathways of reduction and reoxidation are favoured; e.g. a major fraction of the extent of discharge of γ-MnO_2 appears to go through the homogeneous mechanism in the first-electron stage of its reduction while, at CM MnO_2, the heterogeneous pathway is favoured almost from the start of

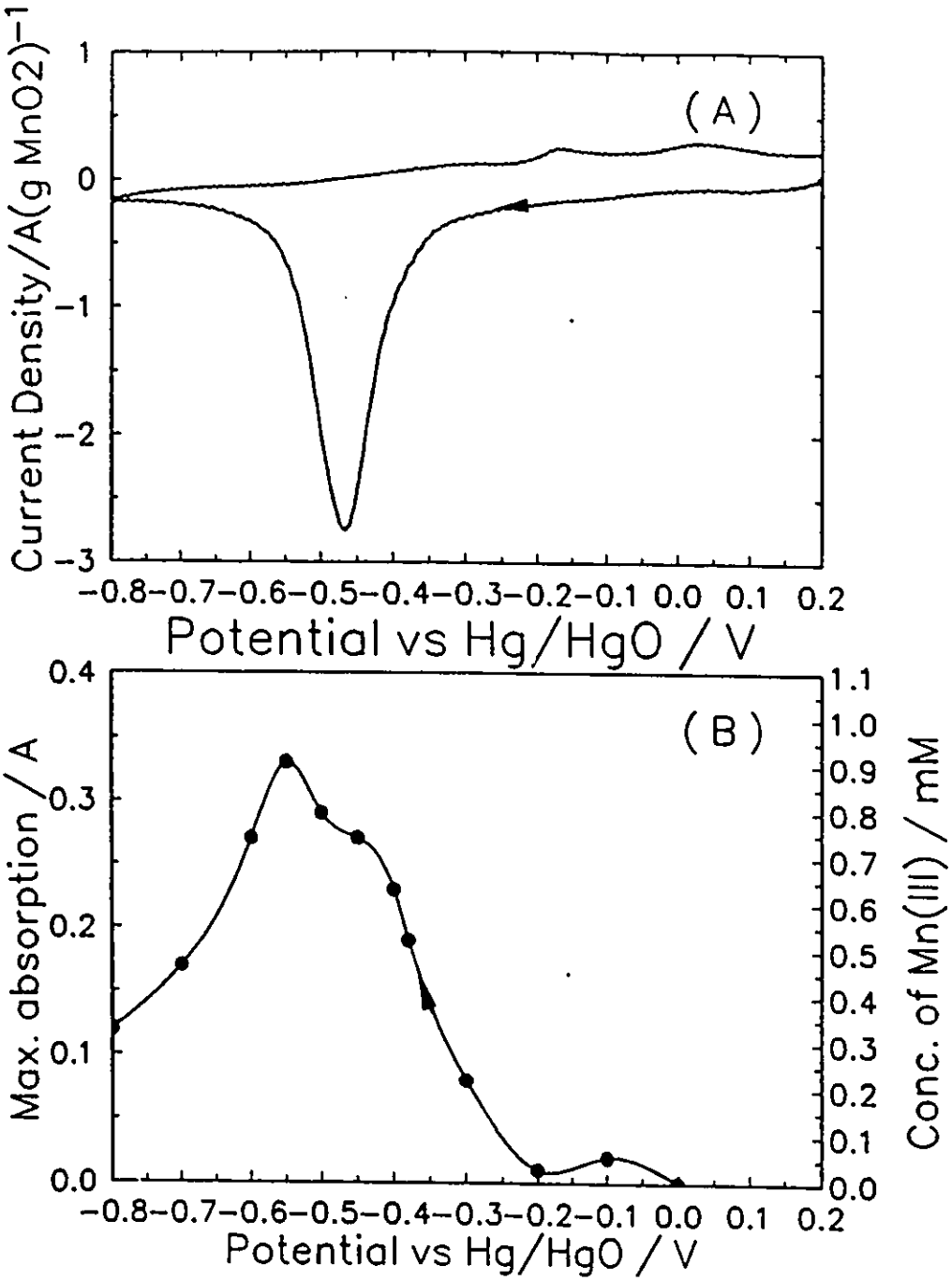

Fig. 41 (A) Correlation of cathodic half-voltammetry current response at 0.5 mV s^{-1} with (B) changes of maximum optical absorption at 465nm for various discharge potentials at a the "blank" MnO_2 electrode. MnO_2/Lonza graphite=1:4.

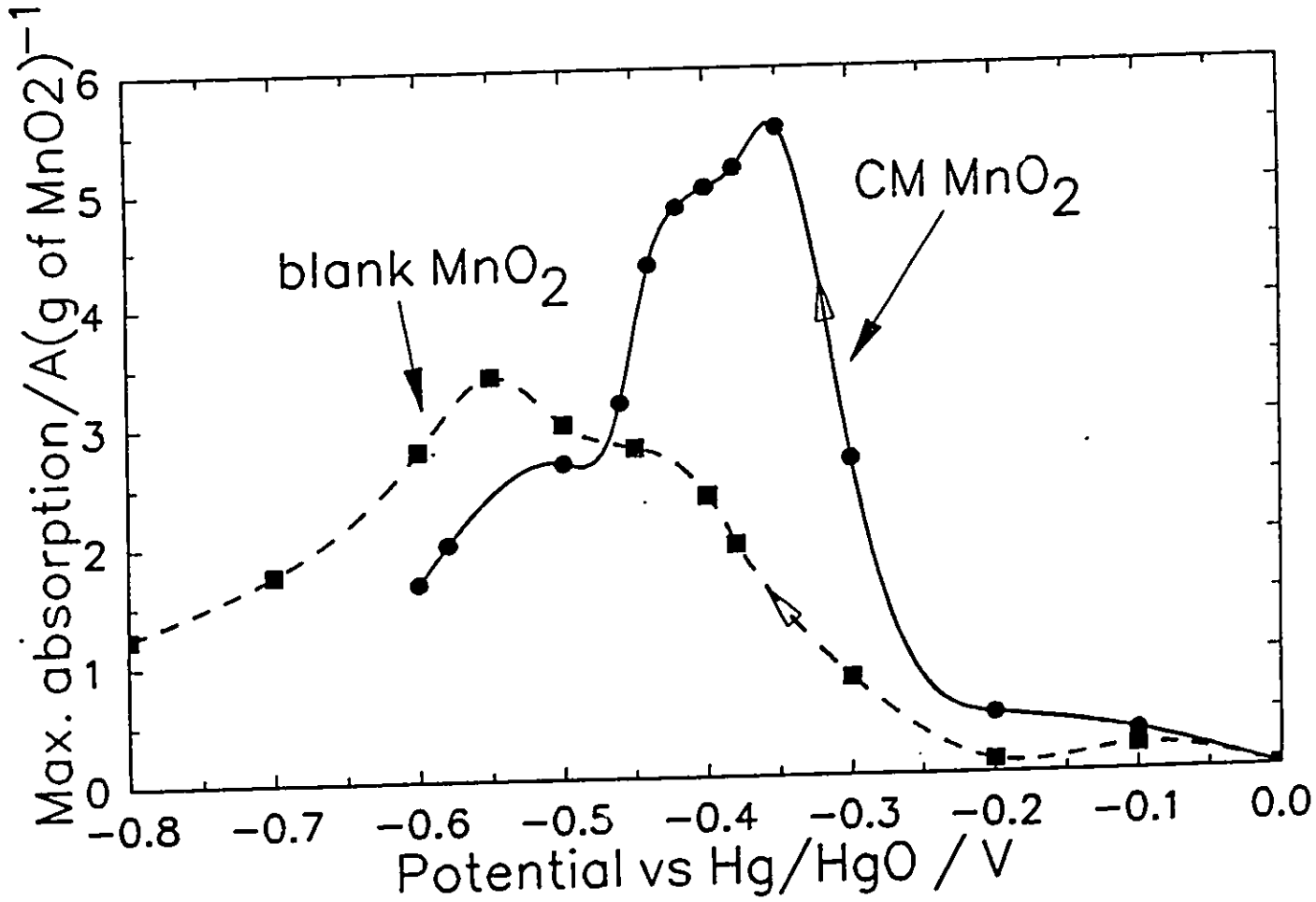

Fig. 42 Comparison of maximum optical absorption at 465nm at various potentiostatically controlled potentials in the discharge process for the CM MnO_2 (solid line) and the "blank" MnO_2 (dashed line). The concentration of Mn(III) species was calculated based on the maximum optical absorption and the extinction coefficient. MnO_2/Lonza graphite=1:4.

discharge.

The extents and rates of appearance of Mn(III) species in solution will depend on potential but, in the case of γ-MnO_2, this effect will mainly be associated with the second electron reduction stage where the heterogeneous mechanism becomes predominant. In that stage, at an appropriate fixed potential, all the remaining material could dissolve into solution under excess free electrolyte conditions,as found in ref. 38.

The substantial differences in the extents of discharge at which significant quantities of dissolved Mn(III) species appear in solution from CM and γ-MnO_2, or Blank MnO_2, require further comment. In so far as the Mn(III) oxidation state must appear in the MnO_2 lattice immediately upon discharge (i.e. initially via the homogeneous mechanism) and thereafter to an increasing extent, it can be seen that, in principle, Mn(III) species could appear in solution early in the discharge half-cycle if there is possible a facile transfer

$$Mn(III),\ lattice \rightarrow Mn(OH)_6^{3-},\ solution$$

Additionally, there could be direct injection of Mn(III) species into solution from the surface of CM or γ-MnO_2 at rates determined by the microscopically-accessible surface areas of the particles. Of course, as already mentioned above, the rates of formation of Mn(III) species, and of their removal to insoluble $Mn(OH)_2$, must depend on potential.

It seems unlikely and experimentally not indicated that most of the Mn^{4+} is first reduced to Mn^{3+} in the lattice

(homogeneous mechanism) and then is subsequently transferred into solution for the 2nd-electron reduction stage. This point receives further support from *in-situ* XANES and EXAFS measurements recently performed on the CM material (see Section III later in this chapter).

In the case of the PM MnO_2 based on γ-MnO_2 plus Bi/graphite, the initial non-rechargeable material becomes rechargeable, as noted in p137.

4.2.6 The rates of formation of the soluble Mn(III) species

The present results show that a *qualitatively different extent* of involvement of the soluble Mn(III) intermediate arises in the reduction (and re-oxidation) process at CM MnO_2 in comparison with that at γ-MnO_2. Of course, the lattice structures and local coordination arrangement in these structure are substantially different. However, on the basis of elementary thermodynamic principles, it is unlikely that the small quantity of Bi(III) present could materially change the equilibrium solubility of the Mn(III) species (e.g. through an "activity coefficient" effect), so the effect of the Bi must be essentially kinetic (or catalytic) in origin, changing the rates, pathway and mechanisms of the reduction and re-oxidation processes involved in the reactions of the MnO_2 electrode. It is also possible that such quantities of Bi(III) dopant could alter the electronic band structure of MnO_2 and its electrical conductivity.

The amounts of soluble $Mn(OH)_6^{3-}$ species formed on discharge and recharge of γ-MnO_2, Blank MnO_2 and CM MnO_2 have been discussed in the previous sections. The *rates* of the formation of the soluble species, however, are also different from one to another among the three types of MnO_2 materials in the respective discharge and recharge processes involved, as shown below.

4.2.7 Kinetic and mechanistic aspects of the discharge processes at the three types of MnO_2 electrodes

In Fig. 35 were shown the "maximum absorption densities" found for production of the intermediate at CM MnO_2, Blank MnO_2 and γ-MnO_2 at various percentages of capacity utilization in the discharge processes. Obviously, the first derivative at any particular point on the curves corresponds to the rate of formation of the soluble $Mn(OH)_6^{3-}$ species in the solution for the given type of MnO_2 at a given discharge percentage (time), assuming the appearance of soluble Mn(III) species is not diffusion controlled[4]. From this diagram, firstly it can be seen that the amount of $Mn(OH)_6^{3-}$ species in the solution increases most rapidly in the case of the CM MnO_2 among the three, and the initial rate of $Mn(OH)_6^{3-}$ formation in the case of Blank MnO_2 is larger than that for γ-MnO_2. In so far as the extents of discharge (or recharge) are related to potential, these amounts of soluble species and their rates of production are also a

[4]The fact that appreciably different rates of appearance of soluble Mn(III) species arise at the three MnO_2 materials, which have the same MnO_2 loadings and preparation conditions, is the basis for this point.

function of potential.

Secondly, at the CM MnO_2 electrode, the process of $Mn(OH)_6^{3-}$ formation is maintained until 40 percent of two-electron capacity has been utilized; then precipitation of $Mn(OH)_2$ begins; at the Blank MnO_2 electrode, the initial rate of formation of $Mn(OH)_6^{3-}$species is moderately high but then the (net) rate decreases to almost zero (the flat plateau in the absorption curve in Fig. 35) before $Mn(OH)_2$ begins to redeposit back on the porous electrode by reduction from the $Mn(OH)_6^{3-}$; in the case of γ-MnO_2, the initial rate of formation of soluble $Mn(OH)_6^{3-}$ species is quite low compared with that at the other two MnO_2 materials, but the rate significantly increases around 25% of two-electron capacity; again, these effects are indirectly dependent on potential.

The rate of formation of soluble $Mn(OH)_6^{3-}$ can be regarded as proportional to the rate of reduction of MnO_2 along the heterogenous pathway. Hence, it appears that for the γ-MnO_2, the initial stage of discharge is mainly through the homogeneous pathway, since the rate of formation of soluble $Mn(OH)_6^{3-}$ intermediates is relatively rather low; in the second stage of reduction, which begins around 25 percent of two-electron capacity, the reaction shifts partly from the homogeneous to the heterogenous pathway, as indicated by the rate of $Mn(OH)_6^{3-}$ formation becoming significantly increased.

It seems to be significant that formation of $Mn(OH)_6^{3-}$ begins only at potential below -0.25 V vs Hg/HgO, i.e. below 1.1 V vs

Zn. However, γ-MnO_2 delivers a substantial fraction of its capacity above this potential (at least at low discharge rates), corresponding to participation of the homogeneous mechanism in the first electron discharge stage. Thus, it appears that γ-MnO_2 can tolerate a substantially greater content of Mn(III) in its crystal lattice than does the CM MnO_2.

These explanations of γ-MnO_2 reduction in terms of mechanisms are satisfactorily consistent with Kozawa's conclusion that the first-electron reduction stage corresponds to a homogenous "electron-proton" solid-state mechanism while the second-electron step involves a heterogeneous "dissolution-precipitation" mechanism. In the case of CM MnO_2, apparently, a relatively greater fraction of the MnO_2 reduction process goes through the heterogenous pathway as the $Mn(OH)_6^{3-}$ formation rate is substantial. The overall mechanism for Blank MnO_2 reduction appears, however, to lie "in between" those for γ-MnO_2 and CM MnO_2, i.e. the fraction of MnO_2 which goes through the heterogeneous pathway is substantially greater than that for γ-MnO_2 but less than that for CM MnO_2. Complementary to that fraction of MnO_2 which is reduced via the heterogenous pathway, the remainder must presumably proceed through the homogeneous pathway.

The shift of the reaction mechanism from the homogeneous to the heterogeneous pathway is well illustrated by the results shown in Figs. 37A and B. The absorption curves for the first constant-current discharge and recharge cycles of PM MnO_2 are

virtually the same as those for γ-MnO_2: the reaction goes mainly through the homogeneous pathway corresponding to the rate of $Mn(OH)_6^{3-}$ formation being quite low. In the subsequent second to fifth discharge and recharge cycles, the rates of $Mn(OH)_6^{3-}$ formation, which can be represented by the initial slopes of each curve, keep increasing, so does the actual amount of soluble $Mn(OH)_6^{3-}$ species formed, approaching the behaviour of the CM MnO_2.

The findings described above suggest that, due to the presence of Bi(III) dopant, the reduction mechanism can shift from one dominated by the homogeneous-pathway (for γ-MnO_2) to one dominated by the heterogeneous-pathway (for CM MnO_2).

In the homogeneous pathway, the "proton hopping" process has been suggested as the rate-determining step. The protons which arise from the decomposition of H_2O molecules at the solid-solution interface on charge are introduced into the lattice, forming OH^- from O^{2-} ions. Since the OH^- in the lattice is librating or rotating, and vibrating, the O-H bond is broken and H^+ can be transferred to an adjacent O^{2-} to form OH^- again. Thus, OH^- can move around in the entire lattice by means of proton jumps from one O^{2-} site to another. Again, it has been supposed that the proton-jumping in the solid phase is probably not a fast step, so the reduction current-density can be limited by the rate constant for that step.

In the heterogenous pathway, however, this rate-determining "proton hopping" step is bypassed by formation of the soluble

$Mn(OH)_6^{3-}$ intermediate, which makes it possible for substantially higher reduction current-densities to pass, as observed and referred to previously (see Fig. 18 and ref.67). Correspondingly O^{-2} ions in the MnO_2 lattice must be equivalently to OH^- ion by proton-transfer steps. In fact, CM MnO_2 can be discharged at high current-densities without significant decrease of the potential of the remarkably flat discharge plateau that is observed (Fig. 18). This characteristic, typical of a 2-phase electrode process, enables CM MnO_2 cathodes to provide high output current-densities (corresponding to up to 6C rates) at a stable useful working potential (1 V vs Zn). This feature would be especially attractive for heavy-duty battery requirements like those for electric vehicles or SLI purposes, notwithstanding the somewhat smaller operating voltage that is involved.

4.2.8 Re-deposition of $Mn(OH)_2$ from $Mn(OH)_6^{3-}$ in the solution on to the porous electrode matrix

The conclusion that the multiple rechargeability of CM MnO_2 arises on account of the possibility that the process can adopt mainly the heterogeneous pathway, is based on (a) the evidence that the processes of formation of soluble intermediates and their re-deposition play demonstrably important roles and (b) that the discharge curves are remarkably flat.

With regard to discharge of the two-electron capacity over a practically useable potential range, the potential for re-deposition of $Mn(OH)_2$ from the solution is quite critical. As mentioned previously in the thesis, it is hard to understand how

the presence of a small mole fraction of Bi(III) could change the thermodynamics of the processes of MnO_2 discharge and recharge. Hence, the dynamic factors of deposition of $Mn(OH)_2$ from, as well as the formation of the Mn(III) species, discussed previously, should be taken into account.

γ-MnO_2 is reduced via the homogeneous mechanism in its initial stages of reduction (Fig. 34), while, as the protons are introduced into the bulk lattice of the MnO_2, it begins to expand but in the initial stages of the discharge, the original structure of the MnO_2 is maintained. It has been supposed that as long as the structure remains unchanged, the material is rechargeable . However, if the lattice collapses as the electrode is further discharged, the products, which may be hausmannite (Mn_3O_4), cannot be electrochemically recharged back to MnO_2, as has been noted in the literature. Thus, the rechargeability of the material is lost. In order to recharge the hausmannite Mn_3O_4 to MnO_2 (not γ-MnO_2 anymore), it has to become further discharged to $Mn(OH)_2$ but such reduction, however, does not practically arise until a potential of ca. -1.0 V vs Hg/HgO had been attained. Furthermore, the reduction involving the second electron is relatively irreversible, so that the current peak becomes smeared out over a wide range of potential (from -0.65 vs Hg/HgO to the potential of H_2 evolution). Thus, in a battery, these conditions are not practically favourable for utilization of the capacity of the active material.

These phenomena are consistent with the behaviour shown in

Fig. 34, where it is seen that the concentration of soluble Mn(III) in the solution does not significantly decrease (Fig. 34B) up to -0.65V vs Hg/HgO (Fig. 34A).

The situation with Blank MnO_2 is quite similar to that with γ-MnO_2 with regard to the second-electron discharge process. As can be seen from both Fig. 33 (solid line) and Fig. 41, $Mn(OH)_2$ is not deposited from the soluble $Mn(OH)_6^{3-}$ species onto the porous electrode matrix until potentials of -0.55 V vs Hg/HgO or 0.7 V vs Zn are reached.

Dramatic differences between the reduction mechanisms at CM MnO_2 and γ-MnO_2 were indicated from the "potential-holding experiments" referred to in Section I which showed that the "two electrons" of CM MnO_2 are capable of being fully utilized for discharge at -0.4 V vs Hg/HgO and the resulting discharge products could be recharged. In fact, the reduction products of CM MnO_2 at *any* depth of discharge can be re-charged back to the original state of MnO_2 which is thus almost completely rechargeable. Hence, it appears that hausmannite (Mn_3O_4), which cannot be electrochemically re-oxidized, may in fact not be substantially formed in the presence of Bi(III); this has been further confirmed by means of *in-situ* X-ray absorption experiments [72].

From a kinetic point of view, the large overpotential that is found to be necessary for further reduction of $Mn(OH)_6^{3-}$ to solid $Mn(OH)_2$ to occur at non-Bi(III)-doped MnO_2 results from apparently high activation energy of the processes of second

electron transfer and nucleation of $Mn(OH)_2$. Since these processes can arise at a much more positive (ca. 0.5V) potential or at a much lower overpotential at the CM MnO_2 than at the other electrode materials, the effect of Bi(III) dopant must, practically, be kinetic and only indirectly structural in origin. It seems that Bi(III) must perform as a sort of catalyst which can reduce the activation energy of both the electron transfer and the nucleation processes associated with phase transformation from soluble Mn(III) species; that is, speculatively, the overpotential for the second electron reduction can be dramatically reduced.

Considering the mechanism involving parallel homogenous and heterogeneous pathways, it can be proposed that γ-MnO_2 is rechargeable only in the initial stage of discharge so long as the known "layer structure" is maintained. If the structure collapses, the material can only be partly recovered by deep discharge to low potentials. The characteristic which makes the fully discharged γ-MnO_2 and Blank MnO_2 practically non-rechargeable results from the substantial overpotential required for the second electron reduction of haussmanite, Mn_3O_4, in the solid phase to occur. With the help of the Bi(III) dopant, the homogeneous pathway can be bypassed and the formation of hausmannite, which cannot be electrochemically re-oxidized, might be avoided through formation of the soluble $Mn(OH)_6^{3-}$ intermediate. Furthermore, corresponding to the overpotential of the second electron transfer being dramatically reduced, the

reaction itself is accelerated. Thus, the discharge of the second electron becomes attainable at a practically useable potential (1 V vs Zn) and at a very favourable discharge rate ([21], and see Fig. 18 and in Section I).

It is these characteristics which make it possible for the CM MnO_2 to be used as a rechargeable cathode material in practical battery embodiments.

Fig. 37 provides a useful illustration of the mechanism described above, showing how the γ-MnO_2, which is non-rechargeable after deep discharge, gradually becomes (refer to the sequence of curves 1 to 5 in that figure) a rechargeable material simply by physically introducing some Bi with graphite into the γ-MnO_2 mechanically. Thus, the shift of reaction pathway from the homogeneous one at γ-MnO_2 to the mainly heterogeneous one at CM MnO_2 is clearly implied in this Fig. 37 (curves in B) by the increased involvement of $Mn(OH)_6^{3-}$ species in the solution from the first to the fifth cycle and beyond.

Section III. *In-situ* and *Ex-situ* X-ray Absorption Spectroscopy Coupled with Electrochemical Methods

The UV-visible spectrophotometric measurements enabled the production and consumption of a soluble Mn(III) species that are produced on discharge or recharge, to be followed at the CM MnO_2 in comparison with the behaviour at γ-MnO_2 (I.C. sample no. 2) and at unmodified Blank MnO_2. The X-ray absorption (XAS) experiments provide complementary information on the following:

a) changes of oxidation-state of the reactive species during discharge and recharge and

b) the coordination environment (from EXAFS) of the reactive species.

Also X-ray absorption experiments can provide *in situ* information during discharge or recharge.

A cursory examination of the XAS data (see Figs. 43, 44 and 45) indicated that the *ex situ* and *in situ* data were identical at the Bi L_3 edge for the undischarged CM material and CM material that had been discharged to the one-electron (formally Mn(III)) level. The *ex situ* data also revealed that when the material had been discharged to the two-electron level, the Bi was in the form of incompletely oxidized Bi metal. Under similar circumstances, the *in situ* data indicated the presence of unoxidized Bi, i.e. the Bi (III) in the original preparation of the CM MnO_2 had become reduced to Bi(0). However the *ex situ* data at the Mn K-edge indicated that all discharged Mn materials

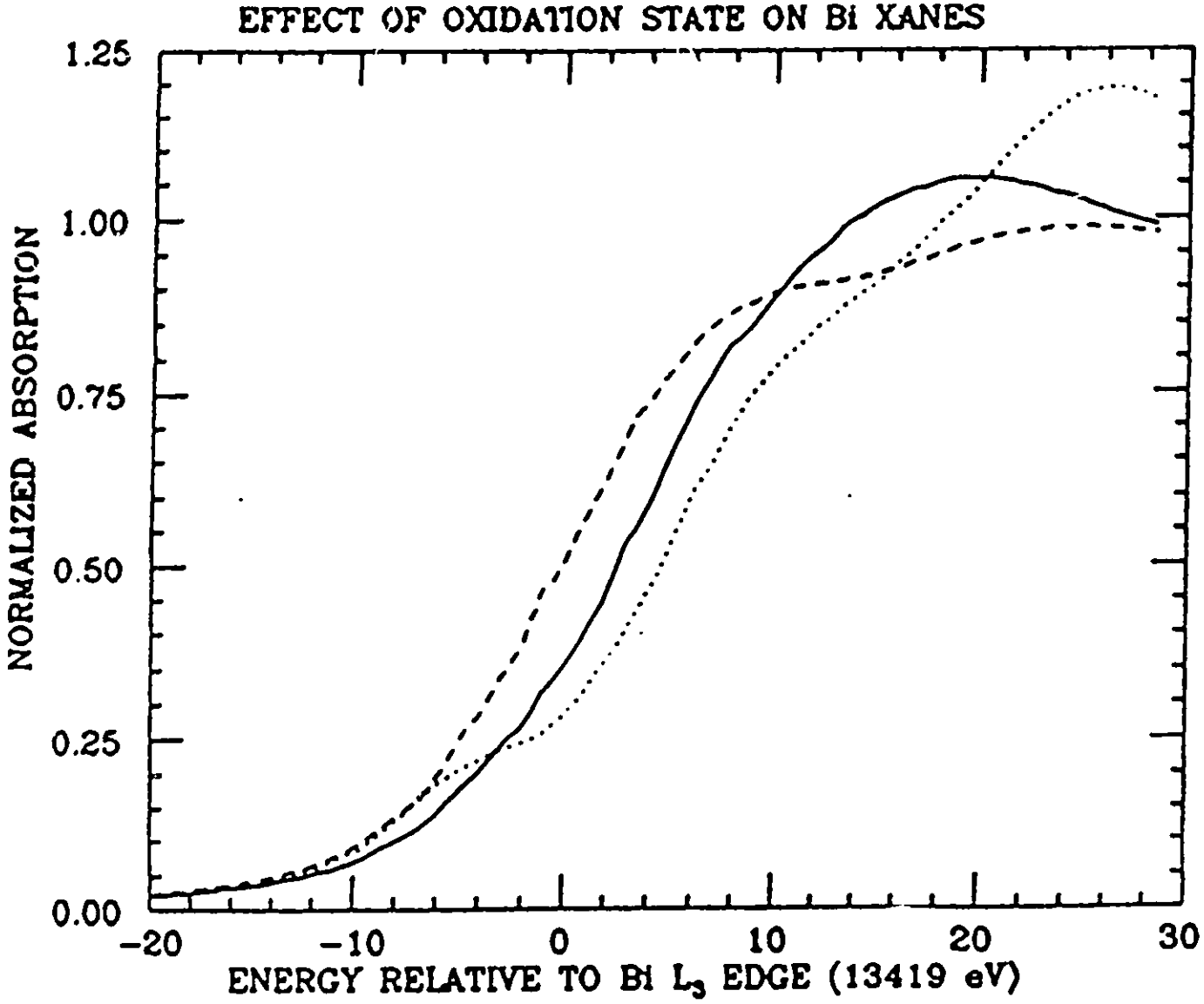

Fig. 43 Dependence of XAS of Bi on its oxidation state: —Bi(0) ——Bi_2O_3; · · · · ·$NaBiO_3$.

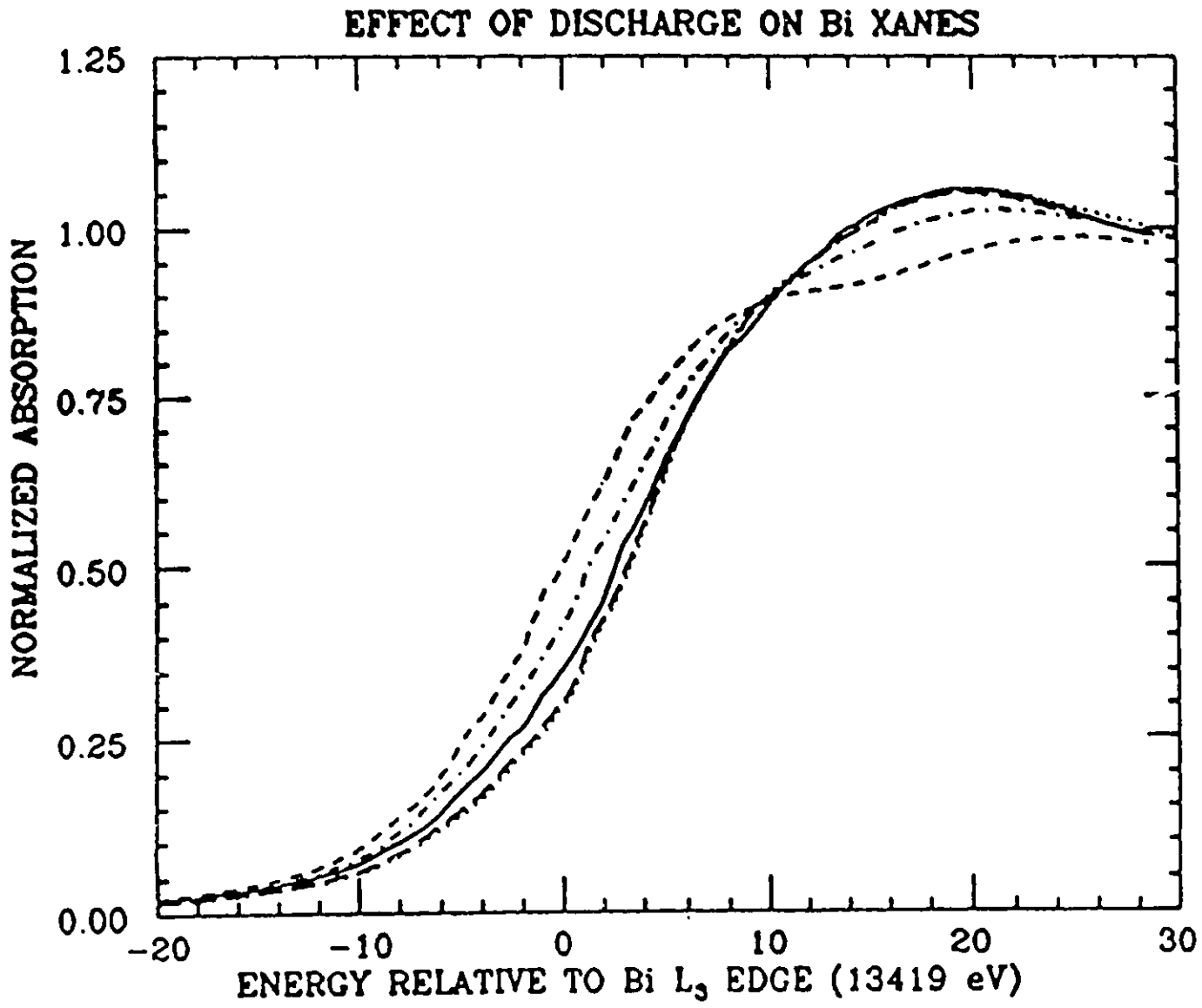

Fig. 44 Effect of charge state (during discharge) of the CM MnO_2 electrode on the *in-situ* Bi XANES: ---fully charged; • • • 1 e/Mn discharge; - - - - 2e discharge; —Bi_2O_3 reference; ----Bi(0).

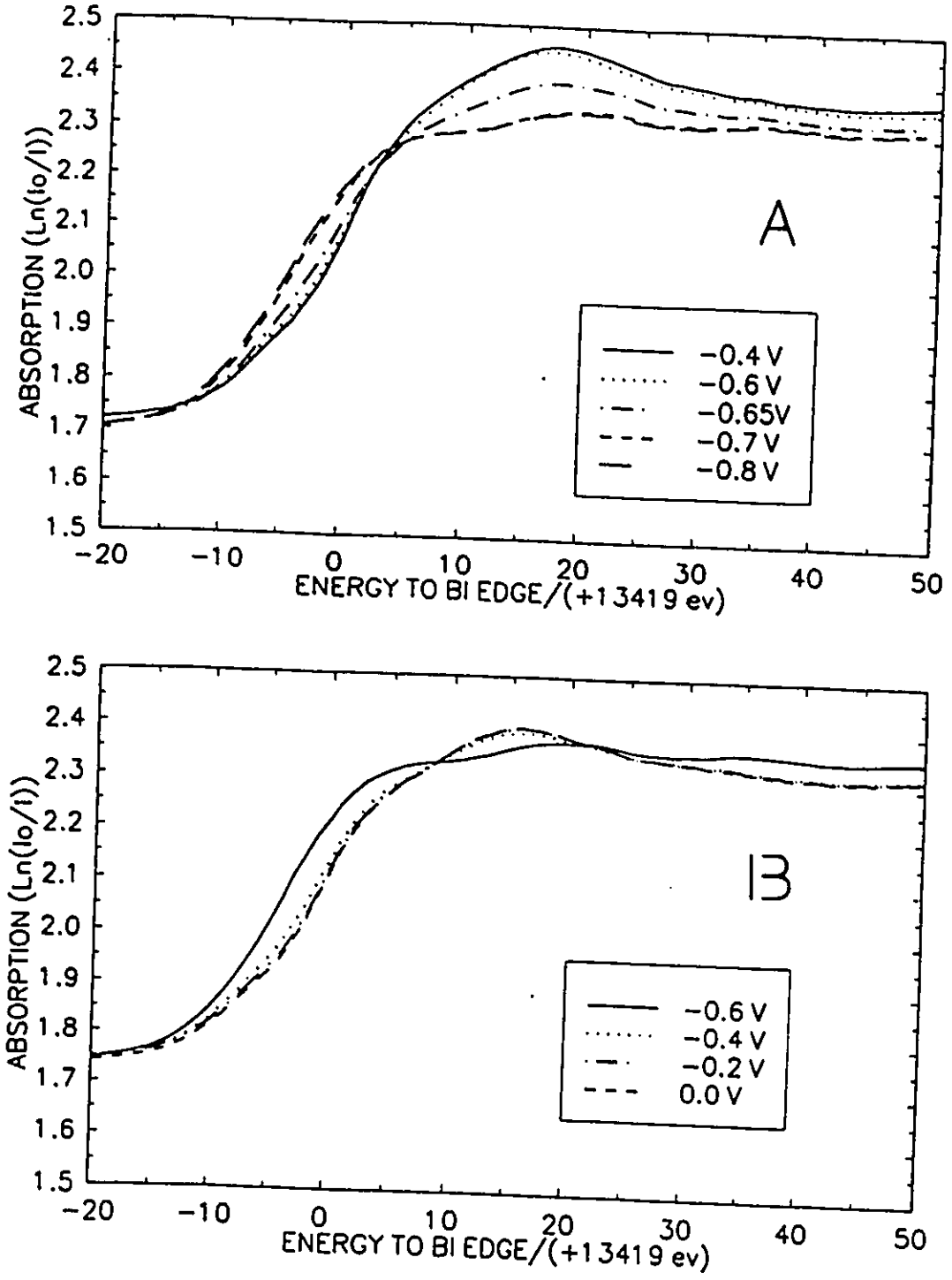

Fig. 45 Series of *in-situ* Bi XANES for a CM MnO_2 at various potentials (A) in the discharge process (B) in the recharge process.

had become reoxidized, presumably by O_2 of the air, during sample preparation. Accordingly, both the *in situ* and *ex situ* Bi data for the oxidized, i.e. charged, materials are considered reliable. Correspondingly, the only reliable *ex situ* Mn data are those for the undischarged materials. For the completely discharged electrodes, only the *in-situ* Bi data are reliable. In the case of the results for Mn, none of the *ex situ* data is to be considered reliable for electrodes that have undergone any degree of discharge, i.e. reduction, because of the possibility of aerial reoxidation during sample handling. This indicates the importance of conducting the complementary *in situ* measurements.

4.3.1 Introduction to EXAFS data treatments [92]

In order to make the rest of this section easier to be understood, a brief introduction to EXAFS data treatments is necessary. The purpose behind the analysis of EXAFS data is to be able to extract information related to interatomic distances, numbers and types of backscattering neighbours. In order to accomplish this, there are a number of steps involved in the data analysis, and these include:

1) Background subtraction and normalization
2) Conversion to wave vector form
3) κ weighting
4) Fourier transforming and filtering
5) Fitting for phase
6) Fitting for amplitude

1. Background Subtraction and Normalization: The background subtraction is separating the modulation in the absorption coefficient from the smooth atom-like absorption (that is the absorption for an isolated atom). However, since the latter is usually not available, it is generally assumed that the smooth part of $\mu(E)$ at large energies beyond the absorption edge is a good approximation to $\mu_0(E)$ (see 4.5.3).

Background removal routines employ polynomial splines of some order (typically second or third order). These are defined over a series of intervals, with the constraint that the function and a stipulated number of derivatives be continuous at the intersections. In addition, the observed EXAFS oscillations need to be normalized to a single atom value, and this is generally done by normalizing the data to the edge jump intensity.

2. Conversion to Wave Vector Form: In order to extract structural information, the EXAFS must be expressed in terms of a wave vector κ which can be expressed as follows:

$$\kappa = \sqrt{\frac{2m\ (h\nu\ -\ E_0)}{h}}$$

The threshold energy E_0 is required. The choice is important because of its effect on the phase of the EXAFS oscillations, especially at low κ values. The difficulty in determining E_0 arises from the fact that there is no way of identifying an edge

feature with E_0. One procedure is to have E_0 as an adjustable parameter in the data analysis, and its value is changed until the observed phase shifts are in good agreement with theoretical values. When good model compounds are available (vide-infra), the use of a fixed value for E_0 works well. However, in many cases it is difficult to assess *a priori* whether a given material is a good model compound.

3 κ Weighting: Once the data has been transformed to wave vector form, it is generally multiplied by some power of κ; typically κ^2 or κ^3. The weighting is important because it prevents the large amplitude oscillations (typically present at low κ) from dominating the smaller ones (typically at high κ). This is critical, since the determination of interatomic distances depends on the frequency, and not the amplitude, of the oscillations.

4 Fourier Transforming and Filtering: Examination of the EXAFS formulation in wave vector form reveals that it consists of a sum of sinusoidal signals differing in phase and amplitude. Sayers, Lytle and Stern [91] were the first to recognize the fact that a Fourier transform of the EXAFS from wave vector form yields a function that is qualitatively similar to a radial distribution function (rdf) and is given by the equation below:

$$\phi(r) = \frac{1}{\sqrt{2\pi}} \int_{\kappa_{max}}^{\kappa_{min}} \kappa^n \chi(\kappa)\, e^{(2i\kappa r)}\, d\kappa$$

Such a function exhibits peaks that correspond to interatomic distances between the central atom and the individual coordination shells, but are shifted to smaller values because of the influence of electron clouds of neighbouring atoms. This finding was a major breakthrough in the analysis of EXAFS data since it allowed ready visualization of short-range atomic arrangements. However, because of the shift to shorter distances and the effects of truncation, such an approach is generally not employed for accurate distance determination. However, it allows the use of Fourier filtering techniques which make possible the isolation of rdf's for individual coordination shells. After Fourier filtering, the data is back-transformed to κ space where it is fitted for amplitude and phase. The basic principle behind the curve-fitting analysis is to employ a parametrized function that will model the observed EXAFS, and the various parameters are adjusted until the fit is optimized. Usually this can be done quite accurately.

5 Fitting for Phase: Accurate distance determination depends critically on the accurate determination of phase shift. There are two general approaches to this problem: a theoretical and an empirical determination. Use of the theoretical phase shifts requires the use of an adjustable E_0 in the data analysis (vide-supra). The empirical approach based on the use of model compounds and the concept of phase transferability is more commonly employed. This approach consists of employing a

compound of known structure (e.g. as determined by X-ray diffraction) and which has the same absorber/backscatterer combination as that of the material of interest. The EXAFS spectrum of the known compound is obtained, and the oscillatory part of the EXAFS is fitted. Since r is known in this case, the phase shift can be determined. Typically the phase shift is parametrized as a quadratic expression.

Implicit in this treatment is the application of phase transferability which states that, for a given absorber/scatterer combination, the phase shifts can be transferred to any compound with the same absorber/scatterer combination without regard to chemical effects such as ionicity or covalency of the bonds involved. This is based on the idea that, at sufficiently high kinetic energies for the photoelectron (e.g. about 50 eV above threshold), the EXAFS scattering processes are largely dominated by core electrons, and thus the measured phase shifts are insensitive to chemical effects. Thus, determination of the phase shift for an absorber/scatterer pair in a system of known r allows determination of the distance in an unknown involving the same atom pair.

6 Fitting for Amplitude: Fitting for amplitude is employed in order to determine the types and numbers of backscattering atoms around a given absorber. The problem can be divided in two parts: identification of the types of backscatters, and the determination of their numbers. In the absence of any

information as to the probable nature of the backscatterer, identification is difficult. especially among atoms that have similar atomic numbers such as nitrogen and oxygen. This is because the backscattering amplitudes are not a very strong function of atomic number.

If the identity of the backscatterer is known, a main point of interest is determination of the number of near neighbours. In this case, one needs to compare the amplitude of the EXAFS of the material of interest (unknown) to that for a compound of known coordination number and structure.

4.3.2 *In-situ* and *Ex-situ* Bismuth XANES

Figure 43 shows the effect of oxidation state on the Bi XANES (p.59) as a standard of reference. There is an orderly shift in edge energy in going from Bi(0) to Bi(III) and up to Bi(V). In the case of $NaBiO_3$, there is a pre-edge shoulder due to transitions into empty 6s states.

Figure 44 shows *ex situ* XANES curves for the CM MnO_2 electrode materials at various stages of discharge. Reference data for Bi foil and Bi_2O_3 are shown for comparison and clearly indicate at least partial reduction to Bi metal in the completely discharged electrodes. The overall edge in the oxidized material is, however, somewhat narrower than for Bi_2O_3. This suggests a higher degree of symmetry around the Bi than that found in Bi_2O_3. The Bi in the undischarged MnO_2 material is in the Bi(III) state and in CM electrodes discharged to the one-electron level.

Fig. 45 shows the *in-situ* Bi XANES data for the CM MnO_2 electrode at the Bi edge. Fig. 45A shows Bi XANES at various potentials in the process of discharge, while Fig. 45B shows corresponding curves at various potentials in the recharge process. The data in Fig. 45A indicate that Bi remains in the Bi(III) state until -0.6 V vs H/HgO. Bi(III) starts to be reduced to Bi metal at -0.65 V. At -0.7 V almost all the Bi is in the Bi(0) state. However, in the recharge process, as shown in Fig. 45B, the Bi(0) becomes oxidized between -0.6 V and -0.4 V vs Hg/HgO. These results, which show the change of oxidation states of Bi in the processes of discharge and recharge for a CM MnO_2 electrode, are consistent with our previous assumption, that the pair of satellite peaks in the CV profile (see Fig. 11) represent the reduction and reoxidation of Bi.

As described previously (cf. 5.1.1), the two-electron capacity of CM MnO_2 electrode can become discharged between -0.2 V and -0.6 V vs Hg/HgO, and the same amount of charge can be delivered back on recharge (see Fig. 11), no matter if the electrode had been discharged previously to -0.4 V (where bismuth is in the Bi(III) state as Bi_2O_3) or to -0.6 V (where bismuth is in the Bi(0) state, as metal).

4.3.3 Bismuth EXAFS

Figure 46A shows the raw *ex situ* Bi EXAFS data obtained for an undischarged electrode at 298K. Almost identical data were obtained at 77K. This was true for both the undischarged material and material that had been discharged to the one-

electron level. The lack of variation of the EXAFS with temperature indicates interestingly a high degree of static disorder. However, change of temperature had a major effect on the Bi EXAFS for the case of the completely discharged electrode.

Table III. Fourier transform parameters for isolating Bi-O contributions in Bi-doped MnO_2 and for performing Fourier transforms on reference material

Material	k^n	$\Delta k(\text{Å}^{-1})$	$\Delta r(\text{Å})$
Ex Situ			
Undischarged, 298K	3	2.68-12.85	0-2.24
1e discharge, 298K	3	2.63-12.0	0-2.42
Undischarged, 77K	3	2.63-12.5	0-2.22
1e discharge, 77K	3	2.80-12.2	0-2.22
In Situ			
Charged	3	2.63-12.7	0-2.22
Discharged to -0.8 V	3	2.60-15.8	-
Recharged to -0.2 V	3	2.60-12.2	0-2.22
Reference Materials			
PbO (tetragonal red)	3	2.87-17.3	0-2.40
Bi foil (electroplated)	3	2.60-15.9	-

Figure 47 shows Fourier transforms of the *ex situ* Bi data for the undischarged electrodes and electrodes discharged to the

one-, and two-electron levels. Changes in the radial distribution function with discharge are clearly observable. A comparison of the rdf of the completely discharged electrode material at 77K with that found for a Bi foil at 77K clearly reveals the presence of Bi metal species. The major differences between the undischarged material and that discharged to the one-electron level are seen at around 3Å in the rdf.

Figure 46B shows the raw *in situ* Bi EXAFS data for an electrode recharged to -0.2 V. This is the potential region where the Bi is oxidized and manganese is charged to the one-electron level. The data are to be regarded as of high quality.

The first check of the Bi EXAFS data was made by comparing the Fourier transforms for the Bi in the undischarged electrodes and in Bi_2O_3, as shown in Fig. 48. The Bi is clearly not present simply as Bi_2O_3 but must be associated in some way with the MnO_2 structure.

Figure 49A shows a comparison of the Fourier transform for the Bi EXAFS in undischarged electrodes at 77 K and 298 K. The data plots are almost identical. The Fourier transform for the *in situ* data in Fig. 46B is shown in Fig. 49B. The results in Fig. 49B closely resemble the *ex situ* data obtained for the CM material after discharge to the one-electron level (see Fig. 47). Integration of slow-sweep current-potential profiles (cf. Fig. 11) indicates that, at this potential, the electrode is charged to the one-electron level.

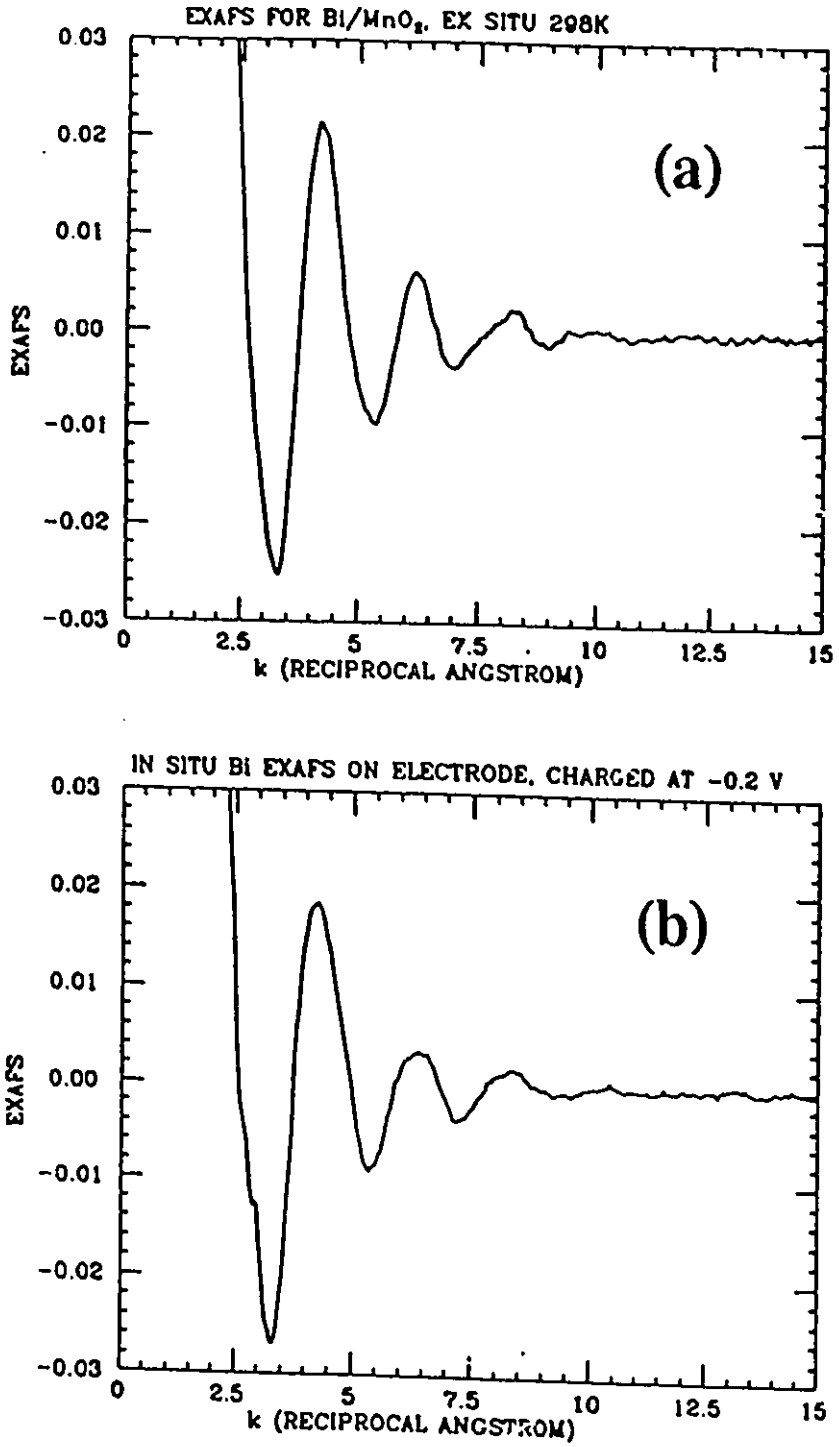

Fig. 46 Raw Bi EXAFS data; (a) for *ex situ* undischarged CM electrode 298 K; (b) *in situ* CM electrode recharged to -0.2 V.

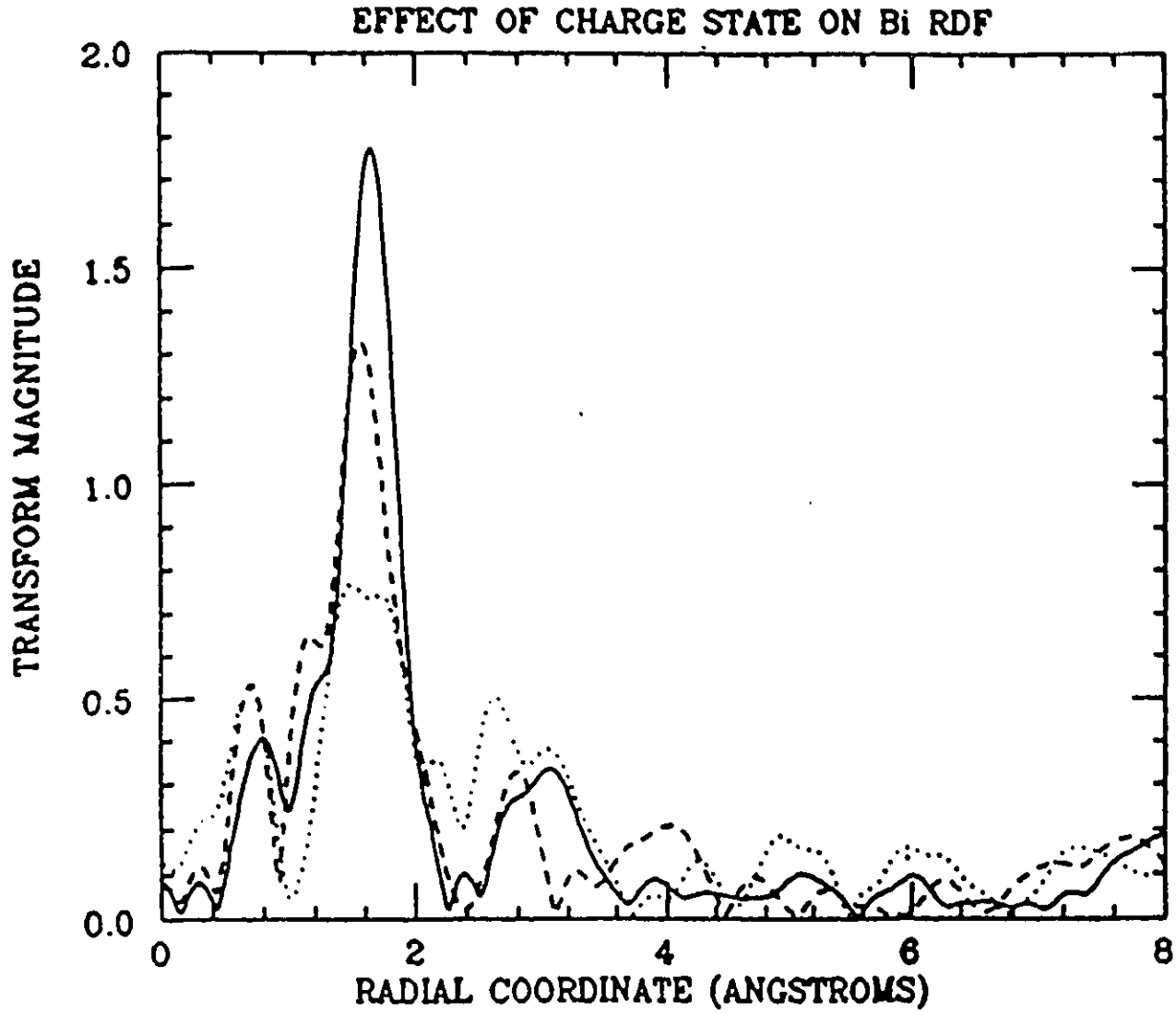

Fig. 47 Comparison between RDF's for Bi in CM MnO_2 in three states of charge: ——fully charged; --- 1e discharge; • • • • 2e discharge. Δk = 2.6-12.9 $Å^{-1}$, k^3 weighted.

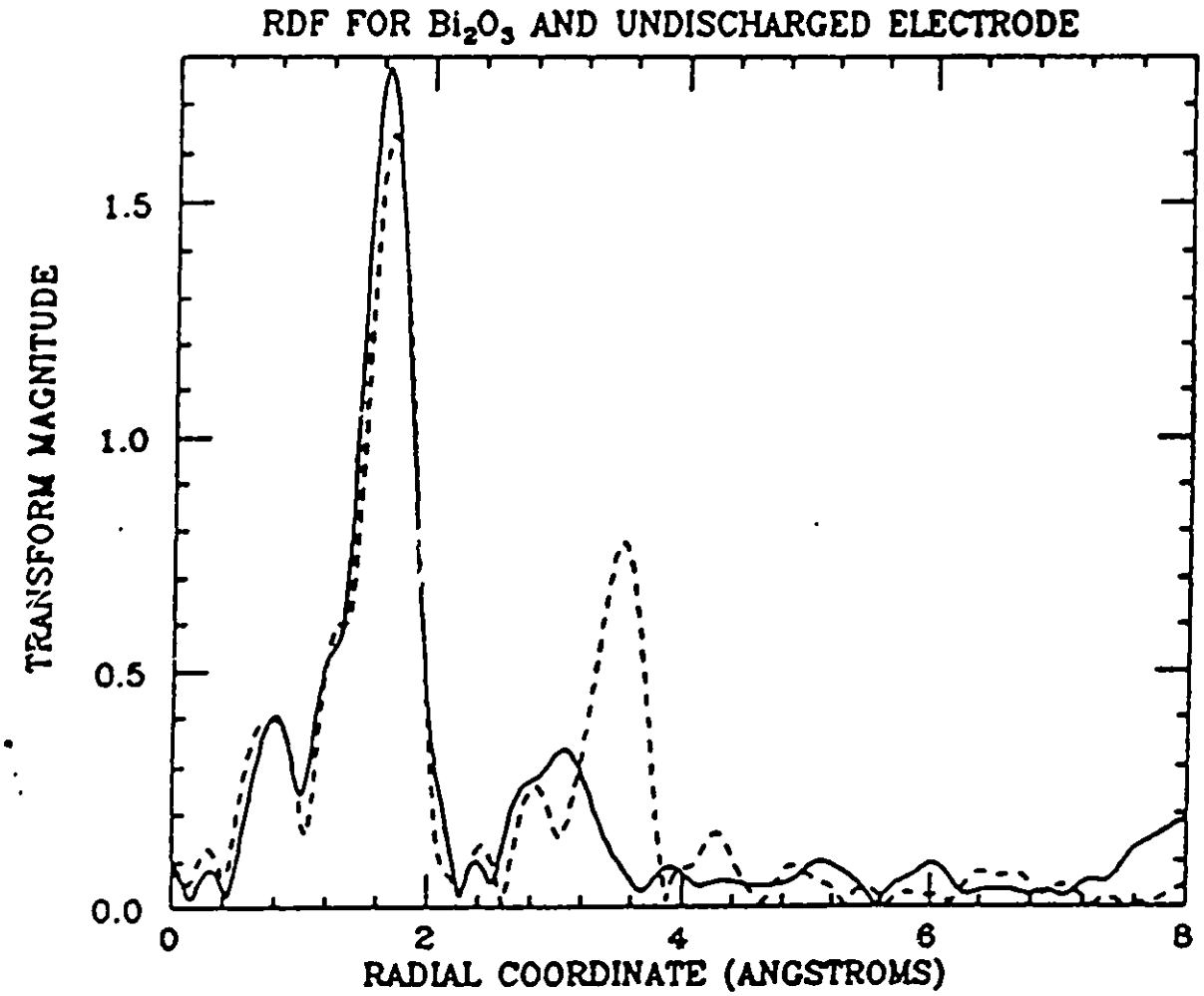

Fig. 48 RDF's for Bi in Bi_2O_3 and in the undischarged electrode; ——— Bi in electrode; ---Bi_2O_3. Δk = 2.6-14 $Å^{-1}$, k^3 weighted.

4.3.4 EXAFS Analysis of Bi-O Coordination

Preliminary analysis of the first peak in the Fourier transform of the Bi EXAFS data for the oxidized materials indicated that it corresponded to Bi-O coordination shells. Considerable difficulty was encountered, however, in generating good Bi-O phase and amplitude data.

Initial attempts to generate these from the FEFF programme of Rehr [90] failed to yield reasonable results. Data for comparative purposes were obtained on BiOCl at 77K. However, it was difficult to separate the Bi-O and Bi-Cl contributions. Finally, it was decided to use red tetragonal PbO as a reference material. Pure red PbO was prepared and data were obtained at 77K. The phase purity was checked by X-ray diffraction.

The Fourier transform parameters used in isolating the Bi-O contributions in Bi-doped MnO_2 are given in Table III. The parameters used in analyzing the PbO reference material are also given there.

All attempts to fit the data to a single-shell fit failed. Also examinations of Bi-O phase-corrected Fourier transforms indicated the presence of more than one shell. Accordingly, a two-shell fit was tried. Excellent fits were then obtained both in k-space and r-space for the two-shell modelling. These results are presented in Figs. 50 and 51. Excellent fits were also obtained for the imaginary part of the Fourier transform.

Table IV lists the fitting parameters for the two-shell fits. The fitting procedures for two-shell fits have been

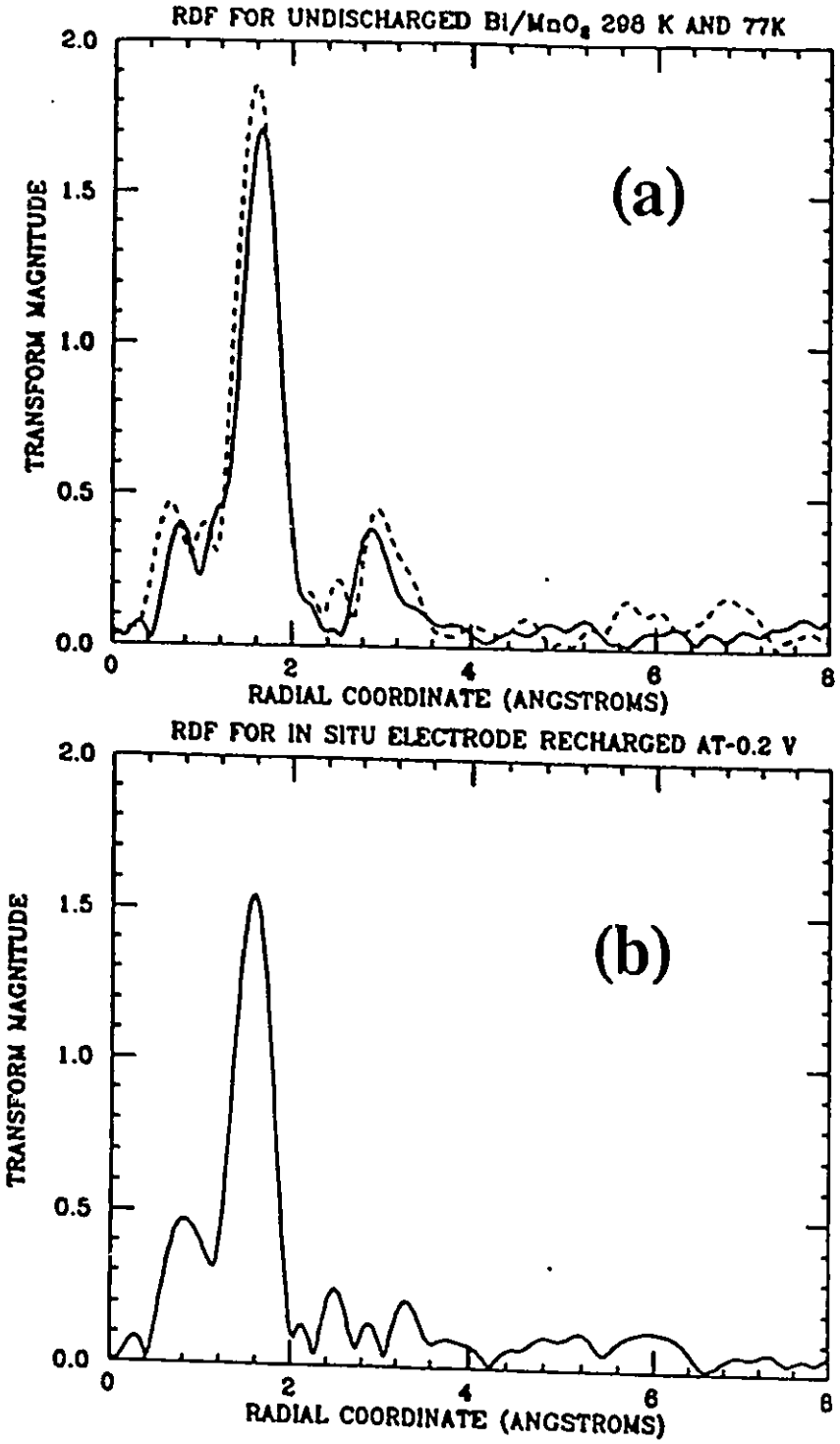

Fig. 49 Fourier transforms of EXAFS data; (a) *ex situ* undischarged electrode at 77 K (---) and 298 K (——), (b) *in situ* electrode recharged to -0.2 V. Fourier transform parameters are given in Table 1.

described in detail elsewhere [84]. All fits gave two shells with coordination numbers close to 4.0 and 2.0. In the final fit, these were fixed at these respective two values. When this was done, the fitting parameters were almost identical for k^1 and k^3 weighted fits.

Table IV Fitting parameters for the two Bi-O shells in Bi-doped MnO_2 materials

Material		Calculated Parameters N	R(Å)	$\Delta\sigma^2$(Å^2)	ΔE_o(eV)
Ex Situ					
Undischarged, 298K	(1)	4.0	2.20	-0.00075	-0.65
	(2)	4.0	2.32	-0.0036	18.9
Undischarged, 77K	(1)	4.0	2.17	-0.001	1.68
	(2)	2.0	2.31	-0.004	18.9
1e discharge, 298K	(1)	4.0	2.16	-0.0002	6.28
	(2)	2.0	2.26	-0.007	18.2
1e discharge, 77K	(1)	4.0	2.19	-0.004	3.16
	(2)	2.0	2.30	-0.007	18.2
In Situ					
Charged	(1)	4.0	2.19	-0.0026	1.68
	(2)	2.0	2.31	-0.006	18.9
Recharged, -0.2 V	(1)	4.0	2.16	-0.001	2.24
	(2)	2.0	2.29	-0.005	18.3

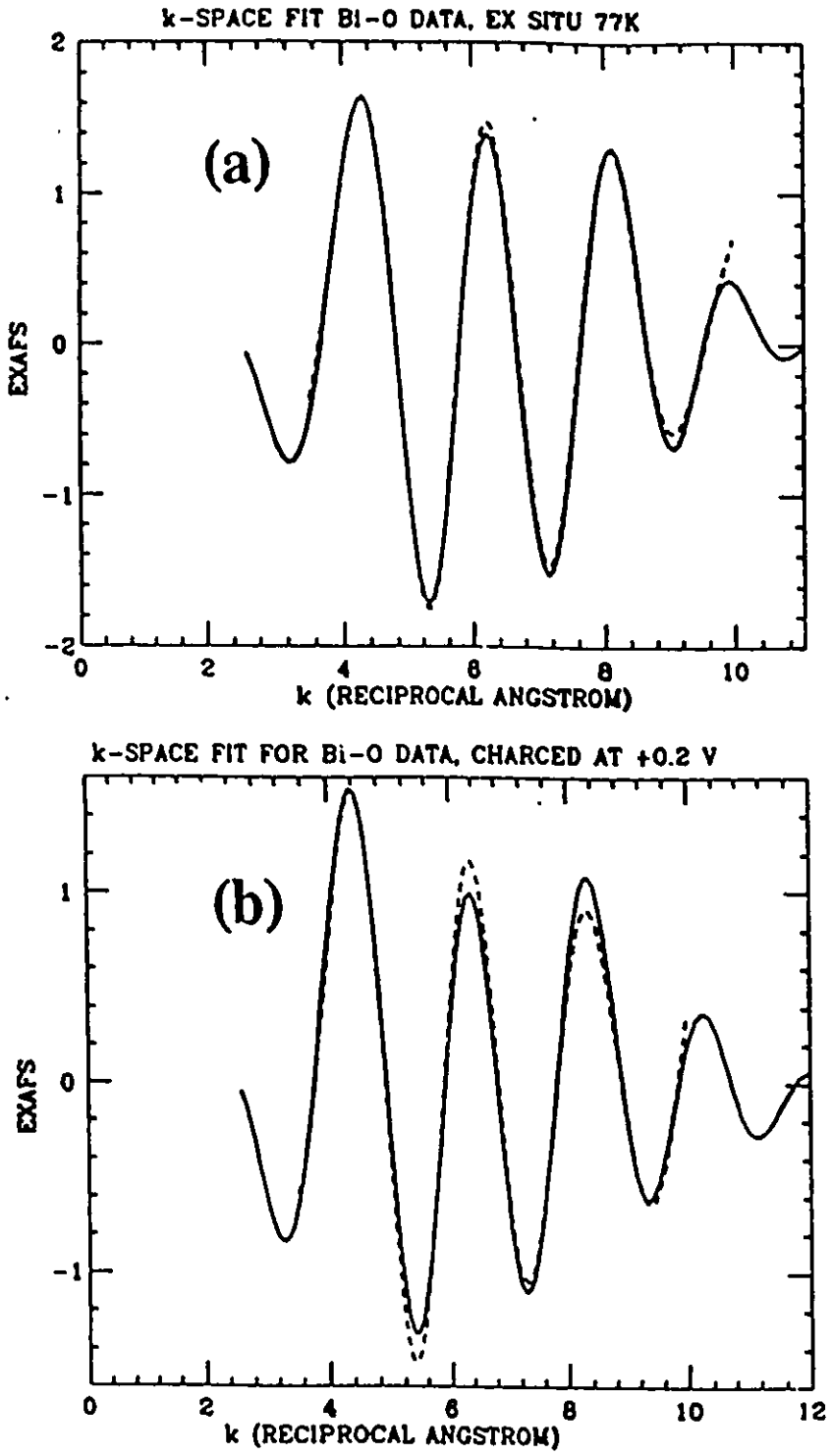

Fig. 50 Fits in k-space to Bi-O data: (a) *ex situ* data for undischarged electrode at 77K; (b) *in situ* electrode recharged to +0.2 V. The data are k^3 weighted and the fitting parameters are given in Table 2. (——) experimental data, (---) fitted.

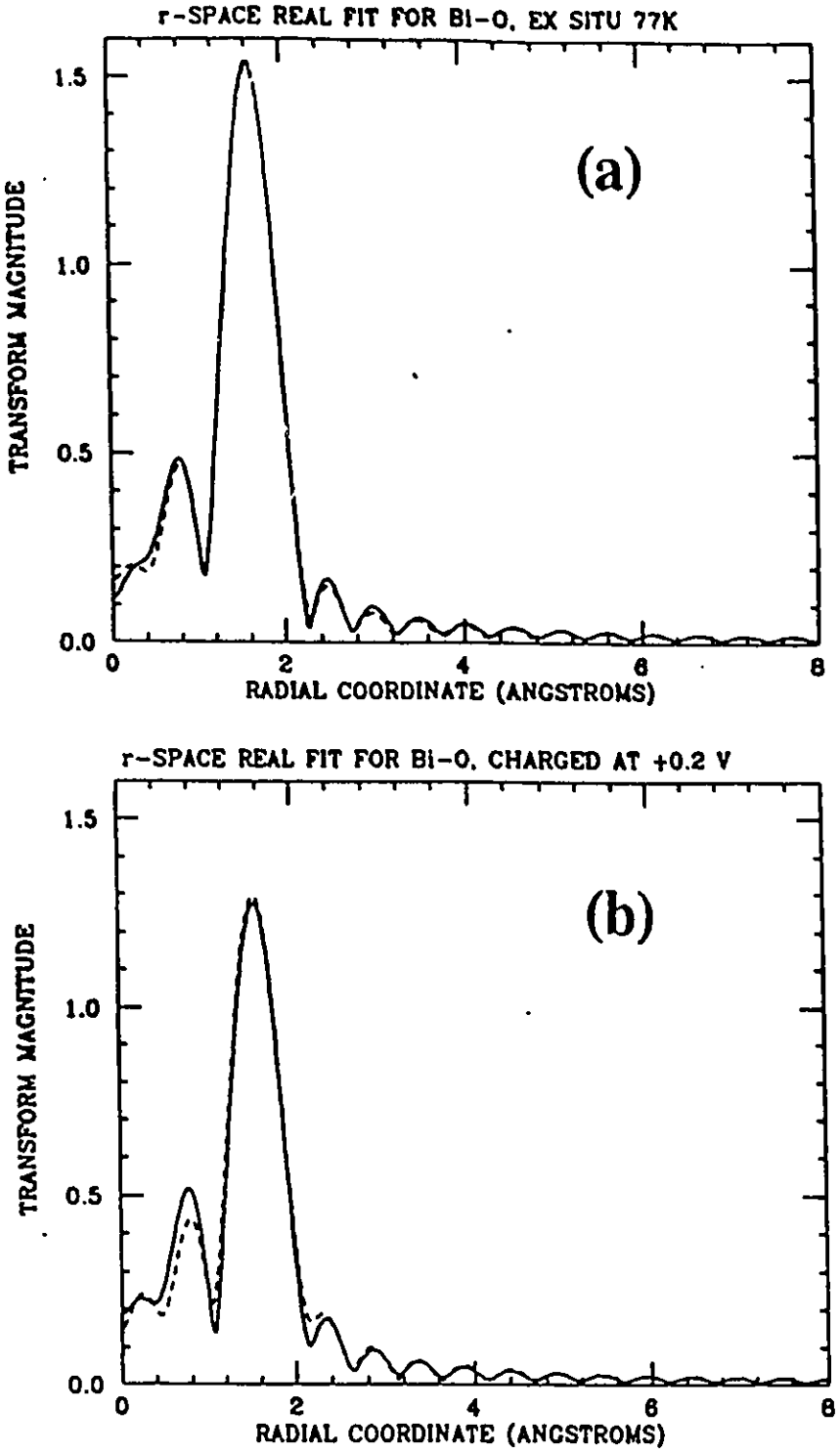

Fig. 51 Fits in r-space for Bi-O data; for (a) data in Fig. 13(a), (b) data in Fig. 13 (b). The transforms are k^3 weighted; Δk = 3.7-9.5 $Å^{-1}$. (—) experimental data; (---) fitted.

Attempts were made to fit the second peak in the Fourier transform for the charged material, at about 3Å. The back-transformed data indicated that this peak was most likely due to a Bi-Mn interaction, since the amplitude of the k^3 weighted EXAFS peaked symmetrically at $k=8Å^{-1}$. A Bi-Mn reference was generated using the FEFF program. Reasonably good fits in k-space were obtained but only with N=0.5 and R=3.53Å. The low value of N=0.5 could signify local coordination disorder generated by the presence of Bi in the Mn oxide structure. However, the difficulty in generating a reliable Bi-O reference using the FEFF program casts doubts on these results. There are irregularities in the core-atom phase shifts for high-Z atoms such as Pb and Bi. These would have to be checked against the FEFF theory before any firmer conclusions can be drawn.

It is interesting that the second-peak contribution largely disappears at the one-electron discharge level and when the electrode is recharged at -0.2 V (See Figs. 47 and 49B). This suggests several possibilities: one is that, at this potential, the Bi-O species are only weakly associated with the MnO_2 structure. Thus, there is the possibility that the recharge promotion or "catalytic effect" of the Bi on the initial stages of recharge might arise from an adsorption effect at the *surfaces* of MnO_2 particles.

Figure 52 shows a comparison of the Fourier transform of the *in situ* EXAFS for a deeply discharged electrode and for an electroplated Bi layer on Grafoil. The Bi is clearly present in

the metallic state in the reduced material. However, the decrease in the amplitude of the Fourier transform strongly suggests that very small particles are involved.

4.3.5 Manganese XANES

Two types of MnO_2 electrodes, CM MnO_2 and γ-MnO_2, were used in these measurements for the purpose of comparison.

Figure 53 shows normalized XANES spectra for manganese oxides in which Mn is in various oxidation states. The materials included MnO, Mn_2O_3, Mn_3O_4 and MnO_2 ("CMD", a battery grade, chemically prepared γ-MnO_2). There is an orderly shift in edge position with increase in oxidation state to the negative direction.

Figure 54 shows comparisons of *ex situ* normalized XANES spectra for Mn_2O_3, two types of CM MnO_2 and two types of γ-MnO_2 ("CMD" and "EMD", an electrolytically prepared battery grade material). The shift in edge positions of the CM MnO_2 to lower energies, may be due to partial replacement of Mn^{+4} sites by Mn^{3+} sites upon the introduction of Bi(III). An undoped MnO_2 sample, prepared by a similar precipitation procedure, had a spectrum almost identical to the 14:1 doped material. The more intense "white line" of the CM MnO_2 suggests a higher symmetry in the MnO_6 octahedra. This may be due to the absence of corner-shared octahedra in the structure.

Figs. 55 and 56 show *in-situ* Mn XANES spectra for a γ-MnO_2 electrode at various stages of discharge and recharge. The data in Fig. 55 indicate that the position of the Mn edge starts to

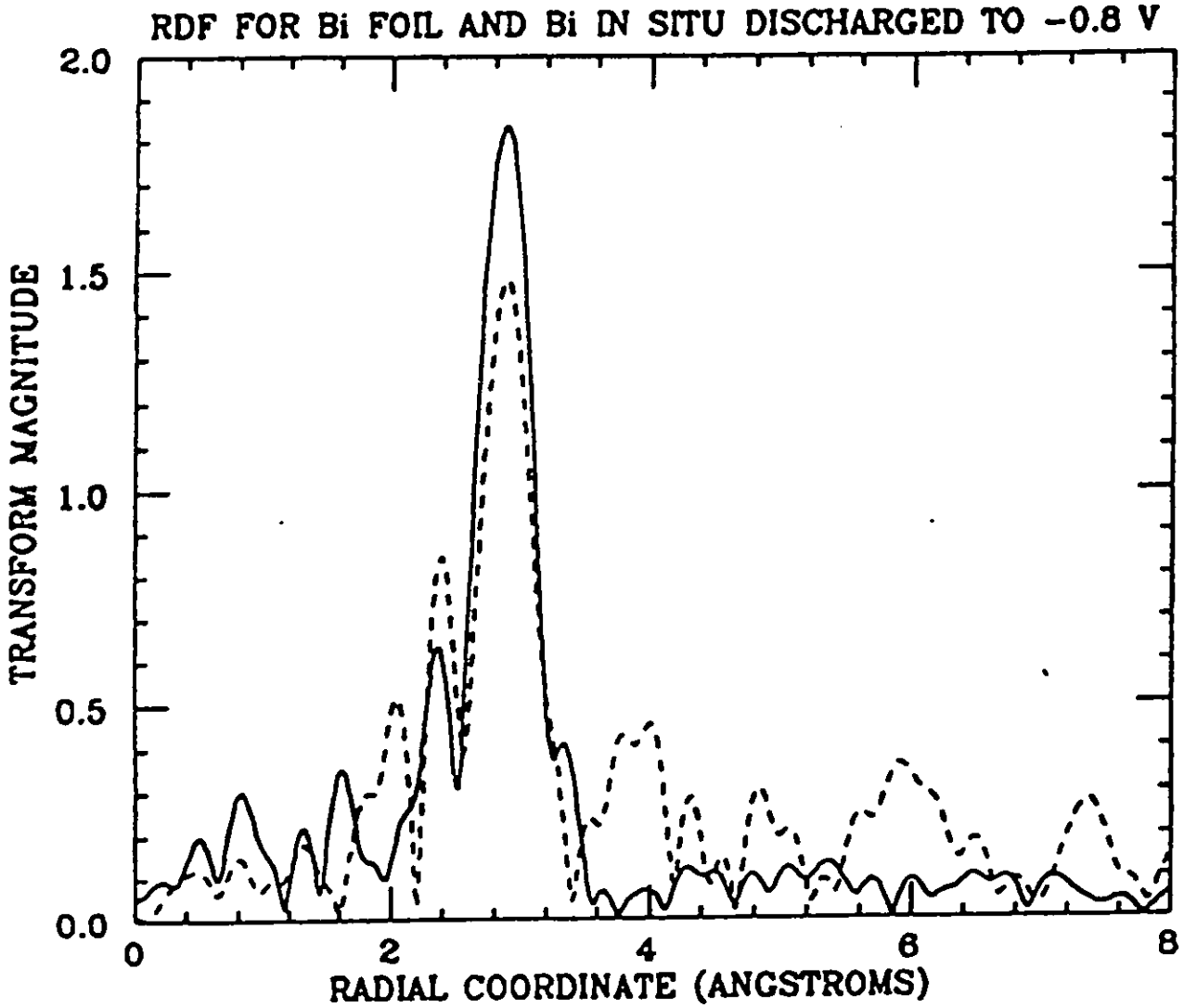

Fig. 52 Fourier transforms for electrodeposited Bi (——) and Bi in CM MnO_2 electrode discharged to -0.8 V.

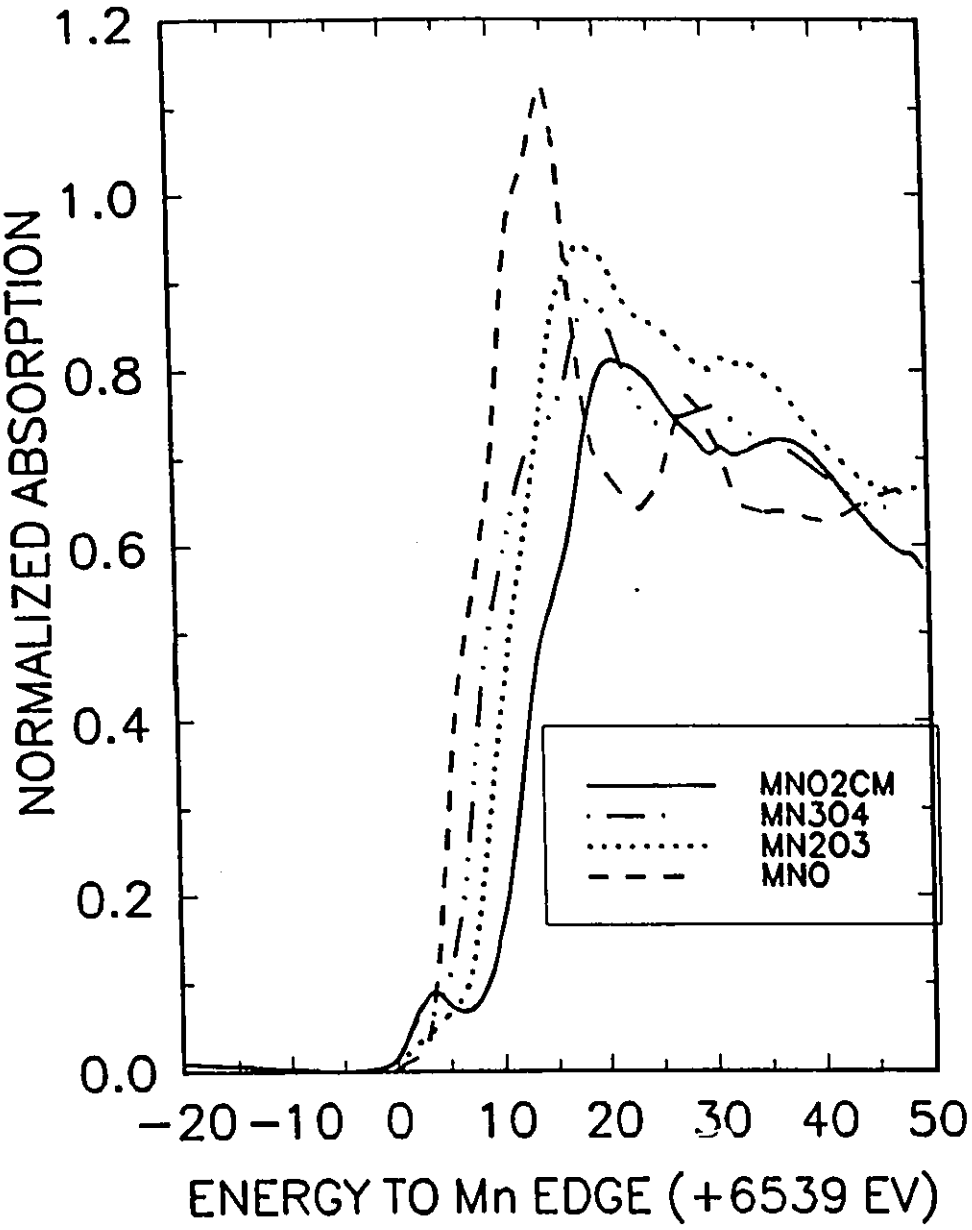

Fig. 53 Comparisons of near-edge Mn XAS for CMD MnO_2 with those for Mn_3O_4, Mn_2O_3 and MnO.

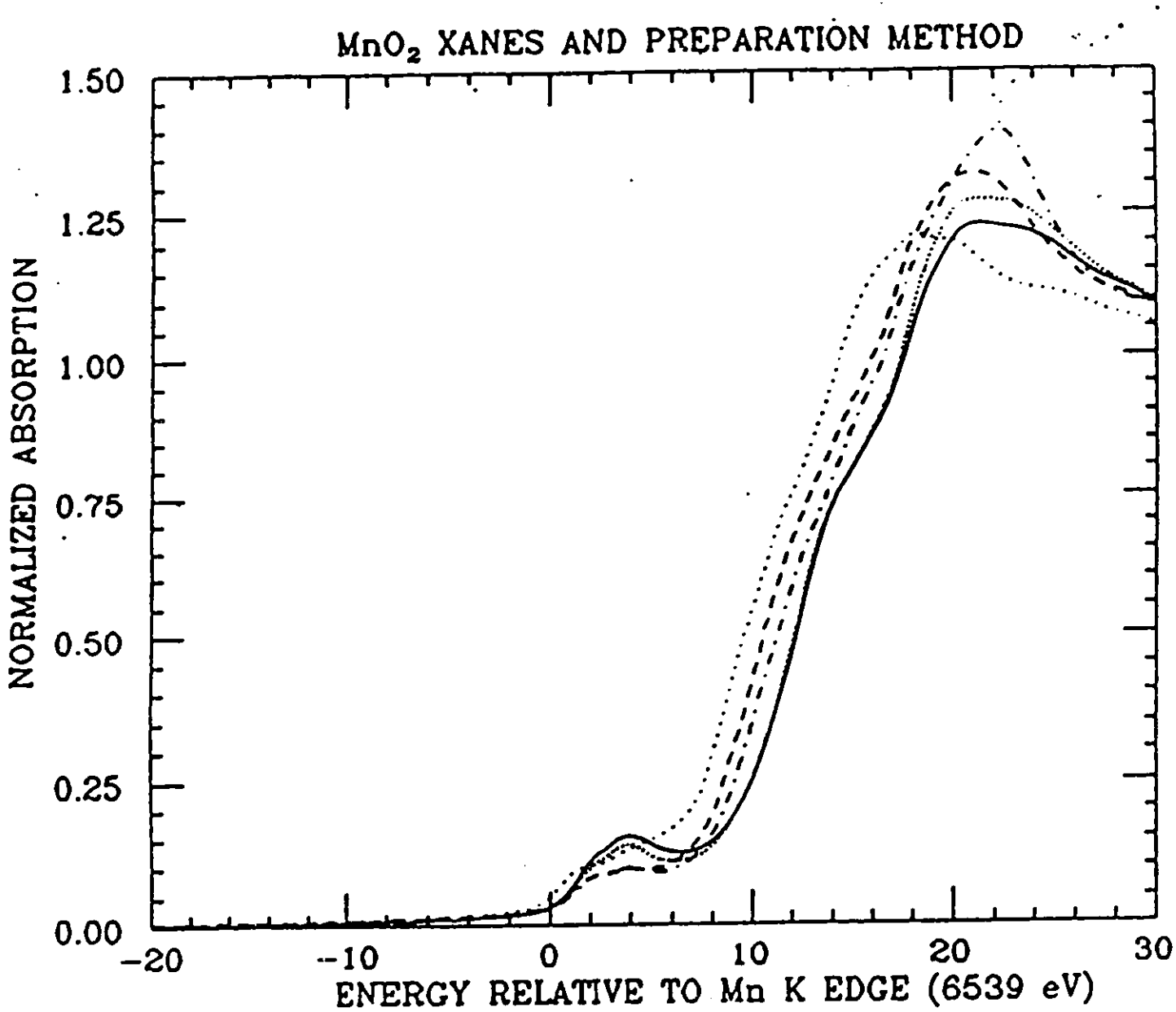

Fig. 54 Comparison of near-edge Mn XAS for Mn_2O_3(.....), CM MnO_2 (8.7:1) (_ o ___), CM MnO_2 (14:1) (_._._), CMD MnO_2 (.....) and EMD MnO_2 (——).

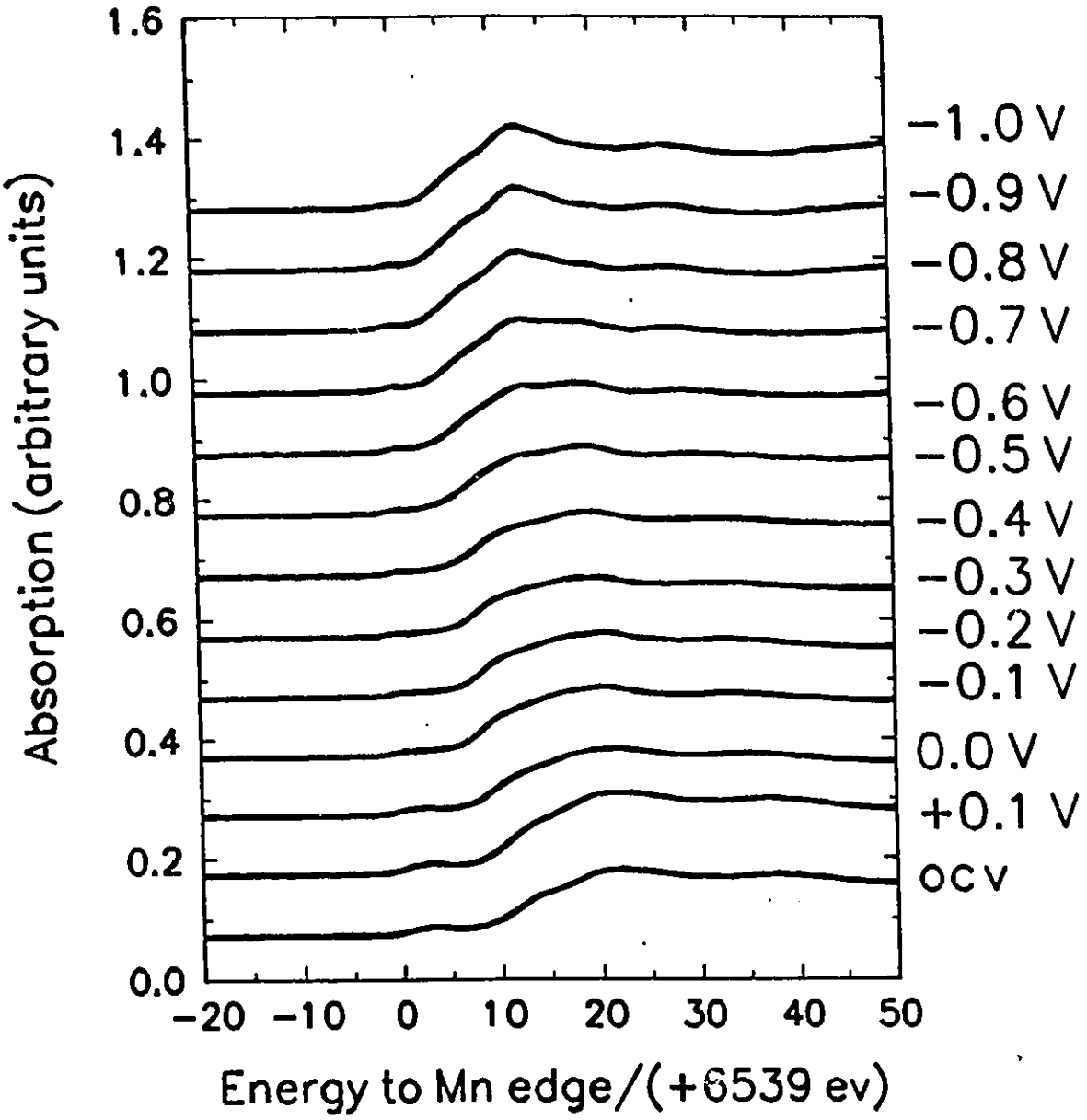

Fig. 55 Series of *in-situ* Mn XANES for γ-MnO_2 electrode at various potentials in the discharge process.

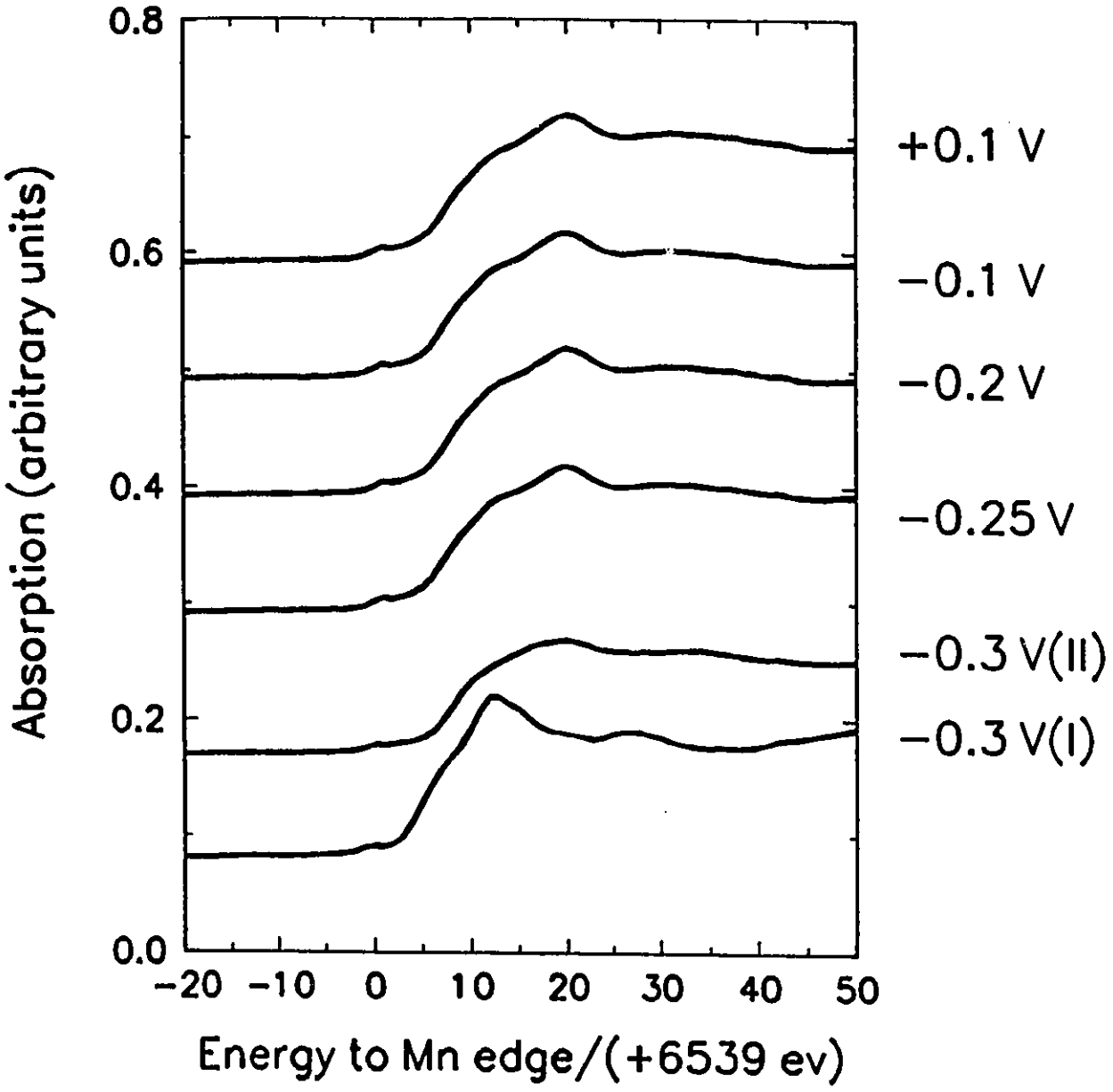

Fig. 56 Series of *in-situ* Mn XANES for a discharged γ-MnO_2 electrode at various potentials in the recharge process.

shift at 0.0 V and continually shifts thereafter in an orderly way to lower energy as the potential increases to -1.0 V vs Hg/HgO, at which potential part of the Mn is in the Mn(II) state as might be expected. The satellite peak at 6554 eV, which represents the Mn(II) state, evidently cannot be observed until the discharge potential reaches -0.6 V vs Hg/HgO (Fig. 55).

In the recharge process (Fig. 56), however, the shift of the Mn edge position, which reflects the oxidation state of Mn in the electrode, cannot be observed until -0.3 V; in other words, the re-oxidation process does not start substantially until the potential reaches -0.3 V v Hg/HgO.

Figures 57 and 58 show *in situ* Mn XANES spectra for CM MnO_2 electrodes at various stages of charge and discharge. The data indicate that, in the fully discharged state, the Mn is in the Mn(II) state, as might be expected. The data also suggest that, at intermediate potentials, there is correspondingly a mixture of oxidation states of Mn.

By comparing Fig. 57 with Fig. 55, and Fig. 58 with Fig. 56, the differences between the CM MnO_2 electrode and γ-MnO_2 electrode can be indicated.

(i) In the case of the CM MnO_2, the shift of the Mn edge position to low energy can be observed only until the potential reaches -0.35 V vs Hg/HgO, while the shift can be observed at a γ-MnO_2 electrode as soon as the discharge begins at 0.0 V. The evidence, however, seems to indicate that the reduction of CM MnO_2 begins

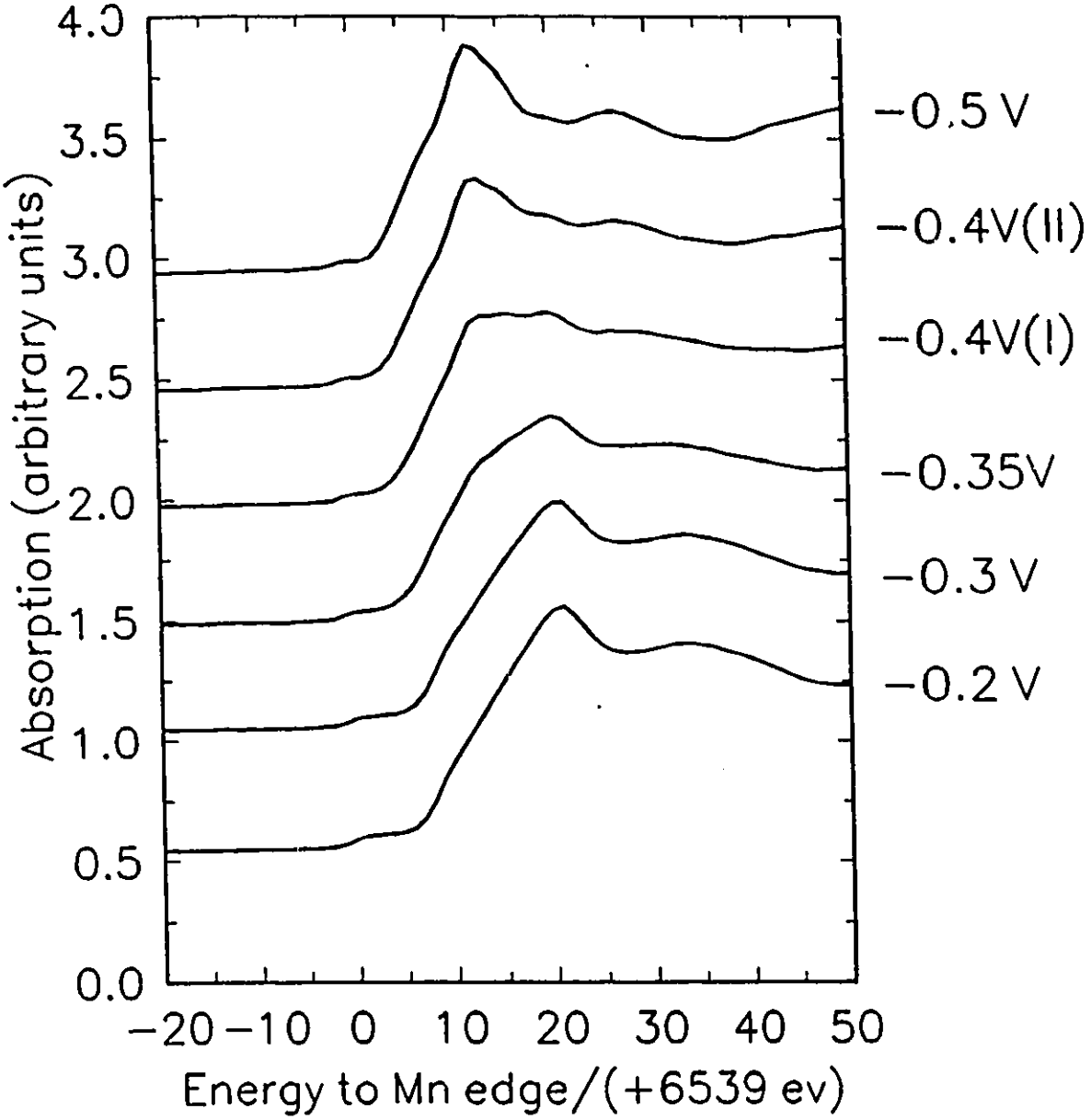

Fig. 57 Series of *in-situ* Mn XANES for a CM MnO_2 electrode at various potentials in the discharge process.

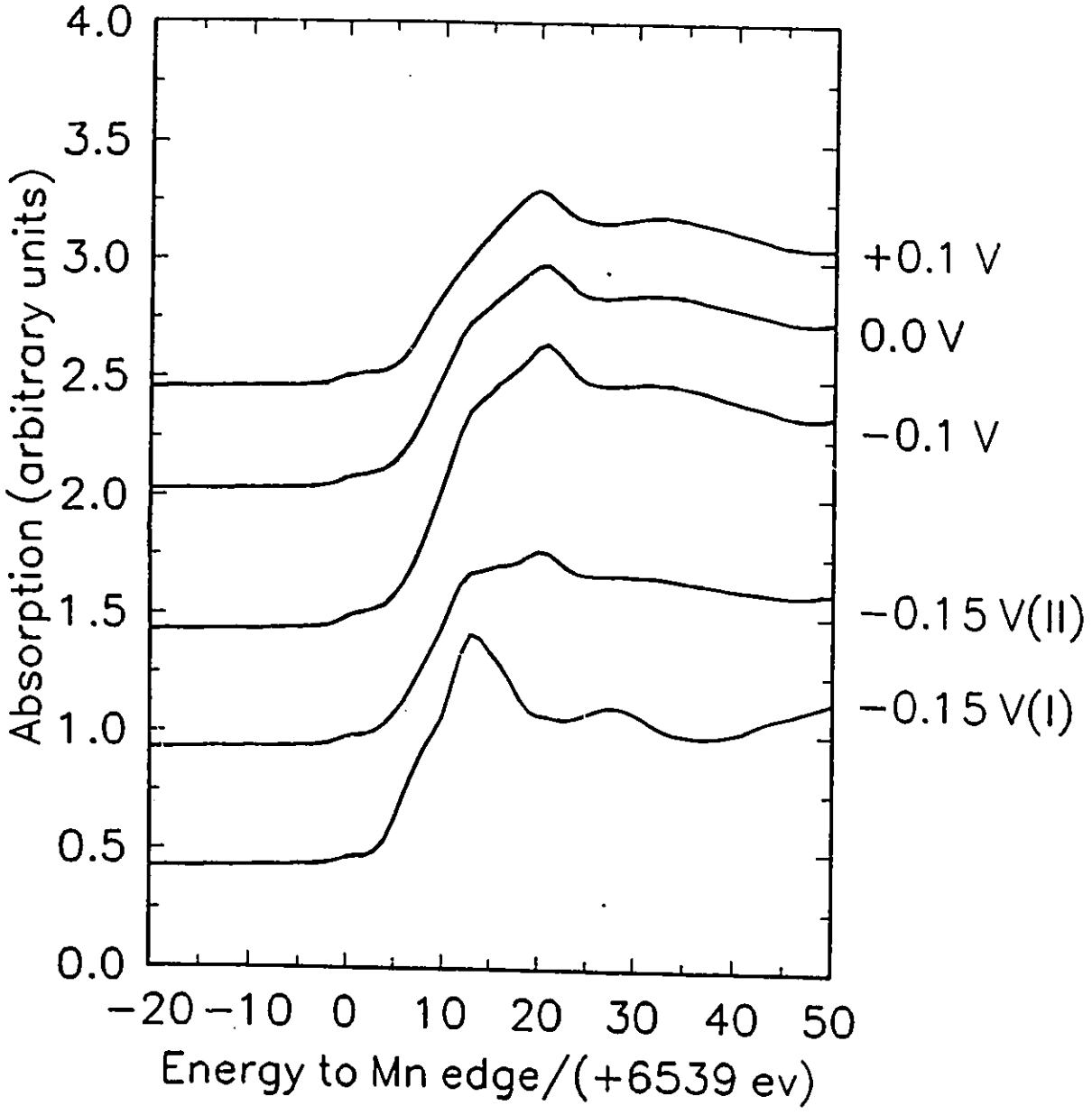

Fig. 58 Series of *in-situ* Mn XANES for a discharged CM MnO_2 electrode at various potentials in the recharge process.

at -0.35 V vs Hg/HgO, and the product is a mixture of Mn oxides in different oxidation states of Mn, mainly IV (i.e. MnO_2), while the reduction of γ-MnO_2 already begins at 0.0 V.

(ii) The major reduction process at the CM MnO_2 electrode arises at -0.4 V vs Hg/HgO, at which potential the MnO_2 can be continually reduced to $Mn(OH)_2$ through the intermediate oxidation state III of Mn, which means, as mentioned in a previous section, that the two-electron reduction of CM MnO_2, beginning at -0.35 V, can be completed at -0.4 V. This conclusion is in agreement with results presented and discussed in Sections I and II of this chapter. On the other hand, however, there is no evidence of the formation of Mn(II) at γ-MnO_2 until the potential reaches -0.6 V vs Hg/HgO, and the product at -1.0 V is still a mixture of Mn(II) and Mn(III). The conclusions that the second electron reduction at γ-MnO_2 cannot begin until -0.6 V and that the material cannot be fully reduced, even at -1.0 V, are consistent with the results of McBreen's work(36).

Complementary kinetic information can be obtained by studies of the *in-situ* time-resolved XANES at MnO_2 electrodes. Figs. 59 and 60 show the shift of the position at the Mn edge *with time* while the potential was held at -0.35 V and -0.4 V vs

Hg/HgO, respectively. A satellite peak, which corresponds to low valence Mn, can be observed after 40 mins of potential holding at -0.35 V. With the potential being held at -0.4 V vs Hg/HgO (Fig. 60), however, the Mn edge continually shifts to lower energy.

Figs. 61 and 62 show the time-resolved Mn edge position shift at the γ-MnO_2 electrode while the potential was held at -0.2 V (Fig. 61A), -0.3 V (Fig. 61B), -0.6 V (Fig. 62A) and -0.7 V (Fig. 62B). Slow but significant shifts of the Mn edge position can be observed, while potentials were held at -0.2 V vs Hg/HgO (Fig. 61A) and -0.3 V. (There was no significant edge shift at -0.4 V). The appearance of the satellite peak at 6551.5 eV, which corresponds to the formation of Mn(II), can evidently be discerned at -0.6 V (Fig. 62A). The Mn(II) peak, however, keeps increasing, while the peak at 6559 eV, which corresponds to development of high-valence Mn, decreases continuously (Figs. 62A and B).

By comparing the case of CM MnO_2 (Figs. 59 and 60) with that of γ-MnO_2 (Figs. 61 and 62), the behaviour observed can be interpreted in terms of kinetic differences between the behaviour of the two electrodes:

(i) the second electron can begin to be discharged at -0.35 V and be completed at -0.4 V at the CM MnO_2 electrode, while the second electron cannot begin to be involved in reduction until -0.6 V at the γ-MnO_2 electrode. A 200 mV difference of potential can be

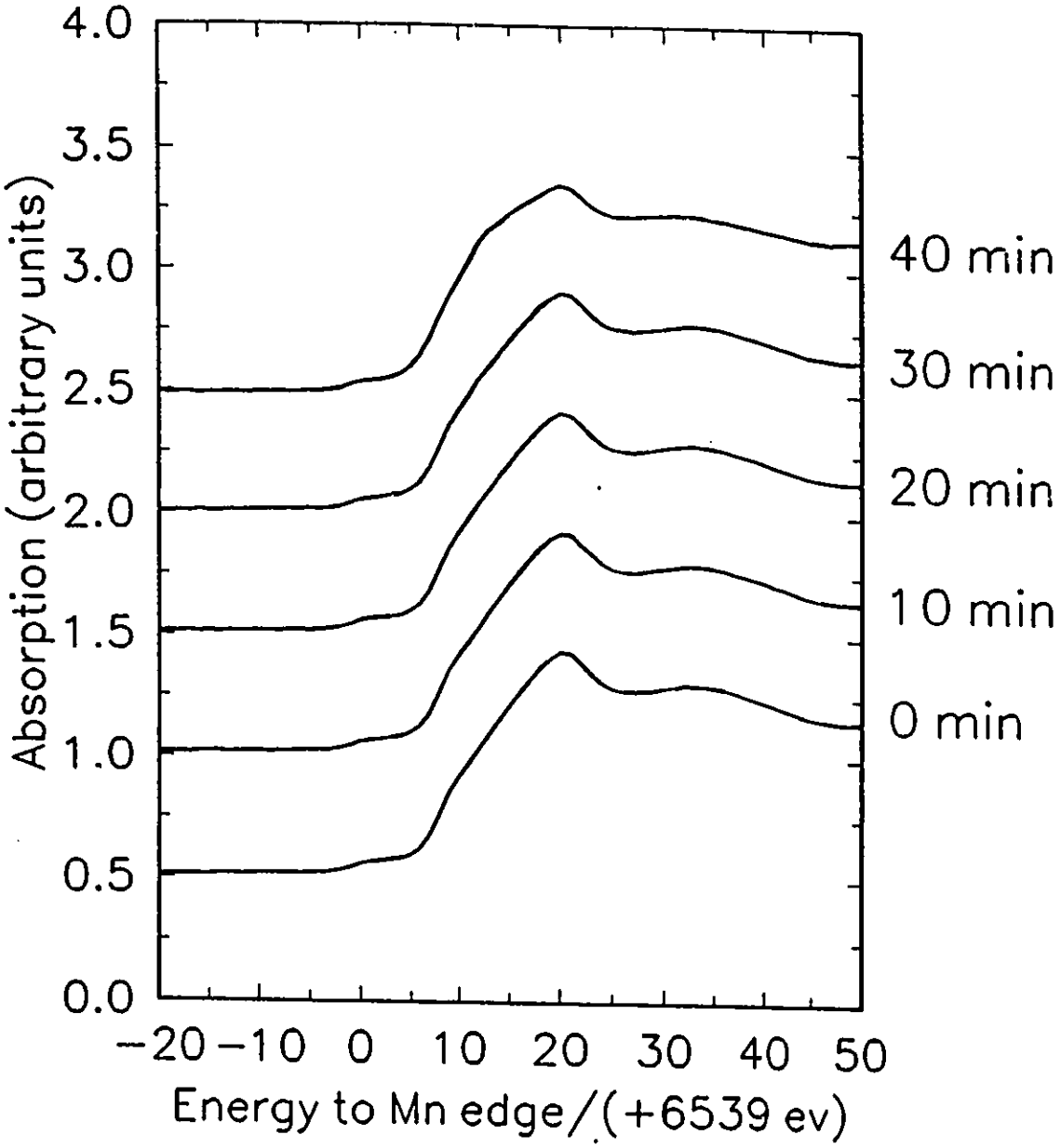

Fig. 59 *In-situ* Mn XANES for a CM MnO_2 electrode discharged at -0.35 V vs Hg/HgO, recorded over a series of times.

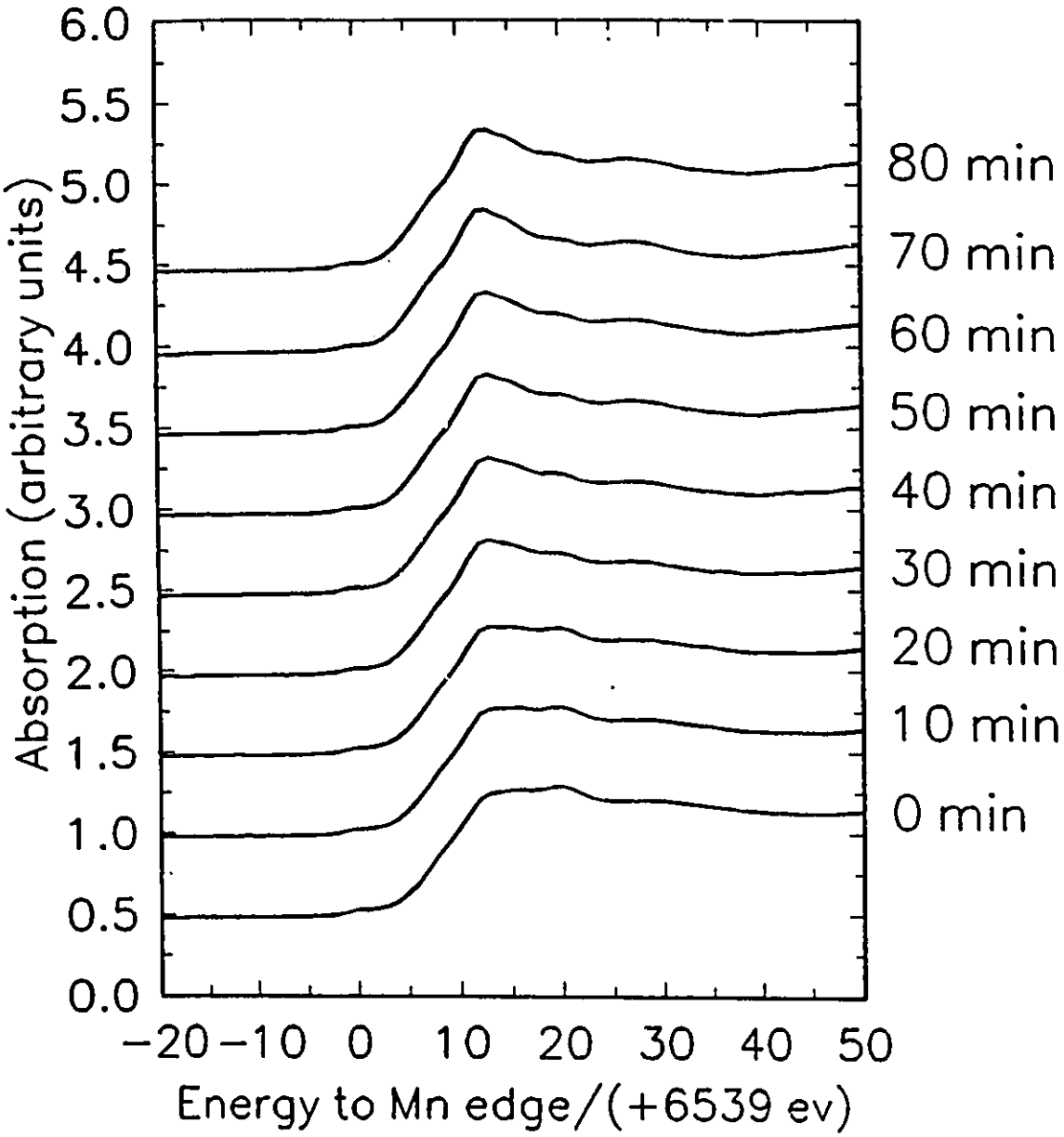

Fig. 60 *In-situ* Mn XANES for a CM MnO_2 electrode discharged at -0.4 V vs Hg/HgO, recorded over a series of times.

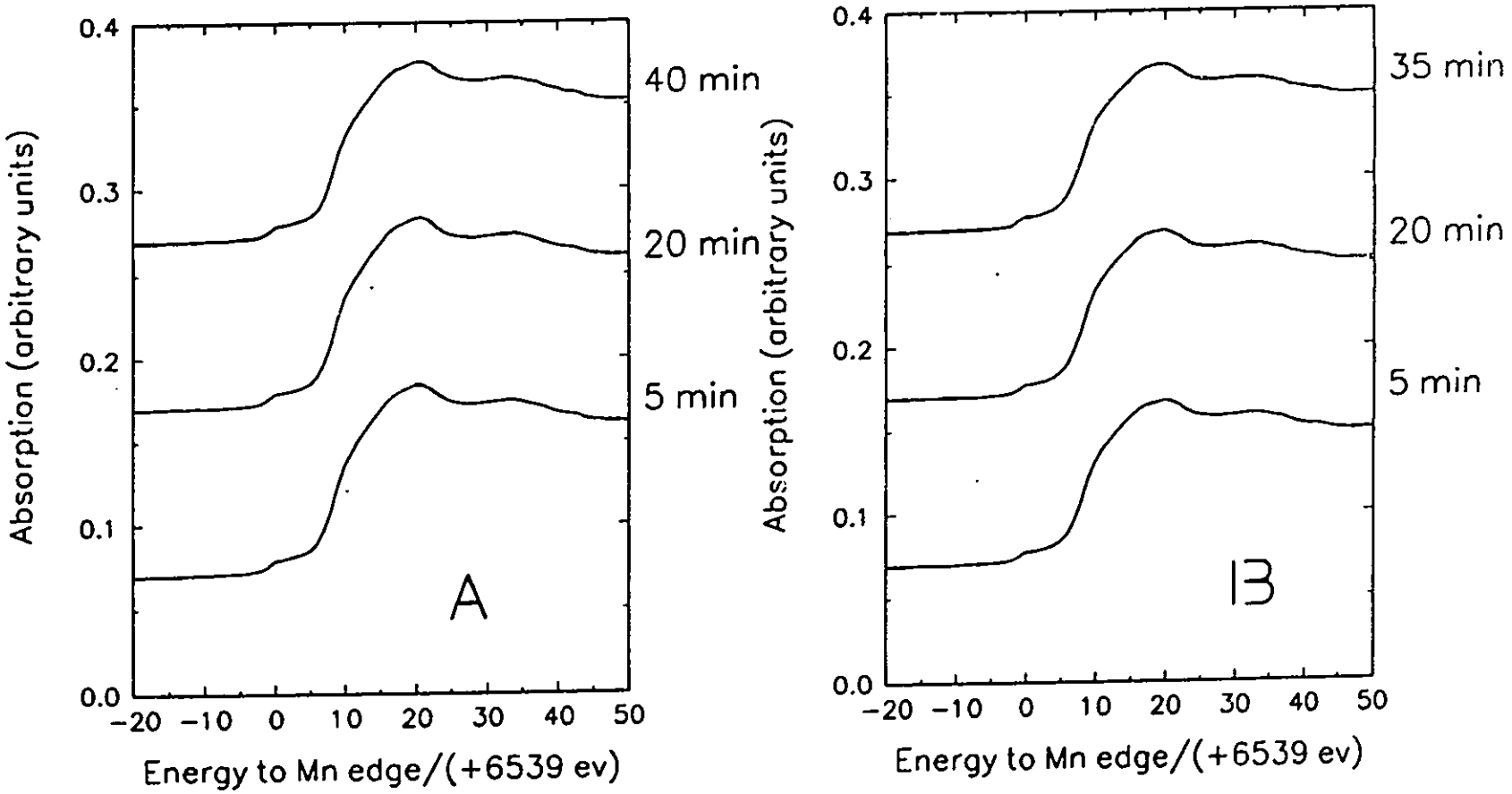

Fig. 61 *In-situ* Mn XANES for a γ-MnO_2 electrode discharged at -0.2 V (A) and -0.3 V (B), recorded over a series of times.

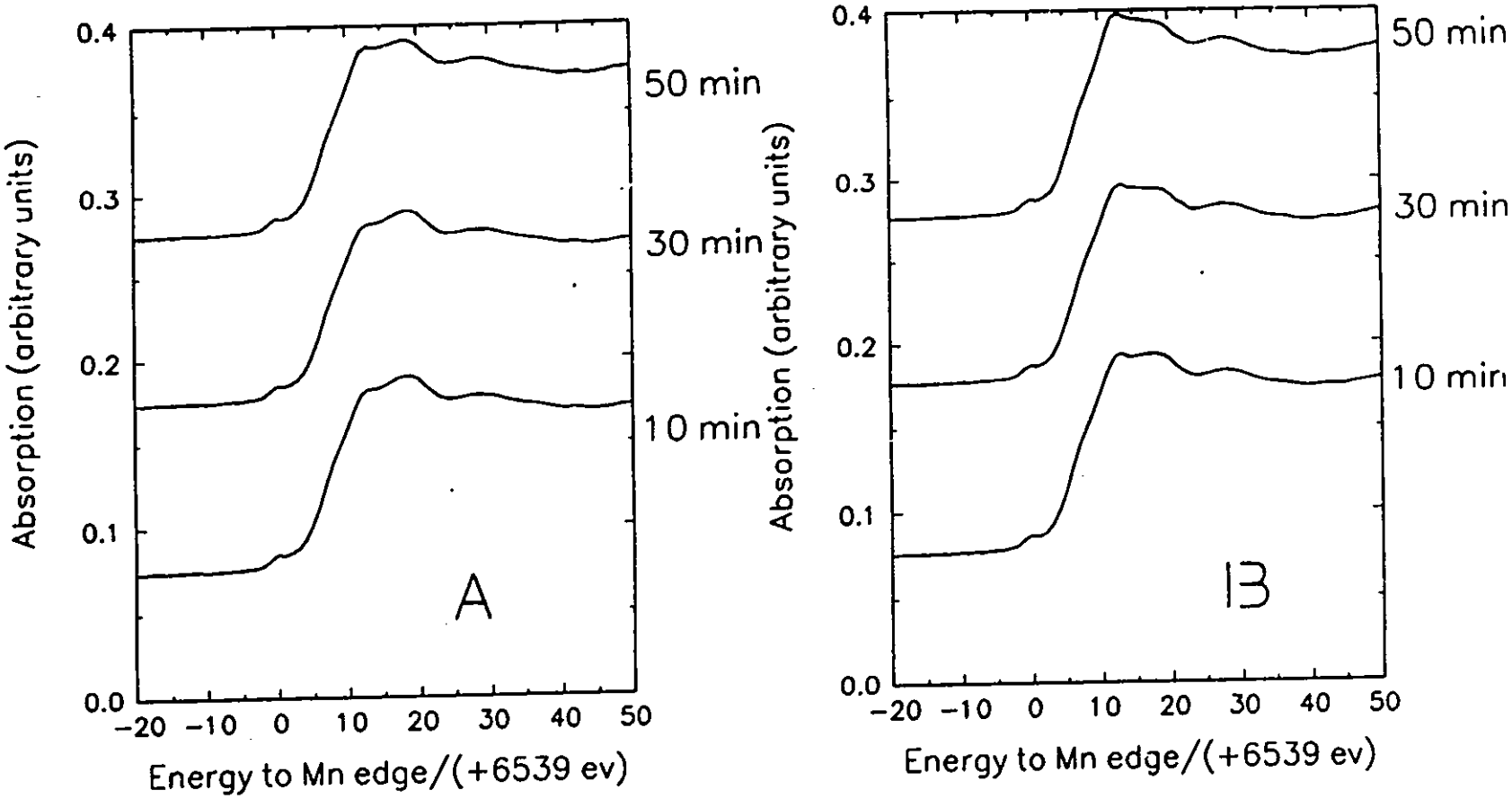

Fig. 62 *In-situ* Mn XANES for a γ-MnO_2 electrode discharged at -0.6 V vs Hg/HgO (A) and -0.7 vs Hg/HgO (B), recorded over a series of times.

observed (in agreement with other results presented earlier, cf. Fig. 42).

(ii) the rate of reduction at the CM MnO_2 electrode, at a given potential, is substantially greater than that at the γ-MnO_2 electrode. Approximately, the passage of 2-electron reduction charge can be completed at -0.4 V within 100 mins at CM MnO_2 (Fig. 60), but the one-electron reduction at γ-MnO_2 can hardly be completed within 80 mins (Fig. 61).

Fig. 63A shows a comparison of the Mn XANES data for an undischarged γ-MnO_2 electrode and a fully recharged one, while Fig. 63B shows a corresponding comparison of an undischarged CM MnO_2 electrode with a fully recharged one. It is clearly seen that the product of recharged CM MnO_2 is identical with the undischarged materials (the slight edge shift for the recharged electrode results from residual low valence Mn, which remains un-recharged inside the electrode). However, in the case of γ-MnO_2, the recharged MnO_2 electrode is evidently different from the undischarged one, from the point of view of structure.

These results are important in demonstrating that "structural reversibility" is realized in discharge and recharge of CM MnO_2 . but not with γ-MnO_2 . Correspondingly the UV-visible spectroelectrochemistry showed that the discharge/recharge processes were "chemically" reversible.

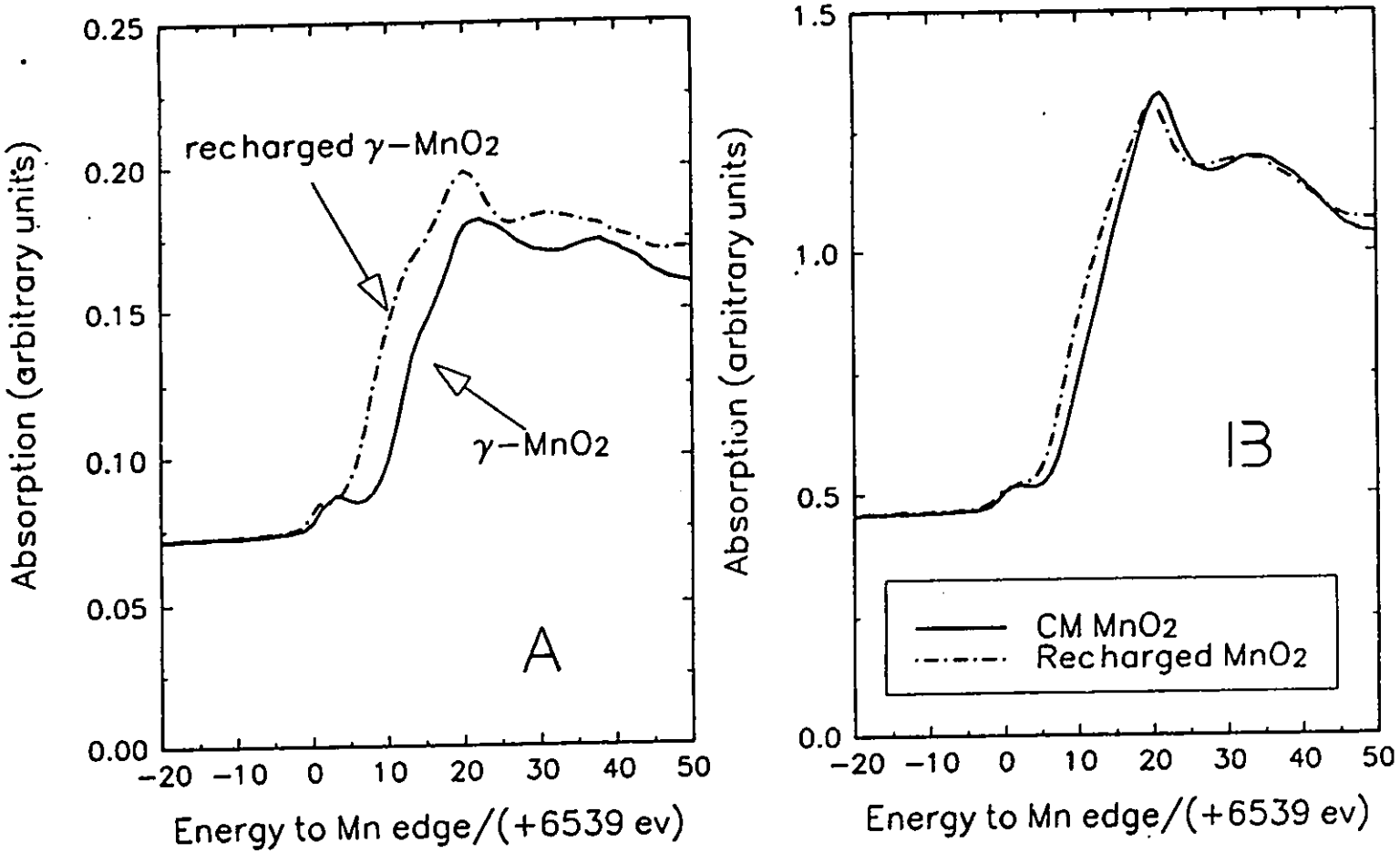

Fig. 63 Comparison of Mn XANES data for the undischarged γ-MnO_2 electrode (solid line in A), CM MnO_2 (solid line in B) with the fully recharged "γ-MnO_2"electrode (dot dashed line in A) and recharged CM MnO_2 electrode (dot dashed line in B).

4.3.6 *In Situ* Manganese EXAFS

Figures 64(A) and 64(B) show the progress of the Mn RDF profiles with various stages of discharge. The data for the undischarged and completely discharged product are similar to those found for the Ni.O.OH/$Ni(OH)_2$ couple [78], in that the reduced material has all the features of the oxidized material but with peaks at larger R values. This is consistent with a layer-type MnO_2 being reduced to a layer-type $Mn(OH)_2$ with extended Mn-O and Mn-Mn bond lengths.

The reduced amplitude of the peaks for the material at the intermediate stage of discharge suggests that a disordered material has been generated. Figure 65(B) shows a comparison of the data for an electrode in undischarged and recharged states. The results are identical and thus elegantly confirm the reversibility of the system, especially with respect to structure changes.

Figure 65(A) shows the development of the Mn EXAFS pattern during charge. At -0.15 V, behaviour corresponding to the disappearance of the discharged product and the formation of the corresponding charged product can be clearly seen. Once again the data indicate that the intermediate, presumably some Mn(III) species, has a much weaker EXAFS pattern than either the charged or the completely discharged material. Elucidation of this will require further data analysis and extension of the experimental work. (Note that availability of experiment time on the synchrotron line is strictly limited - 1 week in 6 months for

external users).

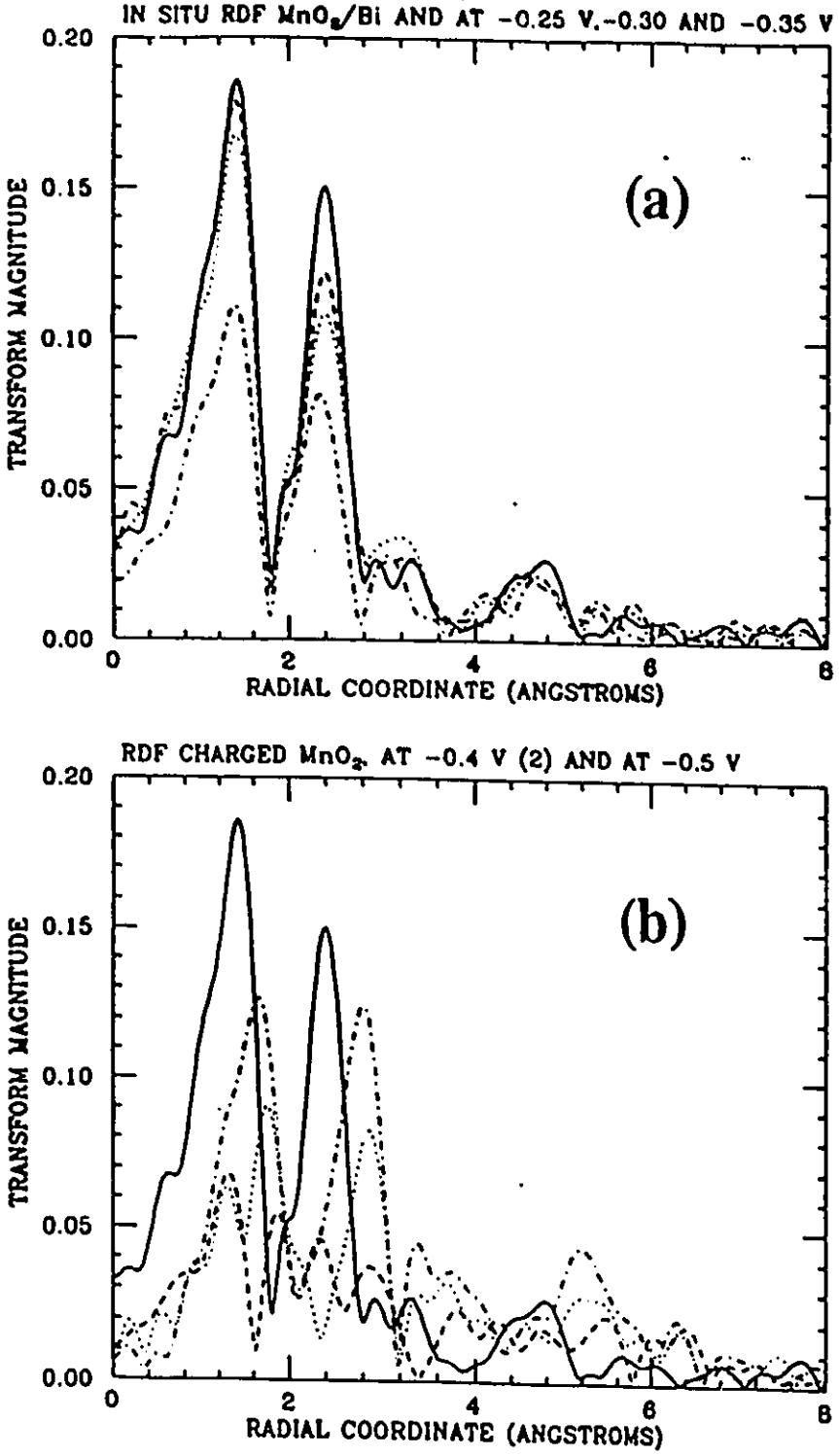

Fig. 64 Fourier transforms of the *in situ* Mn EXAFS data during discharge; (a) undischarged electrode (——), after discharge to -0.25 V (---),-0.3 V (....) and -0.35 V (-.-.-_); (b) undischarged electrode (——), first scan at -0.4 V (----), second scan at -0.4 V (.....), after discharge to -0.5 V (-.-.-). Δk=2.7-11.3 $Å^{-1}$, k^1 weighted.

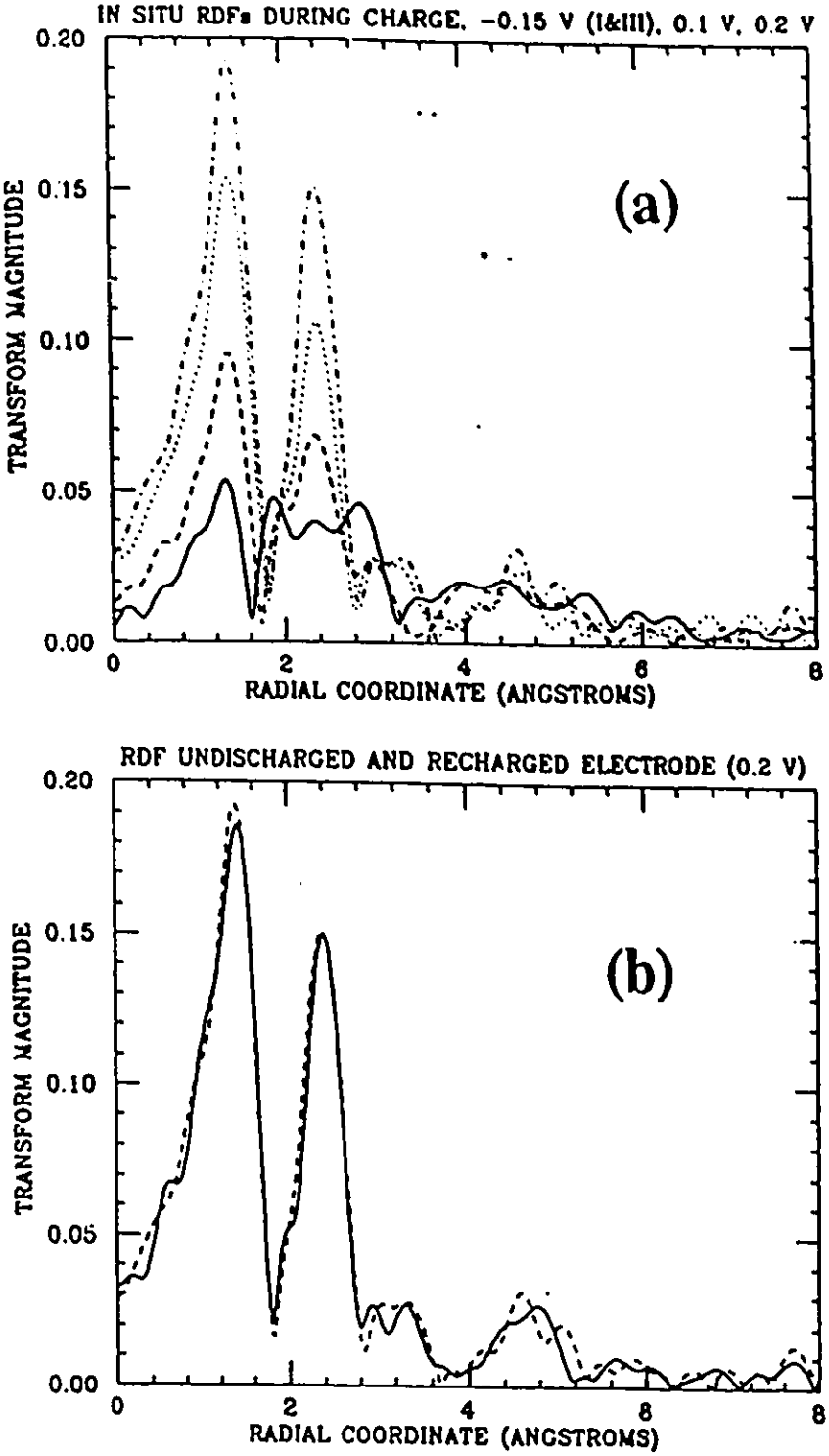

Fig. 65 Fourier transforms for *in situ* Mn EXAFS data during CM MnO_2 recharge; (a) first scan at -0.15 V (——), second scan at -0.15 V (----), at 0.1 V (....), at 0.2 V (-.-.-). (b) comparison of data for undischarged electrode and electrode recharged to 0.2 V (---), Δk=2.7-11.3 $Å^{-1}$, k^1 weighted.

Section IV Rechargeability of Cell Modules Containing CM MnO_2 Electrodes

In the course of the present work and in the earlier published research [60-64, 66-74], the rechargeability of Chemically Modified MnO_2 material has been fully demonstrated; also, the physico-chemical and electrochemical behaviours of the material related to the nature of factors impeding or imparting rechargeability were also extensively studied and are now quite well understood. However, from the technical point of view, several problems still remain ahead. One is the high percentage of carbon loading in the electrode required to achieve good practical discharge rates; another is the influence of zincate ion, if zinc is used as the anode. Various attempts have been made by the research team at University of Ottawa to examine this matter and good progress has been made. The results, however, are in the process of being filed for patent protection.

4.4.1 Percentage of carbon loading

Good cycle life and rate capacity in the current and previous work (59-64) were obtained only at electrodes containing a high carbon (graphite) loading (usually 1:10 MnO_2/carbon weight ratio).

The lower the percentage of carbon, the less is the cycle life and the smaller is power density that can be achieved.

However, use of electrodes having high carbon loadings does not lead to any problems in the mechanism studies, from the basic scientific points of view, but such electrodes cannot be used in practical full cells, because of the low power-density and limited rechargeability.

The loss of capacity at electrodes having low percentage carbon loading is related to the formation of soluble $Mn(OH)_6^{3-}$ species in the processes of discharge and recharge. If the percentage of carbon or graphite in the electrode is sufficiently high, most of the soluble Mn(III) intermediates can remain absorbed uniformly within the pores of the porous electrode matrix, or adsorbed on the particles of the matrix, and this quantity of absorbed species in the dissolved state can be further reduced to $Mn(OH)_2$ in the discharge process or re-oxidized to MnO_2 in the recharge process. The processes involving redeposition of $Mn(OH)_6^{3-}$ take place *inside the bulk of the electrode matrix*, so the distribution of the formed $Mn(OH)_2$ (on discharge) or MnO_2 (on recharge) is uniform in the electrode matrix and good contact of the formed $Mn(OH)_2$ or MnO_2 with the graphite matrix can be maintained. On the other hand, if the percentage of carbon in the electrode is relatively low, two factors can be considered as influencing the rechargeability of the electrode.

Firstly, a relatively large quantity of soluble $Mn(OH)_6^{3-}$ can diffuse into the bulk of the electrolyte solution (the saturation concentration of $Mn(OH)_6^{3-}$ in 9M KOH solution can be

reached; (cf. 4.2), and some fraction of this dissolved material can, obviously, disproportionate. Actually, as was noted earlier in our long-period cycling experiments, after two days, solid MnO_2 could be found deposited on the walls of the cell compartment in which the MnO_2 electrode was accommodated, even at a high percentage (1:10 MnO_2/graphite ratio) of carbon.

Secondly, in the process of redeposition from $Mn(OH)_6^{3-}$ species, which are in the bulk of the electrolyte solution, the $Mn(OH)_2$ (on discharge) or MnO_2 solid (on recharge) can only be formed *on the surface of the porous electrode* instead of *inside the porous electrode structure*.

After several cycles, the electrode matrix, which is a good conductor initially, can become covered by a layer of pure MnO_2 or $Mn(OH)_2$ which are semiconductors. Thus, the conductivity of the electrode tends to become decreased and ohmic polarization at the electrode can increase dramatically.

These problems could be solved in principle by use of conditions which maintain localization of the soluble $Mn(OH)_6^{3-}$ species inside the electrode matrix.

4.4.2 The influence of zincate ion

In alkaline aqueous electrolytes, the highest cell voltage can be achieved by coupling the MnO_2 electrode with a Zn anode. Unfortunately, zinc is highly soluble in alkali, in which the concentration of zincate ions can reach over 2M (in 9M KOH) under electrochemical cycling conditions and, in fact, become supersaturated. The presence of zincate ions in the electrolyte

shortens the cell life, leading to the well-known phenomena of shape change, densification, and/or dendritic growth of redeposited Zn at the Zn anode.

However, besides the inherent problems of the zinc electrode itself, migration and diffusion of zincate ions to the MnO_2 electrode is known [60,61] to lead to the formation of electrochemically inactive hetaerolite in the MnO_2 cathode. The same phenomenon was shown to arise in modified Mn-oxide/Zn cells by Ford's research staff(60,61).

In order to solve this problem, it is necessary to block the soluble zincate ion from reaching the MnO_2 electrode. Attempts to suppress the zincate ion concentration by addition of a number of organic materials (61), or by using various commercial separators (61) have been made by Wroblowa et al. However, none of the results of those attempts is satisfactory in practice.

A Nafion-type ion-selective membrane separator, functioning as a barrier to ZnO_2^{2-} ion transfer, like the Nafion membrane used by Wroblowa (61), was initially employed in the present work for investigation of the operation of the Bi-modified MnO_2 in a secondary alkaline CM MnO_2/Zn cell module, i.e. with the CM MnO_2 worked against a rechargeable Zn anode. The function of the separator is to prevent the soluble ZnO_2^{2-} ions diffusing to the MnO_2 electrode where such ions react with the active cathode material and cause serious loss of its rechargeability, as found initially by Wroblowa (61). It also serves to minimize any Bi-

ion transfer in the opposite direction, arising from the very small solubility of Bi(III) species in the aq. KOH.

Fig. 66 shows plots of percentage of theoretical two-electron capacity vs cycle number for (1) with the separator present and (2) without such a separator. The results in this figure are based on constant current discharge/charging curves for the CM MnO_2/Zn system in a plate-geometry cell (see Fig. 4B) using a cut-off cathode potential of -0.6 V vs Hg/HgO. Fig. 66 illustrates clearly the effectiveness of the an ion-selective separator, enabling, in these tests, 52 cycles to be attained still with 80% of the two-electron capacity remaining electrochemically accessible.

In order to avoid the influence of zincate ions, various other anode materials could be chosen to replace the Zn. In aqueous alkaline cells, a metal-hydride, Fe or cadmium could be considered as alternative anode materials. Of course, each combination of anode/cathode material has its own problems; for example, the unfriendly influence of Cd on the environment, the relatively low cell voltage of the Fe/MnO_2 couple and self-discharge problems with metal-hydride/MnO_2, etc. are well known difficulties.

In non-aqueous electrolytes, modified MnO_2 materials can be coupled with lithium as anode material, and also probably the sodium electrode, to form a rechargeable system, with the MnO_2 used as the Li-intercalation host material (Bi dopants can also be considered as intercalated into the lattice of CM MnO_2). The

advantage of such cells lies in their high operating voltages, unattainable in aqueous system, and potentially high energy and power densities. Such less familiar systems could have both conventional and special-purpose applications.

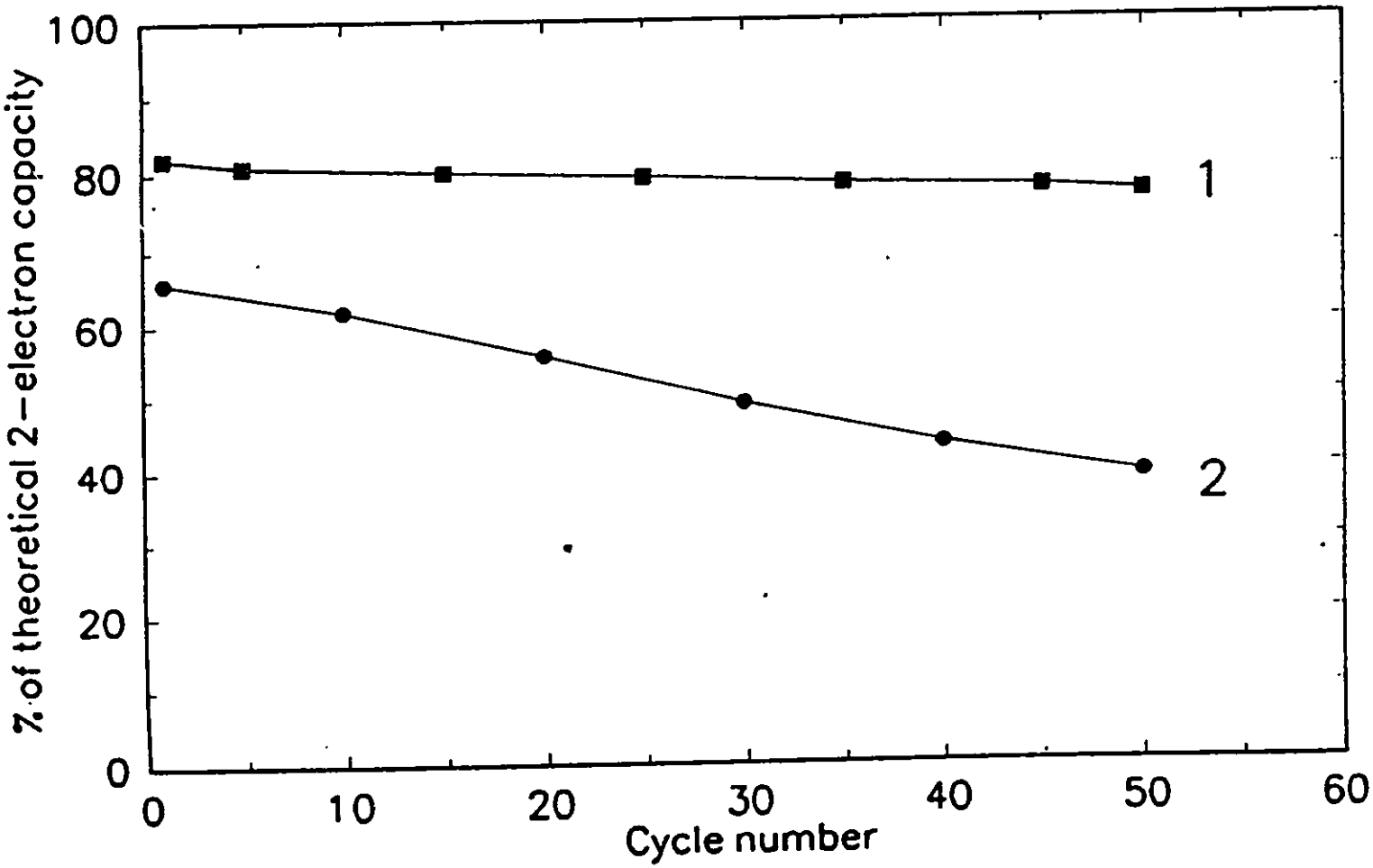

Fig. 66 Plots of percentage of achievable two-electron capacity vs cycle number for a combined CM MnO_2/Zn cell system, (1) with, and (2) without the presence of an ion-selective separator in the cell.

Chapter V

Conclusions

1 From the results of three types of detector experiments (constant current discharge with a detector electrode, use of the RRDE and the *in-situ* spectroelectrochemical method), it was concluded that a soluble Mn(III) species, which was indicated as $Mn(OH)_6^{3-}$, is formed in significant amount, even at the beginning of a discharge half-cycle in the case of the CM MnO_2, and this behaviour differs from that found with γ-MnO_2. It was also demonstrated how soluble $Mn(OH)_6^{3-}$ species are formed in each of the cases of γ-MnO_2, Blank MnO_2 and CM MnO_2 reduction, but the amounts of $Mn(OH)_6^{3-}$ species involved are substantially different from one to another for electrodes having the same "Mn" loading. Related effects are observed on recharge. Correspondingly, rates of formation and consumption of $Mn(OH)_6^{3-}$ species are greatest at the CM MnO_2.

2 *In-situ* and *ex-situ* XANES experiments on Bi and Mn give results that enable characterization of the states of oxidation of both Mn and Bi to be made in the processes of discharge and recharge of both CM MnO_2 and γ-MnO_2. The Bi dopants are found to catalyze the

second electron stage of MnO_2 discharge/recharge at more positive potentials (about 200 mV higher than for undoped γ-MnO_2) .

3 The *in-situ* and *ex-situ* EXAFS results for Bi and Mn give specific information on the Bi-O, the Bi-Mn and Mn-Mn coordination distances through the evaluated radial structure functions.

4 A *parallel* composite pathway, in which the soluble $Mn(OH)_6^{3-}$ species are involved in an "heterogeneous" step coupled with an "homogeneous" "electron-proton" pathway is proposed as the overall mechanism of discharge and recharge of MnO_2. However, different types of MnO_2 favour relatively different extents of participation of the two reaction pathways, the heterogeneous one being preferred at the CM MnO_2.

5 The "proton hopping" process is regarded as the rate-determining step in the homogeneous pathway but the latter can be bypassed by discharge or recharge going through the heterogeneous pathway involving a soluble Mn(III) species. Thus, types of MnO_2 such as CM MnO_2,

for which the heterogeneous pathway is shown to be favoured, have the advantage of passing high density of current, an attribute which could be used favourably in "heavy duty" batteries like those required for electrical vehicles or SLI ("Starting, lighting and ignition") applications.

6 Bi(III) dopant not only makes the processes of discharge and recharge of MnO_2 favour the heterogeneous pathway, but this is also apparently associated with a diminished activation energy of the process of deposition of $Mn(OH)_2$ from the soluble $Mn(OH)_6^{3-}$ intermediate back on to the porous electrode structure, i.e., a kinetic or catalytic effect is involved. Thus, the overpotentials for further reduction or re-oxidation of $Mn(OH)_6^{3-}$ tend to be decreased.

7 In the case of Bi(III)-doped MnO_2, the reduction does not need to be restricted to the first-electron "homogeneous" discharge pathway in order to maintain "rechargeability", as is evidently required with γ-MnO_2. Hence the depth of discharge does not need to be limited in the way that is required for cycling of γ-MnO_2, viz. restricted to less than the one-electron

range. In fact, recyclability to 90% depths of discharge can be achieved.

8 The rechargeability of CM MnO_2 relies, in part, on the redeposition of the soluble species. In practical battery embodiments, there would be *no* problems arising from this situation since a restricted electrolyte volume is used and virtually no free liquid electrolyte is present, as it is in the present optical and detector-electrode experiments.

9 The CM MnO_2 cathodes have the following unique combination of advantages which would be especially suitable, amongst other possibilities, for electric-vehicle applications:

(a) Rechargeability: up to 1000 cycles or more;

(b) High theoretical specific capacity and specific energy, at least twice that of nickel oxide and lead dioxide cathodes.

(c) Capability of high charge/discharge rates: over 6C, or even up to 10C, at electrodes having high graphite: MnO_2 ratios to minimize internal resistance

sufficiently.

(d) A flat discharge profile, after an initial decline, giving a constant working voltage (1 V vs Zn) over a wide range of current densities or C rates.

(e) The materials are non-toxic, inexpensive and abundant.

By means of an ion-selective separator, the CM MnO_2/Zn cell system can achieve 52 cycles without any serious decline of the rechargeability: about 80% of theoretical two-electron charge still remains accessible after the 52-cycle-life tests. Further development of a better separator material will lead to improved performance against a Zn anode; Such work is in progress.

Chapter VI

Claims to Original Research

In the present work, classical electroanalytical[66-69], in-situ UV-visible spectro-electrochemistry[70,71] and *in-situ* X-ray absorption methods[72-74] have been used in studying Ford's CM MnO_2 in order to further elucidate the role and behaviour of the soluble Mn(III) intermediate involved in multiple cycling of MnO_2, in relation to the role of Bi dopants. Thus, the purpose of the spectroelectrochemical experiments was to examine if there are significant differences in the production of soluble Mn(III) species from discharge and recharge of CM MnO_2 in comparison with blank MnO_2 (no Bi) or γ-MnO_2, and hence obtain an indication of whether the role of the intermediate stage is changed by the doping of MnO_2 by Bi(III).

The *in-situ* X-ray absorption experiments provide direct and complementary experimental evidence for both the change of oxidation state of Mn and Bi, and the change of co-ordination environment of Mn-Bi, Mn-Mn, Mn-Bi and Mn-O during the processes of discharge and recharge. By comparing the results obtained at CM MnO_2 and γ-MnO_2, valuable information on the redox mechanism steps has been obtained , as well as on the role of Bi dopants in the reaction pathway.

In complementary work on comparison of the kinetics of charging and discharging of CM MnO_2 with that at γ-MnO_2, we have observed that the CM material can sustain much higher current-densities (per g of active material), both on charge and discharge, than the γ-MnO_2 material, over a well defined and flat discharge potential plateau.

In the light of the works done by previous researchers, the Bi-modified cathode materials, both Chemically Modified (CM) and Physically Modified (PM) have been extensively studied in comparison with γ-MnO_2 and "blank" MnO_2 by means of various complementary experimental techniques:

1) classical electrochemical methods, including cyclic-voltammetry, use of a rotating ring-disk electrode, constant-current discharge and recharge methods, etc.
2) A new *in-situ* spectro-electrochemistry technique and
3) *In-situ* and *Ex-situ coupled* X-ray absorption (XAS) - electrochemistry measurements.

The role of the Bi dopant, as well as the role and behaviours of the soluble Mn(III) intermediate(s) involved in multiple cycling have been further elucidated. Mainly, two major directions of work have been carried out:

i) The reaction mechanisms of discharge and recharge of Bi-doped MnO_2 materials have been extensively studied, especially the physical, physico-chemical and electrochemical aspects which lead to major

improvement of the rechargeability of the cathode material.

An heterogeneous reduction mechanism was proposed, coupled with the well-known "homogeneous" mechanism for γ-MnO_2, based on experimental results derived from the following four stages of the investigation:

1) fundamental electrochemical aspects, by means of classical electrochemical methods.
2) the role of soluble Mn(III) intermediates in the reaction in the solution, arising from the MnO_2 electrode (by means of a new *in-situ* UV-visible-electrochemical method).
3) information on structure change, especially the co-ordination environment of reactive species during discharge and recharge processes (by means of the combined *in-situ* and *ex-situ* EXAFS-electrochemical method).
4) information of the change of oxidation state of the reactive species, Mn and Bi, during the discharge and recharge (by means of *an in-situ* XANES-electrochemical technique).

All the above information was obtained in comparative studies on CM MnO_2 vis à vis γ-MnO_2 and "blank" MnO_2.

ii) Several tasks have been completed which enable the

work to proceed to full cycle-life testing by using a newly developed and the being patented membrane separator with the longer term aim of commercial development and evaluation.

Based on the information obtained from the mechanism studies, full cell (MnO_2/Zn) testing was performed by:

(i) selecting and modification of proper ion-selective membranes, which could be used to prevent the soluble zincate ions from diffusing into the vicinity of, and into the MnO_2 electrode.

(ii) trying to increase the percentage of CM MnO_2 in relation to that of carbon to a practically useable level by efforts at keeping the soluble Mn(III) species from diffusing into the bulk of the electrolyte by localizing them in pores of the MnO_2/C electrodes matrices.

In conclusion, the successfully synthesised, rechargeable Bi-doped MnO_2 was subjected to various electrochemical and *in-situ* optical evaluation procedures (including a new *in-situ* UV-visible spectro-electrochemistry procedure and a new X-ray absorption-electrochemistry method) in order better to understand the reaction mechanism(s) of rechargeability of the MnO_2 material.

Good progress was made with several of the above

distinguishable aspects, leading not only to more fundamental understanding of the reaction mechanisms thermodynamically and kinetically, but also to some understanding of the Bi(III) doping effect.

The parallel heterogeneous mechanism of reduction and re-oxidation, in which the soluble Mn(III) species are involved, has been postulated and now experimentally characterized, and is coupled with the widely adopted homogeneous mechanism at the MnO_2 electrode. Bi(III) dopant was found not only to favour the heterogeneous pathway, but also to act as a "catalyst" to reduce the activation energy (overpotential) of the re-deposition of soluble $Mn(OH)_6^{3-}$ intermediates, which form in the reduction and re-oxidation processes at MnO_2, on to the porous electrode in both discharge and recharge of MnO_2. The Bi(III) species also promote the reduction and re-oxidation of Mn involving the *second* electron redox stage.

It was shown how the proposed "heterogeneous" mechanism can, however, explain one of the main characteristics of CM MnO_2, i.e. that of passing high current-density, which is achieved by the rate-determining step of solid-state "proton hopping" in the lattice of γ-MnO_2 becoming bypassed by the heterogeneous mechanism involving production of soluble Mn(III) ion. This important characteristic of the CM MnO_2 makes it substantially different from the γ-MnO_2 cathode and is also very important in providing better power density for possible electric-vehicle power-train applications.

The rechargeability of the electrode material has been improved, especially in the system involving the presence of ZnO_2^{2-} ions, with the help of ion-selective membranes.

At the "molecular" level, the microscopic origin of the effect of Bi(III) on rechargeability is still elusive, but the preliminary results of the *in-situ* XAS studies have begun to shed some light on this question in terms of local coordination changes and interactions.

Major References:

1) W. Konig, Forsch. Forschr., 14(1),8,(1938).

2) A. Volta, Phil. Trans. Roy. Soc., 90,403 (1800).

3) W. Cruikshank, Tilloch's Phil Mag., 7, 337 (1800).

4) J.F. Daniell, Phil. Mag. III8, 421 (1836).

5) W. Grove, Phil. Mag. III, 14, 388 (1839).

6) W. Grove, Phil. Mag. III, 15, 287 (1839).

7) R.W. Bunsen, Pogg. Ann. Physik., 54, 417 (1841).

8) G. Lechanche, French Patent 69980 (1866).

9) H.S. Wroblowa, Electrochemistry in Transition, Plenum Press, New York and London, page 147-159.

10) Report of Business, The Globe and Mail, May 6, 1992, Toronto, Ontario, Canada.

11) K.J. Euler, J. Power Source 8, 133 (1982)

12) R.Huber, in: Batteries, Vol. 1 (K.V. Kodesch, ed.), Marcel Dekker, New York (1974).

13) G. Leuchs, German Patent 24,552 (1882).

14) S.Yai, U.S. Patent 746,227 (1903).

15) W.S. Herbert, U.S. Patent 2,650,945 (1953).

16) J.P. Brenet, *Reun.* CITCE 1956, Madrid, 8, 394 (1956). Butterworth, 1958.

17) J.P. Brenet, Electrochimica Acta 1, 231 (1959).

18) J.P. Brenet, A. Grund, C.r. hebd.seance Acad. Sci. Paris 240, 1210 (1955).

19) J.P. Brenet, 4th Int. Power Source Symp. Brighton, 1964, pp. 2. 247. Pergamon (1965).

20) N.C. Cahoon and M.P. Korver, J. Electrochem. Soc., 100(1959)745.

21) G.S. Bell and R. Huber, J. Electrochem. Soc., 111(1964)1.

22) K.J. Vetter, Z. Elektrochem., 66(1962)577.

23) k.J. Vetter, J. Electrochem. Soc. 110(1963)597.

24) A. Kozawa and J.F. Yeager, J. Electrochem. Soc., 115(1968)1003.

25) A. Kozawa and R.A. Powers, J. Electrochem. Soc., 113(1966)870.

26) A. Kozawa and R.A. Powers, Electrochem. Tech., 5(1967)535.

27) A. Kozawa and R.A. Powers, J. Electrochem. Soc., 115(1968)122.

28) A. Kozawa and B. Kagaku, BMRA Symposium, Brussels 38(1983).

29) A. Kozawa and J.F. Yeager, J. Electrochem. Soc., 112(1965)959.

30) A. Kozawa and R.A. Powers, J. Chem. Educ., 49(1972)587.

31) A. Kozawa, T. Kalnoki-kis and J.F. Yeager, J. Electrochem. Soc., 113(1966)405.

32) J. Fitzpatrick, F.L. Tye, J. Appl. Electrochem., 21(1991)130.

33) K.A.K. Lott and M.C.R. Symons, J. Chem. Soc., (1959)829.

34) P. Ruetschi, J. Electrochem. Soc., 123(1976)495.

35) H.Y. Kang and C.C. Liang, J. Electrochem. Soc., 115(1968)6.

36) J. McBreen, Power Source, 5(1975)525.

37) J. McBreen, Electrochimica Acta, 20(1975)211.

38) P. Ruetschi, J. Electrochem. Soc., 135(1988)2657.

39) P. Ruetschi, J. Electrochem. Soc., 131(1984)2737.

40) P. Ruetschi and R. Govanoli, J. Electrochem. Soc., 135(1988)2663.

41) W.C. Vosburgh and Pao-soong Lou, J. Electrochem. Soc., 108(1961)485.

42) D. Boden, C.J. Venuto, D. Wisler and R.B. Wylie, J. Electrochem. Soc., 114(1967)415.

43) A. Era, Z. Takehara and S. Yoshizawa, Electrochimica Acta, 13(1968)207.

44) J.B. Fernandes, B.D. Desai and V.N. Kamat Dalal, Electrochimica Acta, 29(1984)181.

45) D. Boden, C.J. Venuto, D. Wisler and R.B. Wylie, J. Electrochem. Soc., 115(1968)333.

46) J. McBreen, in: Power Sources 5 (D.H. Collins, ed), Academic Press, London (1975), paper #31 and disscussion.

47) K. Kordesch, J. Gsellmann, M. Peri, K. Tomantschger and R. Chemelli, Electrochimica Acta, 26(1981)1495.

48) W.C. Vosburgh, J. Electrochem. Soc. 106, 839 (1959).

49) R. Giovanoli, Proceedings of the MnO_2 Symposium, Tokyo, 1980, Vol. 2, paper #7.

50) J.P. Brenet, J.P. Chevillot, and J. Brenet, Schweitzer Archiven 1, 10(1960)

51) A. kozawa and R.A. Powers, Proceedings of the MnO_2

Symposium, Cleveland, Ohio, 1975, Vol 1, p.4

52) K. Miyazaki, J. Electroanal. Chem. 21,414 (1969).

53) K, Miyazaki, J. Electrochem. Soc. 116, 415 (1969).

54) K. Miyazaki, J. Electrochem. Soc. 117, 821 (1970).

55) K. Kordesch, BMRA Symposium, Brussels 81(1983).

56) K. Kordesch, J. Daniel-Ivad, E. Kahraman, R. Mussnig and W. Toriser, Paper#910052. 26th International Energy Conversion Engineering Conference, Boston, Massachusetts (1991).

57) S. Fletcher, J. Galea, J.A. Hamilton, T. Tran and R. Woods, J. Electrochem. Soc.,133(1986)1277.

58) Xi Xia and Chingwen Li, Extended Abstracts, 1(91)28, Electrochemical Society Spring Meeting (1991), Washington, D.C.

59) Y.F. Yao, N. Gupta and H.S. Wroblowa, J. Electroanal. Chem., 223(1987)107.

60) H.S. Wroblowa and N. Gupta, J. Electroanal. Chem., 238(1987)93.

61) M.A. Dzieciuch, N. Gupta and H.S. Wroblowa, J. Electrochem. Soc., 135(1988)2415.

62) Y.F. Yao, U.S. Patent 4,520,005 (1985).

63) M.A. Dzieciuch, H.S. Wroblowa and J. T. Kummer, U.S. Patent 4,451,543 (1984).

64) H.S. Wroblowa, N. Gupta and Y. F. Yao, BMSI (1985)203.

65) R. C. Kainthia, D. J. Manko, U.S. Patent 5,156,934

66) D.Y.Qu, B.E. Conway, L. Bai, Y.H. Zhou and W.A Adams,

J. Applied Electrochemistry, 23(1993) 693-706.

67) L. Bai, D.Y. Qu, B.E. Conway, Y.H. Zhou, G. Chowdury and W.A. Adams J. Electrochem. Soc. 140 884(1993).

68) L.Bai, D.Y. Qu, C. Castledine, B.E. Conway, Y.H. Zhou, G. Chowdury, J. Wilinski and W.A. Adams, Abstract No.8, The Electrochemical Society Fall Meeting, Toronto, Canada(1992).

69) D.Y. Qu, L. Bai and B.E. Conway, Y.H. Zhou and W.A. Adams, (Part I), The Electrochemical Society 184th Meeting, New Orleans, Louisiana, October (1993)

70) D.Y. Qu, L. Bai, B.E. Conway and W.A. Adams, J. Electroanal. Chem. in press (1993).

71) D.Y. Qu, L. Bai and B.E. Conway, Y.H. Zhou and W.A. Adams, (Part II), The Electrochemical Society 184th Meeting, New Orleans, Louisiana, October (1993)

72) B.E. Conway, D.Y. Qu and J. McBreen, Proc. NATO Conference on X-ray Absorption Spectroscopy in Electrochemistry, Madeira, December(1992), Proceeding in press(1993).

73) J. McBreen, D.Y. Qu and B.E. Conway, The Electrochemical Society 184th Meeting, New Orleans, Louisana, October (1993).

74) J. McBreen, D.Y. Qu and B.E. Conway, in preparation.

75) L. Bai, B.E. Conway, W.A. Adams and D.Y. Qu, material on file.

76) J. McBreen, W.E. O'Grady, K.I. Pandya, R.W. Hoffman

and D.E. Sayers, Langmuir, 3(987)428.

77) J. McBreen, W.E. O'Grady, G. Tourillon, E. Dartyge, A. Fontaine and K.I. Pandya J. Phys. Chem., 17, 93(989)6310.

78) K.I. Pandya, R.W. Hoffman, J. McBreen and W.E. O'Grady, J. Electrochem. Soc., 237(1990)3883.

79) J. McBreen, W.E. O'Grady, G. Tourillon, E. Dartyge and A. Fontaine, J. Electrochem. Chem. 307(991)229.

80) P. Stephen, Cramer, O. Keith, Hodgson, Prog. Inorg. Chem. 25(1979).

81) P. Eisenberger and B.M. Kincaid, Science 4349, 200(1978)1441.

82) M. J. Fay, A. Proctor, D. P. Hoffmann and D. M. Hercules, Anal. Chem. 21, 60(1988)1225.

83) Boon-Keng Teo, Acc. Chem. Res. 13(1980)412.

84) K.I. Pandya, W.E. O'Grady, D.A. Corrigan, J. McBreen and R.W. Hoffman, J. Phys. Chem. 21, 94(1990).

85) W.J. Wruck, B. Reichman, K.R. Bullock and W.H.-Kao, J. Electrochem. Soc., 138(1991)3560.

86) Handbook of Batteries and Fuel Cells, D. Linden (ed.), McGraw-Hill Inc., NewYork (1984).

87) M. Ibers and J.T. Davidson, J. Amer. Chem. Soc. 72(1950)4744.

88) R. Drummond and M waters, J. Chem. Soc. (1953)435.

89) K.A.K. Lott and M.C.R. Symons, J. Chem. Soc., (1959)829.

90) J.J. Rehr R.C. Albers and M. de Leon., Physica B., 417(1989)158.

91) D.E. Sayers, E.A. Stern and F.W. Lytle, Phys. Rev. Lett. 27(1971)1204.

92) H. D. Abruna, Chapter 1, "Electrochemical Interfaces: Modern Techniques for In-Situ Interface Characterization" , Edited by H. D. Abruna (VCH).

General References:

1) "Electrochemistry in Transition from the 20th to the 21th Century", Edited by O.J. Murphy, S. Srinivasan and B.E. Conway, Plenum Publi. Corp., NewYork (1992).

2) "Surface Electrochemistry A Molecular Level Approach" Edited by J. Bockris and S. Khan, Plenum Publi. Corp., NewYork (1993).

3) "Modern Battery Technology" Edited by C.D.S. Tuck, Ellis Horwood.

4) "Handbook of MnO_2", The International Battery Material Association.

5) T.D. Gregory, R.J. Hoffman and R.C. Winterton, J. Electrochem., Soc., 2, 137(1990)775.

6) T.Ohzuku, M. Kitagawa and T. Hirai, J. Electrochem. Soc., 11,136(1989)3169.

7) K. Takahashi, Electrochimica Acta, 10, 26(1981)1467.

8) H.S. Wroblowa, Proceedings of the Symposium on History

of Battery Technology, Vol. 87-14, p.74, Edited by A.J. Salkind, The Electrochem. Soc., Battery Division.

9) A. Kozawa and R.J. Brodd, Manganese Dioxide Symposium, Vol. 1, Cleveland, 1975.

10) B. Schumn, H.M. Joseph and A. Kozawa, Manganese Dioxide Symposium, Vol.2, Tokyo 1980.

11) A. Kozawa and M. Nagayama, Battery Material Symposium, Vol.1, Brussels, 1983.

12) K.V. Kordesch and A. Kozawa, Battery Material Symposium, Vol. 2, Graz, 1985.

13) A. Kowawa, Battery Material Symposium, Vol.2, Graz, 1985.

14) Batteries, Vol.2, Edited by D.H. Collire, Pergamon Press (1964), Oxford.

15) H. Laig-Horstebrock, J. Electroanal. Chem., 180(1984)599.

16) Proceedings of the BMRA Symposium, Brussels, 1982.

17) B.A. Lopez De Mishima, T. Ohtsuka, H. Konno and N. Sato, Electrochimica Acta, 9, 36(1991)1485.

18) D. Gosztola and M.J. Weaver, J. Electroanal. Chem., 271(1989)141.

19) I. Taei and T. Hirai, Electrochimica Acta, 1, 27(1982)149.

20) T. Yamamoto and T. Shoji, Inorganica Chimica Acta, 117(1986)L27.

21) T. Shoji and T. Yamamoto, Inorganic Chimica Acta,

129(1987)L21.

22) M.B. Liu, B.R. Faulds, G.M. Cook and N.P. Yao, J. Electrochem. Soc., 10, 128(1981)2049.